LBL-16594 c.2

Lawrence Berkeley Laboratory

UNIVERSITY OF CALIFORNIA

RECEIVED
LAWRENCE
BERKELEY LABORATORY

NOV 1 1983

LIBRARY AND
DOCUMENTS SECTION

Materials & Molecular Research Division

ALKALI MONOLAYERS ON TRANSITION METAL SURFACES:
ELECTRONIC PROMOTION IN CATALYSIS

E. Garfunkel
(Ph.D. Thesis)

August 1983

TWO-WEEK LOAN COPY

This is a Library Circulating Copy which may be borrowed for two weeks. For a personal retention copy, call Tech. Info. Division, Ext. 6782.

LBL-16594 c.2

Prepared for the U.S. Department of Energy under Contract DE-AC03-76SF00098

DISCLAIMER

This document was prepared as an account of work sponsored by the United States Government. While this document is believed to contain correct information, neither the United States Government nor any agency thereof, nor the Regents of the University of California, nor any of their employees, makes any warranty, express or implied, or assumes any legal responsibility for the accuracy, completeness, or usefulness of any information, apparatus, product, or process disclosed, or represents that its use would not infringe privately owned rights. Reference herein to any specific commercial product, process, or service by its trade name, trademark, manufacturer, or otherwise, does not necessarily constitute or imply its endorsement, recommendation, or favoring by the United States Government or any agency thereof, or the Regents of the University of California. The views and opinions of authors expressed herein do not necessarily state or reflect those of the United States Government or any agency thereof or the Regents of the University of California.

ALKALI MONOLAYERS ON TRANSITION METAL SURFACES: ELECTRONIC PROMOTION IN CATALYSIS.

Eric Garfunkel

Ph.D. Thesis

August 1983

Department of Chemistry, University of California
and
Materials and Molecular Research Division, Lawrence Berkeley Laboraotry
Berkeley, California 94720

This work was supported by the Director, Office of Energy Research, Office of Basic Energy Sciences, Material Sciences Division of the U.S. Department of Energy under Contract Number DE-AC03-76SF00098.

Alkali Monolayers on Transition Metal Surfaces: Electronic Promotion in Catalysis.

by Eric Garfunkel

Department of Chemistry, University of California
and
Materials and Molecular Research Division, Lawrence Berkeley Laboratory
Berkeley, California 94720

ABSTRACT

The chemical and physical properties of alkali metal monolayers on transition metal surfaces were studied under both ultrahigh vacuum (UHV) and atmospheric pressure conditions to determine how catalyst surfaces are affected by alkali additives. The interactions of alkali adatoms with the substrate, molecular coadsorbates, and other alkali atoms were studied in UHV. In addition, CO hydrogenation reactions were carried out at 32 psig on well characterized transition metal catalysts.

Potassium monolayers on the platinum (111) crystal surface were studied most extensively. Ultraviolet photoelectron spectroscopy (UPS) showed a large decrease in the work function of the surface when potassium was adsorbed, implying charge flow from potassium into the platinum surface. The heat of desorption of potassium, as determined by thermal desorption spectroscopy (TDS), decreased significantly with increasing coverage, due to depolarization effects. Low energy electron diffraction (LEED) showed that potassium forms hexagonal (close packed) overlayer structures.

The effects of potassium on the chemisorption of various small molecules on Pt(111) were studied by a variety of surface science techniques. Oxygen and nitric oxide were readily adsorbed and dissociated by potassium, forming stable potassium-oxide complexes on the surface. The heat of adsorption of carbon monoxide on Pt(111) increased significantly with potassium coadsorption, as shown by TDS. High resolution electron energy loss spectroscopy (HREELS) showed that the carbon-oxygen bond of adsorbed carbon monoxide was weakened by potassium. The heat of adsorption of benzene, however, was decreased by coadsorbed potassium. A molecular orbital explanation consistent with photoelectron results was given to explain the potassium induced behavior on molecular coadsorbates. Only adsorbates having orbital energies within about 2-3 eV of the Fermi level of the transition metal can be significantly affected by "electronic promotion".

CO hydrogenation reactions performed on metal foils showed that the addition of alkali adlayers tends to decrease the overall rate of reaction. Changes in selectivity were noted, shifting the product distribution in favor of higher molecular weight species and from alkanes to alkenes, in agreement with known behavior of industrial catalysts. The shift in hydrocarbon chain length with alkali promotion was attributed to an increased probability for CO dissociative adsorption.

TABLE OF CONTENTS

Chapter	page
Abstract	i
Table of Contents	iii
Acknowledgements	vii
1. Introduction	1
1.1 Scientific and Technological Interest in Alkali Monolayers on Transition Metal Surfaces	1
1.2 Overview of the Thesis	3
1.3 Alkali Monolayers	4
1.4 Alkali Coadsorption Systems	6
1.5 CO Hydrogenation Studies	8
2. Experimental	10
2.1 Apparatus	11
2.2 Methods	14
2.3 Sample Preparation	19
2.4 Dosing	23
2.5 Overview of techniques to study promoter effects	24
2.5.1 Classical techniques	25
2.5.2 Modern ultrahigh vacuum (UHV) techniques	27
2.5.3 Modern "in situ" techniques	28
3. Alkali metal and alkali oxide adlayers	31
3.1 The Work Function	32
3.2 Pure Alkali Monolayers	37

3.2.1 Thermodynamics: AES and TDS behavior..... 37

3.2.2 Structure: LEED studies..... 44

3.2.3 Electronic properties: UPS studies..... 48

3.3 Alkali Oxides: K_2O on Pt(111)..... 61

3.3.1 Thermodynamics: TDS studies..... 61

3.3.2 Structure: LEED studies..... 65

3.3.3 Electronic properties..... 69

3.4 Alkali Adsorption on Stepped Surfaces..... 70

4. Coadsorption Studies: Alkalis and Small Molecules on Metal Surfaces..... 71

4.1 CO adsorption on potassium-dosed Pt(111)..... 72

4.1.1 CO bonding to metals..... 72

4.1.2 TDS studies..... 78

4.1.3 HREELS studies..... 86

4.1.4 UPS studies..... 91

4.1.5 Discussion..... 98

4.2 Benzene adsorption on potassium-dosed Pt(111)..... 108

4.2.1 TDS studies..... 108

4.2.2 UPS studies..... 113

4.2.3 Discussion..... 119

4.3 NO adsorption on potassium-dosed Pt(111)..... 124

4.3.1 TDS studies..... 124

4.3.2 Discussion..... 125

4.4 PF_3, CH_3CN, and C_4H_8 adsorption studies..... 139

4.4.1 TDS studies..... 139

4.4.2 Discussion..... 142

4.5 Literature review of alkali coadsorption studies..... 147

4.6 Conclusion..... 155

5. The Use of Alkalis as Promoters: CO Hydrogenation Reactions... 157

5.1 Introduction..... 157

5.2 Experimental..... 161

5.3 Results..... 162

5.4 Discussion..... 173

5.5 Literature Review..... 177

6. References..... 182

Appendices..... 190

A. Classification of additives..... 191

A.1 Introduction..... 191

A.2 Operational (Macroscopic) Categories of Catalyst Additives..... 192

A.3 Fundamental (Microscopic) Categories of Catalyst Additives..... 193

B. Thermal Desorption Spectroscopy: Practice and Theory... 197

B.1 Theory of Rate Processes..... 198

B.2 The Thermal Desorption Equations..... 204

B.3 Aspects of the Thermal Desorption Experiment..... 212

B.4 Problems in Thermal Desorption Analysis..... 216

C. Sulfur as an additive..... 220

C.1 Introduction..... 220

C.2 Experimental..... 221

C.3 Results..... 223

C.3.1 Chemisorbed Carbon Monoxide..... 223

C.3.2 Chemisorbed Benzene..... 226

C.4 Discussion..... 228

C.4.1 The Effect of Potassium..... 228

C.4.2 The Effect of Sulfur..... 229

D. Review of related uses of alkali promoters in catalysis... 232

D.1 Carbon Gasification..... 232

D.2 Ammonia Synthesis..... 238

E. PET computer programming for surface science..... 240

E.1 Introduction..... 240

E.2 Computer Controlled Thermal Desorption Spectroscopy E-2..... 241

E.3 Computer Control for Photoelectron and Auger Spectroscopy..... 242

E.4 Auger/ESCA Display Program..... 243

ACKNOWLEDGEMENTS:

I would like to acknowledge all those who made my graduate years in Berkeley both an enjoyable and educational experience. First, I must mention Professor Gabor A. Somorjai, my advisor, whose enthusiasm and creativity is an inspiration to all who work with him. I am especially appreciative of his patience and support. I will never forget the time I had to tell him (somewhat timidly) that I had just accidently galvanized the inside of my vacuum chamber. He managed to smile and say that it would be a good chance for me to see all the instruments from the inside. After one month of cleaning every bolt, ceramic, and filament, I decided that I could have done without the experience.

The work reported in this thesis is the product of several other researchers in addition to myself and Professor Somorjai. I would like to thank Dr. Michel Van Hove for numerous helpful discussions at all stages of my work. John Crowell was my coworker for the CO/K/Pt(111) studies. The crucial surface vibrational experiments were performed in his chamber (and are reported in more detail in his thesis - John Crowell, PhD 1983.) Dr. Mario Farias was involved in several other coadsorption studies, including all the sulfur work. Dr. J.J. Maj helped in the NO studies, and Drs. M. Kudo and M. Jazzar in the photoemission experiments. John Parmeter and more recently Brian Naasz have been involved in the catalysis experiments.

A large group of other people were very helpful to me in both experimental and conceptual problems concerning my work. In the first years these included Drs. P.W. Davies, J.E. Frost, N.D. Spencer, P.R. Watson, G. Ertl, M. Salmeron, L. DuBois, S.M. Davis, R.J. Koestner,

U. Bardi, A. Cabrera, R. Casanova, and M. Quinlan. More recently, I have enjoyed and benefited from useful discussions with Drs. B.E. Koel, S.W. Weng, E.L. Meutterties (and his research group), C. Minot, J.P. Biberian, R.F. Lin, W.E. Tysoe, F. Delanney, T.H. Lin, M. Kahn, V. Ponec, D.W. Goodman, M. Asscher and Msr. F. Ogletree, F. Zaera, M. Logan, R. Yeates, M. Mate, A. Gellman, the water splitters (Drs. J. Turner, C. Leygraf, and M. Hendewerk) and Ravi Narasimhan.

Keith Frank, who deserves a "Doctor of Vacuum Technology", was a great help in all mechanical work. I would also like to thank the continuous support of Steve, Henry, Don, and Dave of the Chemistry Department's Electronic Shop, and J. Katz of LBL. Among other things, they helped the Somorjai group enter the computer age. Tammy Learned and Ann Kahn were also of invaluable help in their administrative and secretarial work.

Finally, I would like to thank Sonia SooHoo, and all those not directly involved in my graduate work, who have helped me enormously throughout my four years in Berkeley. In particular, my parents, sister, and brother were always there for support and diversion when needed. I would also like to thank my surrogate family - Mona, Larry, Butch, Nancy, and of course Andre - for all their help.

CHAPTER 1. INTRODUCTION AND OVERVIEW.

1.1 Scientific and Technological Interest in Alkali Monolayers on Transition Metal Surfaces.

In 1912, while trying to commercialize an ammonia synthesis process, B.A.S.F. researchers found that the reaction rate increased when they added potassium oxide (K_2O) to an iron catalyst. This was one of the first examples of catalyst additives being used in an industrial process. In addition to ammonia synthesis, alkali metals are used to promote the hydrogenation of carbon monoxide, commonly called the Fischer-Tropsch reaction, and several other reactions such as coal gasification and ethylene oxidation. However, there is still no definitive model of how additives such as K_2O work. There are only scattered papers on "promoters" considering electronic, structural and/or textural effects. My graduate work has been directed toward contributing to the development of such a model by exploring the surface chemistry of alkali metal additives.

Several hypotheses have been put forward in the past few decades attempting to explain the particular ability of alkalis to promote chemical reactions. Some have argued that alkali metals keep the surface clean of unreactive carbon during CO hydrogenation. Others have claimed that certain reactions which do not occur on the "active metal" component (as distinct from the catalyst support material and the additives) will take place on an alkali oxide or hydroxide island. A third possibility is that the alkali islands help keep the surface clean by acting as a sink to scavenge poisons such as chlorine or sulfur. The most

widely held view, however, is that the dominant effect of alkalis is to change the electronic properties of the metal surface, which then changed the reactivity. The results reported here support this last proposition, lending much credence to the idea that alkali metals act as "electronic" promoters on transition metal catalysts.

In my thesis, surface modifier effects are classified as follows (a more complete account is given in Appendix A):

a) For an electronic effect, the important property of the additive is to change the electronic structure of the active transition metal component of the catalyst surface. One can imagine several types of electronic interactions which vary in the strength and range. In addition, charge transfer to a molecular adsorbate from the additive can occur via the transition metal substrate, while with others, a direct interaction between the promoting addditive and the molecular adsorbate occurs.

b) For a structural effect, the dominant change in reactivity can be ascribed to a change in a structural parameter of the surface. Structural effects can be subdivided in several categories. In the most simple case, the adatom merely blocks sites for adsorption. A somewhat different phenomenon is the ensemble effect where it is presumed that a given chemical reaction requires a certain number of metal atoms in a cluster before the reaction becomes allowed. By alloying the active metal with an inactive one, the number of ensembles (of some minimum size) can then be decreased. In a third type of structural effect the adatom stabilizes a certain crystallographic orientation of the metal crystallites (on a supported catalyst). Other structural effects of

additives involve changes in the support, which in turn affect the degree of dispersion or the degree of phase mixing between support and metal.

Scientific interest in alkali monolayers comes not only from their catalytic applications, but also from their unique photoelectron and thermionic properties. As early as 1923, Langmuir had shown that adsorbed cesium greatly increased the electron emission from hot tungsten surfaces because of the decrease of the work function of the metal (the minimum energy needed to extract an electron from the surface). This finding has had many applications in the design of thermionic converters and photocathodes (Mayer, 1940).

1.2 Overview of the Thesis.

Following the Introduction (Chapter 1) and Experimental Section (Chapter 2), the body of the thesis is organized into three general categories. In Chapter 3, the properties of alkali metal and alkali oxide monolayers on transition metal surfaces under ultrahigh vacuum (UHV) conditions are discussed, concentrating on the system studied in most detail: potassium on the platinum (111) surface. Chapter 4 is concerned with the way in which alkali adatoms modify the chemisorption of various small molecules on a metal surface (also in UHV). The systems most extensively studied were carbon monoxide (CO), benzene (C_6H_6), and nitric oxide (NO) when coadsorbed with potassium on Pt(111). In Chapter 5, results for high pressure CO hydrogenation reactions on iron and rhenium foils are presented. The effects of alkalis, as well as other additives, on the reaction rates and product distributions are shown and discussed in the context of what was learned from the

studies done in UHV (chapters 3 and 4). Five appendices are included which cover: A) A classification scheme of the macroscopic and microscopic role of additives; B) Thermal desorption theory and practice; C) The role of sulfur as an additive/modifier; D) A literature review of the use of alkalis in catalysis (except for CO hydrogenation, i.e. Chapter 5); and E) The use of the PET-Commodore computer for surface science studies. In addition to our studies on alkali effects, several other papers have recently appeared in the literature on systems related to those that we have studied. The results of these studies will be discussed both in the appropriate chapters and in the appendices. The rest of the introduction will be devoted to summarizing the results.

1.3 Alkali monolayers.

The properties of potassium monolayers on the Pt(111) crystallographic face were studied by thermal desorption spectroscopy (TDS), low energy electron diffraction (LEED), Auger electron spectroscopy (AES), and ultraviolet photoelectron spectroscopy (UPS). The results were presented in Chapter 3. Our results for potassium on platinum were similar to the those of alkali metals on most transition metal surfaces: see for example the recent studies by Lee (1980) and Broden (1979). Pure potassium adlayers assume a hexagonal structure on Pt(111). Because of their size, the alkali atoms are relatively mobile at room temperature, and displayed no LEED pattern until near monolayer coverages. Lower coverage LEED structures have been observed by cooling the sample. Orientational reordering of the alkali adlayers, similar to the behavior of noble gas overlayers, was observed by LEED, implying a relative insensitivity to substrate potential variations. (Throughout this

thesis, I use the convention that one monolayer of potassium defines $\Theta_K=1$, and is equal to a coverage of 5.4×10^{14} atoms/cm^2. This is 36% the atomic density of the Pt(111) surface. Others define saturation monolayer coverage to be $\Theta_K = \sigma_K sat/\sigma_{Pt} sat = 0.3$. To convert my coverages to this other convention, one can divide by 3.)

We find from thermal desorption spectroscopy that potassium desorbed with a broad peak, starting at about 300K for monolayer coverages, and extending to 1100K at low coverages. This corresponds to a decrease in heat of adsorption from 60 kcal/mole to 25 kcal/mole as the coverage is increased. This change, as with the change in work function, can be understood by assuming that potassium is highly ionized at low coverage, but becomes depolarized at high coverage. The depolarization results in a nonlinear drop-off in the work function and the eventual attainment of a constant heat of desorption approximately equal to the heat of sublimation of potassium.

UPS results on Pt(111) showed that potassium overlayers caused a decrease in work function (as expected), a sharp drop in emission just below E_f, and an increase in the secondary electron emission yield. We also noted the appearance of a peak at about 20 eV binding energy, below the secondary electron edge, which should not conventionally be allowed. This feature is interpreted with a model of localized electrostatic potentials.

When oxygen is added to the potassium monolayer, a surface potassium oxide is formed. This oxide is quite stable compared to a pure potassium monolayer, and exhibits a whole series of new LEED patterns. The stabilizing ability of oxygen is probably of importance on real catalyst

surfaces as discussed below.

1.4 Alkali coadsorption systems.

In Chapter 4, various coadsorption systems are analyzed. The most important ones are carbon monoxide, nitric oxide, and benzene with potassium on Pt(111). The effects of potassium on these molecules were the most dramatic of the coadsorption systems examined.

The bonding of CO to metals involves a donation from the 5σ CO orbital into the metal, and a back-donation from the metal into the 2π CO orbitals (Blyholder, 1964). The major experimental findings for the CO + K + Pt(111) system can be summarized as follows: the addition of submonolayer amounts of potassium continuously increased the heat of adstoption of CO on Pt(111) from 25 kcal/mole for clean Pt(111) to 36 kcal/mole for near monolayer coverages. Associated with the increased heat of adsorption was a large decrease in the stretching frequency of CO from 2000 cm^{-1} on clean Pt(111) to as low as 1400 cm^{-1} with 0.6 monolayer of coadsorbed potassium. At a constant potassium coverage, the CO vibrational frequencies for both linear and bridge adsorption sites decreased substantially with decreasing CO coverage. On the potassium-free Pt(111) surface, CO preferred to occupy top adsorption sites, while on the potassium-covered surface, CO adsorbed preferentially on bridged sites. The work function of the Pt(111) surface decreased by about 4 eV upon the adsorption of about one-third of a monolayer of potassium, but increased by as much as 1.5 eV when CO was coadsorbed.

When potassium is adsorbed, it donates charge into the surface, thereby lowering the work function. The changed electronic properties

at the surface make it a better electron donor (more basic), which in turn results in an increase in electron back-donation into the 2π (CO) orbitals. The increase in 2π orbital occupancy strengthens the metal - carbon bond as noted in the TDS study. It also weakens the carbon - oxygen bond, and even leads to the dissociation of CO on most other metal surfaces. (Platinum, palladium, and the group IB metals are notoriously poor at dissociating CO.)

Nitric oxide was studied as an analog to CO. NO adsorbed molecularly on the clean Pt(111) surface. NO dissociated with potassium on the surface, but only in an amount proportional to the potassium coverage. It was not clear in this study if potassium interacted directly with the NO causing it to be dissociated, or if the interaction was indirect, mediated by the substrate, as was the case for CO. The dissociation products, as monitored by TDS, were N_2O, N_2, and some form of a surface potassium oxide.

The benzene/potassium coadsorption system also showed interesting behavior. Upon heating a benzene overlayer on clean Pt(111), some of the benzene desorbed intact while the rest decomposed, giving off hydrogen and leaving a carbon residue. The benzene desorption temperature was lowered significantly by coadsorbed potassium, and the amount of benzene which decomposed was decreased. Thus for benzene, a large weakening of the benzene - metal bond was observed, just the opposite of what was observed for CO.

The desorption (or decomposition) temperature of other molecules adsorbed on Pt(111), such as PF_3, C_4H_8, CH_3CN, and NH_3, remained practically constant when potassium was coadsorbed. So, how can we predict

whether or not the chemisorptive state of a molecule will be altered by a given additive? The answer we offer is based on a qualitative molecular orbital analysis. Our hypothesis is that only those molecules with energy levels within about 3 eV of the Fermi energy (E_f) can be significantly affected by electronic promotion in catalysis. In the case of CO (as noted above), the gas phase $2\pi^*$ CO orbital interacts with the metal d-orbitals at the surface, forming a conjugate d-2π orbital lying about 2 eV below E_f. By lowering the work function, we enable more charge to flow into the 2π orbital. The conjugate d-2π level is "bonding" between the metal and carbon atoms, and "antibonding" between the carbon and oxygen. For benzene, on the other hand, the nearest level to E_f which could be filled by a drop in work function is the e_{1g}^* orbital. This orbital is antibonding between the metal and carbon ring. Thus the idea of potassium causing a weakening of the benzene-metal bond is in agreement with a qualitative molecular orbital analysis. A review of the literature shows that no molecular orbital levels exist within 3eV of E_f for most of the other molecules studied. The absence of an electronic effect therefore is not surprising.

1.5 CO hydrogenation studies.

The effects of alkali metal and oxygen additives on iron and rhenium foils for CO hydrogenation reactions are presented in Chapter 5. Iron showed greater activity and increased selectivity towards higher molecular weight species as compared to rhenium. The addition of submonolayer amounts of alkali on both surfaces decreased the overall rate of reaction, but caused a selectivity change from methane towards

longer chain hydrocarbons and from alkanes to alkenes. This agrees with known industrial catalytic behavior (Anderson, 1956). Oxidation usually caused a higher selectivity towards methane, and a decreased rate of carbon build-up, but the overall rate of methanation remained relatively constant. The increased selectivity towards longer chain hydrocarbons (when potassium is added) is correlated with an increased probability for CO dissociative adsorption, as noted in Chapter 4. We also suggest that the alkane to alkene shift, with potassium addition, results from a lower heat of adsorption of the alkene, in analogy to the benzene TDS shifts reported in Chapter 4.

CHAPTER 2: EXPERIMENTAL

Contents: page

2.1 Apparatus 11

2.2 Methods 14

2.3 Sample Preparation 19

2.4 Dosing 23

2.5 Overview of techniques to study promoter effects 24

2.5.1 Classical techniques 25

2.5.2 Modern ultrahigh vacuum (UHV) techniques 27

2.5.3 Modern "in situ" techniques 28

2.1 Apparatus.

The experiments described in this thesis have been performed by me and various coworkers in four different ultrahigh vacuum chambers. Although all chambers had a variety of available techniques, I will discuss them according to their main function: 1) the TDS chamber, 2) the HREELS chamber, 3) the photoelectron chamber, and 4) the catalysis chamber. The TDS and catalysis chambers are shown in Figures 2.1 and 2.2. The TDS chamber (base pressure 1×10^{-10} torr) was equipped with a Physical Electronics (PHI) single-pass cylindrical mirror analyzer (CMA) for Auger electron spectroscopy (AES), a PHI low energy electron diffraction (LEED) optics system, a UTI quadrupole mass spectrometer (QMS) interfaced to a PET-Commodore micro-computer for thermal desorption spectroscopy (TDS), and an argon ion sputtering gun for sample cleaning. The design and use of the computer is described in Appendix E. Alkali and sulfur guns were also mounted in this chamber as described below.

Details of the design of the HREELS (high resolution electron energy loss spectroscopy) chamber can be found in the thesis of John Crowell (PhD, U.C. Berkeley, 1983). This chamber was equipped with an ion pump providing pressures of 5×10^{-11} torr, with two levels of instruments. The upper level contained a retarding field analyzer (RFA) for LEED and AES, a UTI QMS for TDS, an argon ion sputtering gun for sample cleaning, and an alkali source. The lower level contained the HREELS spectrometer. In the results reported here, the resolution was typically 85 cm^{-1} FWHM in the elastically scattered peak with 20,000 counts/s.

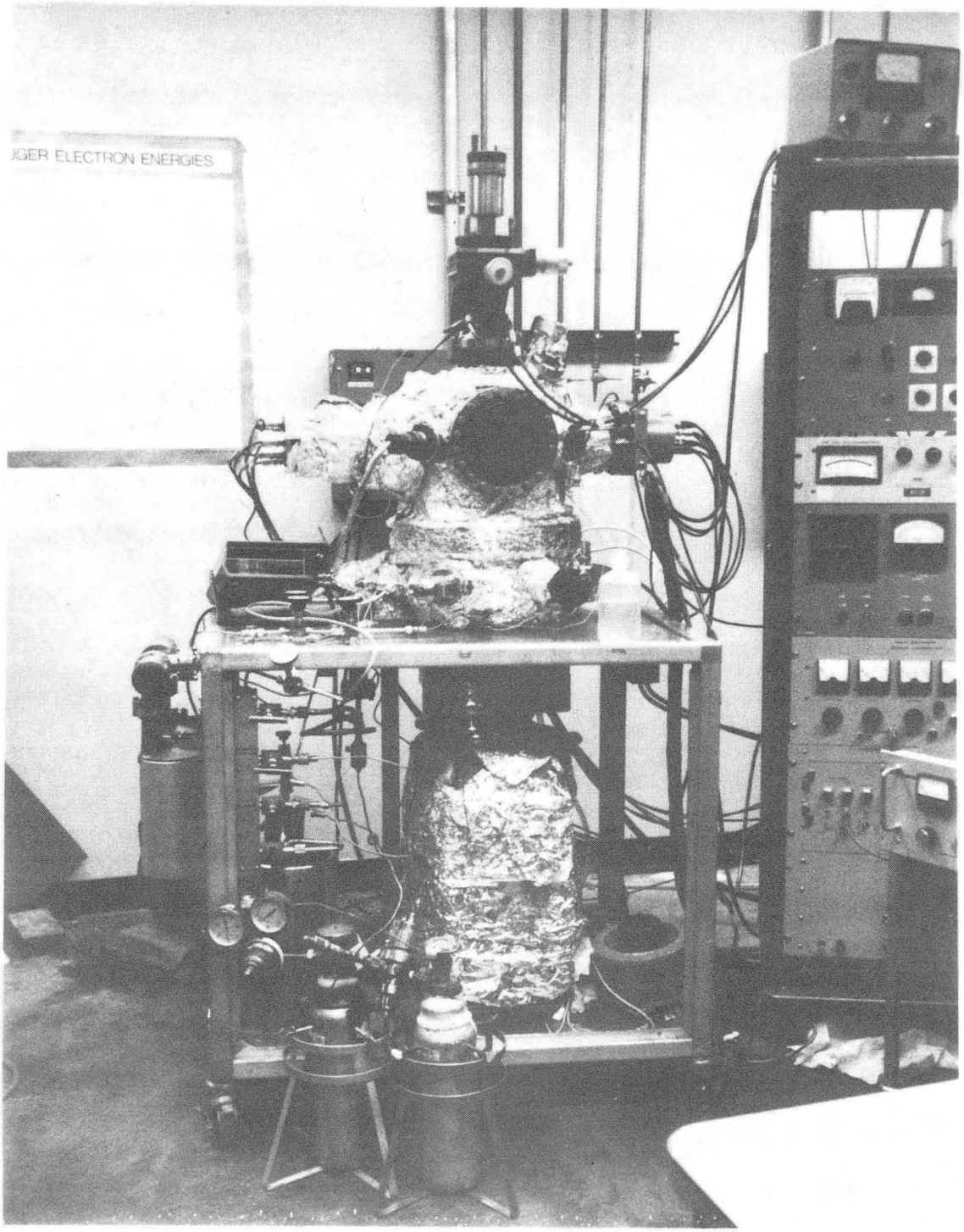

XBB 800-12544

Figure 2.1 The thermal desorption chamber.

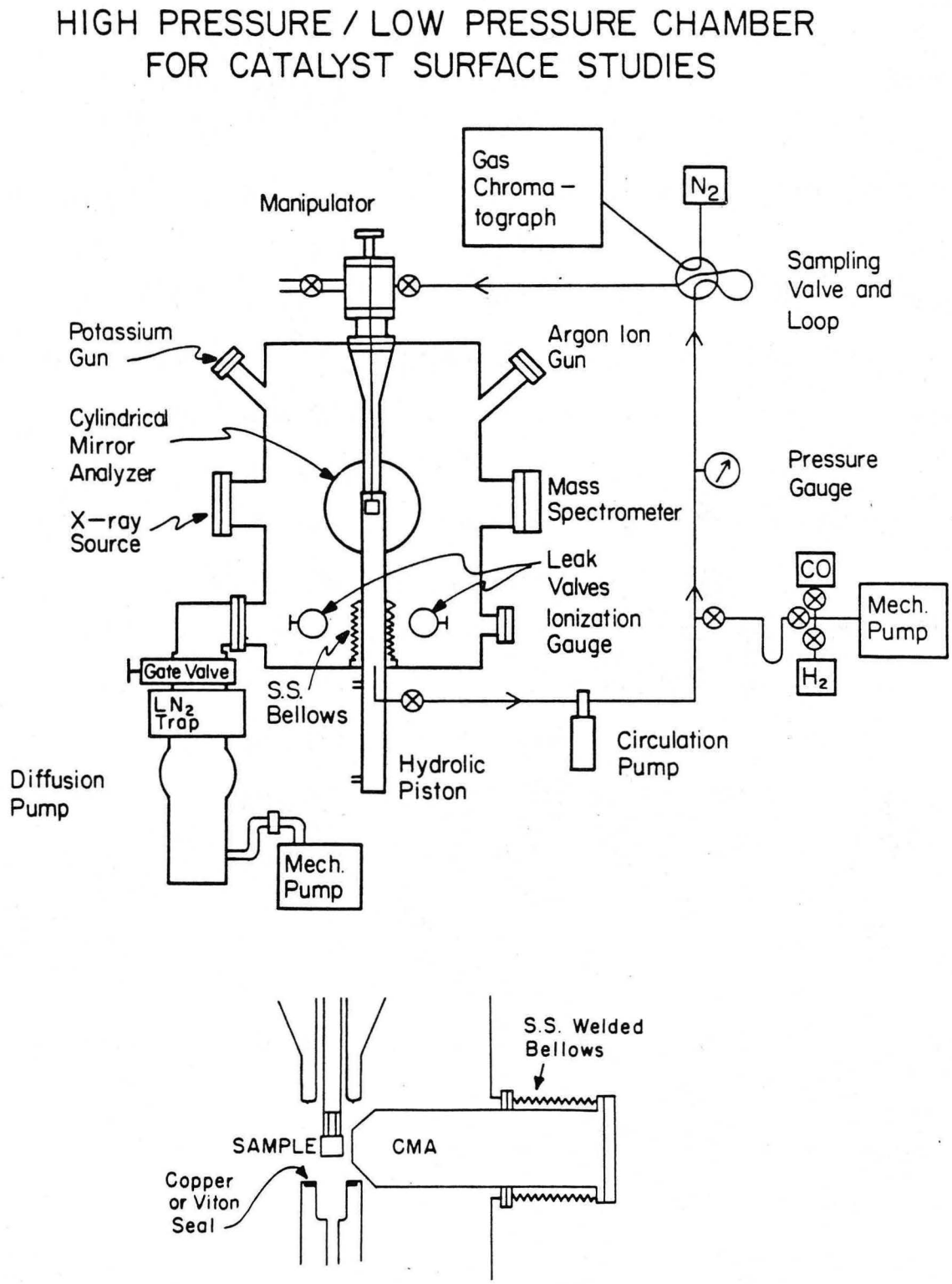

Figure 2.2 Catalysis chamber.

The photoelectron chamber (ion pumped, 10^{-10} torr) was equipped with a QMS, a LEED system, an argon ion sputtering gun, ultraviolet (UV) and x-ray sources, and a double pass CMA for AES, ultraviolet photoelectron spectroscopy (UPS), and x-ray photoelectron spectroscopy (XPS). The data were collected with the aid of the PET computer. The catalysis chamber is shown in Figure 2.2. It was equipped as depicted with both standard UHV instruments as well as an internal high pressure cell. It contained a UTI QMS, and PHI double-pass CMA for AES (and XPS), an argon ion sputtering gun, and an alkali source. In the high pressure mode, the sample (held stationary) was enclosed in a reaction cell mounted on stainless steel welded bellows and was opened and closed with the aid of a hydraulic piston. The pressure in the reactor cell was normally held near two atmospheres in the studies reported here (although it could be pressurized up to 20 atmospheres). Gaseous reaction products were injected into a gas chromatograph from a sampling valve connected to the high pressure loop.

2.2 Methods.

The most common technique used in my studies was thermal desorption spectroscopy (TDS). Appendix B is devoted to a detailed description of the theory and practice of TDS; only a brief account is offered here. In the thermal desorption experiment, one simply heats the sample and monitors the desorbing species by some technique (usually mass spectroscopy) as a function of time or of temperature. By monitoring the temperature of the maximum rate of desorption one can get some idea of the heat of adsorption of the species on the surface, whether it is an adsorbate molecule or a substrate atom. The most common experiment

reported in my thesis involved the predeposition of a small amount of potassium on a metal surface, and then noting how the desorption of a small molecular adsorbate such as CO or benzene was changed by the presence of potassium (see Chapter 4). Most of the discussion in Chapters 3 and 4 can be understood with this simplified description of the thermal desorption experiment, but the interested reader is referred to Appendix B for a more complete treatment.

Auger electron spectroscopy (AES) has now become a standard technique to monitor the atomic composition of surfaces (Ertl, 1974). The Auger experiment (usually) involves a four electron process. First a high energy electron beam (1-2 KeV) is directed onto the surface. One of the several pathways for de-excitation involves the emission of a core electron of a surface (or near surface) atom (Figure 2.3a). The resulting excited atom will usually relax by having an outer shell electron fall into the core hole. In order to conserve energy, the atom must release energy as the electron falls into the core. Two processes can now occur: either an x-ray photon is emitted with a characteristic energy, or, in the so-called Auger process, another electron (the Auger electron) is emitted as depicted in Figure 2.3b. Since the energy of this Auger electron is determined by its original level in the atom as well as the levels of the electron which dropped into the core hole, it is independent of the exciting electron (or x-ray) and characteristic only of the atom. The Auger transitions are relatively sharp in energy (a few eV) and can be readily extracted from the large "secondary electron" background emission by taking the derivative spectrum (using a standard modulated lock-in amplifier technique). Figure 2.3c shows a typical

AUGER ELECTRON EMISSION

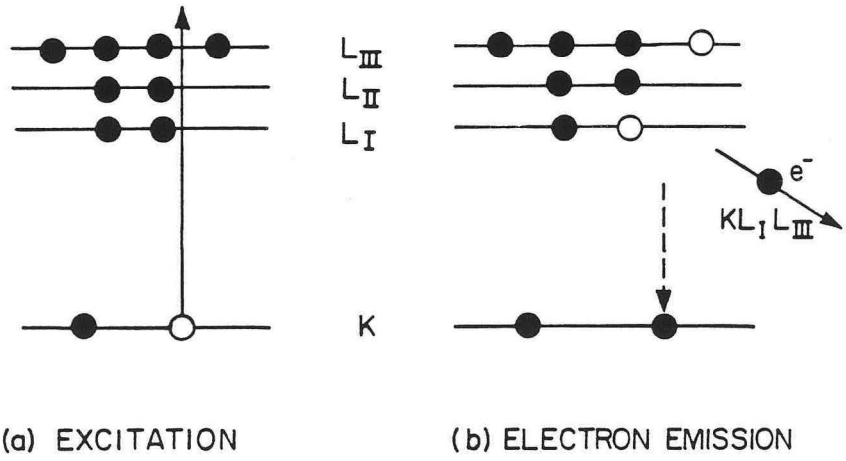

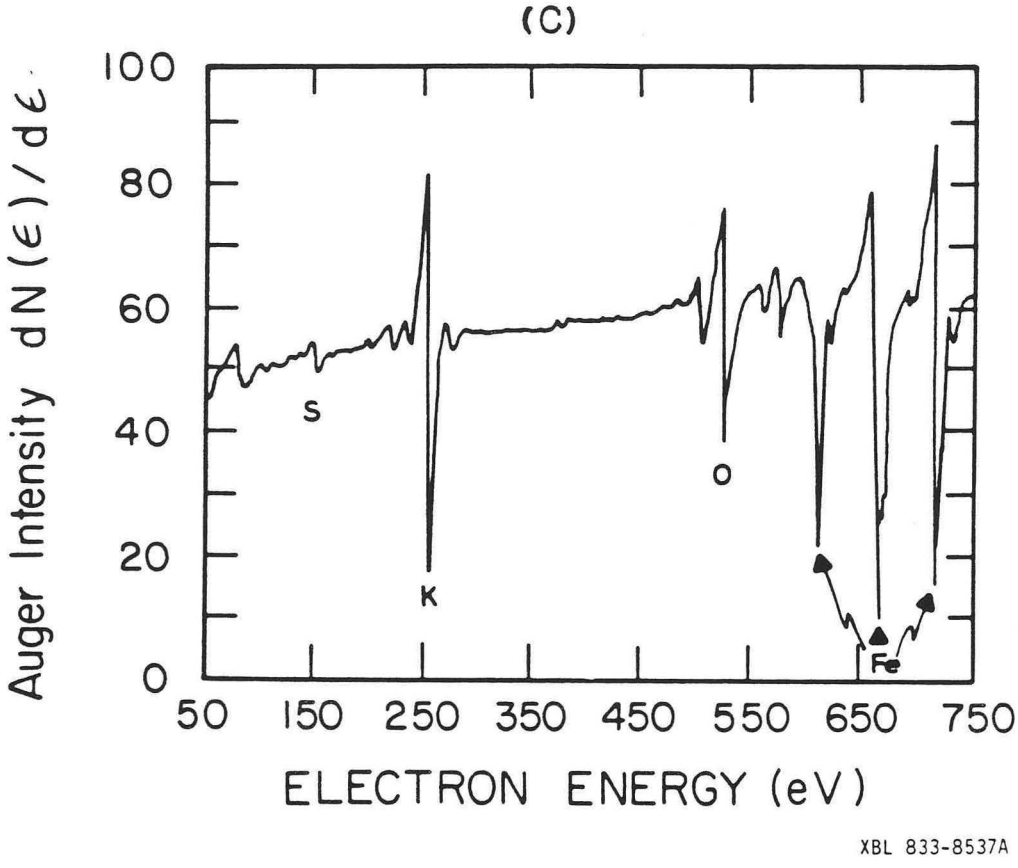

Figure 2.3 (a) and (b), the Auger Emission Process. (c) An Auger spectrum of a promoted iron foil sample.

Auger spectrum of an iron sample promoted with potassium. Many of the Auger electrons have a kinetic energy of 50-1000 eV. Although the high energy electron beam penetrates 50-100 angstroms into the solid, the relatively short mean free path of the analyzed electrons (5-20 Å) in a solid will ensure that the only electrons that reach the detector are those which have been emitted from the near surface region. In fact, by varying the incidence and collection angles one can roughly determine the relative concentration of species not only at the surface but just below it (5-10 Å). Changes in Auger peak shape and position can also occur due to the chemical environment, as noted for carbon in Figure 5.8.

Low energy electron diffraction (LEED) is another, now standard, UHV technique for single crystal surface analysis which has been regularly used in this work. In the LEED experiment, a monochromatic beam of electrons is directed onto a flat, single crystal surface. Some of the electrons are back scattered and can be detected by any number of techniques, including a fluorescent screen. Due to their wave character, some of the back-scattered electrons will be diffracted and will appear as spots on the screen. The diffraction pattern gives a reciprocal space representation of the two dimensional surface periodicity. The (111) crystallographic face of an fcc crystal will give a hexagonal diffraction pattern. If CO is then adsorbed on the surface such that one CO molecule is adsorbed on every second substrate atom, then new spots forming a (2 x 2) overlayer pattern will be observed by LEED. In addition to the two dimensional periodicity of the surface, some three dimensional information can be determined from an analysis of

the LEED spot intensities. Since electrons of 50-500 eV can penetrate the first 2-3 layers of the surface, the intensity of the scattered electron beams depends on their energy (wavelength). An analysis of the LEED spot intensities versus electron energy can thus be used to give information about distances normal to the surface, even for adsorbates. This structural information is an invaluable counterpart to the electronic and thermodynamic information given by other techniques.

Photoelectron spectroscopy is the most useful method for learning about electronic properties of surfaces. A monochromatic beam of photons (x-rays or ultraviolet) is focussed onto the sample and the energies of the emitted electrons are analyzed. XPS studies of core level electrons yield information about the chemical state of the surface atoms. UPS probes the valence levels at the surface yielding both the band structure of the substrate and the position of the valence orbital levels of any adsorbate.

High resolution electron energy loss spectroscopy (HREELS) has been used to determine the vibrational structure of adsorbates. A complete description of the spectrometer, theory, and practice of HREELS can be found in Ibach (1982). A shorter description, as well as an in depth analysis of the HREELS spectra used in this study, can be found in the thesis of my coworker John Crowell (PhD, U.C. Berkeley, 1983). Briefly, the HREELS experiment involves scattering a monochromatic beam of low energy electrons (≈ 5 eV) from a sample and detecting the intensity of the scattered electrons as a function of energy. By scanning from the energy of the elastically scattered peak, to about 500 meV below it, many of the adsorbate vibrations and surface phonons

can be detected. Because of certain selection rules (Ibach, 1982) vibrations normal to the surface are usually more easily detected than ones parallel to it.

The high pressure cell shown in Figure 2.2 was used for all catalysis experiments (Cabrera, 1982b). This design enables the user to determine the surface composition and structure both before and following a high pressure exposure such as would occur in a catalytic reaction. Following sample preparation (see below), the high pressure chamber was closed and high purity gases were introduced. A circulation pump was used to provide a closed loop circulation rate of about 200 ml/min with a total volume of 400 ml in the chamber. If the gases were introduced sequentially, the self-mixing of the circulation system was such that the gases were completely mixed within several minutes. During operation the pressure in the UHV chamber would rise to 10^{-8}-10^{-7} torr (depending on the age of the gasket). The leak enabled us to monitor, by mass spectroscopy, the concentration of the major gaseous components in the high pressure chamber.

A Hewlett Packard HP 5720A gas chromatograph was connected to the catalysis loop through a gas sampling mechanism. Gases could also be injected into the column through a standard injection system. Gaseous catalysis products were separated on Chromosorb 102, 103 and Porapak PS columns, and were then detected using a flame ionization detector (FID). The FID signal was amplified and sent to a "minigrator" to determine retention time and peak areas.

2.3 Sample preparation.

Platinum, rhenium, iron, and palladium single crystals were used

in this work, as well as a series of transition metal foils. Four different platinum crystals (99.998% purity) were used at various stages. The other crystals were of unknown purity. All were cut and polished using standard techniques, and checked for orientation by Laue x-ray back-diffraction. Most of the samples (≈ 1 cm^2) were mounted on platinum, tantalum, or palladium wire (0.015 - 0.030" diameter), although other methods of mounting were used. Heating was accomplished by passing a current of up to 50 amps through the sample. To ensure even heating, the sample shape and support length had to be varied. The temperature of the sample was measured by a 5 mil wire thermocouple (Pt-Pt/Rh or chromel-alumel). The TDS chamber manipulator was also equipped with a liquid nitrogen cooling system. Liquid nitrogen was usually pulled, by an external vacuum through a tube to an electrically isolated reservoir located 5-10 cm from the sample. Copper braids were then connected from the reservoirs to the sample support rods on the manipulator. This method of cooling was reasonably efficient, allowing a base temperature of near 100K, but was limited by the necessity of the somewhat lengthy copper braid needed to permit movement of the "off axis" manipulator. Other less effective methods of cooling were used on the other chambers. Figure 2.4 shows the manipulator design.

Initial cleaning of all samples involved repeated cycles of argon ion sputtering and annealing. Sputtering removed all of the major impurities which segregated to the surface, such as Si, Ca, O, Mg, S, and P. Residual carbon was removed with the aid of medium temperature (500-800K) oxygen treatment, and the resultant oxygen was removed either by flashing to an appropriate temperature, or reducing in hydrogen.

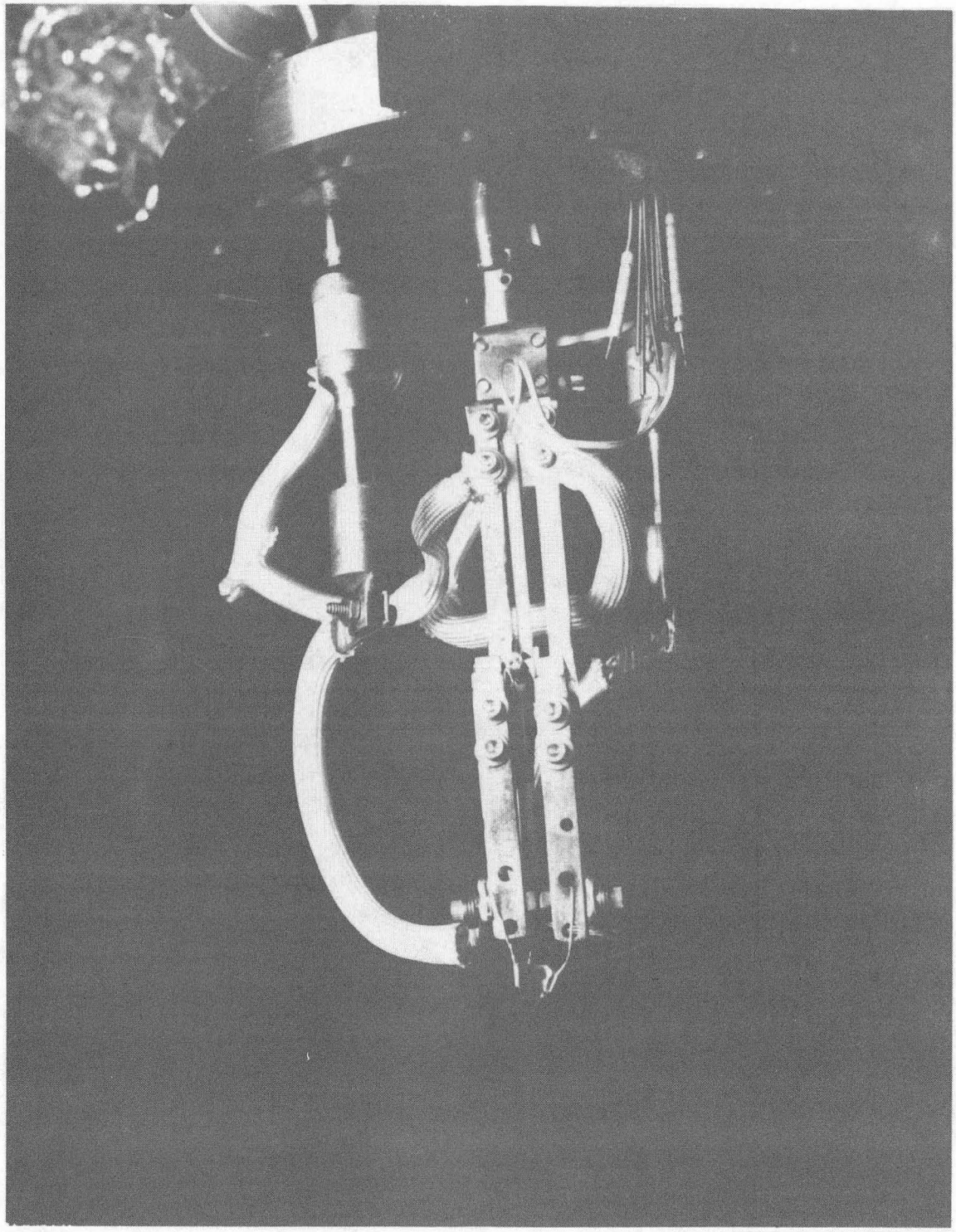

XBB 810-11557

Figure 2.4 Manipulator with Pt(111) sample.

The most troublesome impurities for platinum were Ca and Si. Their removal was most easily accomplished by sputtering the surface at a temperature between 800-1200K.

To clean impurities, it is helpful to find conditions where the impurity is selectively drawn to the surface and sputtered away. The enthalpy of mixing term for the crystal dictates that at equilibrium some impurities should form a separate phase, perhaps an ordered alloy or compound at the surface. The entropy term, which dominates at high temperature, forces the system to mix as randomly as possible (i.e., not to segregate to the surface). These are the two thermodynamic terms contributing to the free energy of the system. Thus, if one wants impurities to be at the surface, presumably to be bombarded off, the sample should be relatively cool. An equally important factor is kinetics. If the sample is cool the impurities will not be mobile enough to segregate to the surface; the system will be in a metastable equilibrium. If possible, the most desirable situation is to find a temperature where the impurity is relatively mobile, yet not so high a temperature that the entropy term (causing equal mixing) dominates over the enthalpy (of segregation) term. At this temperature, the surface will have a high concentration of impurities which can be continually bombarded. Of course, for some impurities, such a dynamic equilibrium cannot be attained, and one must find other methods of sample cleaning. Final cleanliness of metal samples can be determined by most UHV techniques, including AES, LEED, XPS, HREELS, SIMS, etc. AES, however, is most common.

3.4 Dosing.

Several different methods of dosing (with potassium, sulfur, and gaseous molecules) have been used in this work. Potassium was usually deposited with an "SAES Getters" source mounted 3-5 cm from the sample surface. This source consisted of a powdered mixture of potassium chromate and a zirconium-aluminum getter, enclosed in a tantalum "boat" (SAES). By passing a current through the boat to heat it, the chromate decomposes, giving off potassium and oxygen. The potassium migrates through the powder and is emitted through a slit, while the oxygen reacts with the Zr-Al getter. Initally H_2, O_2, H_2O, CO_2, and CO are emitted, but after a sufficient induction period, most sources become pure. The behavior of pure alkali metal monolayers differs markedly from that of alkali oxides in LEED, TDS, and UPS behavior. Hence a source which outgasses is highly undesirable.

Two other types of alkali sources were tried. First, zeolite guns were used which give off potassium ions, but also (unfortunately) a fair amount of O_2, H_2O, and CO_2. These gases readily reacted with potassium on the surface to form stable potassium suboxides. Pure potassium was also tried as a source. Potassium, packed in glass under argon, was inserted into a copper tube which was connected to vacuum through a small valve. By breaking the glass inside vacuum, pumping off the argon, and then heating the copper tube, potassium would vaporize and travel through the small collimating tube to hit the sample. This method was reasonably successful, but required a differentially pumped ante-chamber.

Sulfur was deposited by three different techniques. The best,

although most difficult, technique involved an electrochemical cell. Details of this gun, also useful for halogen deposition, are available in the literature (Wagner, 1953). Briefly, the cell, $Ag/AgI/Ag_2S/Pt$, could be heated while a current was passed through it causing silver to migrate and be reduced, giving off S_2. A second method of sulfur deposition was to introduce H_2S into the chamber. This method is often used by others, but the maximum sulfur coverage usually cannot exceed 0.5 monolayers, and one must contend with H_2S being deposited throughout the chamber. Multilayer deposition is facile using the electrochemical cell technique. A final, rather crude, technique for putting sulfur on the surface was used for iron and rhenium. A new crystal or foil, was heated to a high temperature, which upon cooling would allow bulk sulfur impurity to segregate to the surface.

Molecular gas dosing was accomplished in most cases by opening a leak valve from the gas manifold into a .25" stainless steel tube (in vacuum). The open end of the tube was positioned to within 1-2 cm of the sample, allowing local pressures at the sample to be up to an order of magnitude greater than the rest of the chamber. Exposures were calibrated from various sources including ionization gauge, thermal desorption, LEED and Auger behavior, as well as known sticking coefficients.

2.5 Overview of techniques to study promoter effects in catalysis.

In giving an overview of the techniques used to study promoter effects and catalysis, it is useful to divide these topics first into the more classical, high pressure methods, and then the modern ultrahigh vacuum "surface science" tools. This choice is not rigorous. In

fact, some of the most informative approaches go beyond this distinction and enable the researcher to study the sample under high pressure conditions while still obtaining atomic level information. New "in situ" techniques using neutrons, EXAFS, Raman, FTIR, and NMR probes will be surveyed following a brief discussion of the classical and modern UHV methods. There are several papers and books which give a much more complete description of the techniques used to study catalysts and their reactivity (Thomas, 1980; Somorjai, 1981).

2.5.1 Classical Techniques.

For the most part the techniques originally used in catalysis did not monitor the surface. The early researchers were mainly interested in results: if an element or compound worked for catalyzing a given reaction, it would be used until a better one was found. Although performance under actual conditions is the best judge of a catalyst, this method of analysis does not necessarily lead to a rational way of predicting or designing new ones. A knowledge of chemical bonding and reaction behavior of certain elements can, however, be used in the process of designing catalysts, even in the absence of microscopic analysis (see Trimm 1980, for the best example of this).

The classical method involves running a reaction in a small batch or flow reactor and analyzing product yields and distributions as a function of variables such as time, pressure, and temperature. For this process, one of the most important quantities used to characterize the catalyst is the surface area. The various adsorption isotherm methods (such as BET) help in determining the total surface area as well as pore size and structure of a given catalyst support material.

This is a necessary first step since a measure of reaction rates requires a knowledge of the number of surface (or active) sites on the catalyst. Once the number of active sites on a catalyst is known, a reaction can be run, and rates and selectivities determined. In bench-scale reactions, chromatographic methods (both G.C. and H.P.L.C.) have proven most useful in determining product yields and distributions, while an array of spectroscopic methods including IR, NMR, UV, and mass spectrometry have helped in the analysis of the various products. Of course under actual industrial conditions other methods of product separation, such as fractional distillation, are required. In fact, sometimes the product separation and purification stages are more costly than the catalytic reaction step itself.

To a first approximation, the rate of a reaction (-dN/dt) may be expressed as:

$$-dN/dt = f(\theta)\nu e^{-E_a/RT}$$

By monitoring the reaction rates at various temperatures, the activation energy E_a, for the reaction may be derived from an Arrhenius expression. If the surface area is also known, then the preexponential factor, ν, may be determined. Finally, by changing the partial pressures of the components, the reaction order, $f(\theta)$, can be determined. Pressure dependence studies can, in principle, also give information on the nature of the reaction mechanism. However, these methods do not give direct information about the microscopic dynamics of the systems, consequently, the assignment of a reaction mechanism and determination of intermediates is difficult. This is especially true for heterogeneous multicomponent-multiphase catalysts. This is precisely the point at

which the more modern surface science techniques attempt to prove a certain proposed mechanism, or suggest another.

Another classical technique which has often been used to elucidate mechanisms is isotopic labelling. Here, the results imply that certain reactions could or could not have occured, and have led to the discounting of proposed pathways. For example, Araki (1976) and others showed that the enol-intermediate mechanism for Fischer-Tropsch reactions was not correct.

2.5.2 Modern Ultrahigh Vacuum Techniques.

A qualitative change in our knowledge of promoter effects, and catalysis in general, was enabled by the development of the ultrahigh vacuum (UHV) surface science techniques (Somorjai, 1981). The main advantage of these methods is that they allow a quantitative determination of surface conditions. Since particles (of moderate energy <1 KeV) have very short mean free paths in solids, this makes many of the UHV spectroscopies appropriate for the study of only the outer 2 or 3 layers of a surface.

We are now able to obtain surface composition (SIMS, XPS, AES), surface structure (LEED, EXAFS), electronic structure (UPS, XPS), vibrational frequencies (HREELS), etc. Thus, we can now solve simple problems such as determining what is the stable configuration of CO or N_2 on a surface or how an additive such as sulfur or potassium will affect the dissociation probability of NO. Thus, atomic level catalytic information is now available for a large variety of systems, a few of which are discussed in this thesis.

The major disadvantages of these techniques is that they require

UHV conditions, and they are usually static, meaning that one only observes stable surface species. A knowledge of stable surface species is important, but an understanding of the microscopic reaction dynamics of short-lived reactive intermediates is still missing. As for the extremely low pressure requirement, the objection is often raised that these conditions are too far removed from actual catalytic conditions to be of any use in understanding catalysis. The art is in knowing when and how one can use information learned from UHV experiments to understand high pressure systems. A pressure increase of 12 orders of magnitude will certainly manifest itself in more rapid rates of exchange of surface species. It will also assure that the surface is completely covered with adsorbates at all times. But, in most cases the chemisorption bond itself should not change much. This has been demonstrated for cases such as CO chemisorption where high pressure FTIR studies show similar CO vibrational frequencies as are seen by HREELS at 10^{-10} torr on single crystals.

2.5.3 Modern "in situ" Probes.

Several new in situ techniques are now being used to study catalysts under actual catalytic conditions. In the extended x-ray absorption fine structure (EXAFS) experiment, x-rays from a synchrotron source are allowed to pass through a sample, for instance a supported catalyst, and an absorption spectrum is measured as a function of photon energy. When the photon energy becomes equal to the ionization energy of a core electron, the absorption curve exhibits a sharp maximum. In the energy region slightly greater than the maximum absorption, usually called the absorption edge, a series of oscillations occur due to

interference as the photon scatters off atoms neighboring the original absorbing atom. These interference oscillations give information on the interatomic distances, the coordination number, and the Debye-Waller factor (Joyner, in Thomas, 1980).

Neutron scattering spectroscopy can also be used to give information on crystallographic structure, as well as on surface dynamics. This technique has the added advantage that neutrons can penetrate the stainless steel walls of high pressure catalyst chambers. Of particular relevance to the study of additives, both neutron scattering and EXAFS can determine if the additive forms a separate phase, or is incorporated as an impurity (or alloy) into the active metal component of the catalyst.

Mossbauer and conversion electron Mossbauer spectroscopy have also been used recently for iron catalyst characterization (W. Jones, in Thomas, 1980). Mossbauer spectroscopy is normally bulk-sensitive, but the use of high surface area catalysts and the conversion electron process enable characterization of the surface and near surface, and even adsorbate properties.

Recent developements in lasers and computers have made Raman and infrared spectroscopy much more attractive for surface scientists. For many cases, these methods can be used under both UHV and high pressure conditions. The information they give about the vibrational frequencies and certain electronic transitions of adsorbed species is often useful in the study of catalysis. Both can now be used to study small area single crystals as well as high surface area supported catalysts (Thomas, 1980).

Lastly, nuclear magnetic resonance (NMR) is now becoming more

popular for catalysis studies. This technique is well suited for "in situ" studies which have H, Li, C^{13}, Al, Si, or other elements with appropriate nuclear magnetic properties. One disadvantage is that samples of very high surface area, such as zeolites, are needed if surface information is required, due to the inherent limitations in sensitivity. Many interesting results have recently been confirmed by NMR including studies on the effects that different supports have on the electronic properties of small supported metal clusters, as well as the changes in electronic structure that follow a change in cluster size (De Menorval, 1981). NMR can also be used to give information about atomic distances (positions).

CHAPTER 3. ALKALI METAL AND OXIDE ADLAYERS.

Contents: page

3.1 The Work Function..... 32

3.2 Pure Alkali Monolayers..... 37

3.2.1 Thermodynamics: AES and TDS behavior..... 37

3.2.2 Structure: LEED studies..... 44

3.2.3 Electronic properties: UPS studies..... 48

3.3 Alkali Oxides: K_2O on Pt(111)..... 61

3.3.1 Thermodynamics: TDS studies..... 61

3.3.2 Structure: LEED studies..... 65

3.3.3 Electronic properties..... 69

3.4 Alkali Adsorption on Stepped Surfaces..... 70

3.1 The Work Function.

The study of the alkali metal monolayers deposited on transition metal surfaces has proven to be one of the most intriguing subjects studied by surface scientists since the early work of Langmuir (1923, 1925, and 1933). The most noticeable change observed upon alkali adsorption is the large drop in work function of the metal surface.

The work function of a metal can be defined as the minimum amount of energy needed to remove an electron from a surface (Holzl, 1979; Ertl, 1974), see Figure 3.1a. It is analogous to the ionization potential of an atom or molecule. One can divide the work function of a metal surface into two components:

$$\phi = -\mu/e + \Delta\phi_{DP} \qquad \text{Eqn. 3.1}$$

where μ is the chemical potential, and $\Delta\phi_{DP}$, the surface dipole term, is the difference in electrostatic potential between the inside of a crystal and the region $\approx 10^{-4}$cm outside the surface.

The chemical potential of an electron in a transition metal should stay practically constant when any adsorbate, such as an alkali metal is put on the metal surface. But the second term, $\Delta\phi_{DP}$ will change. For alkali metal adsorption, it is the large change in the surface dipole term that causes the drop in work function. The surface dipole term can be readily understood by examining Figures 3.1b, c, and d.

Inside the metal, all the ion cores are surrounded by an essentially symmetric electron gas. At the surface, however, the electron orbitals extend into the vacuum beyond the ion cores of the atoms such that the electron distribution at the surface is asymmetric, see Figure 3.1b.

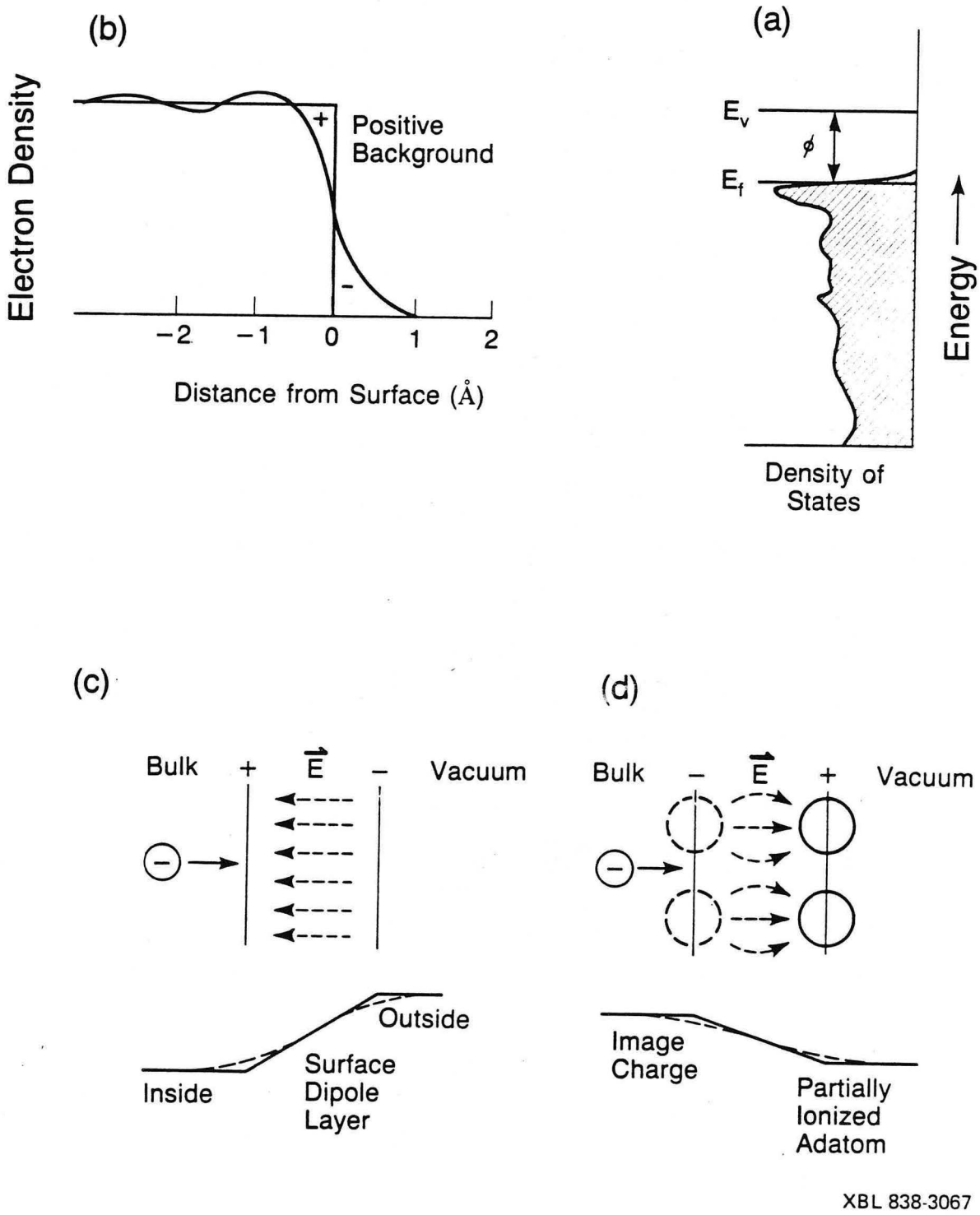

Figure 3.1 (a) density of states vs. energy for a group VIII metal. (b) represents the electron "spillover" in the vacuum which creates the surface dipole layer (c). An electropositive adatom (d) contributes another component to the total surface dipole field.

Because some of the charge extends into the vacuum, an electrostatic dipole field is created at the surface, $\Delta\phi_{DP}$(intrinsic). It can be modeled in a simplified sense by a parallel plate capacitor (Figure 3.1c). Here, an electron in region A or C will experience no net field from the charges on the plates because they cancel each other, but in region B, the electron will be accelerated towards the positive plate, i.e., towards the metal. This is considered the intrinsic component of the dipole term.

If we now place an adsorbate on the surface, which, upon adsorption, results in charge transfer either to, or from, the surface, we might expect a change in the dipole field strength. For alkali metal atoms we expect that the alkali metal will donate charge readily into the surface since its ionization energy (and electronegativity) is low compared to that of transition metals. Although some electron density will always extend beyond the alkali ion cores, a new component to the dipole field is created, $\Delta\phi_{DP}$(extrinsic), at the surface upon alkali adsorption as represented in Figure 3.1d. The work function of the surface will then decrease. (See Shustorovich, 1982, for a theoretical discussion on some of these points).

In Figure 3.2 we show a typical plot of ϕ versus alkali coverage on a metal surface (Fehrs, 1971). The initial slope of the curve yields the dipole field strength caused by alkali atoms and is given by the Helmholtz equation:

$$\Delta\phi = 4\pi\mu N \qquad \text{Eqn 3.2}$$

where μ is the dipole moment, and N is the coverage.

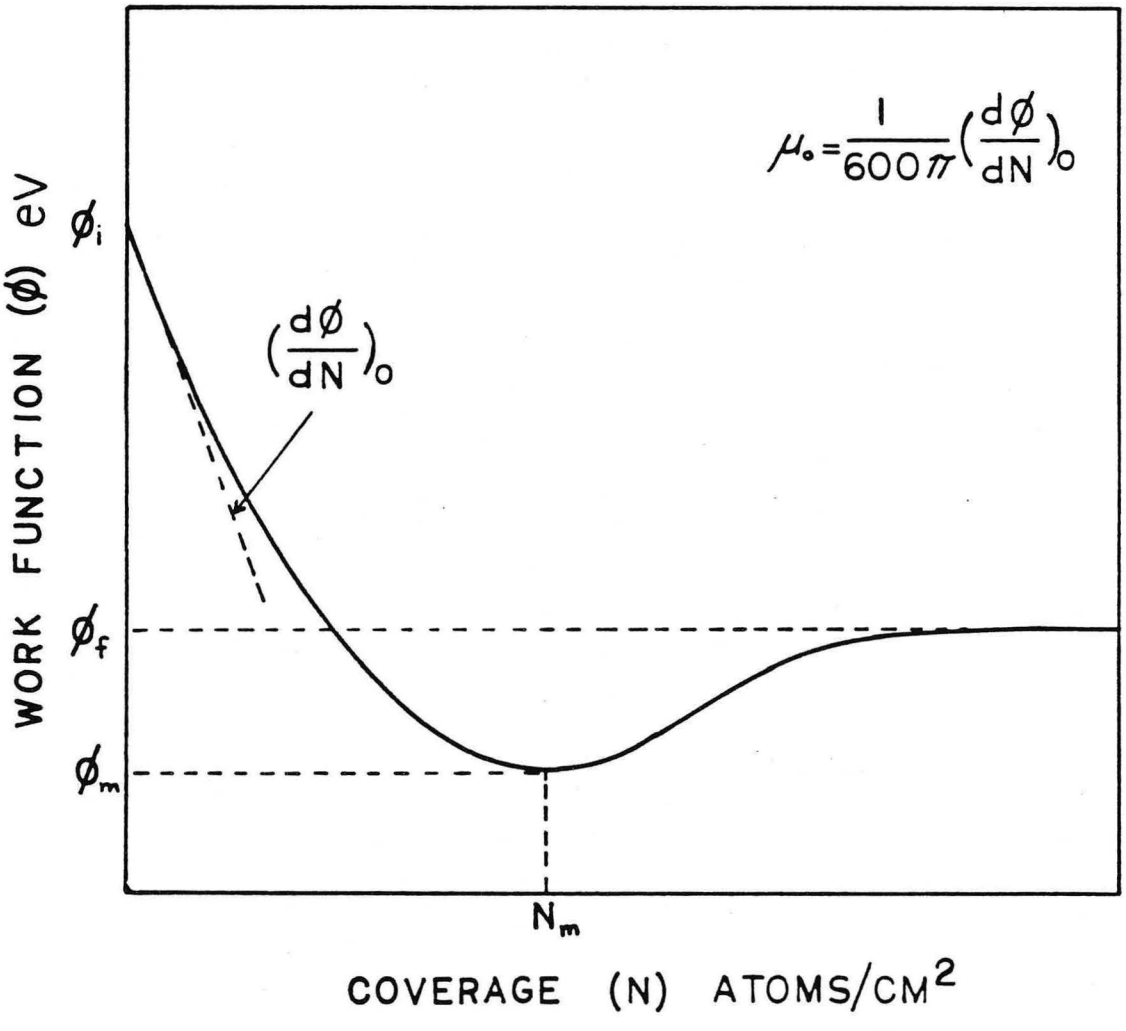

XBL 838-11131

Figure 3.2 Work function versus coverage for alkali adatoms on transition metal surfaces, from Fehrs (1971).

The figure also shows the decreasing ability of an alkali atom to lower the work function with increasing coverage. This is attributable to depolarization effects within the alkali monolayer, and can be roughly approximated by the Topping formula (1929):

$$\phi = 4\pi\mu N/(1 + 9\alpha(N)^{3/2}) \qquad \text{Eqn 3.3}$$

where α is the polarizability.

At low coverage, each alkali atom can be significantly ionized (polarized) without being influenced by neighboring alkali/image dipoles. But, at higher coverages, repulsion between the dipoles becomes important. It is important to notice that the work function does not drop uniformly from the value of the transition metal to that of the alkali metal, but goes below both values at submonolayer coverages. This clearly shows that the extrinsic surface dipole component (Figure 3.1d) between potassium and its image is essential for understanding the total work function. If $\Delta\phi_{DP}$(extrinsic) did not exist, the minimum should not have appeared. The importance of the drop in work function for catalysis will become more obvious in the Chapter 4 where the coadsorption of alkali atoms with small molecules is discussed.

3.2 Pure Alkali Monolayers.

3.2.1 Thermodynamics: AES and TDS behavior.

The potassium Auger signal intensity is plotted against deposition time on the Pt(111) crystal face in Figures 3.3, 3.4, and 3.5. At platinum crystal temperatures slightly above 350 K (Fig. 3.3) the curve, which was linear at first, leveled abruptly to a maximum. The height of the maximum was determined by both the temperature of the crystal and the potassium flux to the surface. At 350 K with a potassium flux of about 0.2 monolayers/min, the potassium adsorption proceeded until the potassium Auger signal was about one half the maximum intensity from a cooled pure potassium multilayer. The growth of multilayer potassium deposits is not observed at these temperatures. Figure 3.4 shows the AES uptake curve with the sample held at 270 K. Here, multilayer adsorption is occuring. The periodic fluctuation in the curve may be the result of clustering; a critical coverage is reached which then clusters in a periodic fashion (Gillet, 1980).

Platinum crystal surfaces cooled well below room temperature showed smoother Auger uptake curves (Figure 3.5). There were slight breaks at the positions corresponding to the first and second layers and these were confirmed by TDS and LEED experiments (see below). The deposition is shown in Figure 3.5 as the ratio between the K 252 eV and the Pt 64 eV Auger peak heights, with the crystal held at 250 K. The first break occurred when the K(252 eV)/ Pt(64 eV) peak ratio was 1.1 (as monitored by our PHI single pass CMA). This was also the coverage at which the most densely packed potassium monolayer LEED pattern was visible (see below). We therefore define this potassium

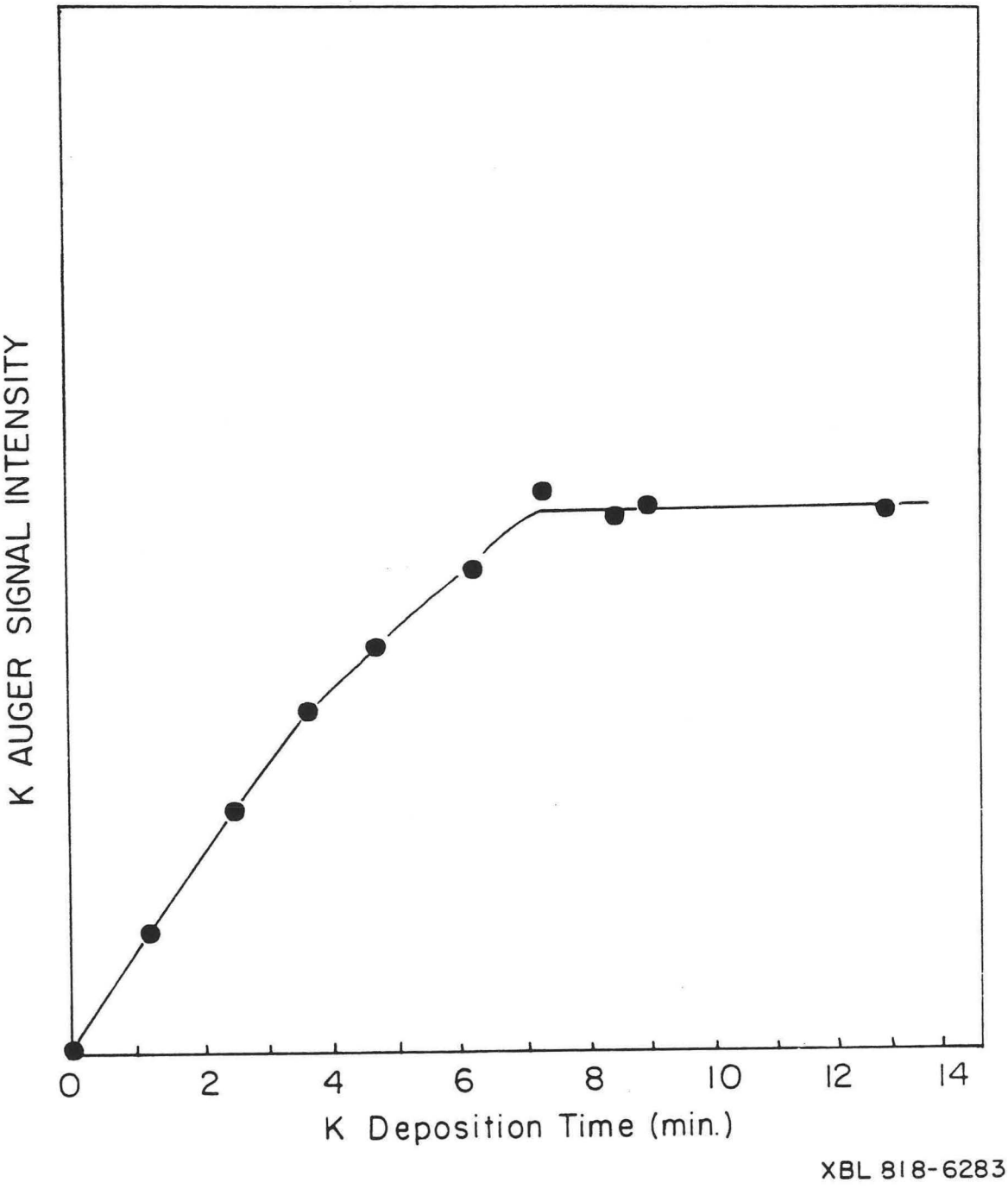

Figure 3.3 Auger uptake curve; 350 K.

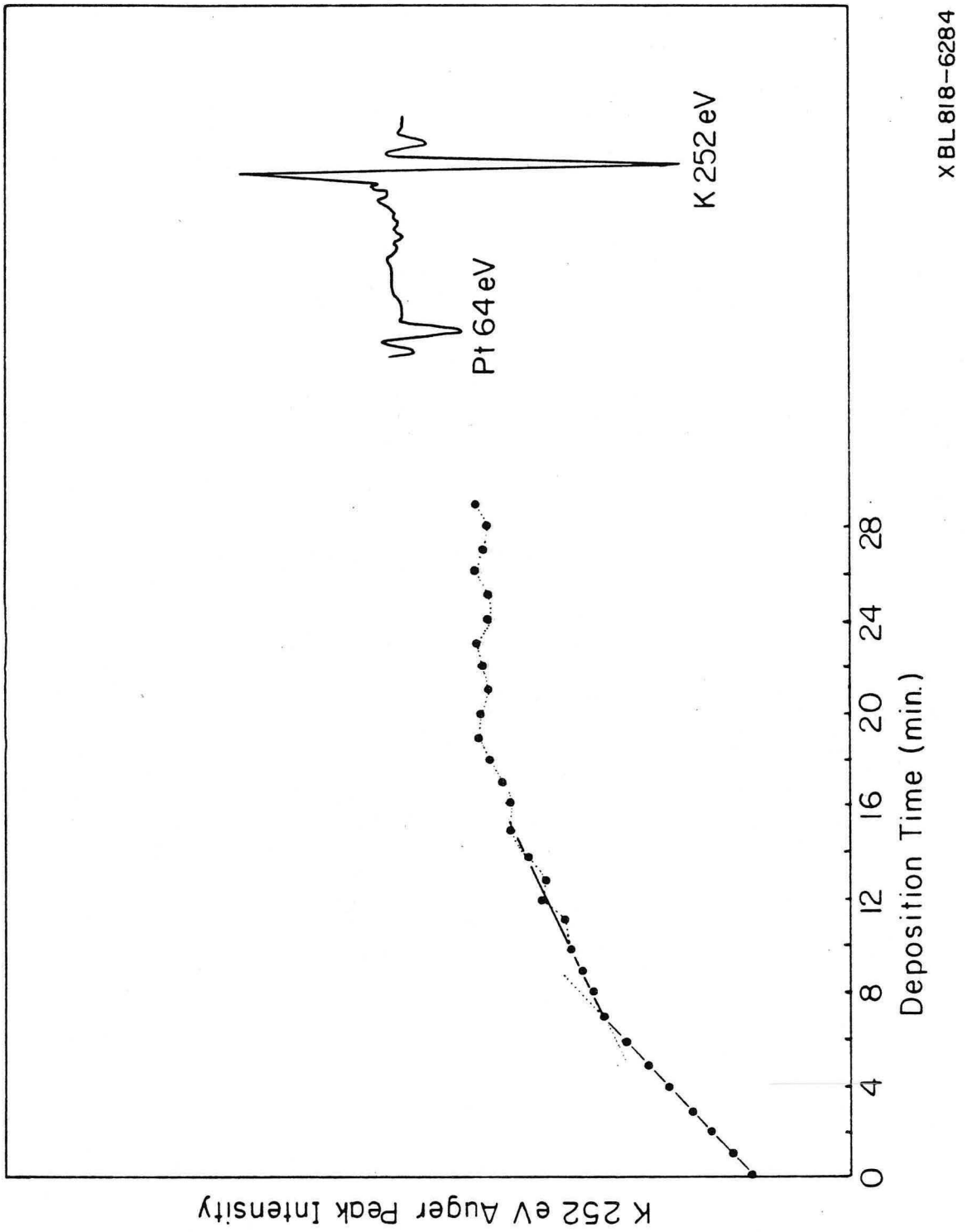

Figure 3.4 Auger uptake curve; 270 K.

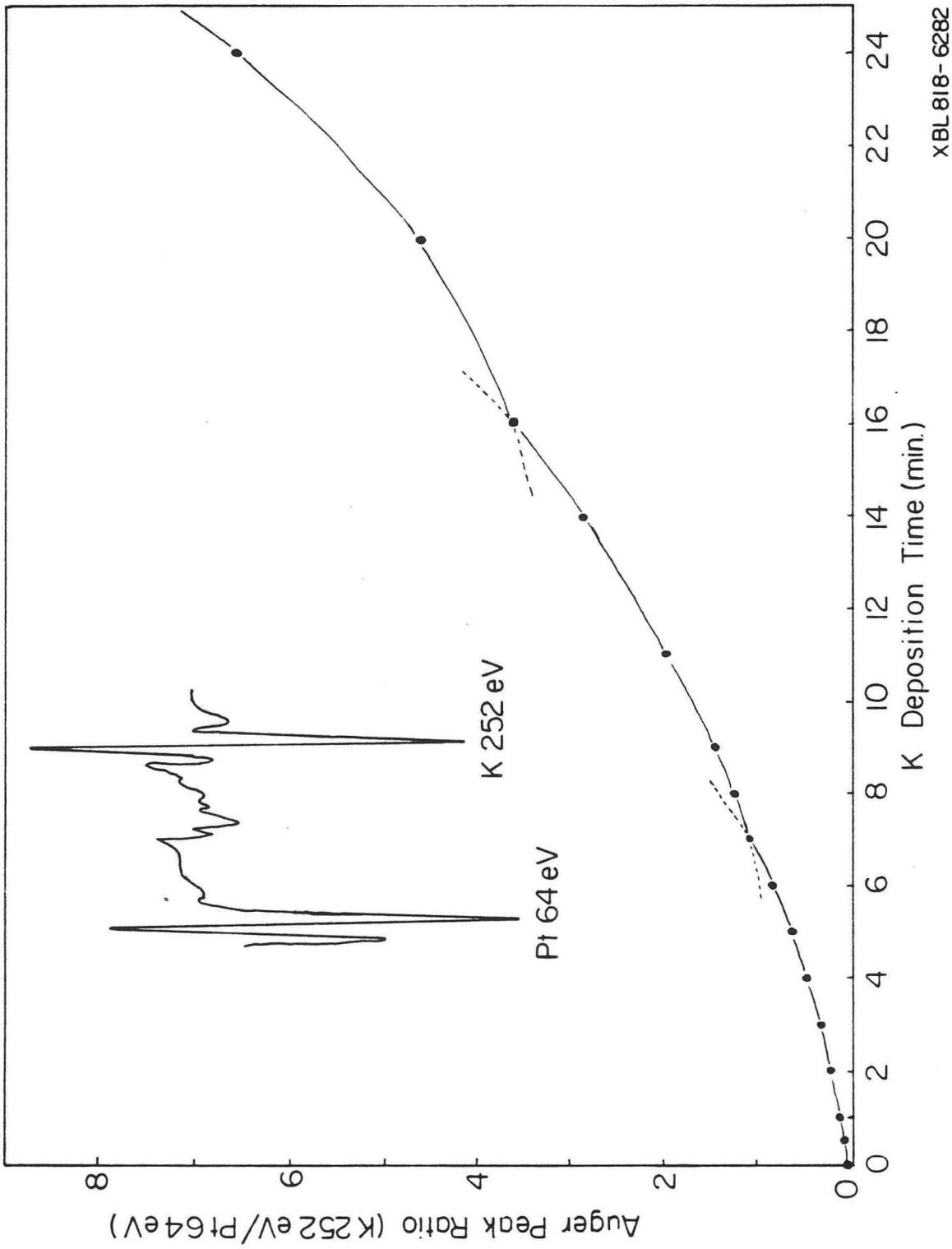

Figure 3.5 Auger uptake (ratio) curve; 250 K. Inset is the Auger signal after 7 minutes and corresponds to 1 monolayer.

coverage (θ_K=1) to be one monolayer; as will be shown below, this corresponds to 5.4 x 10^{14} K atoms/cm^2, or 36% of the surface atomic density of the substrate Pt(111) face. The large difference between the potassium and platinum surface density is due to the much larger radius of metallic potassium.

The results for the thermal desorption of potassium from the Pt(111) surface are shown in Figure 3.6. At coverages of less than 0.1 monolayer, the potassium binds tightly to the surface, desorbing at about 1000 K. As the coverage is increased, the temperature at which the desorption rate is at a maximum decreases continuously, and at one monolayer the desorption temperature is at 400 K. We believe that this shift is due to repulsive lateral interactions between the (slightly ionized) potassium atoms that weakens their bonds with the platinum surface. This is similar to the behavior of alkali atoms on other transition metal surfaces (Gerlach, 1969; Lee, 1981; Broden, 1980). Assuming first order desorption kinetics and a preexponential factor of 1 x 10^{13} s^{-1} that would be characteristic of a mobile atomic overlayer (Somorjai, 1981), the variation of the desorption temperature peak with increasing coverage corresponds to shifts in the heat of desorption from 60 to 25 kcal/mole. The heat of desorption of potassium as a function of coverage calculated from the TDS spectra is shown in Figure 3.7. If other preexponential factors are assumed or derived, the magnitude of ΔH_{ads} will change, but it will still exhibit the same general trend as a function of potassium coverage. The large variation in binding energy with coverage of alkali metals adsorbed on transition metals has been observed by others. For example, Gerlach (1969) showed that the heat

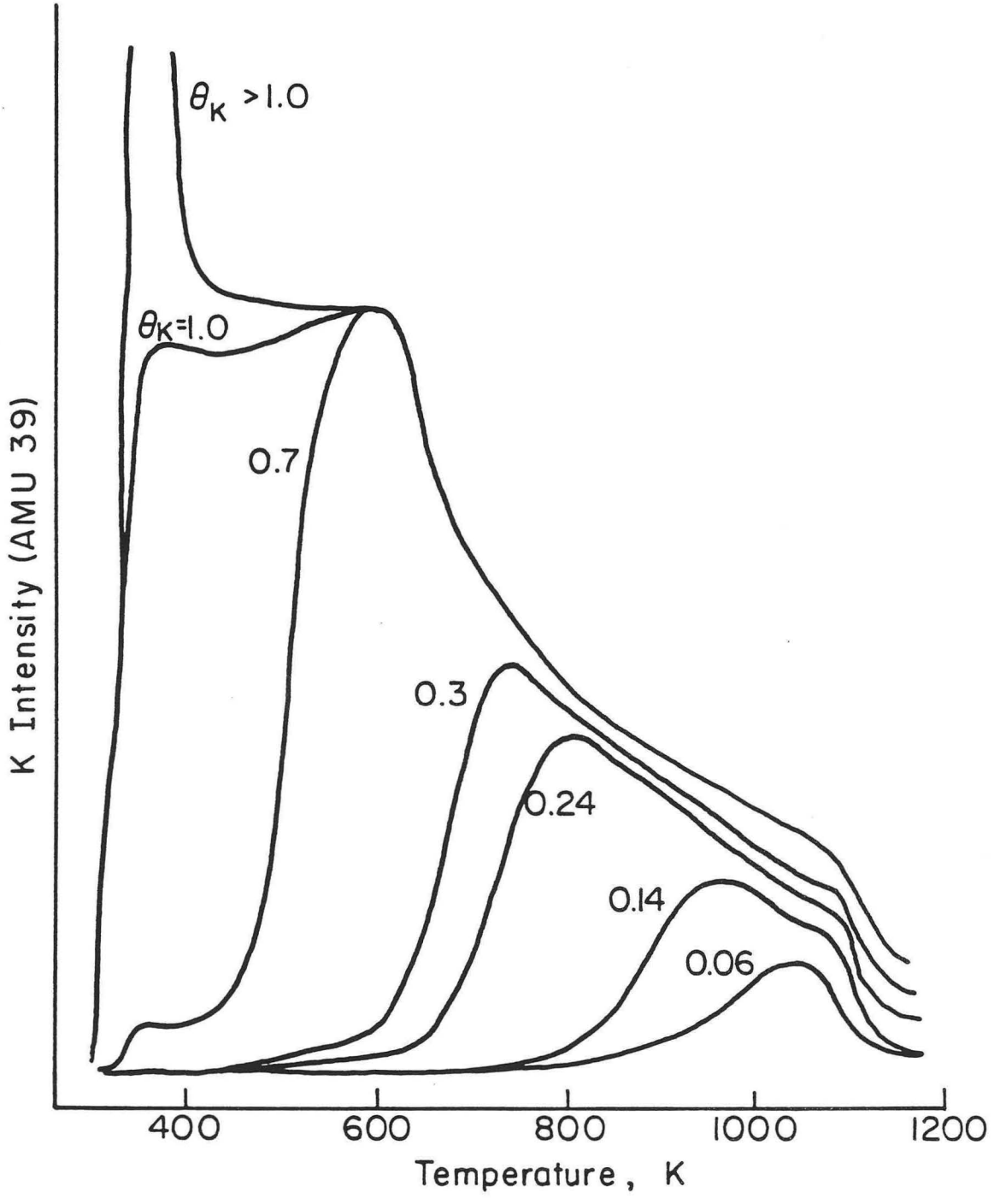

XBL 816-5909A

Figure 3.6 Potassium thermal desorption spectra from Pt(111) surface. Heating rate, 30 K/s. Coverages from peak area and Auger signal.

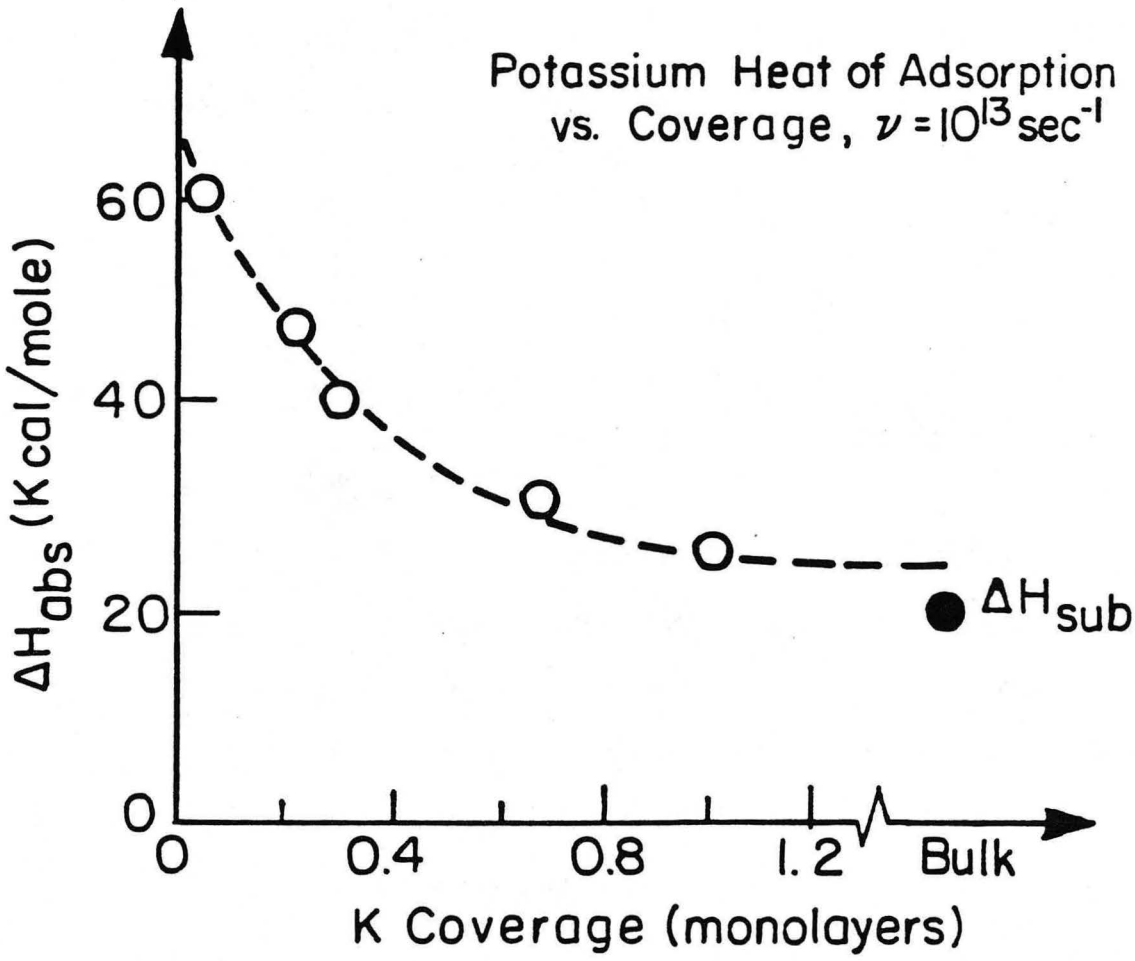

XBL816-5910B

Figure 3.7

of desorption of potassium on Ni(110) drops from 58 to 28 kcal/mole as the potassium coverage is increased from near zero to 0.5 monolayers. All of the models that were proposed to explain this behavior assumed that the decrease in heat of desorption was due to the depolarization of the surface dipoles at high coverages.

Another way to explain the binding energy shift is to consider an alkali atom adsorption potential with two terms:

$$\Delta H_{ads} \approx \Delta H_{sub} + P(\theta) \qquad \text{Eqn. 3.4}$$

Here ΔH_{sub} is the heat of sublimation of pure potassium (≈20 kcal/mole), while $P(\theta)$ is a coverage dependent term, related to the Topping formula (1927), that includes the ionic character of the adsorbed potassium. The surface dipoles would not affect one another at low coverages and $P(\theta)$ would assume a high value. At high coverages, the dipoles would have a significant depolarizing effect on one another, decreasing $P(\theta)$ and therefore ΔH_{ads} (see Figure 3.7).

3.2.2 Structure: LEED studies.

Another interesting feature of alkali adatoms is their spatial position on the surface of transition metals. At low coverages and temperatures the stable configuration for a surface alkali atom is a three or four fold site (Hutchins, 1976; Van Hove, 1976). This permits maximum coordination which is energetically favorable if the partially ionized alkali atom is to be well screened.

As the coverage increases, the alkali becomes slightly less ionized and more weakly bound. Its effective radius increases and the potential

variations along the substrate lattice become less noticeable. Due to the strong repulsive interactions between neighboring alkali atoms (still partially ionized), the alkali may leave its high coordination three and four fold site to maximize its distance from other atoms. This can be easily verified by LEED - see below, Fedorus (1970), or Gerlach (1969 and 1970).

In Figures 3.8a-d we show the progression of LEED patterns obtained from the pure potassium overlayers as the coverage is decreased (by thermal desorption). The pattern in Figure 3.8a was obtained after depositing a monolayer of potassium. For multilayer coverages the LEED patterns became more diffuse.

The inner spots of the LEED pattern of Fig. 3.8a are indicative of an incommensurate hexagonally close packed surface structure. Assuming one potassium atom per unit cell, the potassium overlayer is calculated to have a surface density of 5.4×10^{14} atoms cm^2, in agreement with results found on other surfaces (Lee, 1981). Others define the overlayer coverage as the atomic density of the adlayer divided by the substrate surface density; in our case, the coverage with respect to the surface density of the Pt(111) substrate would be 0.36.

From the LEED pattern we see that the overlayer structure has its axes aligned with the substrate but with an interatomic spacing of 4.6±0.1Å, 66% greater than that of the platinum interatomic distance (2.78Å), and slightly smaller than the known metallic potassium interatomic distance (4.70Å). The real space transformation matrix for this structure is $\begin{pmatrix} 1.66 & 0 \\ 0 & 1.66 \end{pmatrix}$.

As the coverage is decreased by desorption, orientational reor-

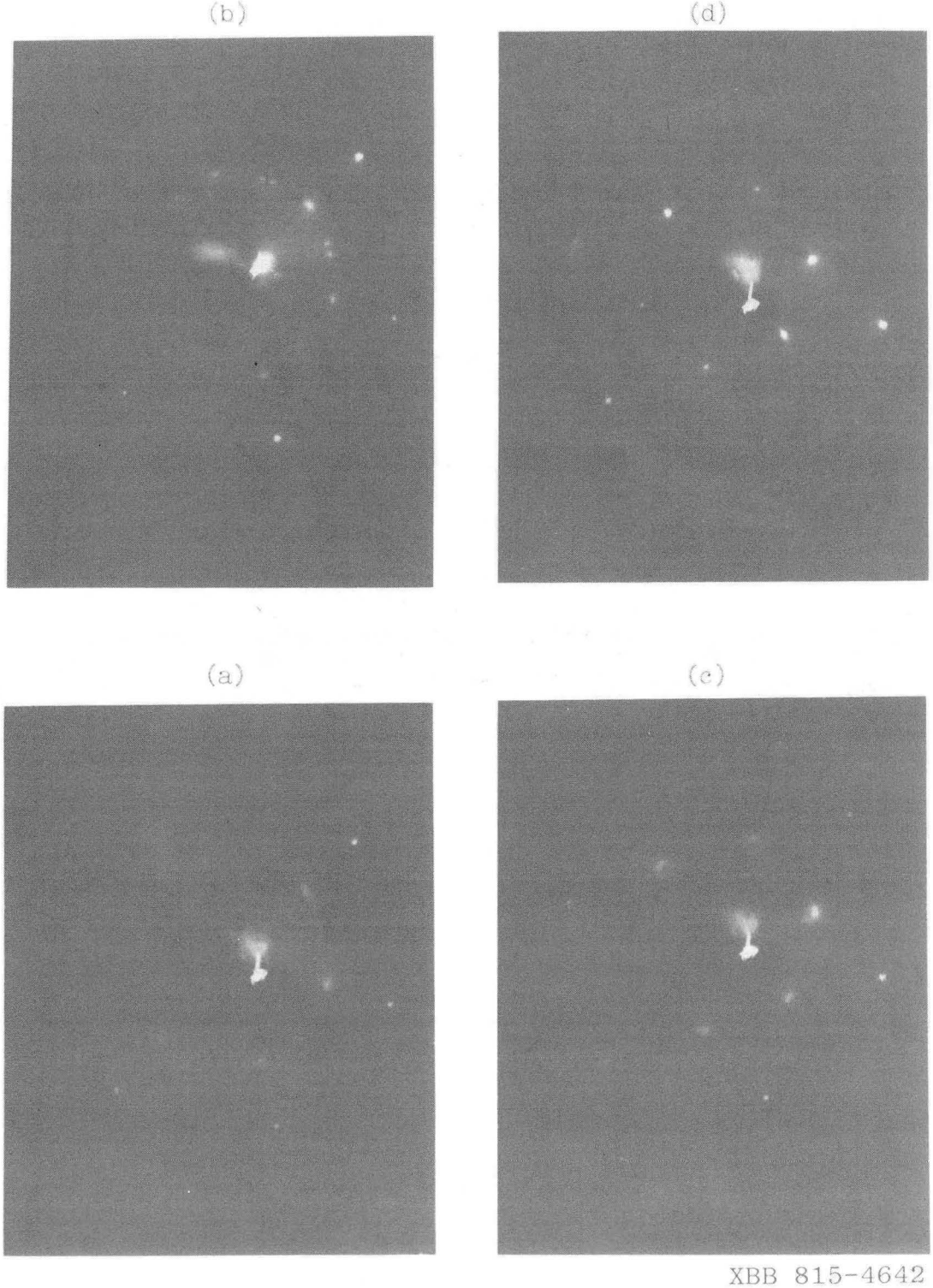

XBB 815-4642

Figure 3.8 Potassium overlayer LEED patterns on Pt(111). (a) is one monolayer, (d) represents a $(\sqrt{3}x\sqrt{3})$ R30° structure.

dering of the overlayer occured. At first, ring-like patterns appeared. Upon desorption, the ring transformed into well defined spot pairs, (Figure 3.8b and c) each pair being split about the (1/3, 1/3) spot position. After further desorption (by annealing the crystal to 400 K and cooling), the split pairs eventually coalesced into the (1/3, 1/3) spot positions, producing a $(\sqrt{3} \times \sqrt{3})R30°$ surface structure (Figure 3.8d), at $\theta_K = 0.9$. Lower coverages only resulted in the the loss of the $(\sqrt{3} \times \sqrt{3})R30°$ surface structure and in the appearance of higher background intensity. It should be noted that the ordering behavior of the potassium monolayer on Pt(111) is very similar both to weakly adsorbed noble gases on metal and graphite surfaces as predicted by Novaco and McTague (1977), and to the ordering behavior of halogen monolayers on metals (Bardi, 1980). In many of these studies, the adlayers were found to have hexagonal symmetry at a coverage of one monolayer, regardless of the substrate symmetry.

From the thermal desorption results which indicate a higher degree of polarization at low coverages, we would also expect lateral interactions to favor hexagonal ordering at less than monolayer coverages. We do not see any ordered structures at coverages less than $\theta_K = 0.9$, unless we use liquid nitrogen cooling. That these lower coverage, ordered structures were not seen with the crystal held above 250 K is probably due to a two dimensional liquid-like mobility of the potassium overlayer in this temperature and coverage region.

3.2.3 Electronic properties: UPS studies.

In ultraviolet photoelectron spectroscopy (UPS), valence electrons are emitted from atoms and molecules and are energy analyzed by an appropriate electron spectrometer. When studying solid surfaces, UPS can give information about the band structure of the substrate, the orbital energy levels of adsorbates, and the work function (see figure 3.9). The Einstein relation determines the energy of the emitted electrons:

$$h\nu = |E_b| + \phi + E_k \qquad (\text{where } E_b = E_{measured} - E_f) \qquad \text{Eqn. 3.5}$$

The work function (ϕ) is usually determined by subtracting the width (E_w) of the emission spectrum from the photon energy. The electrons emitted with the highest kinetic energy (E_k) come from the Fermi level (E_f), while the less energetic electrons are those emitted from states with a "higher" binding energy (E_b).

The d-band in transition metals is usually located within 8 eV of E_f. Emission below the d-band comes from either the broad s-p band, an adsorbate level, or emission from "secondary electrons" (those resulting from multiple scattering de-excitation processes). The secondary electron edge (SEE) is usually 2-3 eV wide and its position is determined by drawing a line tangent to the inflection point and noting where it intersects the baseline (see Figure 3.9).

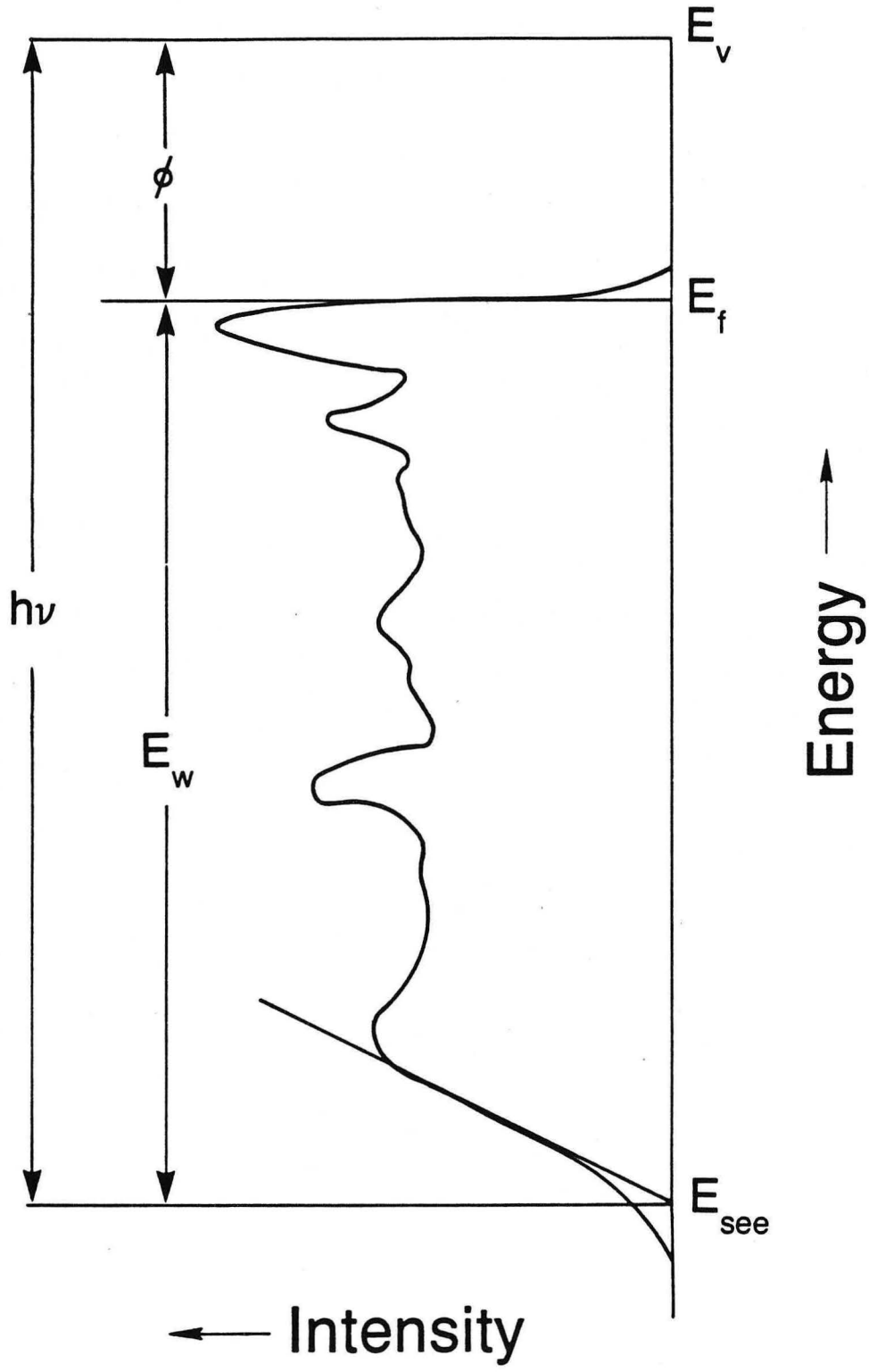

XBL 838-3087

Figure 3.9 Typical ultraviolet photoemission (UPS) spectrum using He(I) radiation, hν = 21.2 eV.

The experiments were performed in the photoemission chamber (see Chapter 2). In Figure 3.10 we show the UPS spectra obtained for potassium on Pt(111) as a function of potassium coverage. (These spectra are not drawn to scale; the secondary electron yield becomes very large at high potassium coverage.) Several features should be noted. First, there is a sharp drop in electron emission at E_f. This drop is observed for most adsorbates on Pt(111), as well as on other metals, and is attributed to an interaction between the surface d-band and the adsorbate. Two other features observed upon alkali adsorption are an increase in the total secondary electron yield and an increase in the width ($E_f - E_{SEE}$) of the spectrum. This is expected since a drop in the work function should permit more secondary electrons to be emitted, since the barrier they must pass through is lowered. Figure 3.11 shows the work function vs. potassium AES signal (coverage). The curve did not bend back up in this case (Figure 3.2) since only low coverage data was obtained.

A fourth observation is the appearance of a peak at about 19 eV, see Figure 3.10. The peak shifts as it should with a change in sample bias, confirming that it comes from the sample, not from the spectrometer or elsewhere. This peak can be attributed to the K(3p) level, as noted in He(II) studies (Broden, 1979; Pirug, 1982). What is interesting is not that it exists, but rather that it appears before the SEE reaches it. Figure 3.12 shows that it does not appear for very low potassium coverages, but only after a threshold coverage is reached. The peak moves closer to the Fermi level with increasing coverage. This shift in position can be explained by an increase in final state screening,

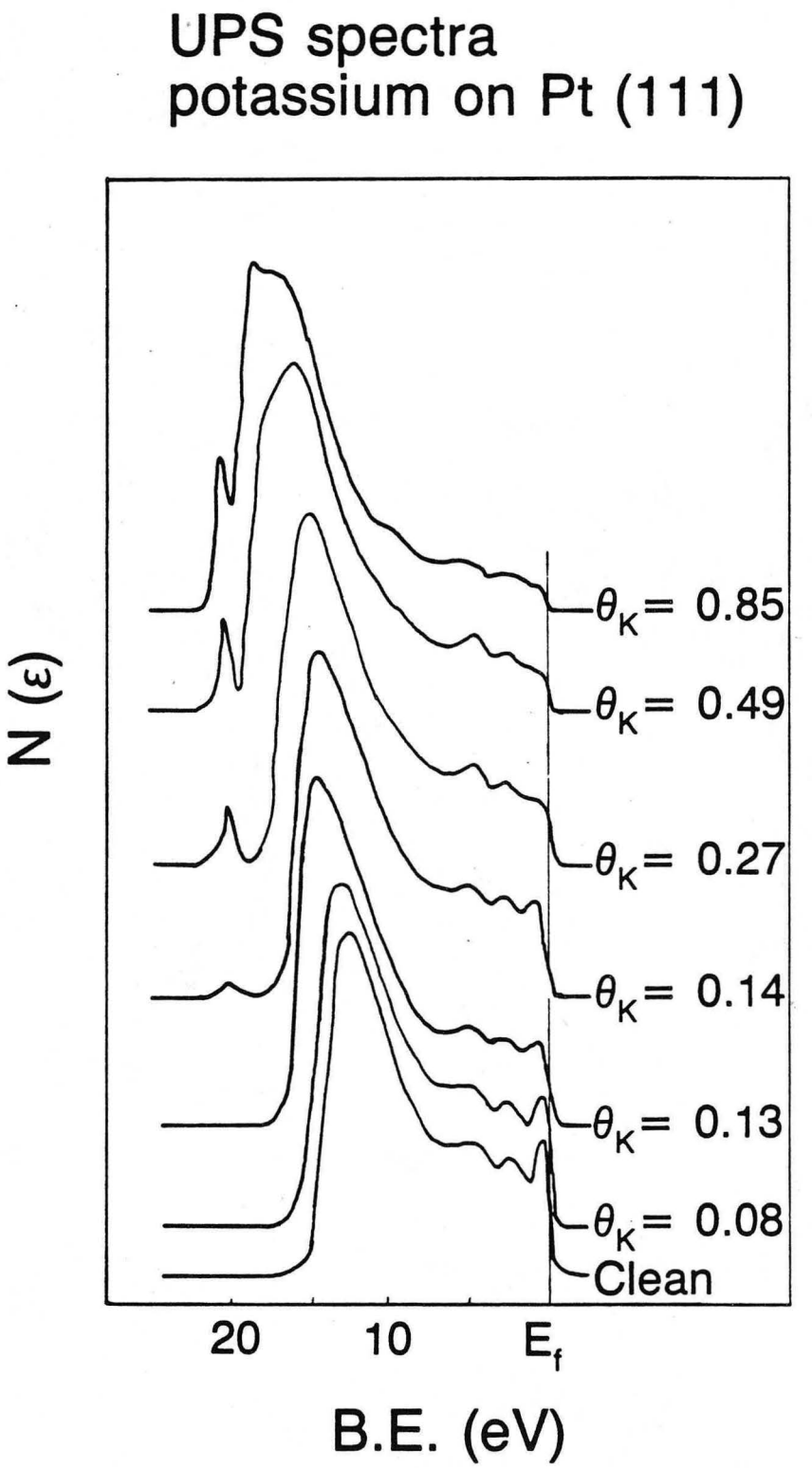

XBL 838-3078

Figure 3.10 UPS spectra for potassium on Pt(111). The different spectra are not drawn to scale.

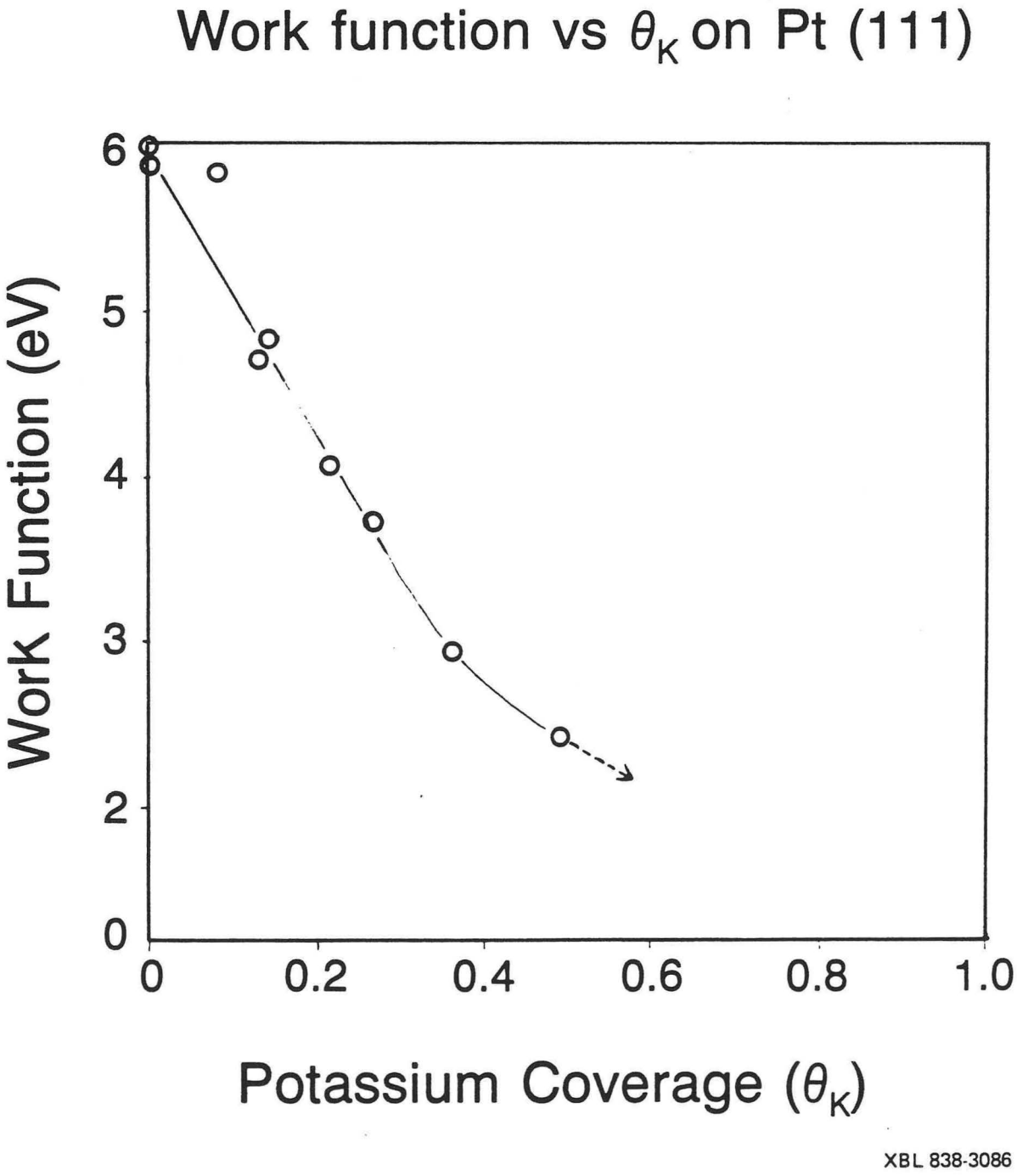
Work function vs θ_K on Pt (111)
Work Function (eV)
6
5
4
3
2
0
0
0.2
0.4
0.6
0.8
1.0
Potassium Coverage (θ_K)
XBL 838-3086

Figure 3.11

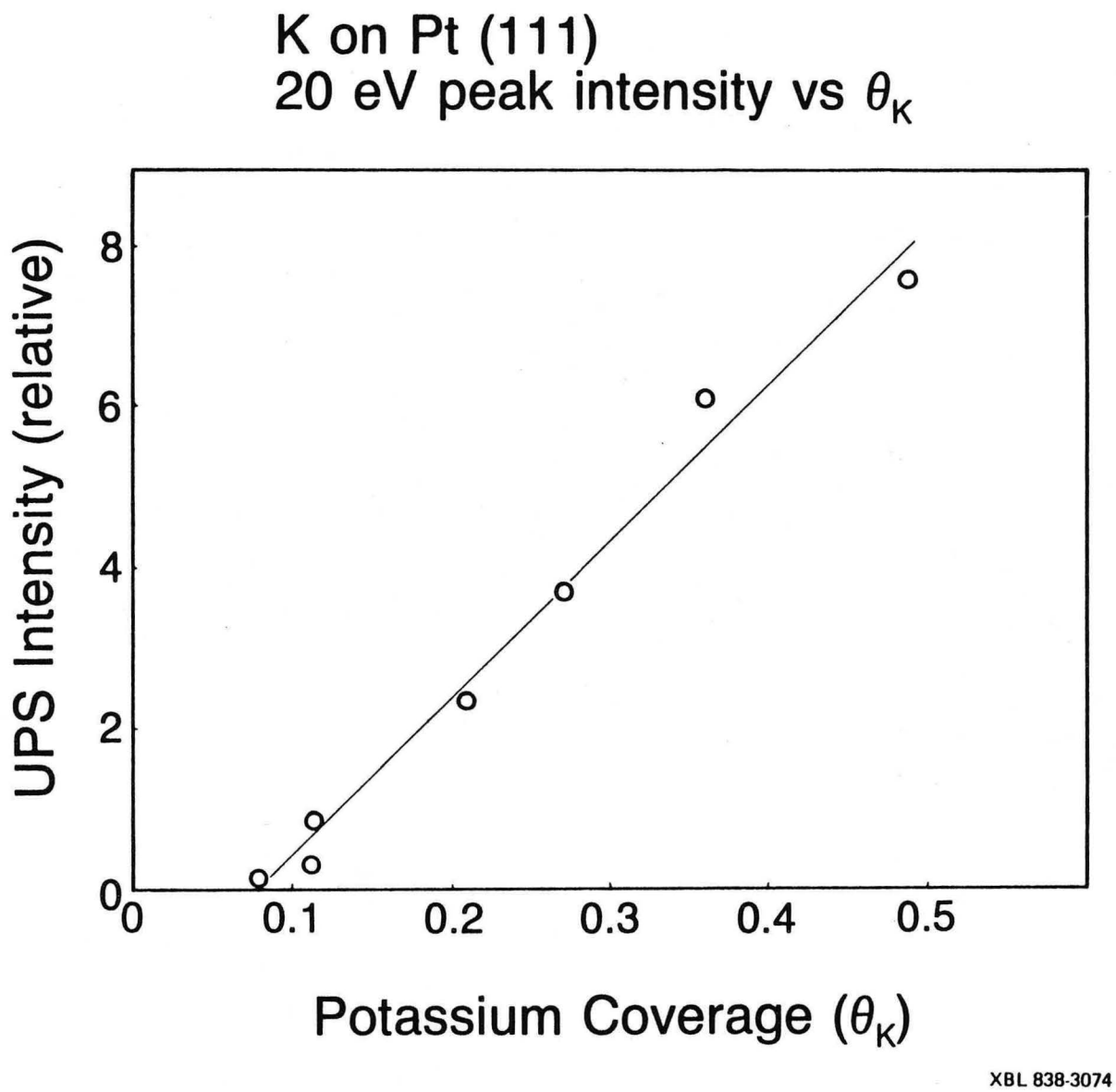
K on Pt (111)
20 eV peak intensity vs θ_K
UPS Intensity (relative)
0
2
4
6
8
0
0.1
0.2
0.3
0.4
0.5
Potassium Coverage (θ_K)
XBL 838-3074

Figure 3.12

The peak has also been observed by Pirug et al (1982). Their explanation is that it results from the He(I) transition at $h\nu$ = 23.1 eV. This argument, however, is not correct since a higher energy photon will shift the spectrum to higher kinetic energy. A new Fermi edge would appear at 1.9eV higher kinetic energy, but the SEE should remain constant. Another possible transition is the He* metastable transition, as used in the metastable quenching experiment. But this, like other rationales which attribute the peak to a different excitation energy, should result in a shifted Fermi edge, not a lower SEE.

Several other possible explanations can be offered to account for this observation. First, since O_2, H_2O, and CO_2 impurities readily react with the overlayer, we considered that small potassium oxide islands could be formed. Such an island would probably have a low local work function, and the UPS spectra would show a superposition of the two spectra. This argument can be discounted because the feature is a real peak, not a second SEE which would result if there were two regions of differing work function.

Another explanation is that the electron emission from a potassium atom on the surface is actually easier than emission from the bulk because of atomic-scale electrostatic potential differences. As noted above, a surface additive does not change the bulk chemical potential term of the work function, but it does modify the surface dipole component. The dipole layer for a metal exists within a few angstroms of the surface. In our case the position of the adsorbate (potassium) within the dipole layer might be determining the extent to which its core electrons see the "full" work

function upon ionization, see Figures 3.13 and 3.14. In other words, an electron coming from the bulk would experience a different field than an electron emitted from a localized potassium core orbital which is positioned half way through the dipole layer. Several problems remain with this interpretation. Why would the K(3p) electron see a smaller dipole field than other valence electrons on potassium? Why wouldn't all electrons be emitted through the potassium if it is the path of least resistance? We can rationalize these problems by noting that the potassium 4s valence electrons are polarized towards and delocalized throughout the metal, unlike the K(3p) electron. So, to be emitted as secondaries, the K(4s) electrons may feel the full barrier as represented in Figure 3.13. This picture is in disagreement with the conventional picture of potential barriers at the surface.

We also coadsorbed CO and potassium on Pt(111), see section 4.2.4. CO caused the work function to increase and the K(3p) signal intensity to decrease, see Figure 3.15a, although there was no change in potassium coverage. The same observation was made when benzene was coadsorbed instead of CO, see Figure 3.15b. This implies that some electronic property, not just the potassium coverage, is determining the intensity of K(3p) emission. The potassium atoms can work collectively to bring down the local electrostatic potential around each potassium atom. A threshold effect could explain why no K(3p) emission was seen at low coverage.

A third possible interpretation is that the photoelectron ionization cross-section changes with a change in work function. Here, the K(3p) peak position would be on the SEE tail, but because of some

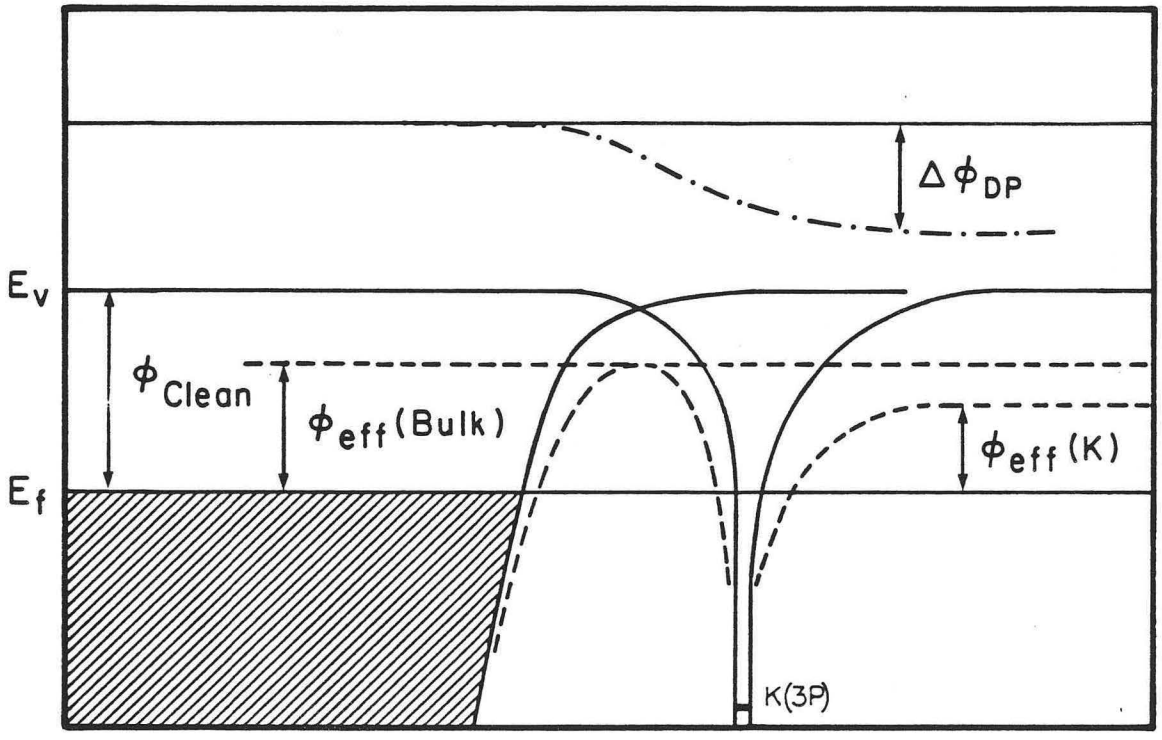

—— unperturbed potential energy of metal and potassium atom

-·-·- perturbation dipole field created by partial ionization of potassium at the surface

--- final potential energy diagram

XBL 838-11076

Figure 3.13 The local electrostatic potential at a surface. Note the difference in the "effective work function" for the substrate and potassium atom.

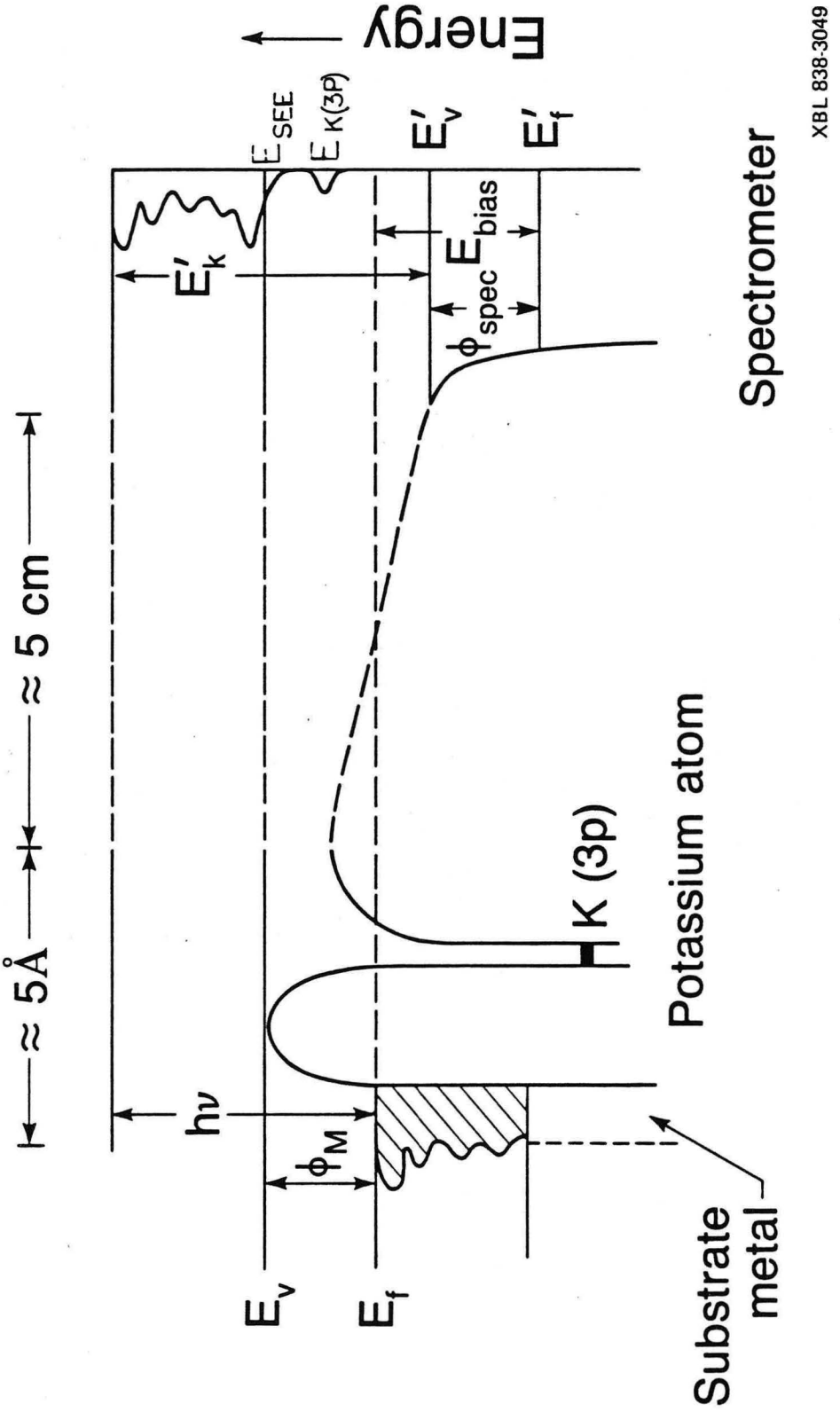

Figure 3.14 Potential energy diagram for sample and spectrometer with bias, showing anomalous K(3p) peak.

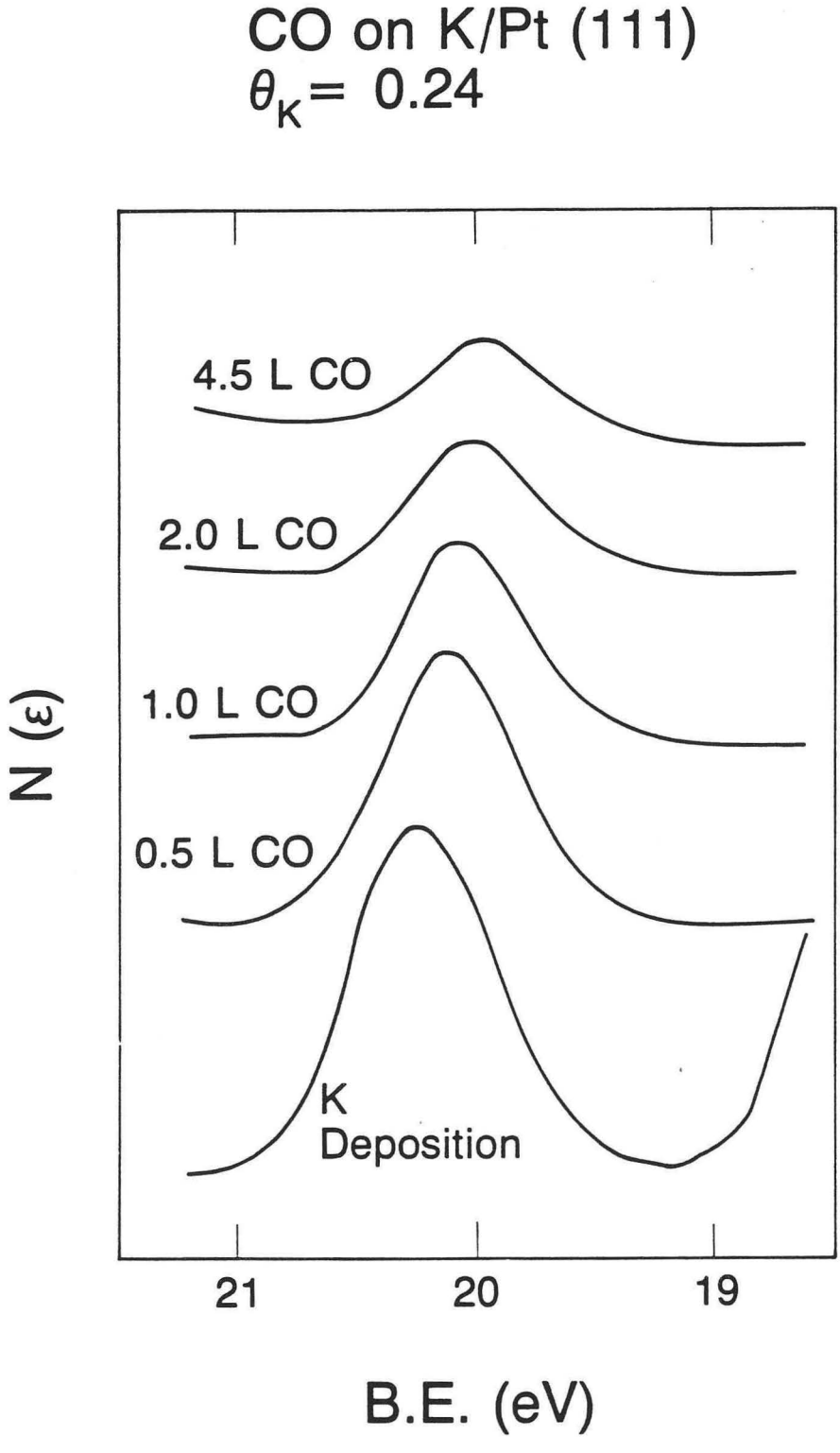

XBL 838-3088

Figure 3.15a K(3p) peak on CO covered surfaces.

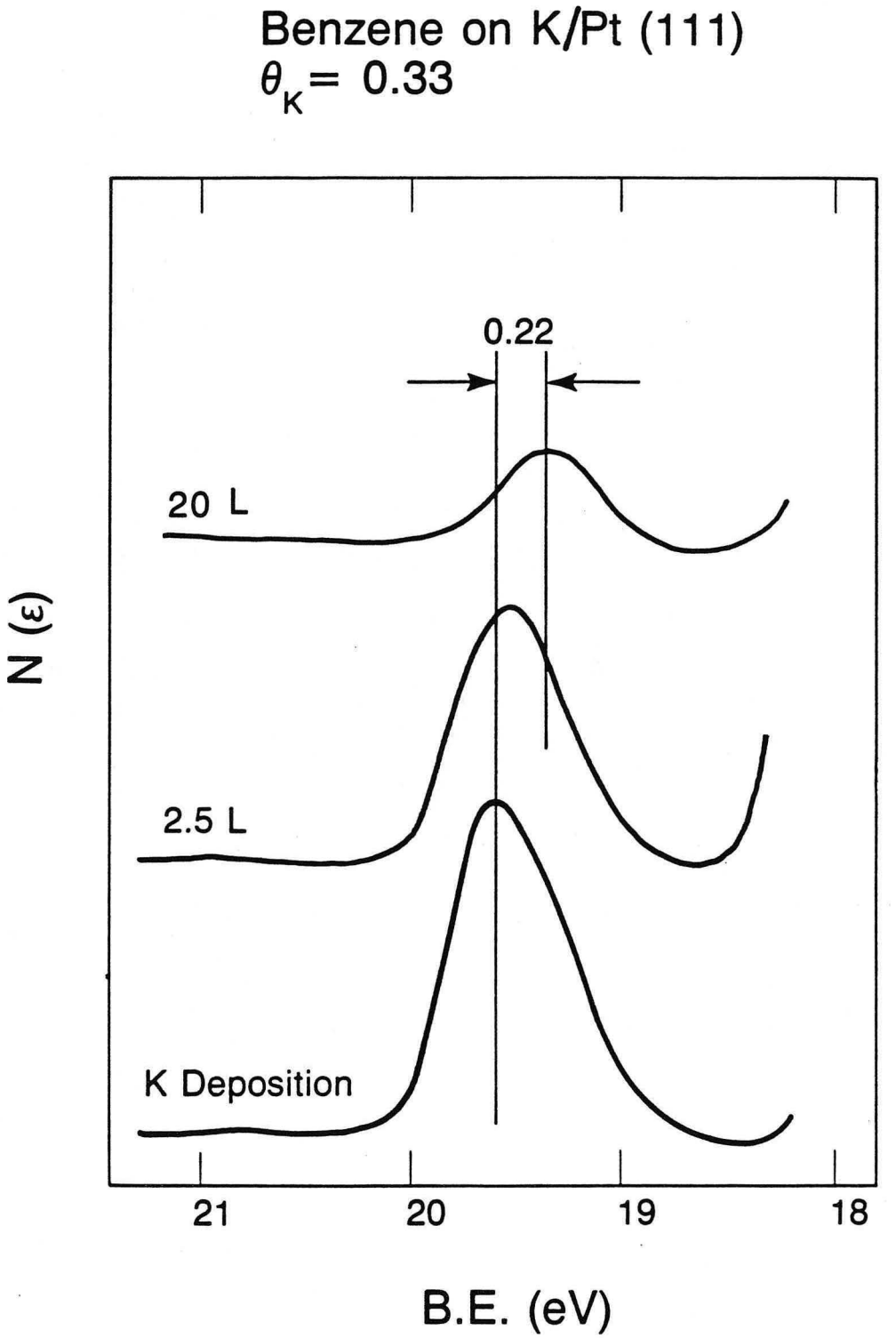

XBL 838-3080

Figure 3.15b K(3p) peak on benzene covered Pt(111).

resonance phenomenon, its cross-section is much higher than that for secondary electron emission. It would thus appear as a peak beyond the SEE, while in fact, it is only a resonance on the tail. (In the previous - second - explanation, the photoelectron cross-section was constant, but the photoelectrons once produced, were more easily emitted from the surface as the work function dropped.) This third interpretation is unlikely as the peak height should change much more sharply with decreasing work function, instead of being a linear function of potassium coverage as in Figure 3.12.

Other workers have also noted interesting local work function properties. In the photoemission of adsorbed xenon (PAX) experiment, performed by Wandelt et. al. (1981), xenon is adsorbed and the position of the Xe(5p) electron level is measured by UPS. Changes in peak position between metals and different crystallographic faces of the same metal are noted and are correlated with the work function of the surface under study. They also note that cooled xenon overlayers preferentially occupy step and kink sites and can thus determine local electronic (work function) properties of these defects, as well as adsorbates. This experiment demonstrates nicely that charge is not completely smoothed out along a real surface, but exhibits local inhomogeneities.

From this perspective, it becomes reasonable to consider that an electron localized on potassium above the surface is more easily ionized than a bulk electron of the same binding energy supporting our second interpretation. Whatever the reason, the observation of this peak below the secondary electron edge does imply that more serious attention

should be given to studying the local electronic properties of surfaces.

Several problems still remain in our understanding of alkali-surface interactions. Although much is known, the exact nature of the charge transfer remains to be fully resolved. In particular, should it be described as an ionization or polarization and what are the localized and delocalized screening properties? The problem of understanding which substrate orbitals interact with the adatoms, and what kind of rehybridization they undergo, is very important for a complete analysis of alkali monolayers.

3.3 Alkali oxides: K_2O on Pt(111).

3.3.1 Thermodynamics: TDS studies.

Metallic potassium on the Pt(111) surface readily promotes the adsorption of O_2. This is in sharp contrast to the low (defect-sensitive) sticking coefficient of O_2 on clean Pt(111), estimated to be in the range of 10^{-2} to 10^{-6} (Monroe, 1980; Weinberg, 1972). The potassium oxide overlayer thermal desorption spectra are given in Figures 3.16 and 3.17. Potassium (mass 39) desorption, is recorded in Figure 3.16 and oxygen (mass 32) desorption in Figure 3.17. The two thermal desorption spectra overlap, indicating simultaneous desorption of potassium and oxygen. While no noticeable desorption of potassium-oxygen cluster could be detected by the mass spectrometer, it is known that K_2O can exist as a vapor species (Drowart, 1964). We must therefore consider the possibility that any potassium oxide cluster that may desorb is broken apart by the mass spectrometer ionizer. Our results, however, only give evidence for the simultaneous detection of K^+ and O_2^+. We cannot say with certainty whether the dissociation

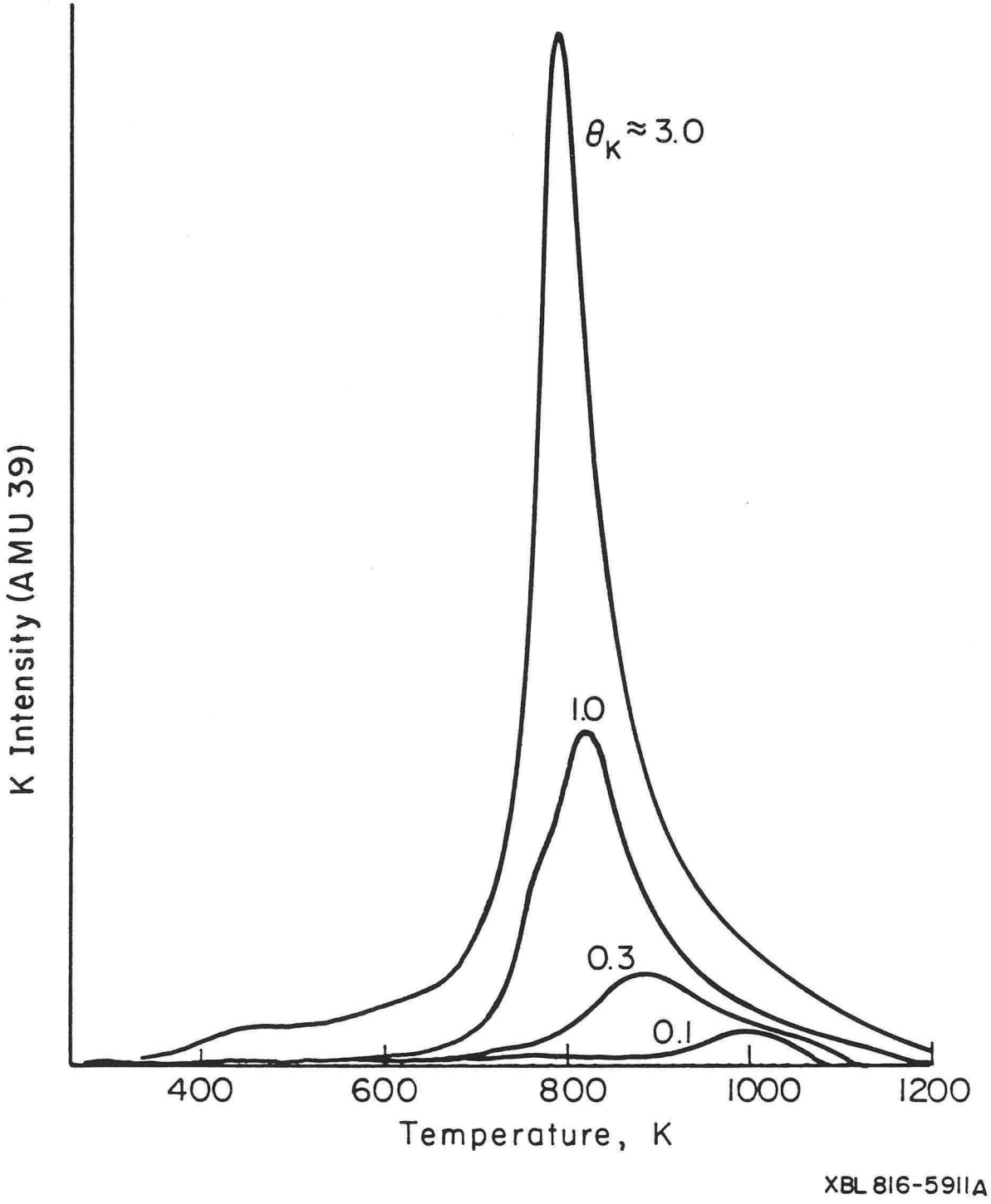

Figure 3.16 Potassium thermal desorption from a "potassium oxide" monolayer on Pt(111).

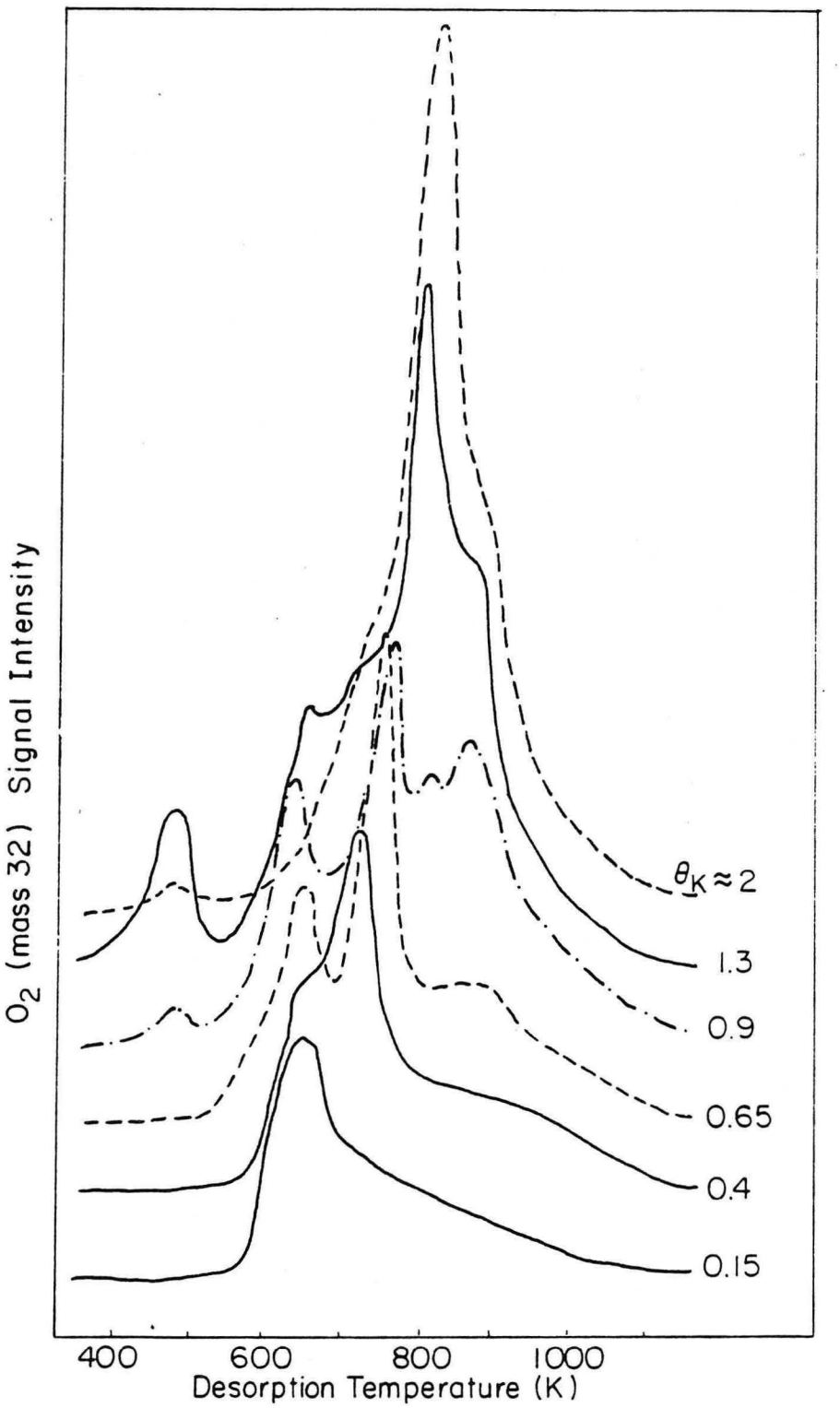

XBL818-6285

Figure 3.17 Oxygen thermal desorption from "potassium oxide" overlayer. 10 Langmuir exposures.

occurs at the surface or in the ionizer.

The potassium (mass 39) thermal desorption spectrum in Figure 3.16 indicates a slight decrease in heat of desorption as the coverage is increased. Again, assuming first order desorption kinetics, the change in desorption temperature corresponds to a heat of desorption shift from 60 to 50 kcal/mole as coverage is increased from 0.1 to 3 layers. This is much less than the 40 kcal/mole shift seen for pure potassium. Here, the potassium coverages are reported in units of overlayer coverage (θ_{KO}), where the K(252 eV)/ Pt(64 eV) Auger monolayer ratio is 1.9, compared to 1.1 for potassium adsorption alone. This means that more potassium fits into a "potassium oxide" monolayer than in a pure potassium monolayer. The desorption temperature for the multilayer remains at about 810 K. We see by comparing the potassium desorption spectra for the pure potassium and potassium oxide overlayers, that for potassium coverages in excess of 0.2 monolayers, the oxygen thermally stabilizes the overlayer. This factor may be of significance under actual catalytic conditions. (Full oxidation of the potassium however, decreases its ability to act as an electronic promoter; see section 4.2.3 below.)

The oxygen thermal desorption spectra are shown in Figure 3.17. After predepositing various amounts of potassium on the Pt(111) crystal face, we exposed the surface to 10 L of O_2. The first major peak to develop in the thermal desorption spectrum appeared at 660 K. This peak had a long tail and retained its position, shape, and intensity, up to potassium coverages in excess of one monolayer. The peak disappeared at these high coverages. As we increased the potassium coverage above

θ_{KO} = 0.2, a second oxygen peak appeared at 730 K, and then moved up to 770 K as the potassium coverage was increased to a monolayer. At higher coverages this peak also disappeared. A third peak then developed at 900 K appearing at coverages of $\theta_{KO}>0.5$. It retained its position and size, even in the multilayer. And lastly, a fourth peak appeared at 820 K, at the completion of the first monolayer. This was found to be the dominant peak in the multilayer. We also note that at potassium coverages between 0.5 and 1.0 monolayer, a low energy peak appeared at 500 K. This might be due to chemisorption of molecular oxygen.

At present we only wish to note that several forms of oxygen are present on the surface, and that some of the oxygen desorbs simultaneously with the potassium although not necessarily as a potassium oxide cluster.

3.3.2 Structure: LEED studies.

Four stable and reproducible ordered potassium oxide surface structures were seen by LEED at specific potassium and oxygen coverages. These structures included three which were commensurate, (4×4), (8×2), and (10×2) overlayer structures (Figures 3.18 and 3.19a) and an incommensurate one (Figure 3.19a). The (4×4) surface structure (Figure 3.18b) was generated by exposing a cooled Pt(111) crystal with $\theta_K \geq 1.5$ to 10 L of O_2, and annealing the crystal at 650-680K for several seconds. This, in effect, desorbed the oxygen associated with the 650 K peak in the TDS spectrum of Figure 3.17. The pattern was observed over a range of coverages for which K(252 eV)/Pt(64 eV) Auger peak ratios of between 1.5 and 2.5 were found. The K(252 eV)/ O(510 eV) peak height ratio was 5 ± 0.2 for the (4×4) surface structure, for both relatively high and low total coverages. The fact that the

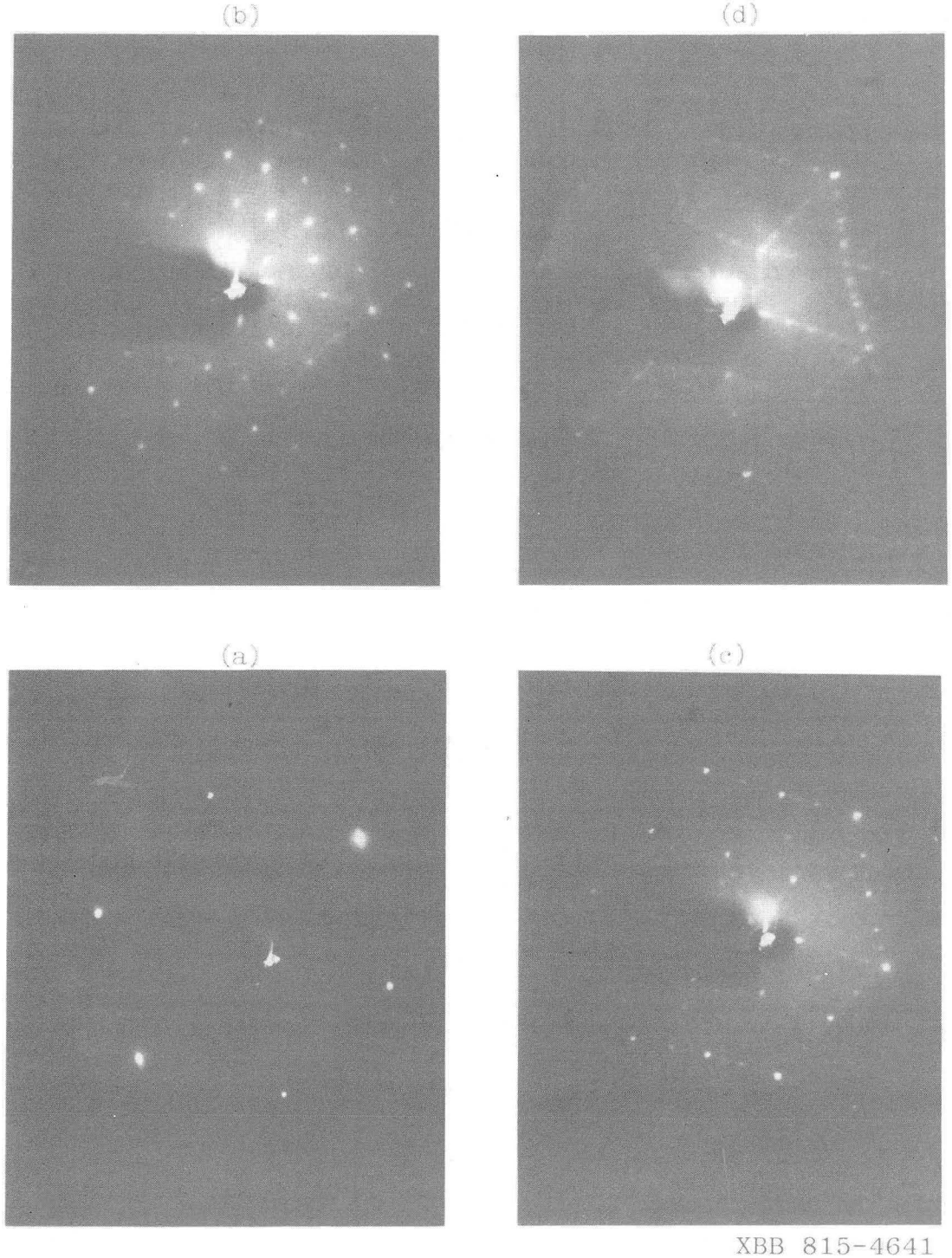

XBB 815-4641

Figure 3.18 LEED patterns of various "potassium oxide" overlayers.

(a)

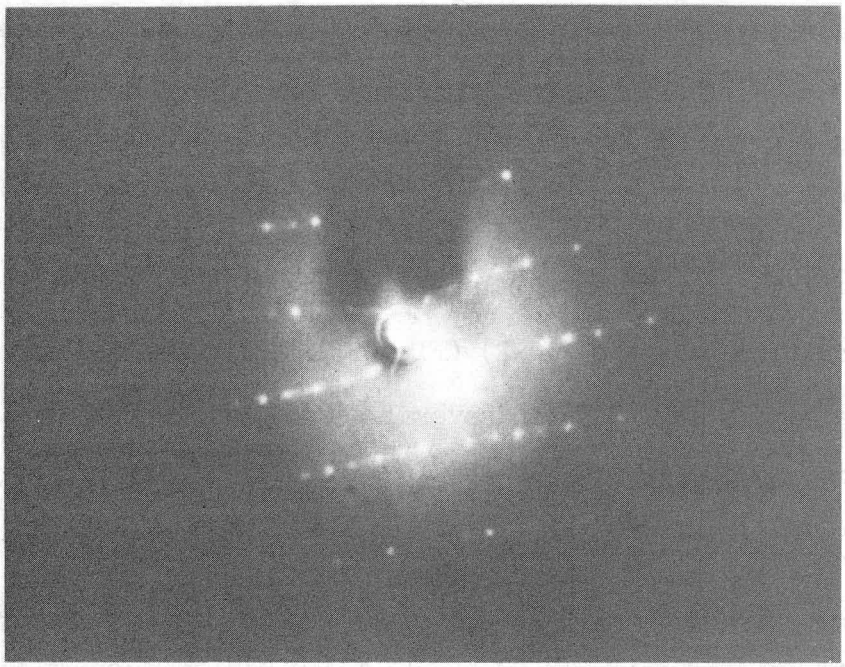

(b)

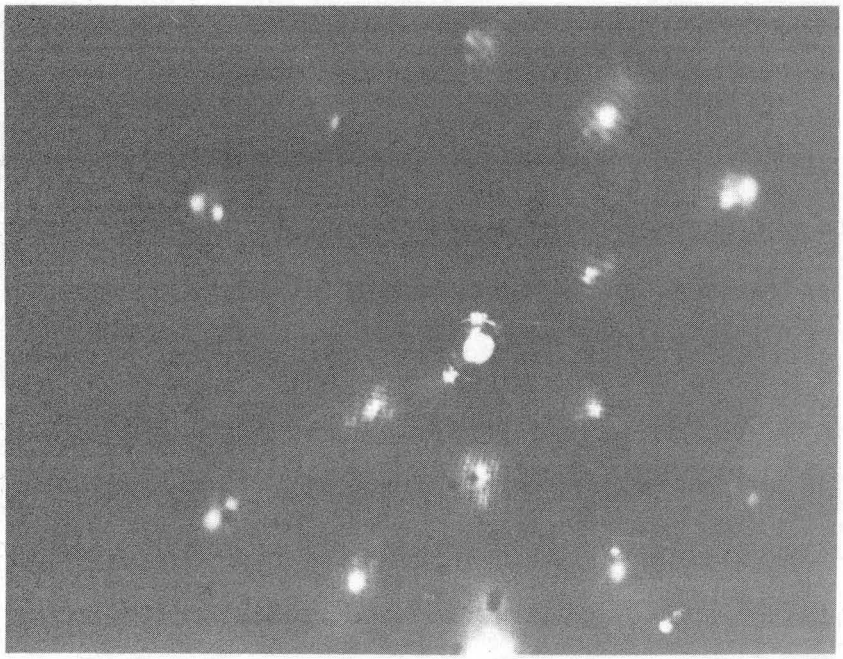

XBB 818-7675A

Figure 3.19 (a) the (10x2) overlayer pattern in one domain. (b) the incommensurate overlayer.

same LEED pattern was observed over a range of "potassium oxide" total coverages, yet where the potassium to oxygen stoichiometry stayed constant, is indicative of ordered domains on the surface at less than monolayer coverages.

After annealing to 700 K and cooling to room temperature, an (8×2) overlayer structure developed (Figure 3.18c). One of the most stable structures was the (10×2) (Figure 3.18d) generated by annealing the sample at 750 K for several seconds. This pattern was visible with K(252 eV)/Pt(64 eV) Auger peak ratios of 1.25-1.6 and with a K(252 eV)/O(510 eV) peak ratio of 7.3±0.3. As Figure 3.19a shows, the (10×2) surface structure could be induced to form one domain. This was accomplished by ion bombarding the surface at a slight angle (about 5°) away from the surface normal during the cleaning stages. The single domain pattern was then readily analyzed to yield the (10×2) surface structure.

The pattern in Figure 3.19b was also generated by heating the crystal to 750 K, but appeared to have slightly less oxygen incorporated into the surface oxide than the (10×2) structure. The K(252 eV)/O(510 eV) Auger peak ratio was found to be 7.7±0.3. Upon close examination of the LEED pattern in Figure 3.19b, one sees that the most intense of the inner spots is not located in the exact half order spot locations, which would imply a (2×2) surface structure. Instead they are shifted slightly outward indicating an incommensurate overlayer. This deviation from the half order spot position (and hence the deviation from a (2×2) overlayer structure) is readily calculated from the positions of the double diffraction spots. The extra spots yield a

hexagonal overlayer unit cell lattice constant of 4.71Å, a 15% contraction from a (2×2) structure.

A likely stoichiometry that could account for this structure is K_2O, in which each oxygen is hexagonally surrounded by 6 coplanar potassium atoms and each potassium by 3 oxygen and 3 potassium atoms. Using the average ionic crystal radii for K^+ (1.33Å) and O^{-2} (1.4Å) the K_2O unit cell lattice parameter should be 4.69Å, very close to the value derived from the LEED pattern. To confirm this model, a more exact LEED intensity analysis will have to be made of the overlayer, and combined with the HREELS and photoelectron spectroscopy results. Triple layer models have been proposed (Broden, 1980; Pirug, 1982) for alkali oxide overlayers, and cannot be excluded.

3.3.3 Electronic properties.

Other changes occur, such as in the work function of the metal, but these depend on the exact stoichiometry of the surface. The work function is sometimes lowered below the alkali value if oxygen is adsorbed before the alkali (or if the coadsorbed layer is annealed): one interpretation for this is that a triple layer develops with alkali on the outside, oxygen in the middle, and then bulk metal on the inside. However, if alkali is adsorbed first, the work function can be observed to increase upon O_2 adsorption (Papageorgopoulos, 1975). The low work function and relatively high stability of alkali oxides is exploited in the design of thermionic and photoelectron devices (Mayer, 1940).

In catalysis, it is still unclear to what degree the alkali is oxidized during a catalytic reaction. Several studies have been made

using various probes including scanning Auger and electron microscopy (Chen, 1973; Ertl, 1983; Hanji, 1981). Some of these have shown that potassium is oxidized on iron catalysts used for the ammonia synthesis. They also showed that most of the potassium oxide resides on the support but that a certain fraction does envelop the active iron grains. In other studies of potassium monolayers on nickel methanation catalysts, it was shown that the potassium was not oxidized during the reaction, but "solvated" by water molecules on the surface (Campbell, 1982). All of these studies, however, were on samples analyzed in vacuum following a reaction and were not actual studies of the alkali made while it was at high pressure.

3.4 Alkali adsorption on stepped surfaces.

We have also carried out the experiments described above on the stepped Pt(755) [or 6(111)×(100)] surface and found only a few minor differences. The thermal desorption spectra of both potassium and potassium oxide were very similar to that of the flat Pt(111) surface. The LEED patterns of pure potassium monolayers were not visible, but single domain patterns of (4×2), (8×2), and (10×2) potassium oxide structures were all seen. Potassium was also found to be distributed evenly among step and terrace sites when titrated with CO (section 4.1.2).

CHAPTER 4. COADSORPTION STUDIES: ALKALIS AND SMALL MOLECULES ON METAL SURFACES

Contents: page

4.1 CO adsorption on potassium-dosed Pt(111) 72

4.1.1 CO bonding to metals 72

4.1.2 TDS studies 78

4.1.3 HREELS studies 86

4.1.4 UPS studies 91

4.1.5 Discussion 98

4.2 Benzene adsorption on potassium-dosed Pt(111) 108

4.2.1 TDS studies 108

4.2.2 UPS studies 113

4.2.3 Discussion 119

4.3 NO adsorption on potassium-dosed Pt(111) 124

4.3.1 TDS studies 124

4.3.2 Discussion 125

4.4 PF_3, CH_3CN, and C_4H_8 adsorption studies 139

4.4.1 TDS studies 139

4.4.2 Discussion 142

4.5 Literature Review of alkali coadsorption studies 147

4.6 Conclusion 155

Very simple UHV experiments, such as thermal desorption spectroscopy, can greatly increase our knowledge of alkali additive effects in heterogeneous catalysis. In addition to our own work, several other authors have recently published papers about the effects of alkali metal monolayers on various molecular and atomic coadsorbates. A variety of techniques have been used including TDS, UPS, XPS, HREELS, work function measurements, and surface penning ionization electron spectroscopy (SPIES). In this chapter, we will first discuss our results for the CO + alkali coadsorbate system in detail, then review the main features of the studies that we have performed on other alkali - molecular coadsorbate systems (NO, benzene, etc.), and end by reviewing the literature on related systems.

4.1 Carbon monoxide adsorption on potassium-dosed Pt(111).

4.1.1 CO bonding to metals.

Blyholder (1964) suggested that the bonding of CO to a metal involved not only a 5σ CO orbital overlapping with metal s and p orbitals, but also d-orbitals from the metal backbonding into the 2π CO orbital. This type of bonding is shown in Figure 4.1a. This model of metal-carbonyl complexing has come under some criticism, but there is now reasonable agreement concerning its general validity. There does, however, appear to be some disagreement about which metal orbitals play the most important role both in the acceptor and donor functions. For instance, some theorists have used the d-orbitals of the metal as acceptors for the 5σ donation, instead of the metal s and p orbitals suggested by others. Moreover, a recent molecular orbital calculation of CO on a lithium cluster has shown significant backdonation from the

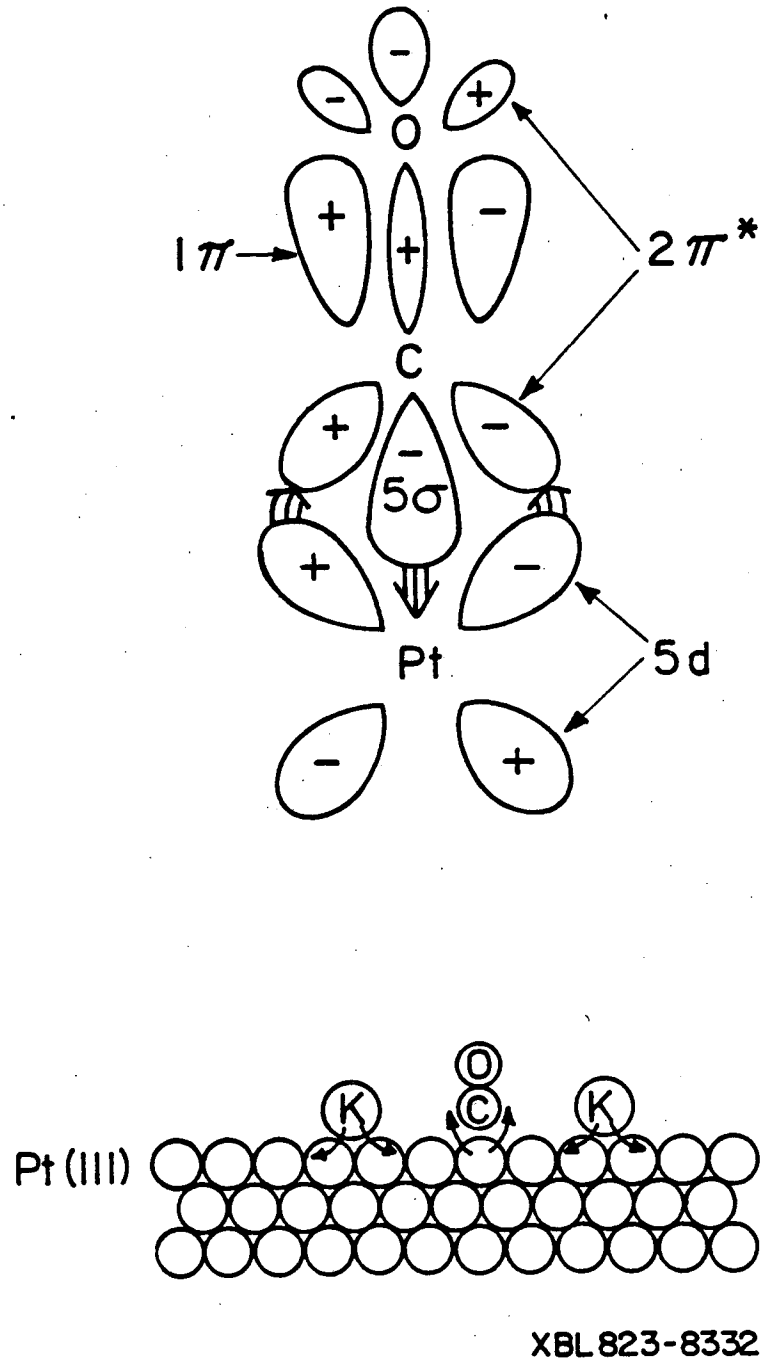

Figure 4.1 (a) important orbitals involved in CO bonding to a metal. (b) diagram of electron flow in coadsorbed K + CO system.

Li 2s and 2p levels into the 2π CO orbital, i.e. no metal d-orbitals were required for backdonation (Post, 1981). It is becoming clearer that more rigorous ab initio calculations are needed because significant rehybridization is taking place, and that approximate treatments have only limited applicability. For most metal-CO systems, the electron orbital levels can be represented as in Figure 4.2.

The adsorption of CO on Pt(111) has been extensively studied; (Steininger, 1982; Campbell, 1981; Crossley, 1980; Winicur, 1981; Norton, 1979; Baro, 1979; Froitzheim, 1977; Ertl, 1977). Figures 4.3 and 4.4 show our TDS and HREELS spectra for several CO coverages on Pt(111). These spectra agree well with other studies. The thermal desorption spectra show there is one desorption peak whose maximum shifts to lower temperature and broadens with increasing coverage. Assuming the recently derived preexponential factor of 10^{13} s^{-1}, for CO adsorption on the flat Pt(111) surface (Winicur, 1981), the heat of adsorption decreases with coverage from its low coverage value of 32 kcal/mole to 27 kcal/mole at saturation. It is now generally agreed that CO bonds with the carbon end toward the surface. The vibrational spectra show that CO adsorbs molecularly on the platinum surface in both linear (2100 cm^{-1}) and bridge-bonded (1870 cm^{-1}) configurations. The corresponding Pt-C stretches occur at 475 cm^{-1} and 355 cm^{-1} respectively. Furthermore, CO is only linearly bonded at low coverages, while with increasing coverage the bridged position becomes partially occupied. Finally, the vibrational frequency of the linearly bonded species increases by 30-40 cm^{-1} as the CO coverage increases.

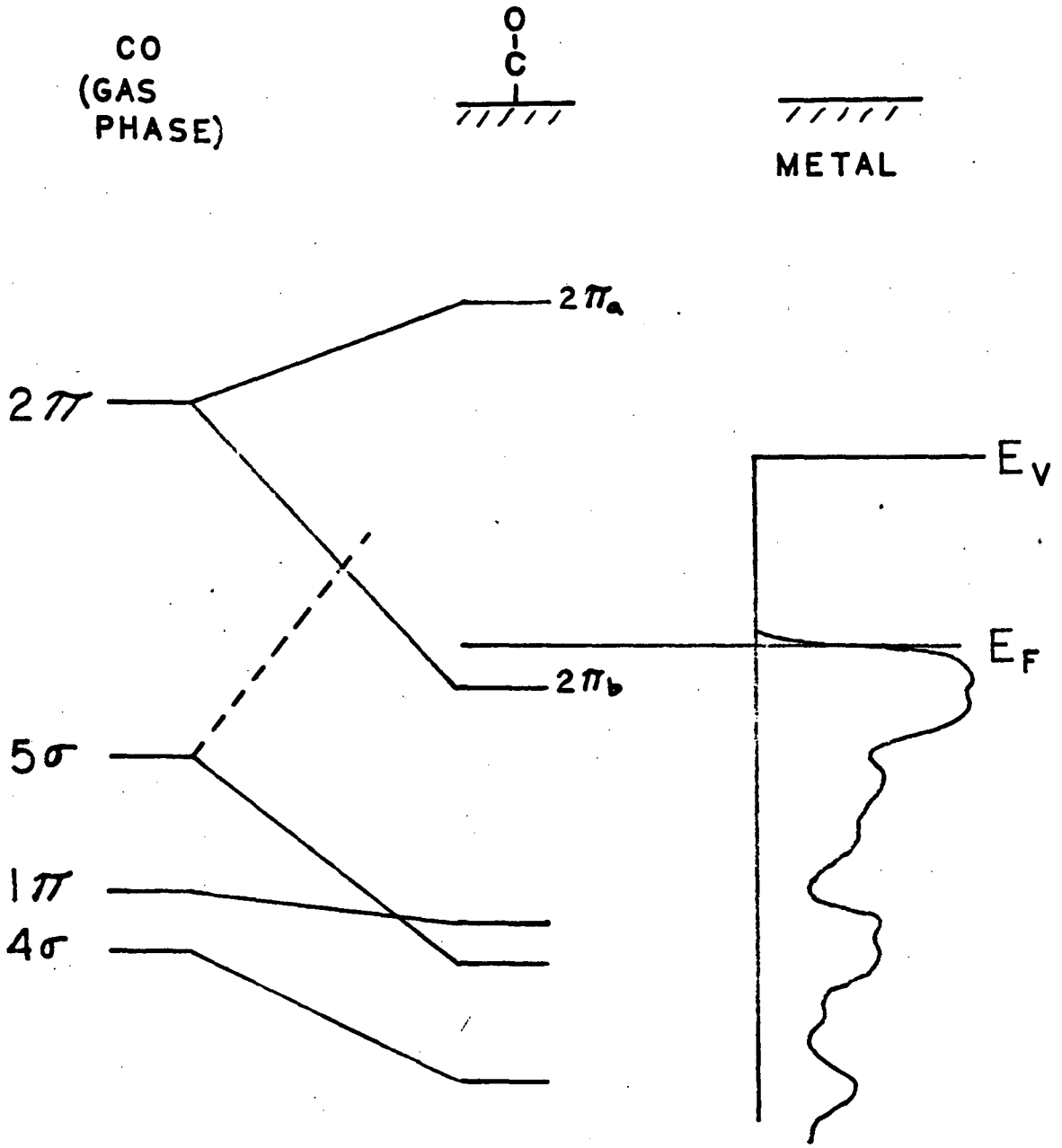

CO BONDING TO METALS

XBL 838-11077

Figure 4.2 Carbon monoxide bonding to a transition metal surface (associatively adsorbed state).

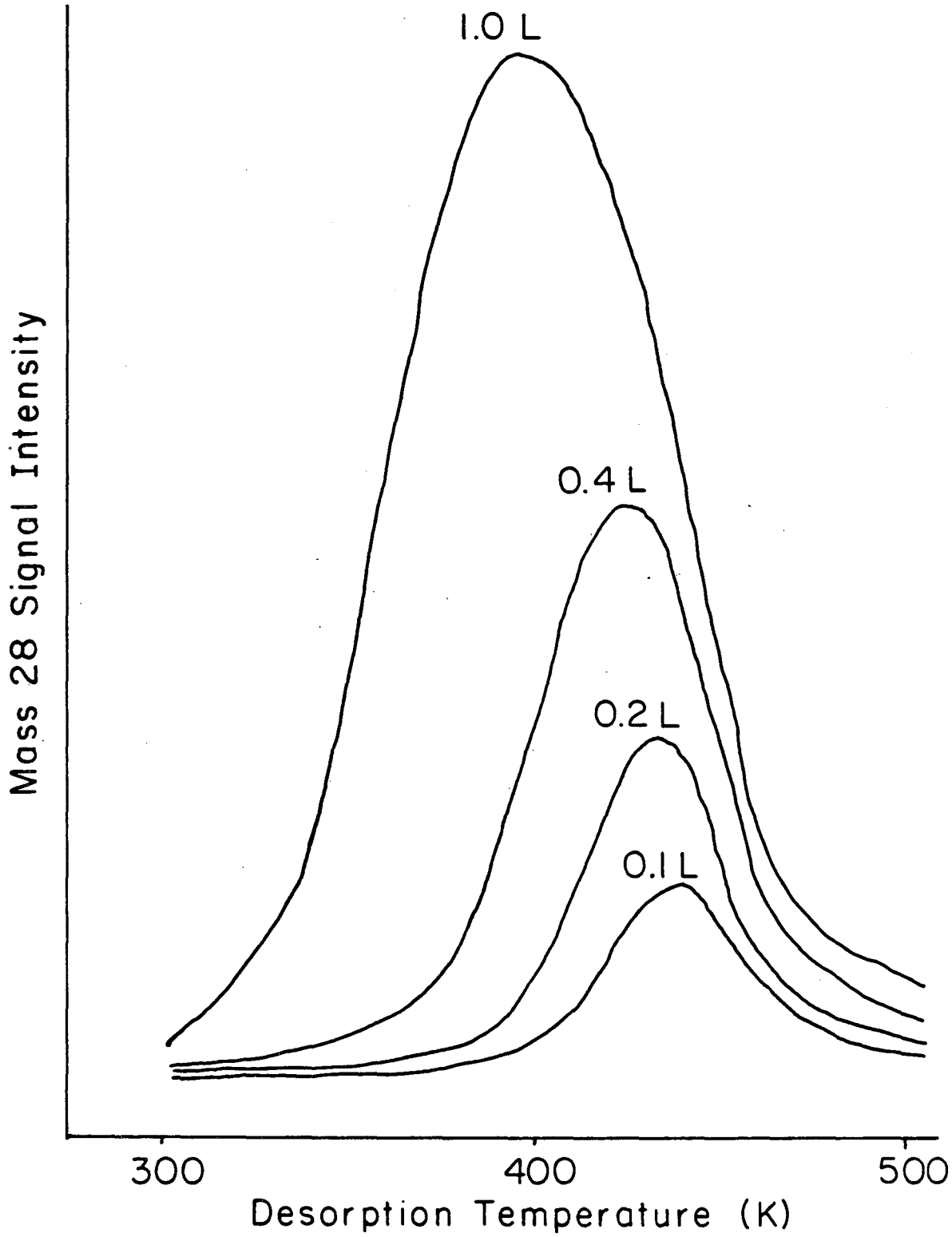

XBL 819-6465

Figure 4.3 Carbon monoxide thermal desorption from Pt(111).

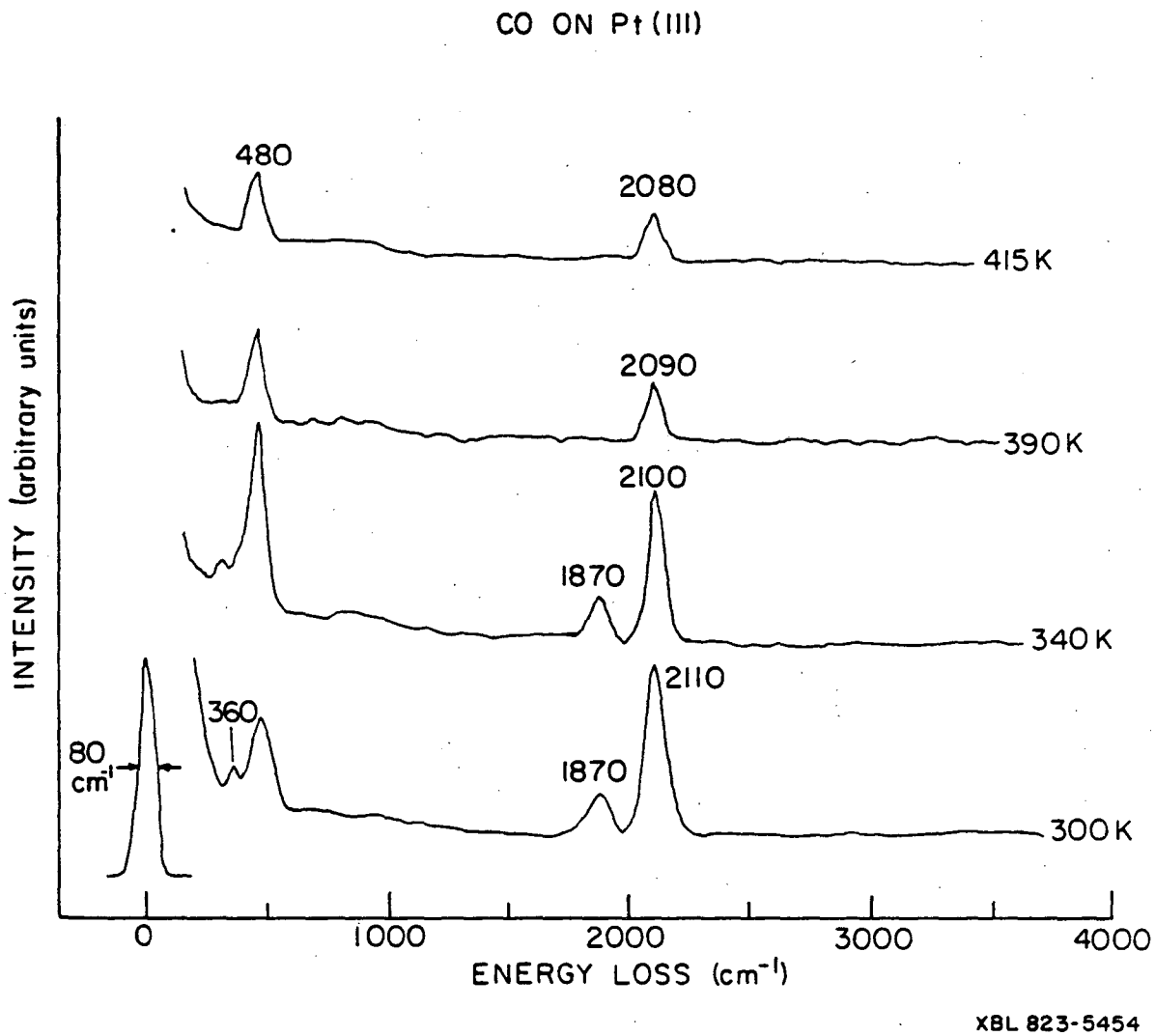

Figure 4.4 Carbon monoxide vibrational spectra (HREELS) on Pt(111).

4.1.2 TDS studies.

Substantial changes in the TDS, HREELS, and UPS spectra occured when potassium was co-adsorbed with CO on Pt(111). No ordered LEED patterns were observed with the co-adsorbed system.

Thermal desorption spectra for various CO exposures on Pt(111) at a constant potassium coverage are shown in Figures 4.5, 4.6, and 4.7. We see, in Figure 4.5 (with Θ_K=0.1) that at low CO exposures (< 0.1L) the desorption peak is centered around 490K, shifted up by about 50K from clean Pt(111). The peak shifts to lower temperature and broadens as the CO coverage is increased. After > 5L exposure, the full width at half maximum (FWHM) of the desorption peak increases to ≈ 120K, and the peak is asymmetric. This trend of shifting peak and increasing FWHM becomes more apparent as the potassium coverage is increased. At Θ_K=0.2 (Figure 4.6) the low exposure (< 0.1L) peak is centered around 520K while it broadens to a FWHM of ~ 160K at saturation CO coverage. At Θ_K=0.3 (Figure 4.7) the peak has shifted as far as 590K for CO exposures less than 0.1L, and the saturation coverage desorption curve has broadened out considerably with the FWHM expanding to 200K. In these figures, it is evident that the desorption peak broadens continuously with both increasing CO exposure and increasing potassium coverage (up to Θ_K=0.5). The mechanism giving rise to the broad desorption peak will be discussed below.

Figure 4.8 shows the thermal desorption spectra for saturation CO coverages on the Pt(111) surface at various potassium coverages. We see the pronounced effect that potassium has on the heat of desorption of CO. At Θ_K=0.05, the CO desorption peak maximum has already shifted

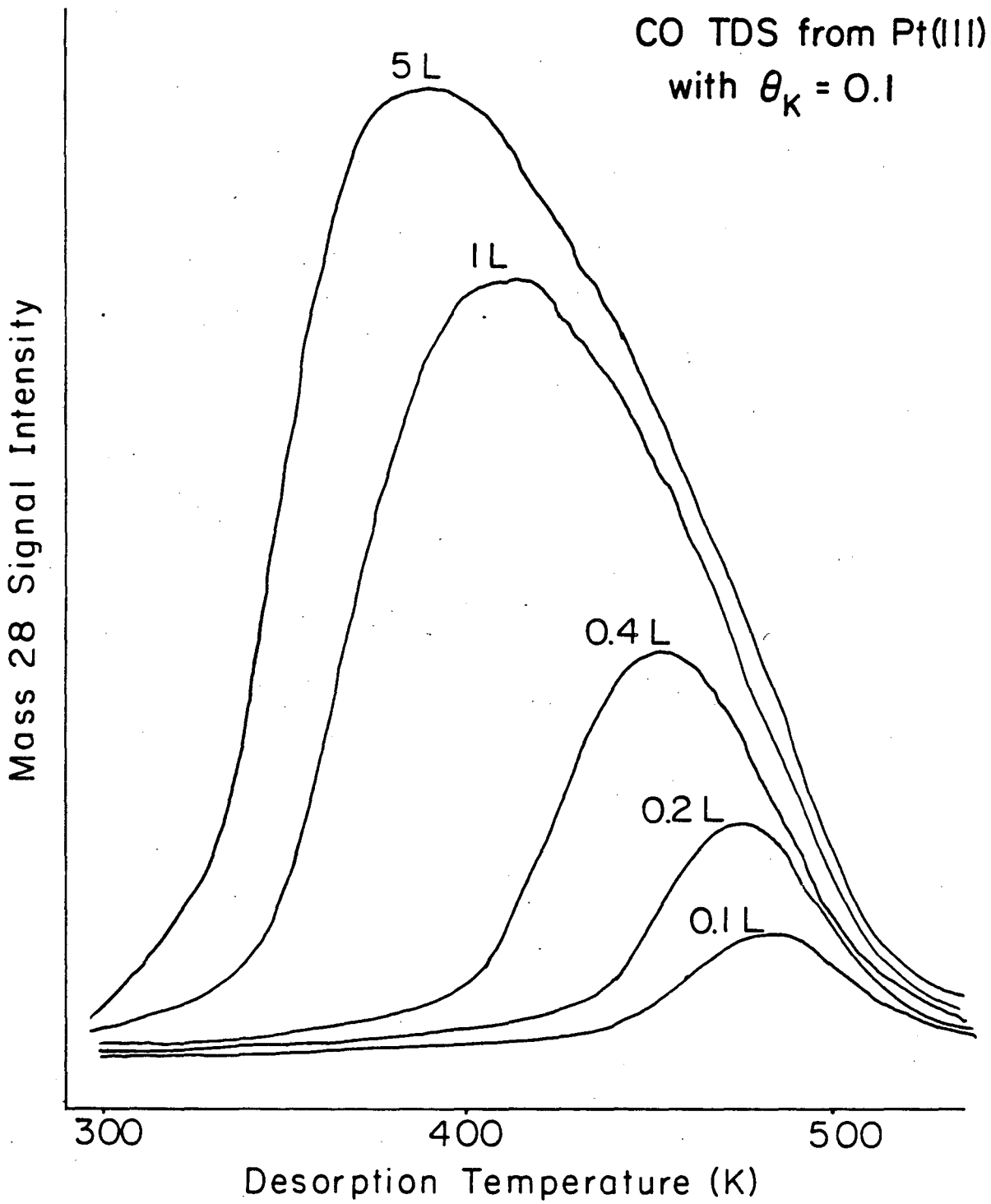

XBL 819-6464A

Figure 4.5

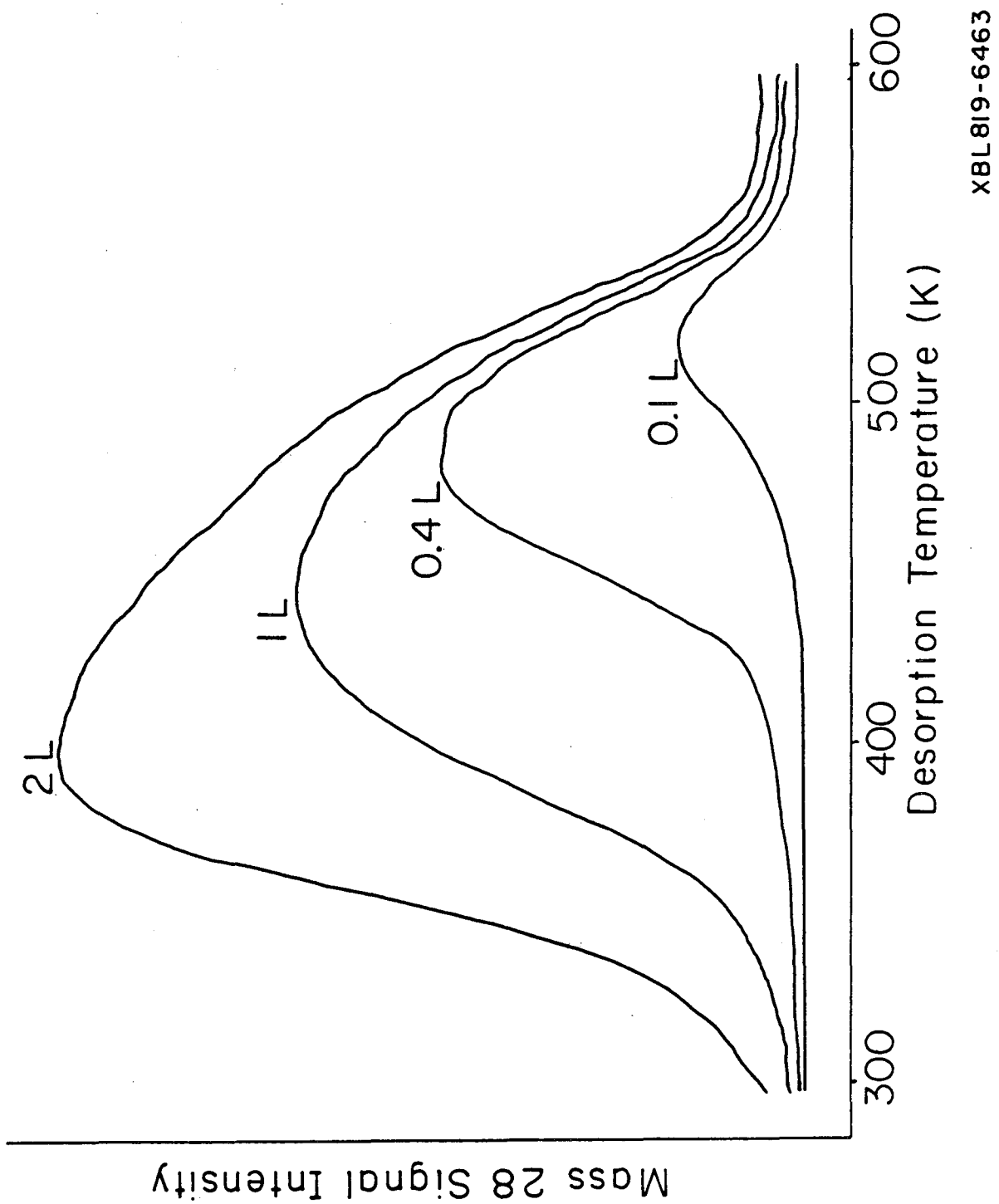

Figure 4.6 CO thermal desorption from Pt(111) with Θ_K=0.2.

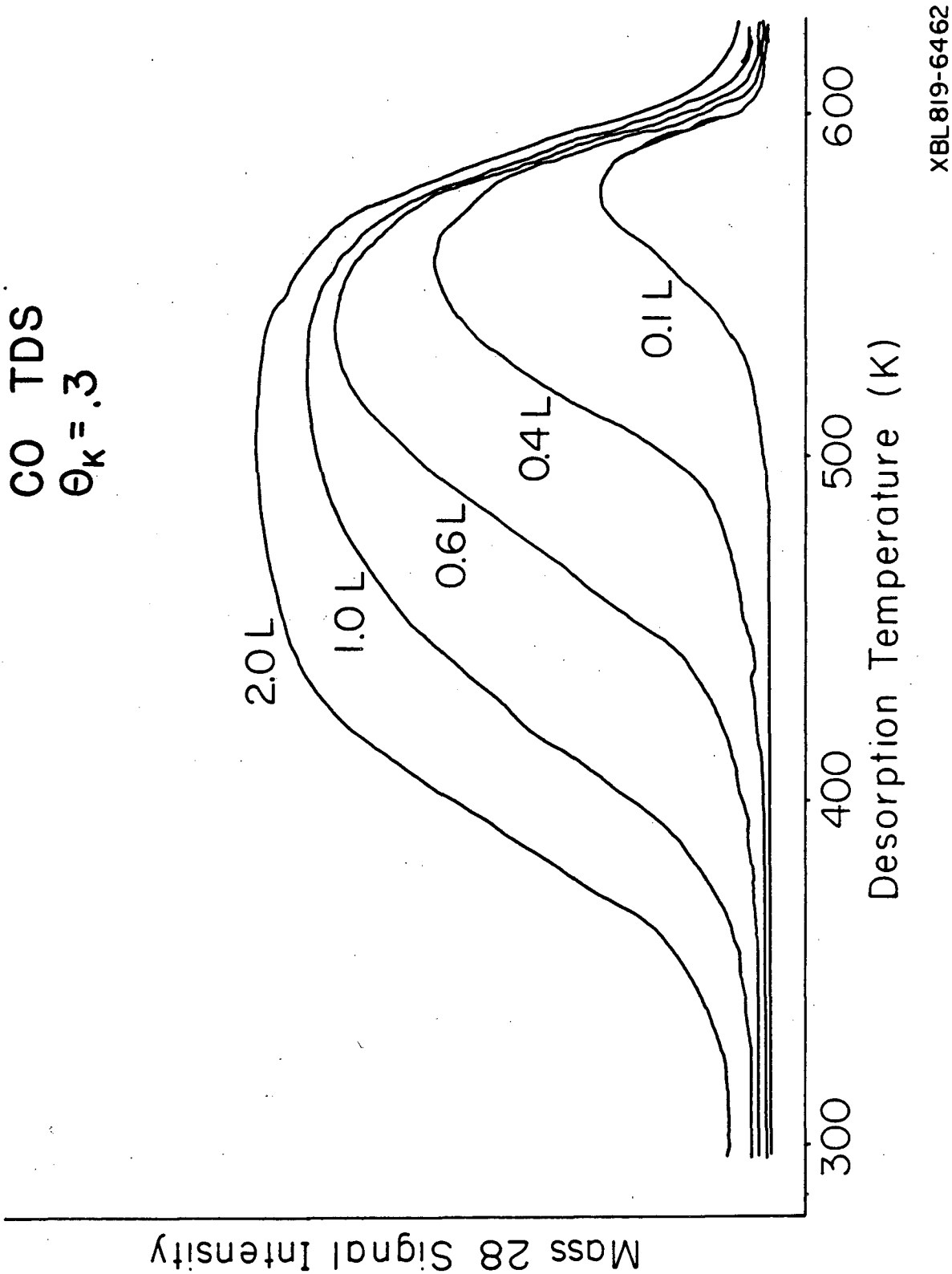
CO TDS
$\theta_K = .3$
2.0 L
1.0 L
0.6 L
0.4 L
0.1 L
300
400
500
600
Desorption Temperature (K)
Mass 28 Signal Intensity
XBL 819-6462

Figure 4.7

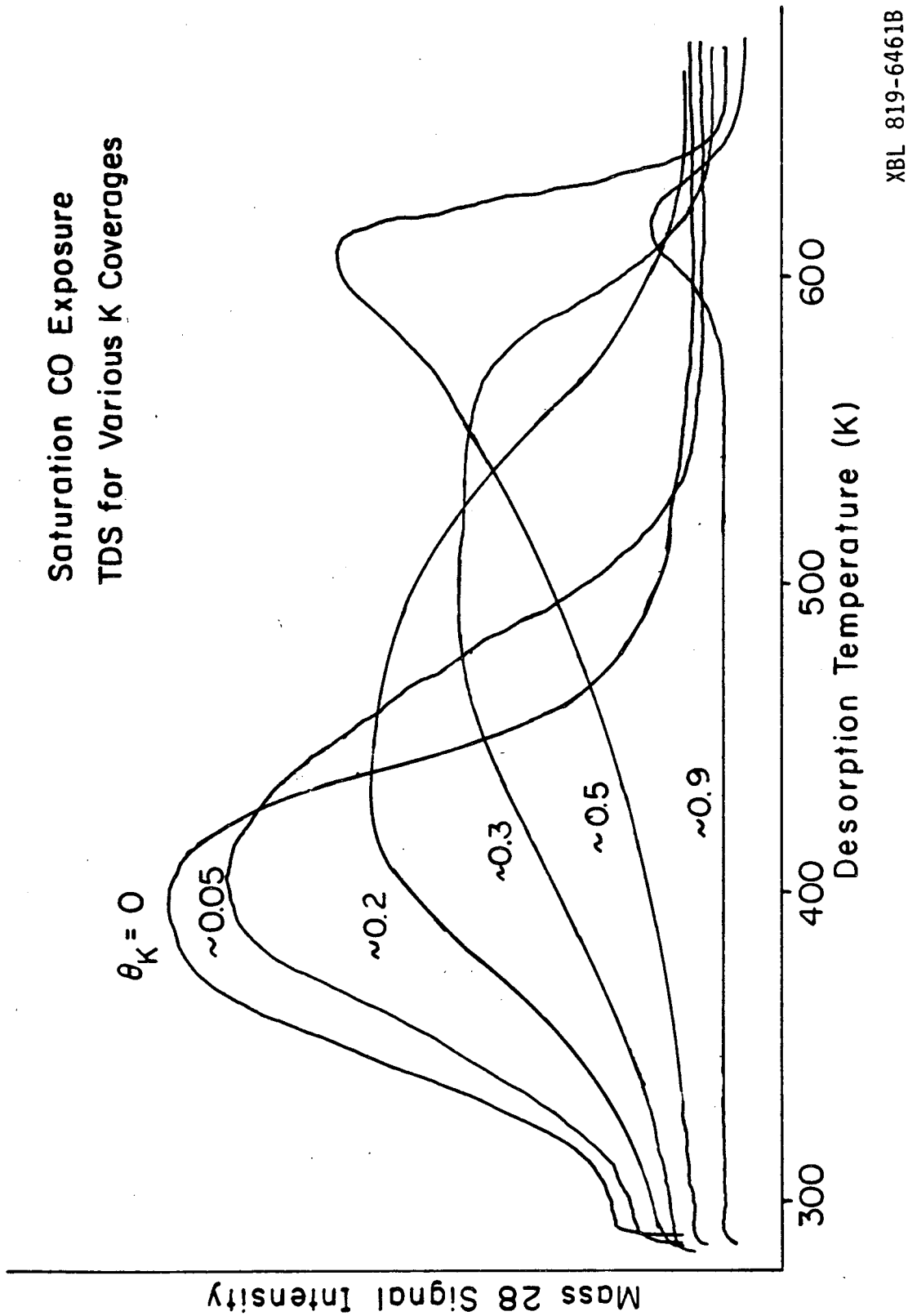
Saturation CO Exposure
TDS for Various K Coverages
$\theta_K = 0$
~0.05
~0.2
~0.3
~0.5
~0.9
300
400
500
600
Desorption Temperature (K)
Mass 28 Signal Intensity
XBL 819-6461B

Figure 4.8

toward higher temperatures from the 400K peak maximum for clean platinum. This shift toward higher temperature continues for Θ_K=0.2 combined with substantial peak broadening on the high temperature side. By Θ_K=0.3, the FWHM is 200K and the peak has shifted to nearly 600K. Above Θ_K=0.5 the maximum CO coverage decreased markedly as determined by TDS peak area, but the CO desorption peak remained at 610K. No CO adsorbed on potassium multilayers. A small amount of residual CO desorption (≈5% of saturation) centered at 420K, which was shown to be due to crystal back, edge, and/or support effects, has been subtracted from all of the spectra. Again, assuming a preexponential factor of 10^{13} s^{-1}, and first-order desorption kinetics, an increase from 400K to 610K in desorption rate maximum corresponds to a heat of adsorption increase from about 25 to 36 kcal/ mole. Finally, no significant irreversible CO dissociation was evident since no carbon or oxygen remained on the surface as determined by AES after heating to 650K.

We have also plotted the CO coverage vs. potassium coverage for 10L CO exposure in Figure 4.9. For room temperature exposure, the maximum coverage of CO increases slightly at first, then decreases at high potassium coverages. This is the result of the competing effects of an increase in CO binding energy due to potassium coadsorption, as well as a blocking of sites by the potassium. At low potassium coverage, the increase in CO binding energy allows for tighter CO packing. This offsets the decrease due to the blocking of exposed Pt surface sites, that dominates at high K coverages.

Figure 4.10 shows the CO thermal desorption spectra from a stepped platinum surface with coadsorbed potassium. The increase in

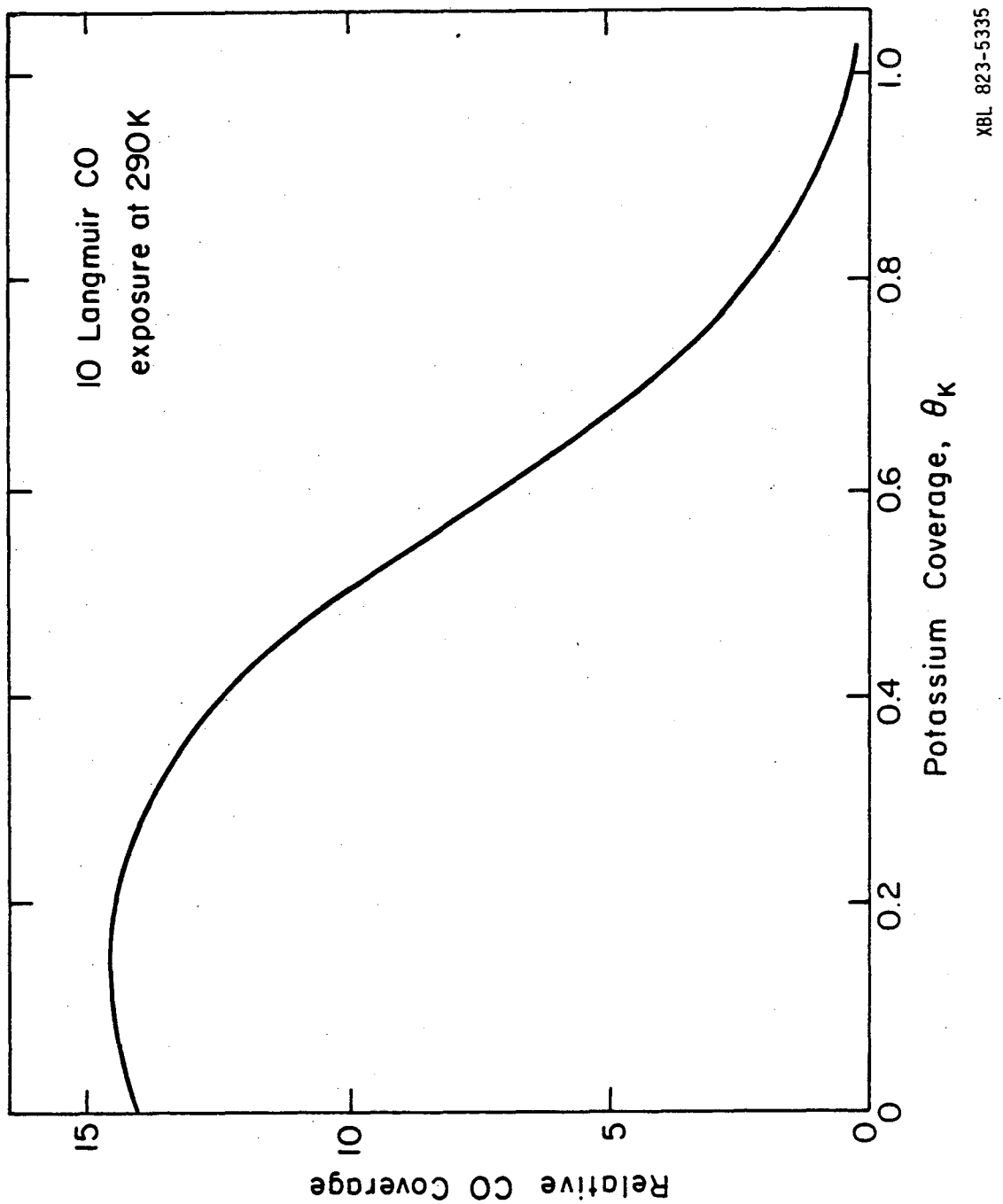

Figure 4.9 CO coverage versus potassium coverage for 10 Langmuir CO exposure.

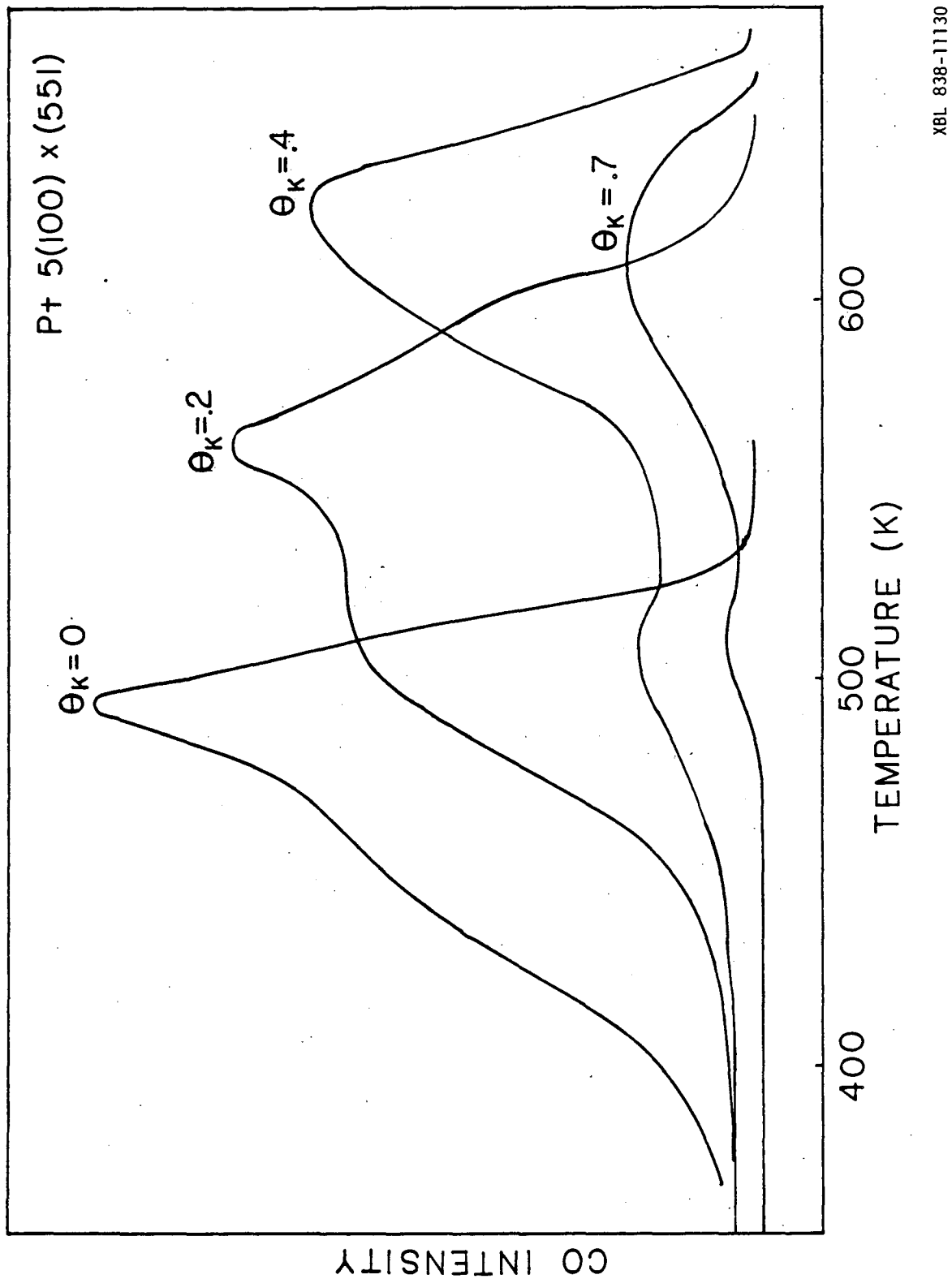

Figure 4.10 Carbon monoxide thermal desorption from a potassium covered stepped platinum surface.

desorption temperature of both terrace and stepped CO peaks implies that the potassium is not localized on either site, but is positioned somewhat evenly across the surface. This should be expected from their strong repulsive interactions (see Chapter 3).

4.3.2 High Resolution Electron Energy Loss Spectroscopy Studies

The effect of potassium on the vibrational spectrum of CO is illustrated in Figures 4.11 and 4.12. Figure 4.11 shows the room temperature HREELS vibrational spectrum for saturation exposures (> 10L) of CO as a function of potassium coverage. Potassium coverages were achieved by depositing a monolayer or more of potassium, then heating the surface to achieve the desired coverage by desorption. The potassium coverages were determined by TDS and AES calibrations, as described in Chapter 3. One should remember that one potassium monolayer, Θ_K=1, has about one-third the atomic density of a Pt(111) surface layer.

Figure 4.12 shows the changes in the vibrational spectrum as the CO coverage is varied at a constant potassium coverage. In these figures the reported temperatures indicate those at which the crystal was annealed for several seconds prior to recording the spectra; all spectra were obtained at 300K. This annealing process is used to vary the CO coverage: the higher the annealing temperature, the lower the CO coverage (although the actual coverage was not determined). Since the partial monolayer potassium coverages were obtained by annealing a monolayer of potassium to at least 700K (e.g. annealing to 700K produced Θ_K=0.3), no noticeable potassium desorption was detected using this process to vary CO coverage.

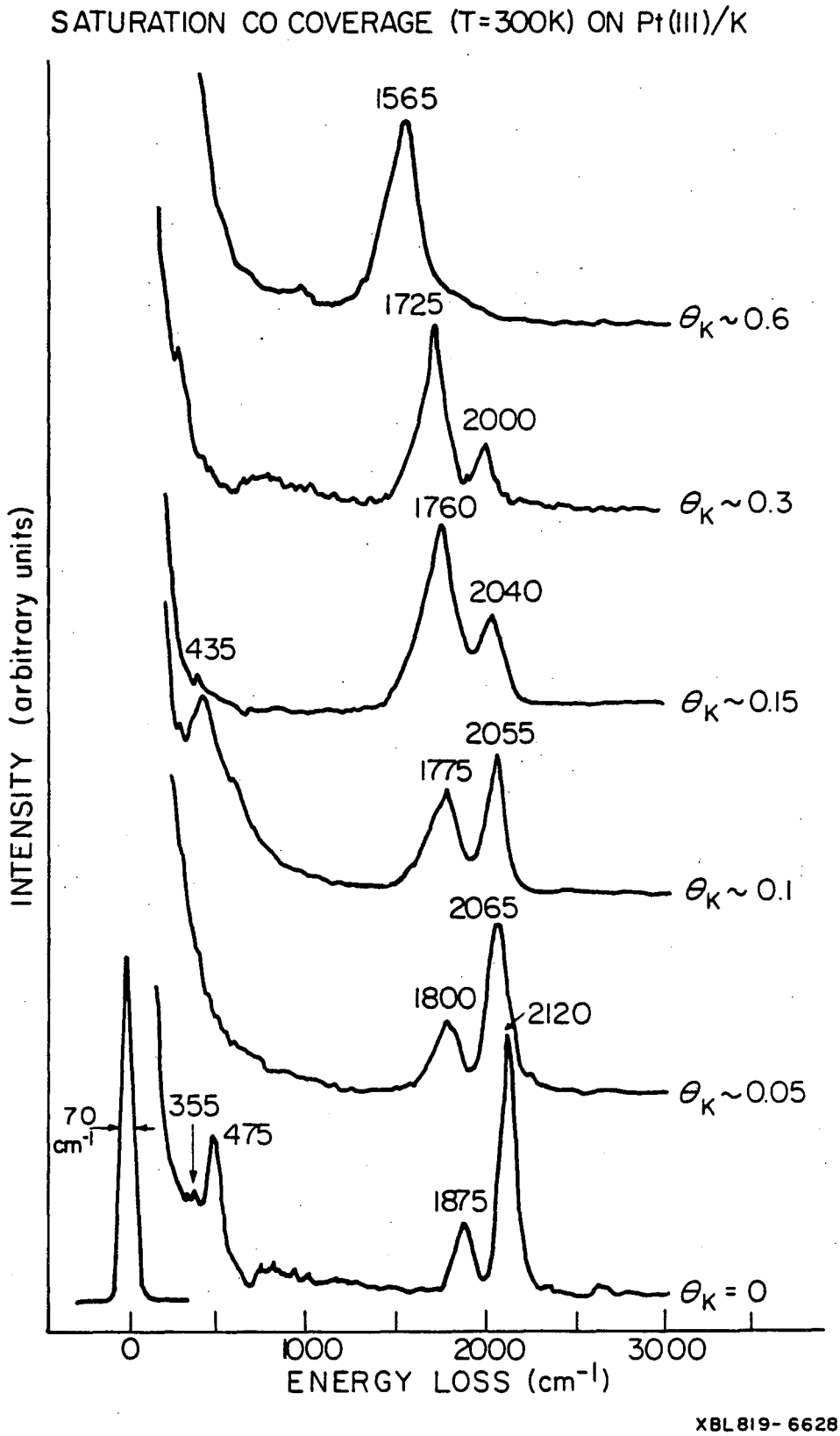

Figure 4.11 Carbon monoxide vibrational spectra (HREELS) with various potassium coverages.

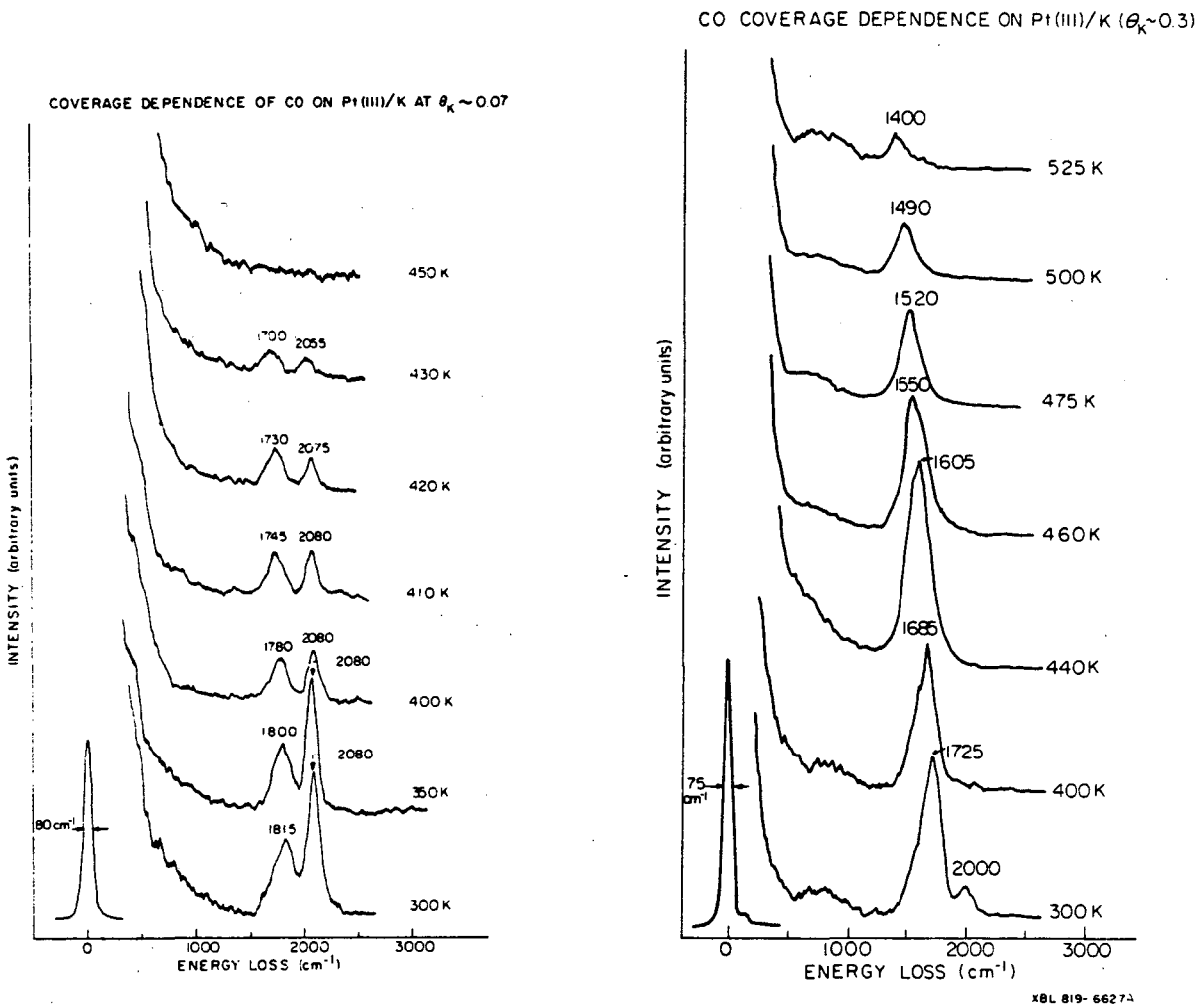

Figure 4.12 Carbon monoxide vibrational spectra (HREELS) for various CO coverages (increased temperature denotes decreased coverage).

In Figure 4.12a we show the vibrational spectra as CO coverage is varied Θ_K= 0.07. In the spectra taken at room temperature, both peaks are shifted slightly from the clean CO saturation coverage values (see Figure 4.4). Only small variations occur until 400K, where the linear stretching frequency is decreased substantially. At 410K, both the linear and bridged species have the same peak height. Note that on clean Pt(111) at this temperature, only the higher frequency species is present (see Figure 4.4), while here both species are present. As the coverage is decreased, the peak height of the linear species continues to decrease faster than the bridged species. The position of the stretching vibration, however, has decreased more substantially for the bridged site than for the linear site (115 cm^{-1} vs. 25 cm^{-1}).

At a potassium coverage of Θ_K=0.05, lower than that shown in Figure 4.12a, similar trends occur with CO coverage as discussed above, however both peaks decrease in height at nearly the same rate, becoming equal only at a very low coverage very near total desorption (425K). The frequency shifts are similar to those shown in Figure 4.12a, with an average frequency shift ~ 20 cm^{-1} less than at Θ_K=0.07.

The trend of decreasing stretching frequency and higher occupation of the bridge site continues for Θ_K=0.10 (not shown). In this case however, the linear and bridged peak heights are nearly the same at saturation CO coverage. The bridged site dominates at CO coverages less than saturation. The stretching vibration decreases to a low of 1715 cm^{-1} for the bridged position with no linear species present after annealing to 435 K.

Figure 4.12b shows the HREELS spectra for Θ_K=0.3. At this potas-

sium coverage we see that most of the CO adsorbs in bridge bonded sites, with a small amount of adsorption occuring in the linear site only at high CO exposures. Both stretching frequencies are strongly affected by the potassium. The bridged CO stretching frequency at 1725 cm^{-1}, already shifted substantially at saturation coverage, continues to shift to lower frequency as the CO coverage decreases. Notice that this shift is continuous with increasing temperature, but that the desorption process occurs over a broad temperature range as was evident in the corresponding TDS curves in Figure 4.7. No spectra were taken on samples heated above 525K where further decreases on CO vibrational frequency might occur. The weakest CO stretching frequency we recorded occurs at 1400 cm^{-1}.

We note that the existence of bridge bonded CO with a vibrational frequency of 1400 cm^{-1} calls into question the conventional assignment of 1300-1500 cm^{-1} vibrational peaks as being due to carbonates and formates. On real catalysts they may instead be the result of multiply bonded CO adsorption on promoted sites. Also the large 470 cm^{-1} decrease in the bridge bonded CO stretching frequency raises the question of the nature of the C-O bond. The 1400 cm^{-1} CO frequency we observe for the CO/K coadsorbed system on platinum is characteristic of a molecule with a bond order of 1.2-1.5 (Pauling, 1960), compared with a bond order of 2.4 for free CO. Thus, the CO bond appears greatly stretched without dissociation of the adsorbed CO species. (Note: a more complete description of these HREELS spectra can be found in the PhD thesis of my coworker, John Crowell, Berkeley 1983.)

4.1.4 Ultraviolet Photoelectron Spectroscopy Studies.

In Figures 4.13-4.16 we show the UPS spectra and their difference spectra for CO adsorbed on Pt(111) with various coverages of potassium. On the clean Pt(111) surface, Figure 4.13, the adsorption of CO is accompanied by several changes in the UPS spectra. As with K, CO caused a drop in emission from the peak, lying just below E_f. This is accompanied by the growth of two features located at 5.3 and 9.5 eV binding energy. For low CO coverages, there is also a peak at 12 eV. This peak becomes lost in the difference spectra at higher coverages because a large peak resulting from a change in the work function appears at 14.5 eV. When CO is coadsorbed with potassium, Figures 4.14 and 4.15, the main features of the spectra seem to be the combination of the results for clean potassium and clean CO overlayers. The peak at 5.3 eV appears not to shift, although by $\theta_K = 0.65$ it has disappeared in the difference spectra. The peak at 9.4 eV broadens further into a doublet at 8.5 and 9.8 eV. The peak at 12.3 eV shifts to about 13 eV, see Figures 4.16a and b, but becomes lost in the large change in the secondary electrons. The work function change decreases slightly with CO exposure on clean Pt(111), while it increases for higher potassium coverages, see Figure 4.17. In Figure 4.18 are UPS spectra taken several years earlier to those shown in Figures 4.13-4.16. This also shows the broad $5\sigma - 1\pi$ level. A more complete version of these results will appear elsewhere.

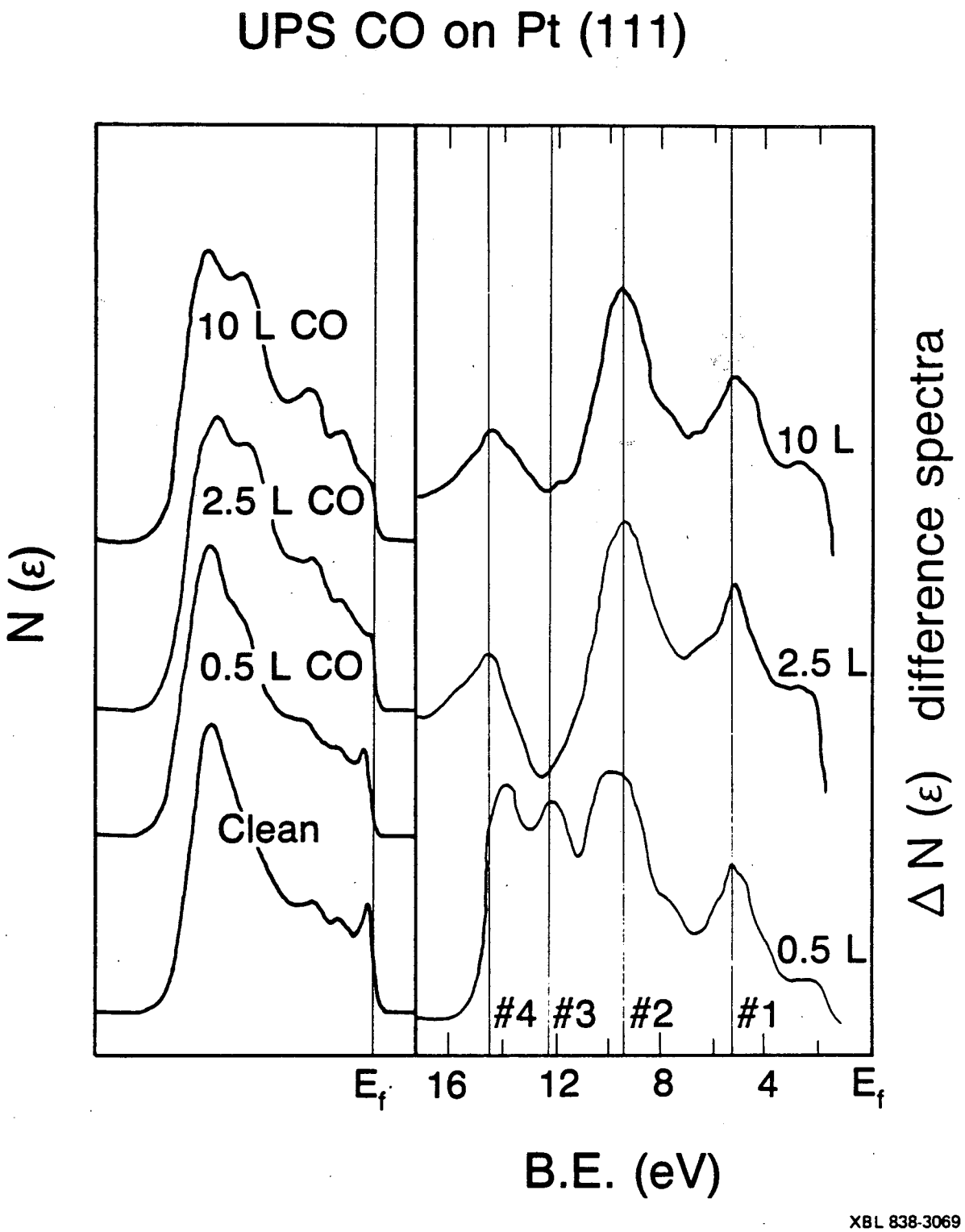

Figure 4.13 Ultraviolet photoelectron spectra of CO adsorbed on Pt(111). Full N(e) spectra are on left panel; right panel shows the difference spectra. Peak heights are not normalized.

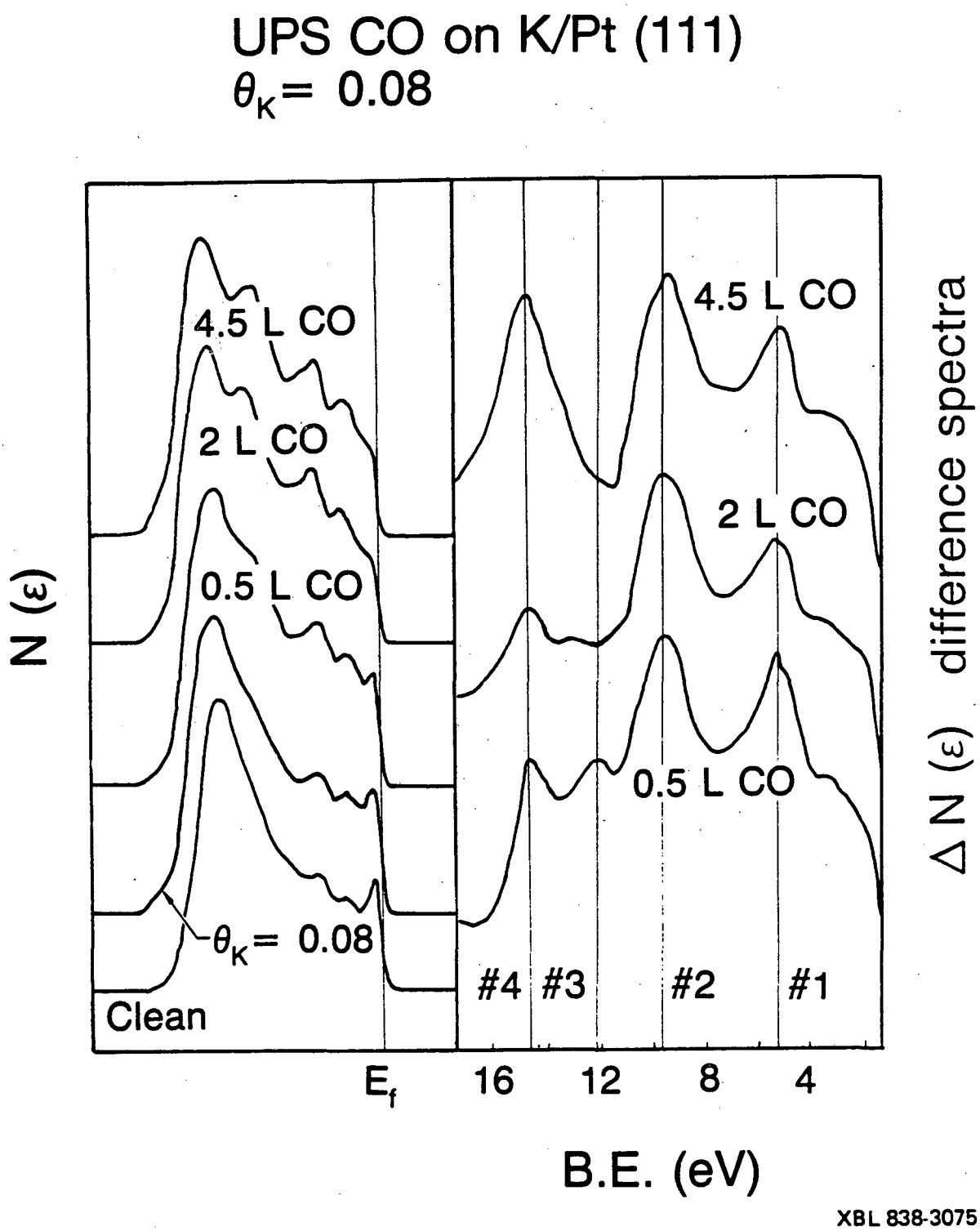
UPS CO on K/Pt (111)
θK= 0.08
4.5 L CO
2 L CO
0.5 L CO
θK= 0.08
Clean
N (ε)
4.5 L CO
2 L CO
0.5 L CO
#4
#3
#2
#1
Δ N (ε) difference spectra
Ef
16
12
8
4
B.E. (eV)
XBL 838-3075

Figure 4.14

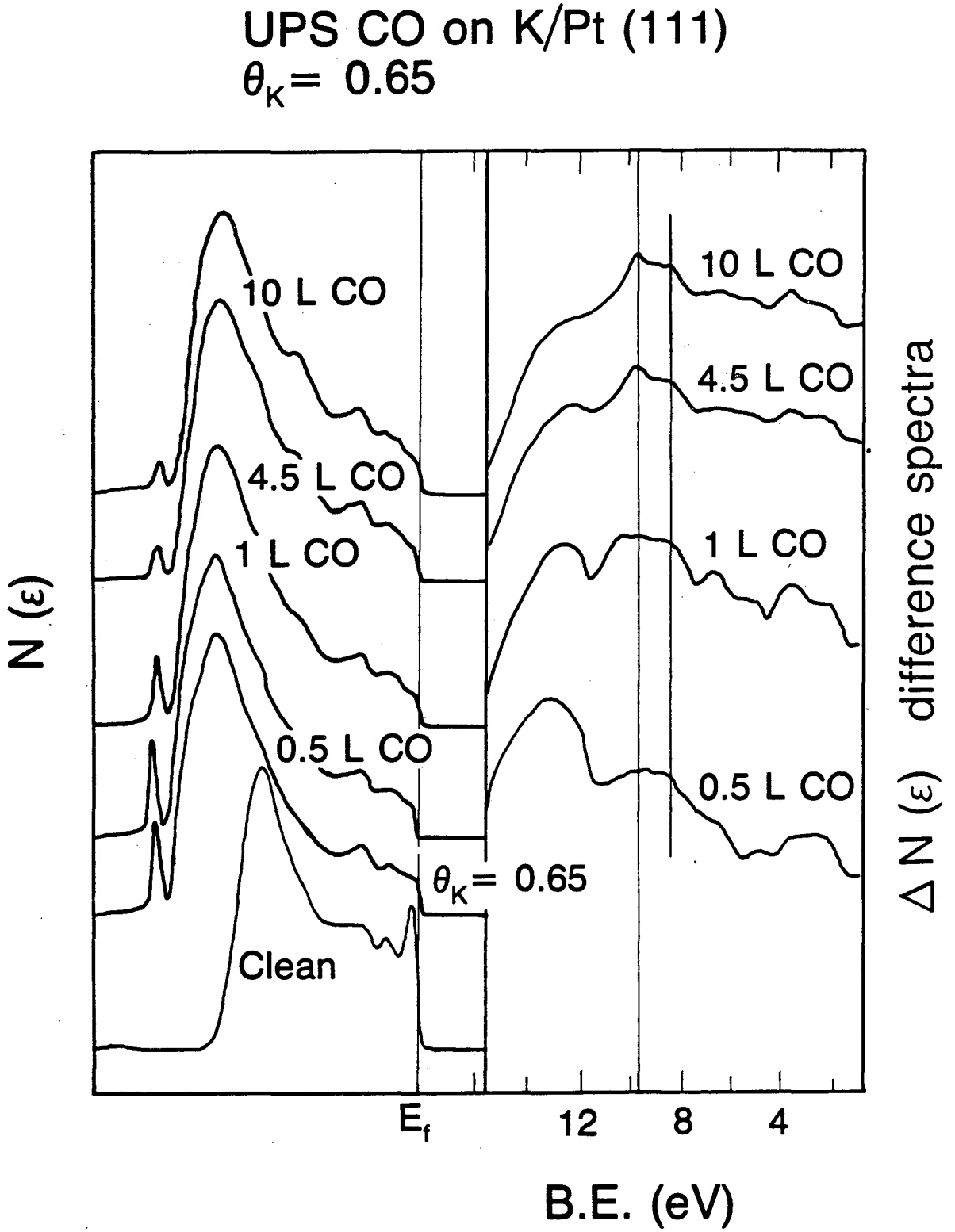
UPS CO on K/Pt (111)
θK= 0.65
10 L CO
4.5 L CO
1 L CO
0.5 L CO
Clean
θK= 0.65
N (ε)
10 L CO
4.5 L CO
1 L CO
0.5 L CO
Δ N (ε) difference spectra
Ef
12
8
4
B.E. (eV)
XBL 838-3089

Figure 4.15

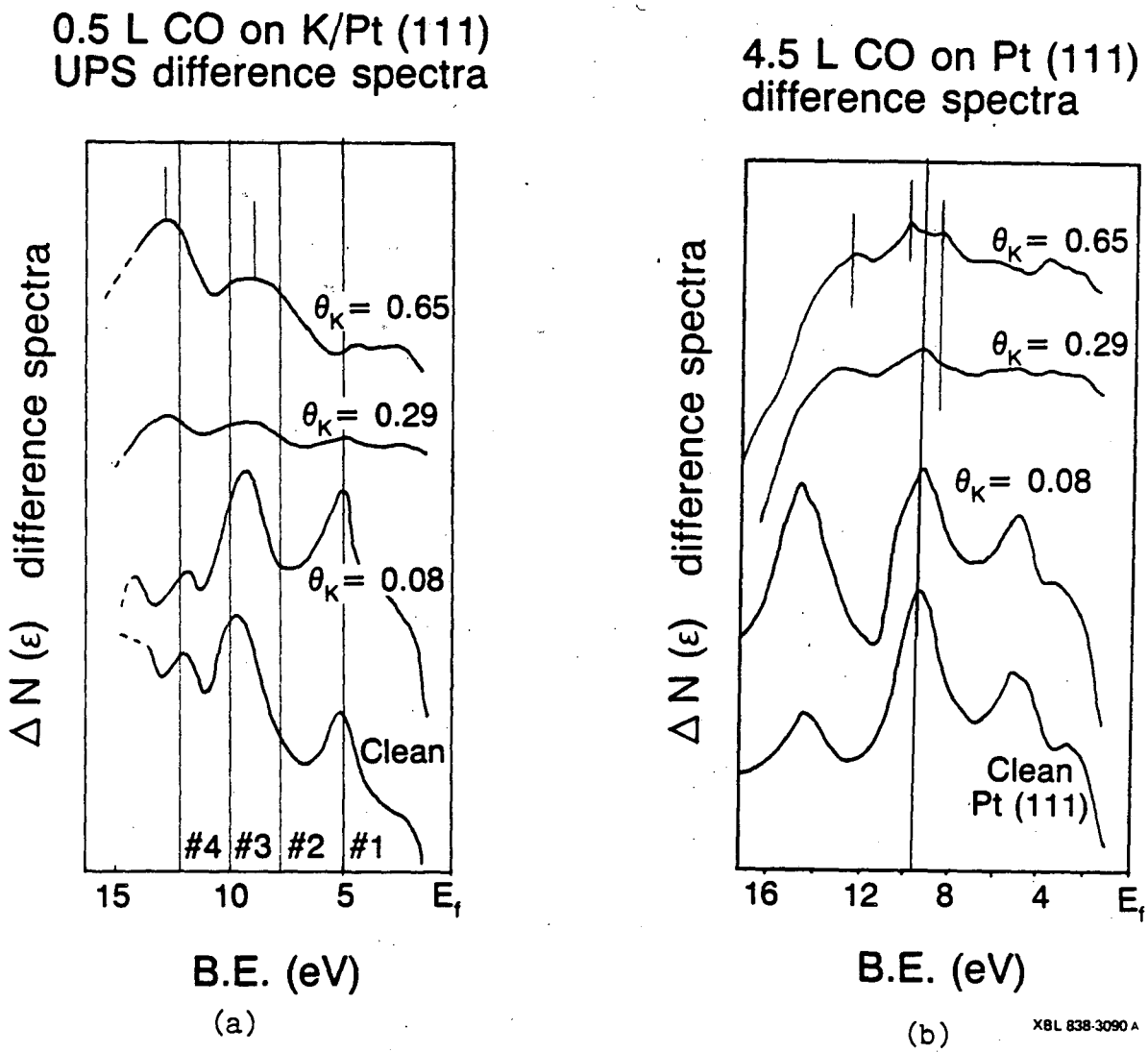
0.5 L CO on K/Pt (111)
UPS difference spectra
ΔN (ε) difference spectra
θK= 0.65
θK= 0.29
θK= 0.08
Clean
#4 #3 #2 #1
15
10
5
Ef
B.E. (eV)
(a)
4.5 L CO on Pt (111)
difference spectra
ΔN (ε) difference spectra
θK= 0.65
θK= 0.29
θK= 0.08
Clean
Pt (111)
16
12
8
4
Ef
B.E. (eV)
(b)
XBL 838-3090 A

Figure 4.16

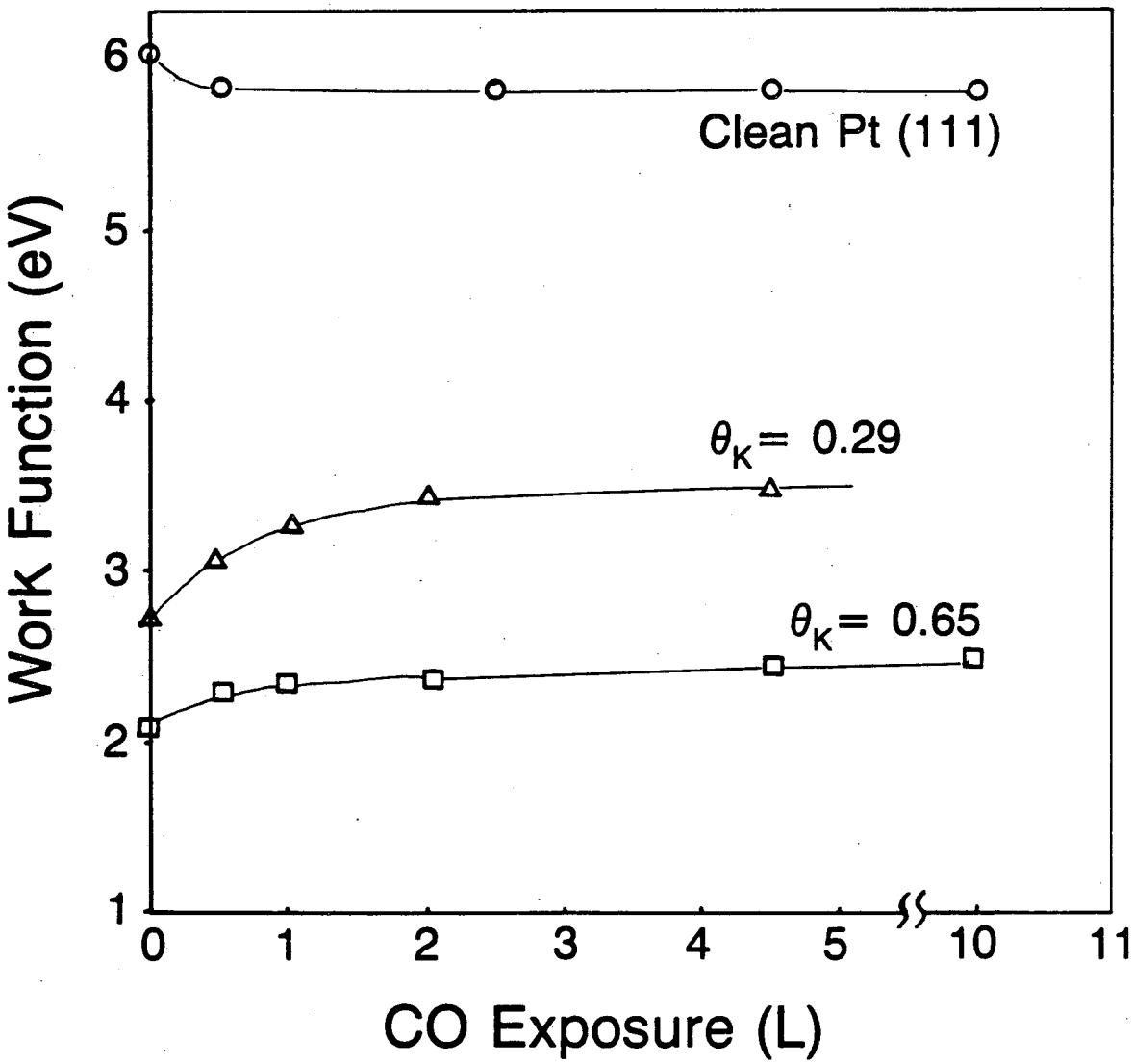

XBL 838-3085

Figure 4.17

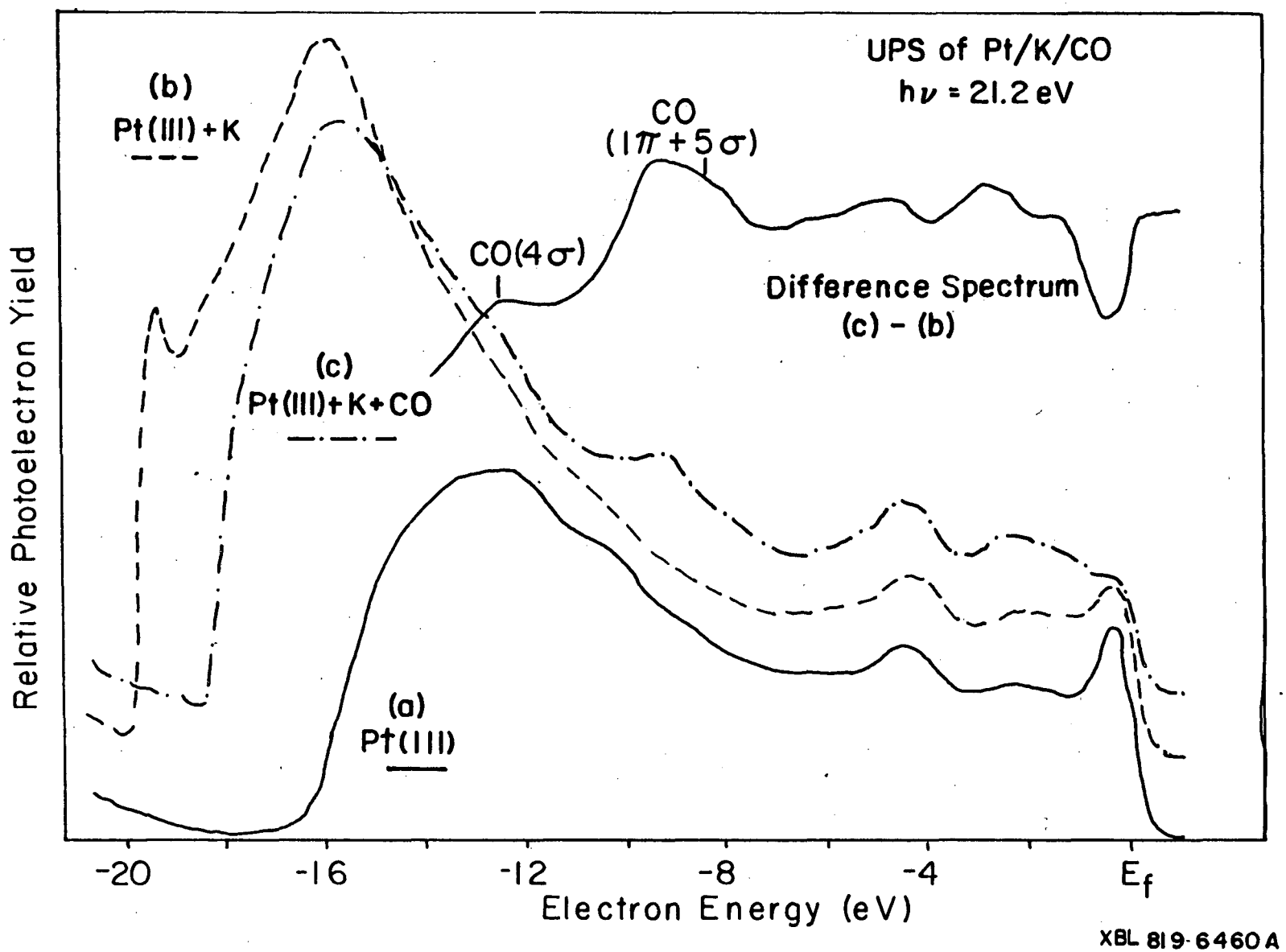

Figure 4.18 UPS spectra for CO + K + Pt(111) system

4.1.5 Discussion.

The preadsorption of potassium has marked effects on the adsorption of CO on Pt(111). The major experimental findings can be summarized as follows:

i) The addition of submonolayer amounts of potassium continuously increases the heat of adsorption of CO on Pt(111) from 25 kcal/mole for clean Pt(111) to 36 kcal/mole for near monolayer coverages.

ii) Associated with the increase in heat of adsorption is a 310 cm^{-1} decrease in the stretching frequency of the bridge bonded CO molecules from 1870 cm^{-1} on clean Pt(111) to 1560 cm^{-1} with 0.6 monolayers of coadsorbed potassium.

iii) The CO thermal desorption peak broadens continuously to a maximum of 200K (FWHM) at saturation CO coverages as the potassium coverage is increased.

iv) At a fixed potassium coverage, the CO vibrational frequencies for both linear and bridge adsorption sites decrease substantially with decreasing CO coverage.

v) On the potassium-free Pt(111) surface, CO prefers to occupy top adsorption sites while on the potassium-covered surface, CO adsorbs preferentially on bridged sites.

vi) The work function of the Pt(111) surface decreases by 4-4.5 eV upon the adsorption of one third of a monolayer of potassium, but increases by 1.5 eV when CO is coadsorbed.

vii) The 4σ CO orbital energy shifts down, and the $5\sigma - 1\pi$ level splits when potassium is coadsorbed.

These results can be interpreted by examining the electron acceptor character of CO and the changes in charge density at the platinum surface as potassium is adsorbed.

The bonding of carbon monoxide to metal atoms involves a simultaneous electron transfer from the highest occupied molecular orbitals of CO (5σ) to the metal and backdonation of metal electrons into the lowest unoccupied molecular orbital ($2\pi^*$) of CO (Blyholder, 1964; Doyen, 1974). The backdonation of metal electrons into the $2\pi^*_{CO}$ orbital leads to a simultaneous strengthening of the M-C bond and a weakening of the CO bond, as seen in Figure 4.1, where the d_{Pt} - $2\pi^*_{CO}$ orbitals are in phase (bonding) between Pt and C, while being out of phase (antibonding) between C and O.

In our experiment, changes in backdonation to CO are induced by using an electron donor, potassium. Charge is transferred from the potassium to the platinum, with electrostatic screening of the resultant positive charge on the potassium by metal electrons. This polarization is displayed by the large drop in work function upon potassium adsorption. Then, upon CO coadsorption, an enhancement (relative to clean Pt) of backdonation into the CO occurs as a result of changes in surface charge density induced by potassium.

Two similar explanations have been used to understand backdonation in similar systems and can be applied here. The first proposes that a potassium-induced change in the platinum surface valence band occupancy and a shifting of the CO molecular levels permits a greater occupancy of the conjugate d_{Pt} - $2\pi^*_{CO}$ orbitals. The second explanation assumes that a conjugate d_{Pt} - $2\pi^*_{CO}$ orbital becomes

fully occupied upon adsorption, but that the surface dipole component of the work function determines the relative occupation of the metal and $2\pi^*_{CO}$ orbitals, i.e. the spatial distribution of charge within the conjugate orbital. In the potassium-free, high work function case, most of the electrons in the orbital would be localized on the platinum atoms. On the potassium covered, low work function surface, however, the electrons in the $d_{Pt} - 2\pi^*_{CO}$ orbital would become less localized on the Pt, shifting their charge density more onto the C and O atomic positions, giving the conjugate orbital more $2\pi^*_{CO}$ character. Both models would account for the observed results of an increased Pt-C binding energy and decreased C-O vibrational frequency.

The UPS experiment offers us the best determination of the energy levels of adsorbed CO in the absence of a more exact determination of energy and relative occupancy. If, by decreasing the surface dipole field we bring the 2π gas phase level closer to the Fermi level, then the overlap between the 2π level and the metal orbitals should increase. In this extreme picture, the molecular orbitals of the adsorbate (at least the 2π level) are not "pinned" to the Fermi level. They do not track the Fermi level as one changes the work function - but rather are at constant energy with respect to the vacuum level. This argument is sometimes invoked to explain the energy level shifts of physisorbed species.

At the other extreme, all of the orbital energy levels of a chemisorbed species are said to be "pinned" to the Fermi level. In this case, however, it is more difficult to reconcile the large changes

in CO chemisorption observed as the work function is changed (i.e. when potassium is added.) If all the electron energy levels moved with changes in work function such that they remained at constant position with respect to the Fermi level, then no changes in bonding should necessarily occur. We see experimentally, however, that this argument is wrong since large changes in chemisorption properties do occur when CO (or benzene see below) is coadsorbed with potassium. A more intermediate situation probably exists where the levels (in particular the CO 2π level) follow neither the Fermi nor vacuum levels exactly.

In the UPS difference spectra we note a peak at 5.3 eV. This does not correspond to any molecular CO level. This feature has been observed by others for adsorbates on platinum (Helms, 1976) as well as other metals, and is thought to be due to subtle changes in the d-band. The CO 2π level exists about 2 eV below E_f, but is not clearly observed by UPS. Its position and occupancy has recently been analyzed by Bosco (1983). The first (in order of decreasing energy) molecular orbitals of CO that are detectable, are the 1π and 5σ levels which appear as overlapping peaks at 9.4 eV. As potassium is added, the peak broadens and a shoulder develops at 8.5 eV. This feature has been observed by others, and is thought to result from a shift in the 1π level towards lower binding energy. The 4σ level, on the other hand, appears to move from 12 to almost 13 eV. This means that the $4\sigma - 1\pi$ spacing increases. From a molecular orbital point of view, the increase in the 1π level position can be expected. Since backdonation into the 2π

level will increase the distance between the carbon and oxygen atoms, the 1π bonding level should be destablized, moving it up in energy. The decrease in position of the 4σ level is somewhat harder to interpret, because it is a nonbonding level. Since the CO molecule has more negative charge on it (in the 2π level) the 4σ level (as well as the other core levels) may be screened better, as observed for the core O(2s) and C(2s) levels (Kiskinova, 1983), but this should cause a shift in the other direction. On the other hand, an initial state shift (to higher binding energy) of the CO core levels should also result from the potassium induced change in local electrostatic fields.

For high potassium coverages, the work function was found to increase with increasing CO exposure, while on the potassium free surface, CO caused the Pt(111) work function to decrease. This behavior can be understood from the donor-acceptor model of CO. The main bonding mechanism, on the clean Pt(111) surface, is a 5σ bonding donation into the metal. On the lower work function potassium covered surface, electrons can be backdonated more easily into the 2π level. CO then becomes an acceptor as well as a donor.

Theoretical calculations are required to determine which of these effects, or others, is dominant in determining the observed results. Recent extended Huckel calculations performed by Anderson (1983) have shown that our results are in agreement with their theoretical predictions.

In that study, the valence state ionization potential (VSIP) of a platinum cluster was decreased by potassium. A second calculation for CO on the cluster showed that when the VSIP was decreased (mimicking the potassium effect), the CO moved from a linear to a bridged and even three fold site, and the metal-carbon bonding became stronger due to increased backdonation into the 2π orbital. Van Santen (1983), however, has shown that direct electrostatic interactions can be important. Other calculations of CO adsorbed on nickel (Rosen, 1979) and lithium (Post, 1981) clusters have shown that the $2\pi^*_{CO}$ orbital can also conjugate with s and p metal orbitals of the proper symmetry, and that CO vibrational frequencies below 1500 cm^{-1} can be predicted.

The 11 kcal/mole increase in adsorption energy of CO (upon potassium coadsorption) supports the model of enhanced electron backdonation. In addition to strengthening the metal-carbon bond, backdonation should also weaken the carbon-oxygen bond as noted above, lowering its vibrational frequency. This indeed occurs since the vibrational frequency of bridge bonded CO at saturation coverage decreases by 310 cm^{-1} as the potassium coverage is increased to 0.6 monolayers. The thermodynamic changes can be represented by Figure 4.19. Here both the molecular adsorption energy and the probability for dissociation increase with potassium coverage (state #1).

Another effect of the platinum mediated potassium-CO interaction is the continuous and large decrease in both top and bridged site vibrational frequencies as the CO coverage is decreased at constant potassium coverage (see Figure 4.12). This observation has its thermal desorption analog in the continuous broadening of the desorption peaks in the Θ_K=0.3 TDS spectra (Figure 4.8). If one considers the CO

THERMODYNAMICS OF CO ADSORPTION ON TRANSITION METALS

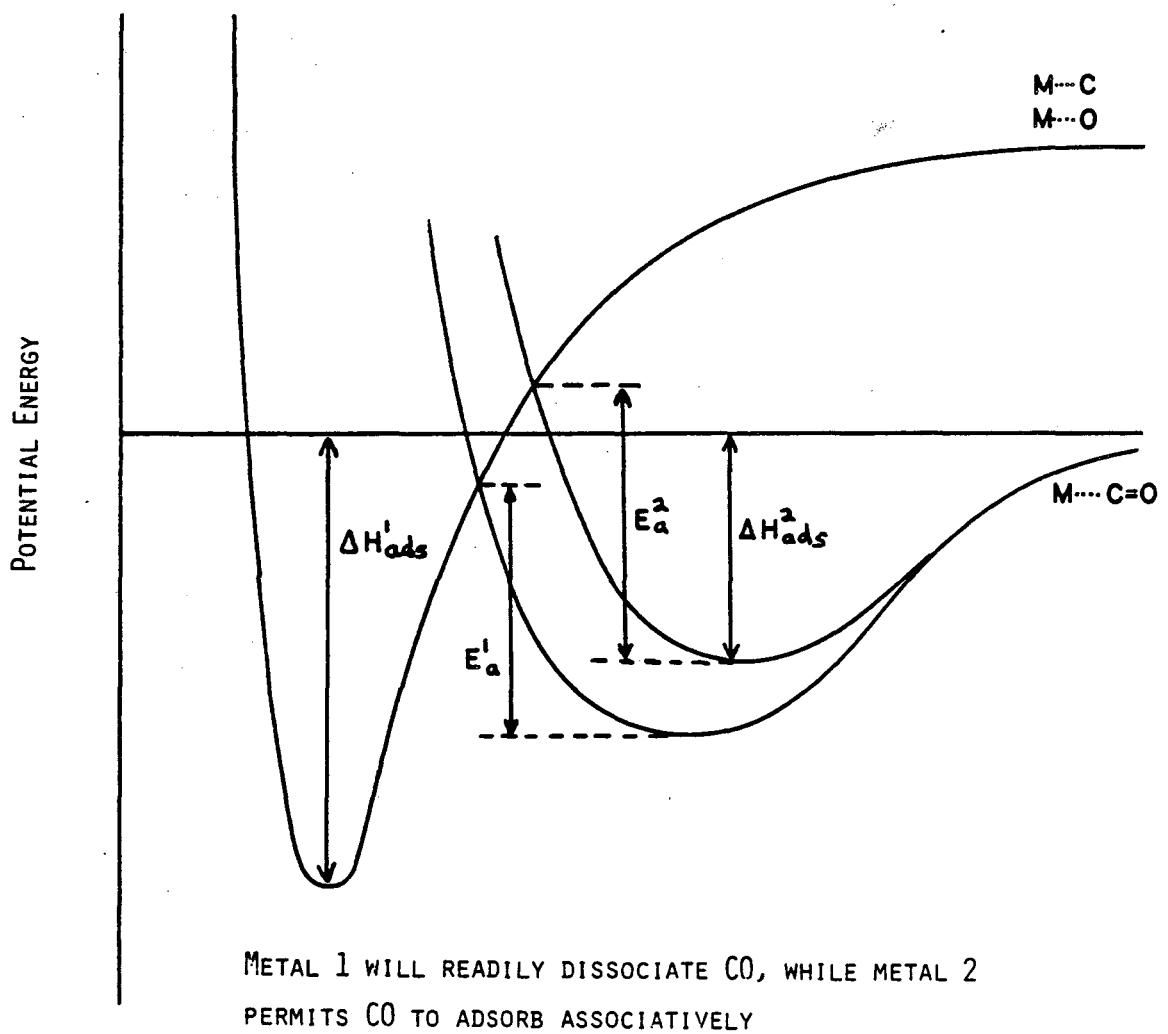

METAL 1 WILL READILY DISSOCIATE CO, WHILE METAL 2 PERMITS CO TO ADSORB ASSOCIATIVELY

XBL 833-8538

Figure 4.19

molecules at various coverages to be in competition for the excess charge on the platinum provided by a fixed number of potassium atoms, then both the TDS and HREELS observations support the model of electron backdonation. When fewer CO molecules are chemisorbed at a fixed potassium coverage, the larger amount of backdonation per CO molecule leads to an increased adsorption energy and decreased vibrational frequency.

The change in CO adsorption site from linear to bridged with increasing potassium coverage is striking. Nieuwenhuys (1981) has shown that the degree of electron backdonation increases with the lowering of the work function of a metal surface. Our results not only indicate an increased heat of adsorption and decreased vibrational frequency due to the decreased work function, but also a change in CO site location. By continuously lowering the work function of the Pt surface by the adsorption of potassium, we are changing the most energetically favorable site location from top to bridged. This tendency has also been noted by Gonzales (1982) in high pressure supported catalyst studies. It must be noted that we cannot rule out the existence of the threefold site CO molecule when the stretching frequencies decrease to their low coverage values.

Dipole-dipole interactions have been postulated for the CO-CO interaction on clean Pt(111), as well as on many other surfaces. As discussed by Crossley and King (1980), the 40 cm^{-1} increase of CO stretching frequency as the CO coverage is increased on clean Pt(111) is due to dynamic dipole-dipole coupling interactions. The corresponding contribution cannot be readily determined for the K-CO coadsorbed

system, but we believe increased backdonation is the dominant contribution accounting for the 325 cm^{-1} decrease in the bridge bonded vibrational frequency as the CO coverage is decreased at θ_K=0.3.

The idea of charge interactions has been proposed for other systems, for instance, to explain the promoting effect of potassium for the catalyzed hydrogenation of CO (Dry, 1969; Benziger, 1980; Broden, 1979) and for the ammonia synthesis (Ozaki, 1979; Ertl, 1979) over iron, and for CO interactions with alkali covered Ni(100) (Broden, 1980). This, however, is the first study that allows one to monitor significant changes in the magnitude of the backbonding effect without other complicating surface reactions occurring, such as dissociation.

The possibility of direct bonding (either covalent or ionic) between K and CO on platinum can be ruled out by our observations. Figure 4.12 shows that for a fixed potassium coverage, the CO stretching frequency merely increases gradually with increasing CO coverage. If direct K-CO interactions dominated, one would expect different vibrational frequencies for the CO molecules depending on their proximity to potassium adatoms. Once all CO sites closest to potassium atoms are occupied, the subsequently adsorbed CO molecules will find only clean platinum adsorption sites. This would give rise to multiple CO stretching peaks with wide variations in frequency. Although we do see some peak broadening, it is not enough to indicate significant bonding interactions.

Similarly, if direct K-CO interactions occurred, at low potassium coverages, the CO thermal desorption spectra should show two peaks, one at 600K for the K-CO species and one at 400K representative of potassium-free adsorption on Pt(111). This does not occur; we see a continuous

increase in the high temperature TDS tail with increasing potassium coverage. Within the range studied, CO molecules on the surface are seeing approximately the same "altered" substrate, regardless of their proximity to the K atoms. Thus the K-CO interaction appears not to be direct or localized, but delocalized over at least two or three interatomic distances.

Although the Pt(111)/K system studied here is different from the multicomponent surfaces used on actual industrial catalysts, the catalytic implications of our results are significant, especially with respect to CO hydrogenation reactions. The increase in backdonation strengthens the M-C bond and weakens the C-O bond, thus increasing the probability of dissociation and hydrogenation (Campbell, 1982). Furthermore, the increased binding energy means that the surface residence time of adsorbed CO will increase. Both these consequences should lead to the formation of longer chain hydrocarbons, as will be discussed in Chapter 5.

4.2 Benzene adsorption on potassium-dosed Pt(111).

4.2.1 Thermal desorption spectroscopy studies.

The thermal desorption spectra for molecular benzene adsorbed on a clean Pt(111) crystal held at room temperature are shown in Figure 4.20. For higher coverages, these spectra are in reasonably good agreement with previously reported results (Tsai, 1982). They show two overlapping desorption peaks centered at approximately 375 and 450K. (At lower coverages Tsai shows two peaks filling simultaneously; our spectra show the peaks filling sequentially.) Generally, 2 L exposures are required to achieve saturation coverage. The benzene thermal desorption peak shoulder in Figure 4.20 extends to room temperature at high exposures. Figure 4.21 shows the benzene desorption spectra when the crystal was cooled with liquid nitrogen. Several new features arise. Most noticeable is that at least two or three more desorption peaks appear whose temperature of desorption (180-250K) is above that of multilayer condensed benzene, yet considerably less than that of the more strongly adsorbed benzene.

The benzene thermal desorption spectra for 1 L exposures (following room temperature exposure) at several potassium coverages are shown in Figure 4.22. As potassium pre-coverage is increased, we see a decrease in the temperature of the maximum benzene desorption rate. This decrease is at first displayed by a broadening on the low temperature side of the peak. Then, at moderate K coverages, the high temperature edge also shifts down. At higher coverages, $\Theta_K > .4$, benzene could no longer be adsorbed at 300K. We show in Figure 4.23 the thermal desorption spectrum of benzene on a liquid nitrogen cooled sample.

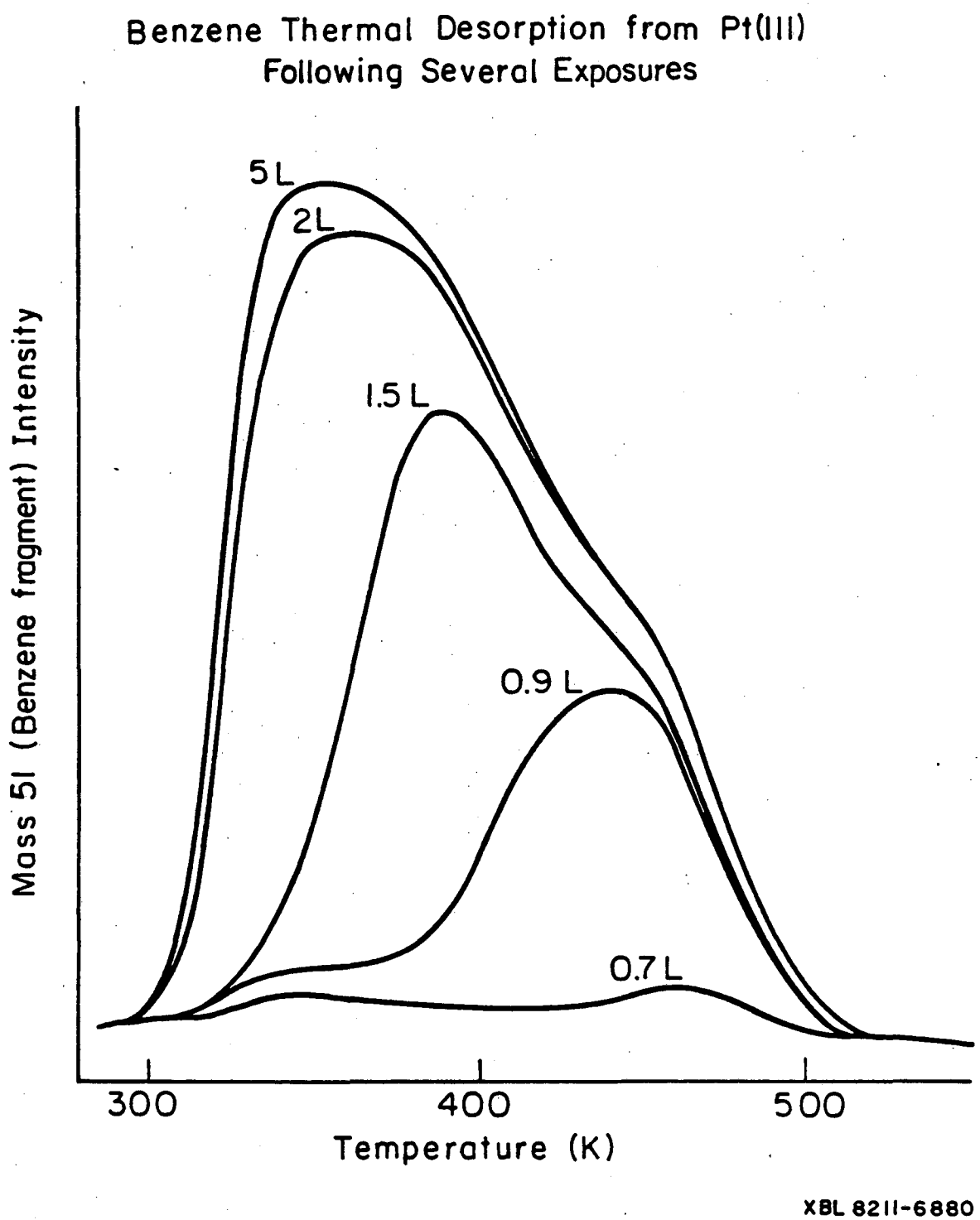

Figure 4.20 Benzene thermal desorption following room temperature exposure to Pt(111).

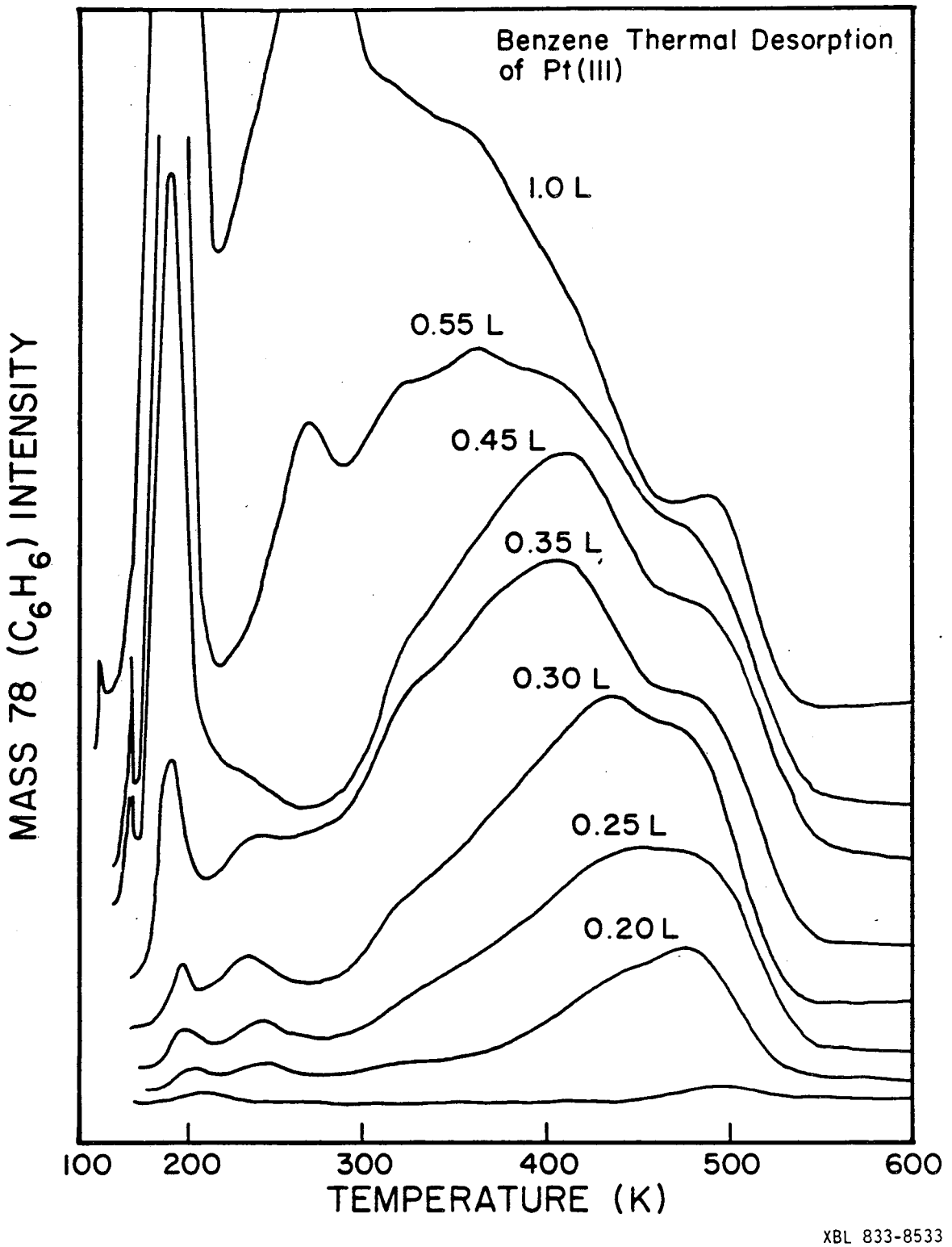

Figure 4.21 Benzene thermal desorption following low temperature exposure.

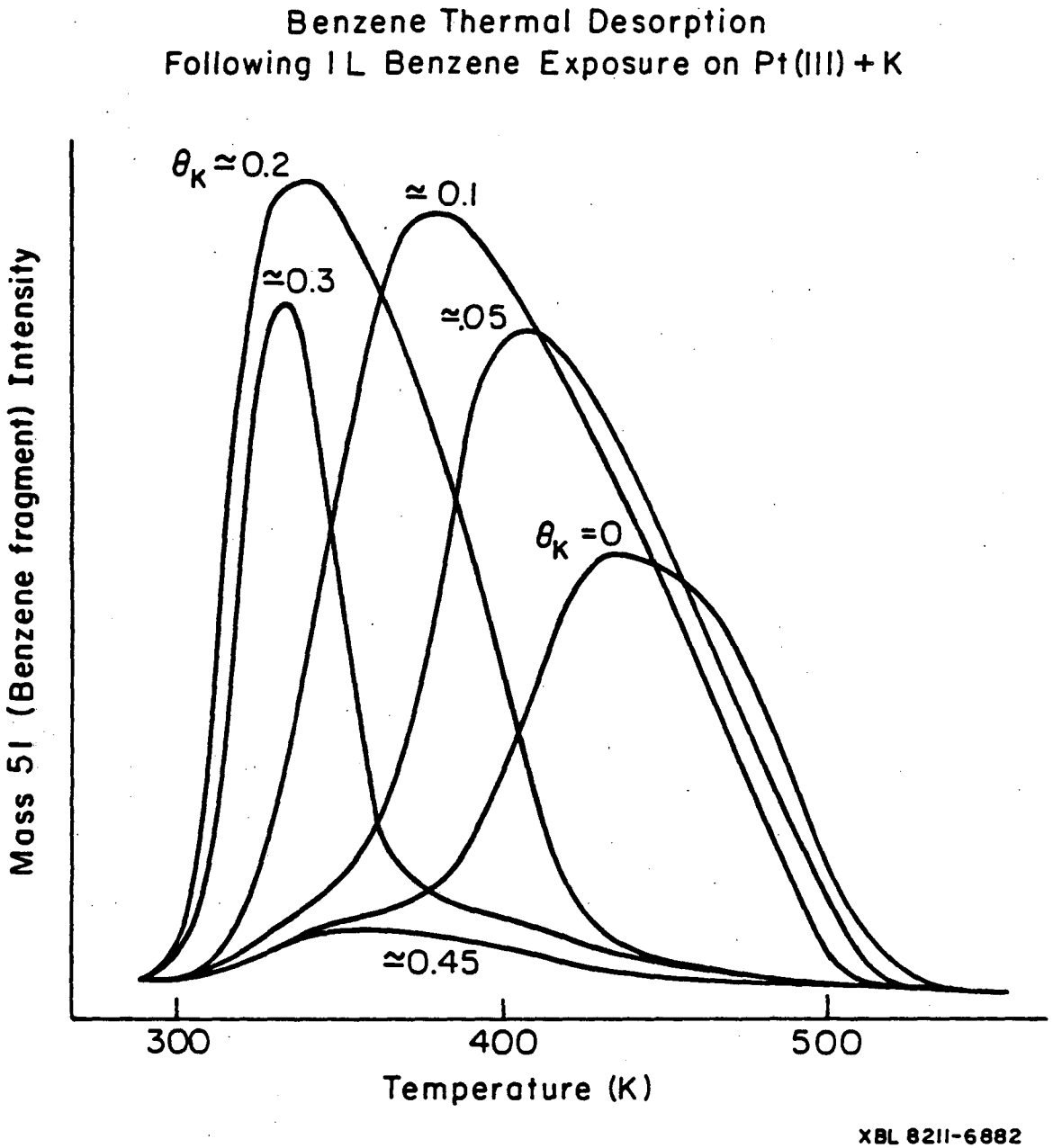

Figure 4.22 Benzene thermal desorption from K/Pt(111) following room temperature exposure.

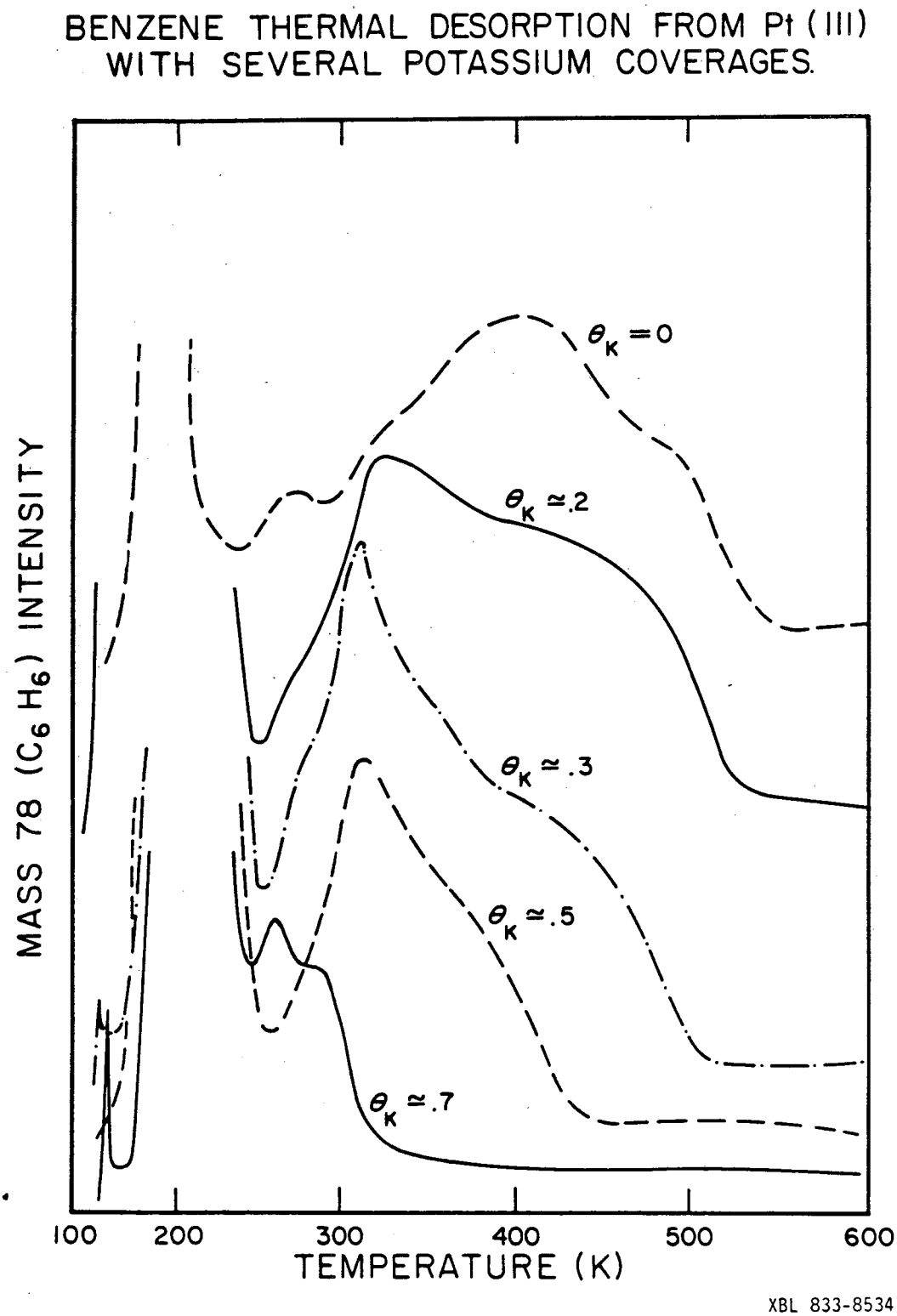

Figure 4.23 Benzene thermal desorption from K/Pt(111) following low temperature exposure.

The same trends are seen as in Figure 4.22, but now the benzene desorption edge maximum is seen to decrease by as much as 200K at high potassium coverages. In Figure 4.24 is shown the benzene thermal desorption spectra from clean, potassium covered, and oxidized-potassium covered Pt(111). It is interesting to note that the oxygen appears to cancel the effect of potassium on benzene.

4.2.2 Photoemission studies.

Figures 4.25 - 4.28 show the UPS spectra for benzene coadsorbed with various coverages of potassium on Pt(111). Benzene adsorbed on clean platinum causes a large decrease in emission from the peak just below E_f (Figure 4.25), similar to what is observed with carbon monoxide and potassium. Three other overlapping features grow in between 3 and 10 eV, labeled #1, #2, and #3 in Figures 4.26 and 4.27. The peaks are also observed for benzene on other metals and can be associated with the π and σ levels of gas phase benzene, as described in the discussion. Also note the large decrease in work function with increasing benzene exposure on the clean Pt(111) surface, supporting the idea that benzene is a donor on metals (Kotz, 1977). Several interesting changes occur as potassium is added. Peaks #1 and #3 shift to higher binding energy, see Figure 4.28. There are also changes in their relative heights: for high potassium coverages the peak heights for #1 and #3 grow much larger than peak #2.

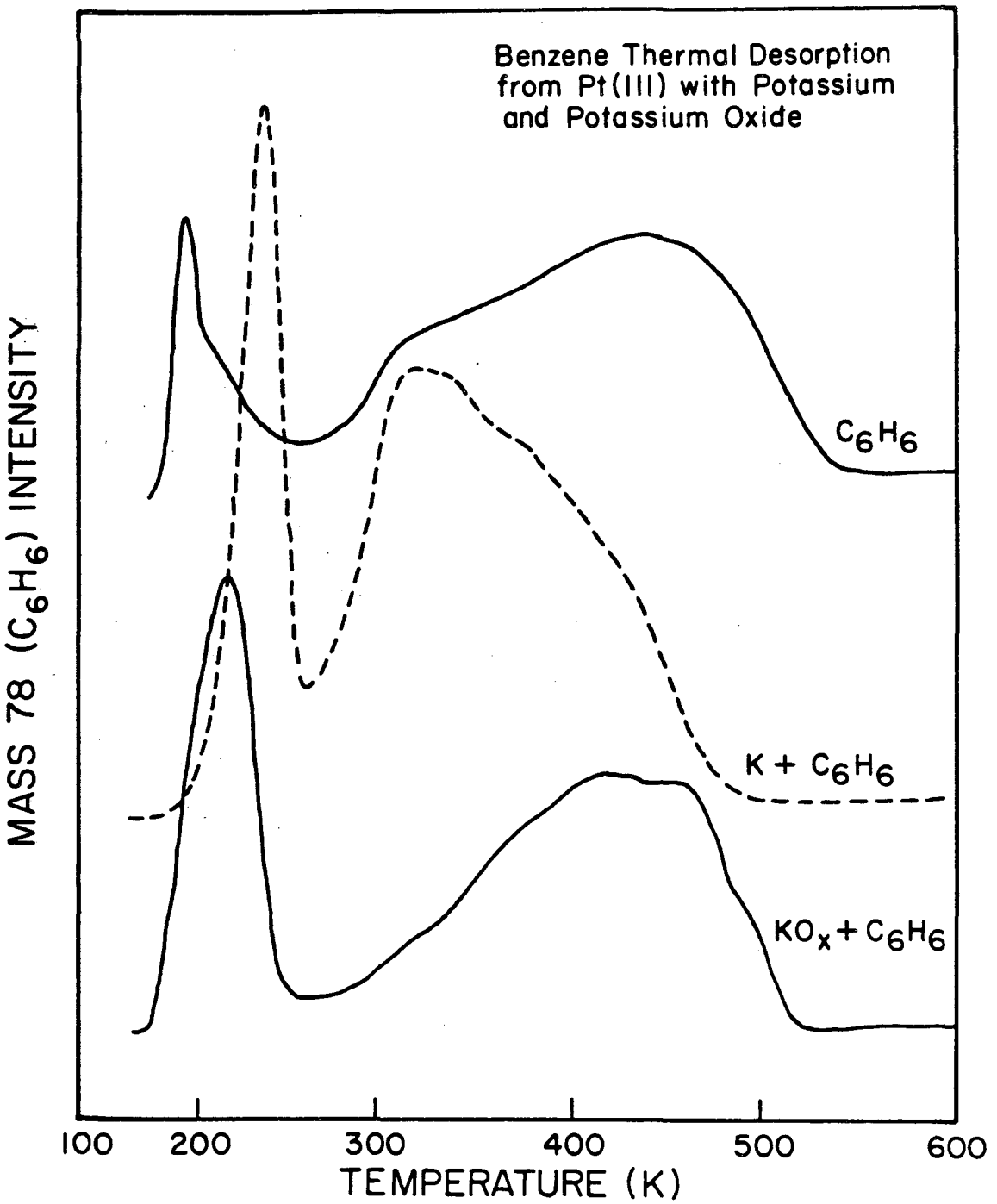

XBL 833-8535

Figure 4.24

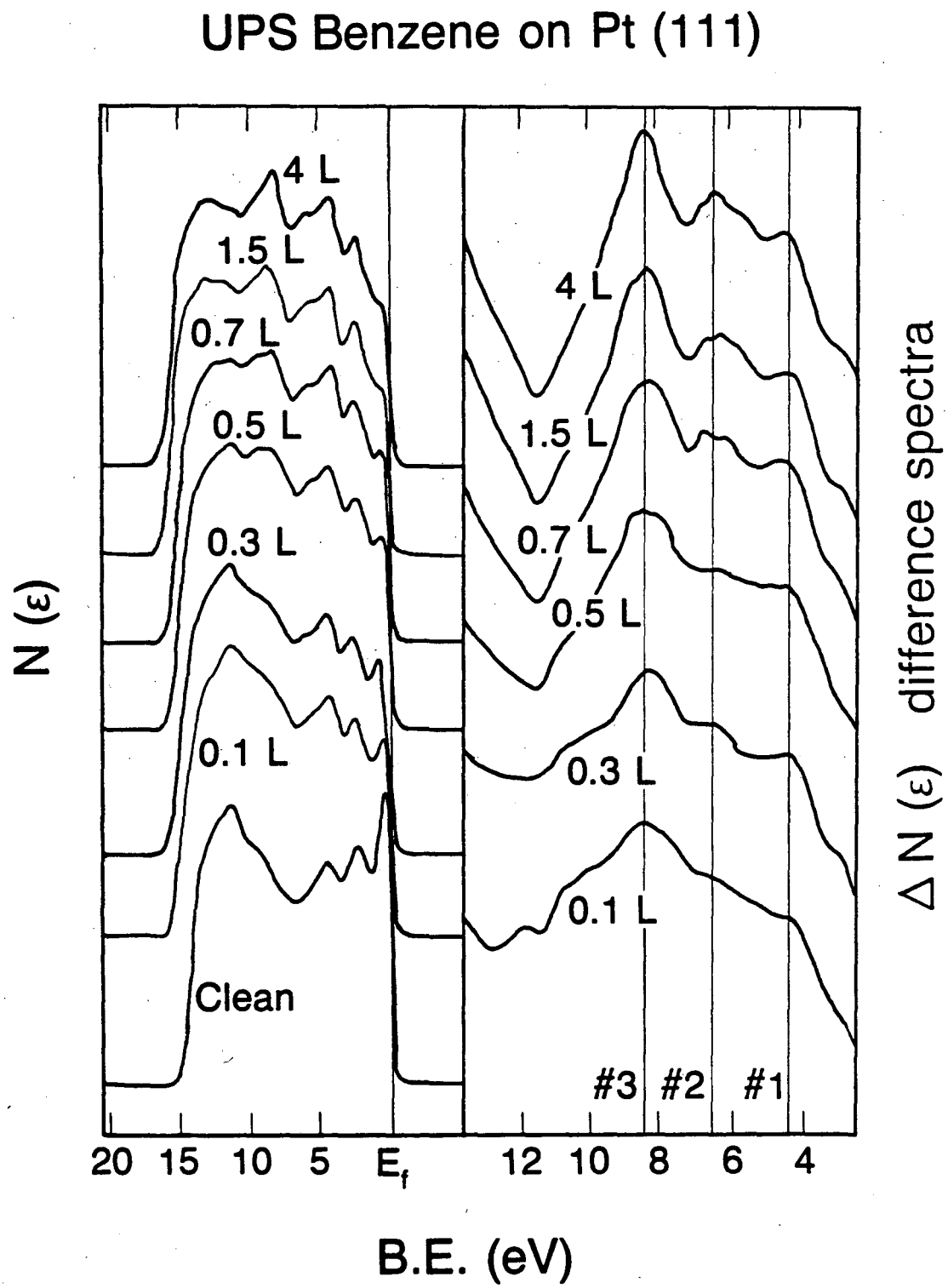
UPS Benzene on Pt (111)
4 L
1.5 L
0.7 L
0.5 L
0.3 L
0.1 L
Clean
N (ε)
4 L
1.5 L
0.7 L
0.5 L
0.3 L
0.1 L
#3
#2
#1
ΔN (ε) difference spectra
20 15 10 5 E_f
12 10 8 6 4
B.E. (eV)
XBL 838-3091

Figure 4.25

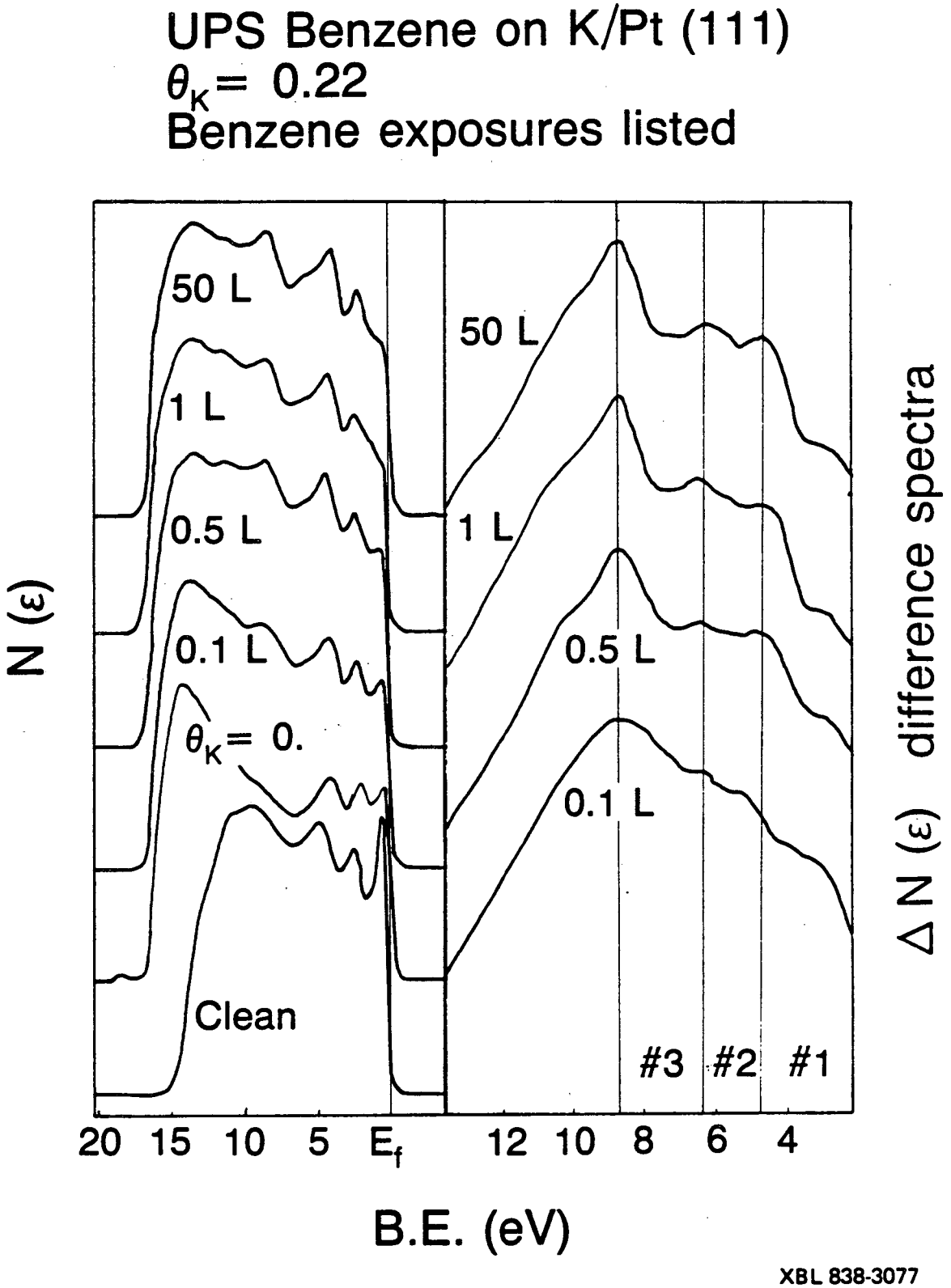
UPS Benzene on K/Pt (111)
θK= 0.22
Benzene exposures listed
50 L
1 L
0.5 L
0.1 L
θK= 0.
Clean
N (ε)
20 15 10 5 Ef
B.E. (eV)
50 L
1 L
0.5 L
0.1 L
#3 #2 #1
12 10 8 6 4
Δ N (ε) difference spectra
XBL 838-3077

Figure 4.26

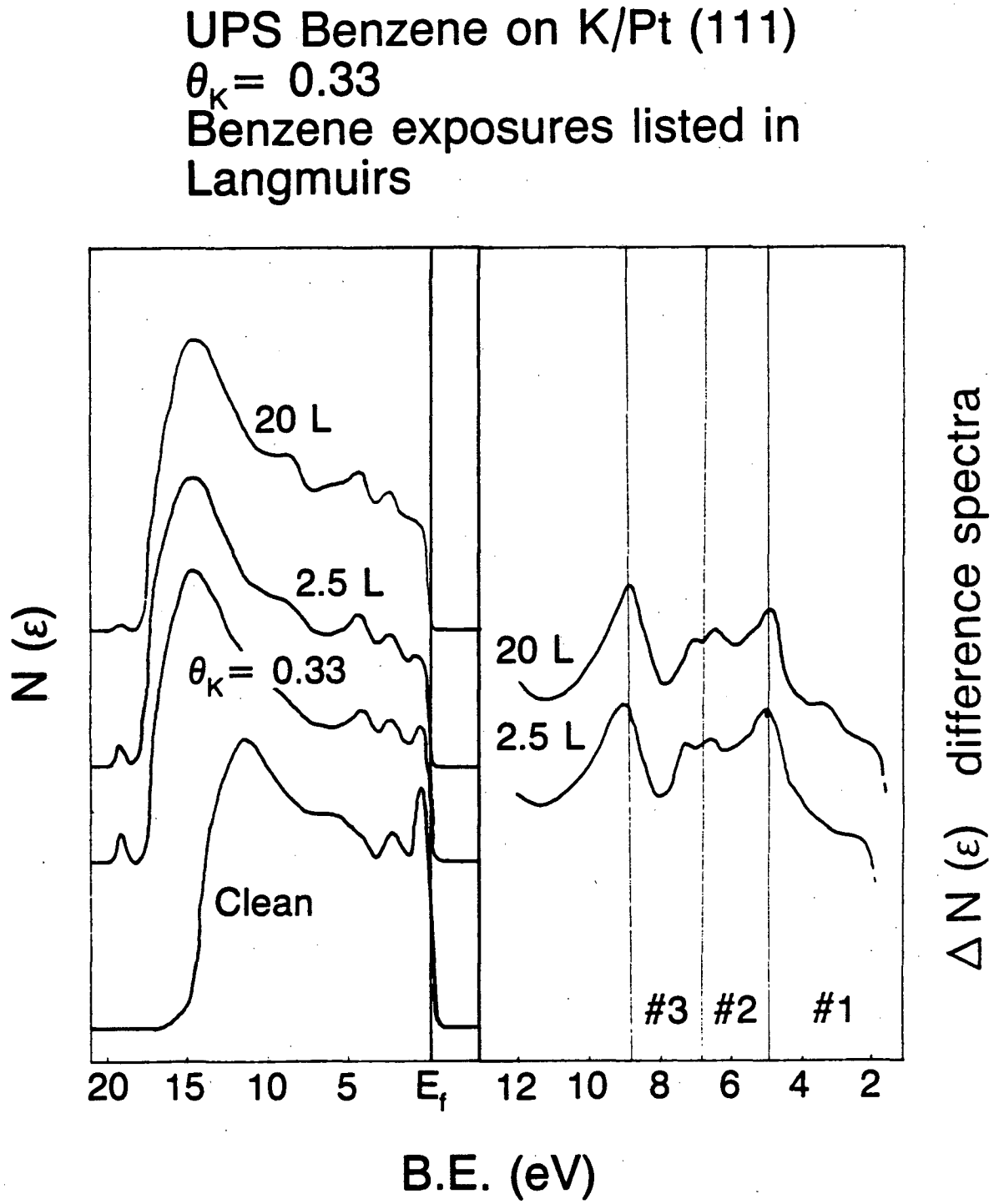

XBL 838-3073

Figure 4.27

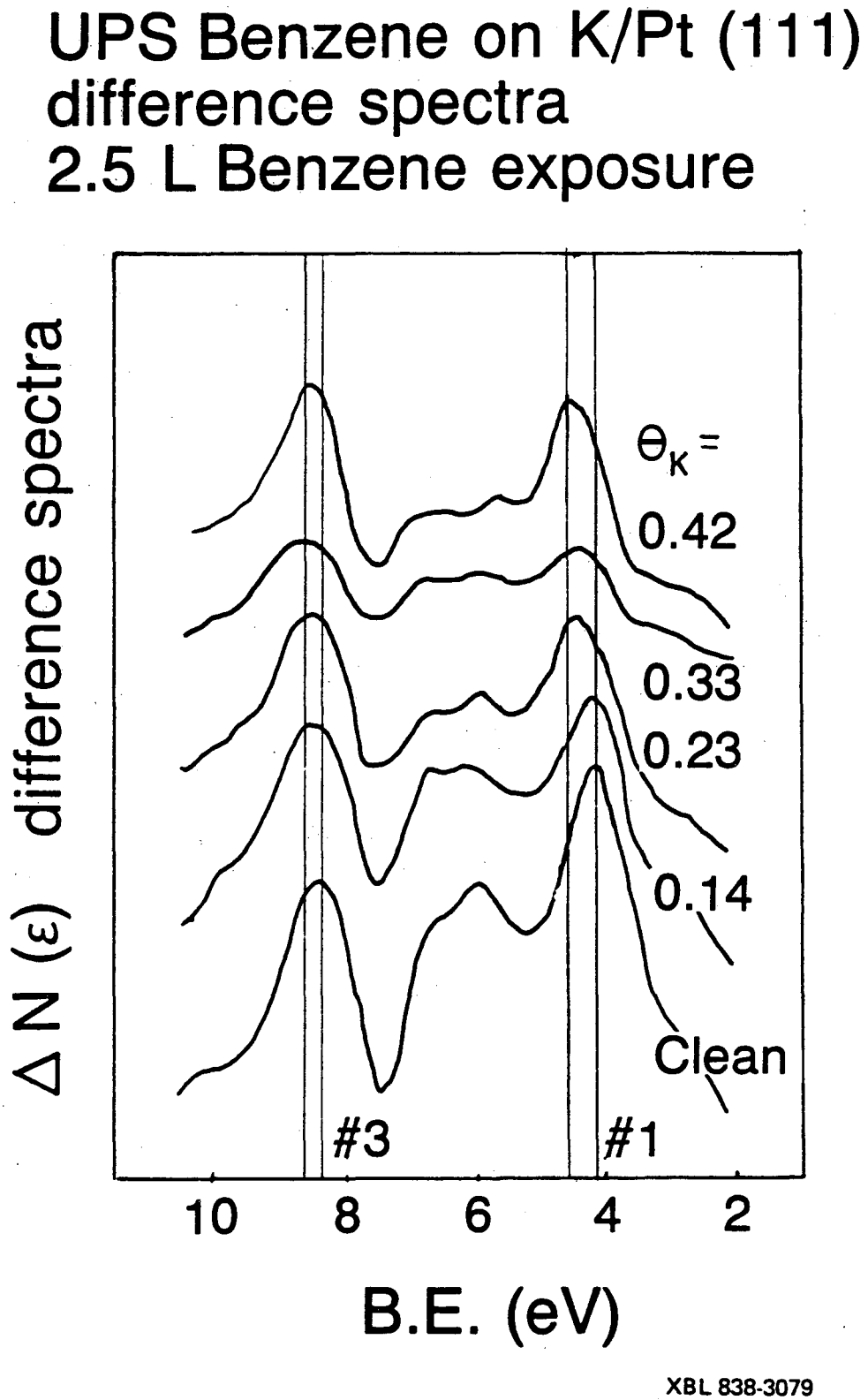
UPS Benzene on K/Pt (111)
difference spectra
2.5 L Benzene exposure
ΔN (ε) difference spectra
θK =
0.42
0.33
0.23
0.14
Clean
#3
#1
10
8
6
4
2
B.E. (eV)
XBL 838-3079

Figure 4.28

4.2.3 Discussion.

Upon heating a benzene overlayer on clean Pt(111), a fraction of the benzene will desorb molecularly at temperatures below 500 K , while the remainder dissociates giving off a broad H_2 desorption peak between 400 and 750K. This behavior is also seen on other transition metals and crystallographic faces, but the Pt(111) surface appears unique in its low activity for C-C and C-H bond-breaking (Somorjai, 1981).

It has been proposed that dissociation of benzene occurs at steps or other defect sites because of geometric (steric) and/or electronic variations at these sites. We found that all of the adsorbed benzene dissociated upon heating for exposures of up to ≈ .4 L, and most of the additional benzene desorbed intact up to exposures of 2 L. For exposures greater than 2 L at room temperature, the sticking coefficient became zero; presumably the first monolayer was saturated at this point. Thus, our results imply that benzene molecules on the flat Pt(111) terraces can readily dissociate upon heating (as well as at step/defect sites) since the amount dissociated is much in excess of the estimated defect site concentration (<5%).

On Pt(111), that fraction of benzene that desorbs molecularly above room temperature yields two peaks in the thermal desorption spectrum at approximately 375 and 450 K. The appearance of these peaks is not yet fully understood although several interpretations are possible to explain their origin: lateral interactions at high coverages, different surface structures (as revealed by LEED), different sites being occupied (presumably top or threefold), etc. (Lehwald, 1978; Lin, 1983).

Much more of the benzene desorbed intact upon heating when the Pt

surface was pre-dosed with potassium: this is seen both from the larger thermal desorption peak area as well as the smaller fraction of carbon that remains on the surface (as detected by AES) after heating. In addition, we observed a lower temperature for the benzene desorption rate maximum as we added potassium. Desorption and decomposition should be viewed as competing reaction pathways: however, only the desorption energy (and pathway) is strongly affected by potassium coadsorption.

Both the decrease in desorption temperature and the increased amount of molecular desorption imply that the benzene-platinum bond strength is weakened when potassium is present. Several explanations can be proposed. Benzene is thought to be an electron donor in transition metal complexes, with the π-orbital often involved in a symmetric coordination with the metal atom or ion (Kotz, 1977; Muetterties, 1983). So, one might expect that if the platinum surface is already "electron-rich" due to charge transfer from potassium, the benzene might not be able to donate charge, hence bond, as strongly.

This type of explanation however, is probably too simplistic, and a more complete understanding of the electron energy levels is required to develop even a qualitative model of the potassium induced changes of adsorption. Figure 4.29 shows the molecular orbital diagram for benzene-chromium (based on Kotz, 1977, and Muetterties, 1983). Of interest here are the molecular orbitals involved near the "Fermi level," i.e. the highest occupied and lowest unoccupied molecular orbitals. All of the filled orbitals in the benzene chromium bond are either bonding or non-bonding between the benzene π-ring and chromium d-orbitals. The

Valence Orbitals of Benzene-Cr: Energy levels are approximate

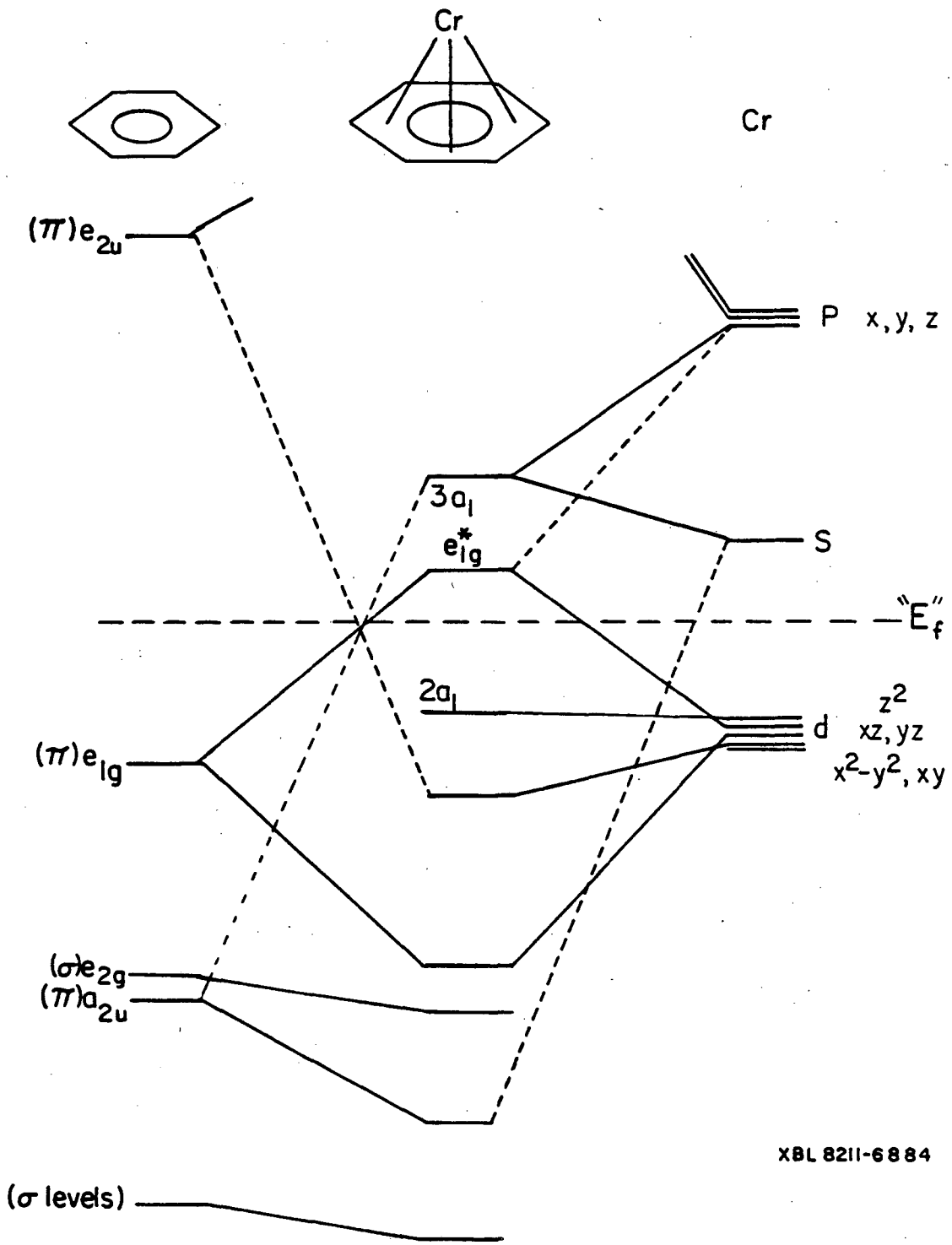

Figure 4.29

lowest unoccupied level, however, is "antibonding" between the benzene and chromium orbitals. Consequently, if one electron were added to the system, this electron would fill the e_{1g}^{*} antibonding level, weakening the metal-benzene interaction.

Of course there is quite a difference between a chromium atom and a platinum surface, but the general character of the bonding is the same. This has been confirmed by recent angularly resolved and photon polarization UPS studies (Nyberg, 1979; Hofmann, 1981; Fischer, 1978; and Netzer, 1983.) In both the gas phase and adsorbed cases, there is a symmetric coordination to the metal atom(s) and benzene can be considered primarily as an electron donor. Two interesting features appeared in our UPS studies. First, the shift to higher binding energy of the benzene peaks #1 and #3 with potassium is consistent with the idea that the benzene levels, or more precisely the benzene vacuum reference level (Luftman, 1983), is moving down relative to the potassium free case. This, it should be remembered, is an initial state effect, since added final state screening by potassium should shift the peaks the other way. That the peaks move to higher binding energy also implies that the e_{1g}^{*} level should now be closer to the Fermi level. The orbital levels are broad enough when adsorbed on the surface that it is reasonable to consider partial occupation, it is not necessary to require that the levels be either fully occupied or empty. Thus, a continuous decrease in the work function could lead to an increasing occupation of the e_{1g}^{*} level. This would then result in a continuous weakening of the metal-benzene bond as was observed by TDS.

The second observation is that peaks #1 and #3 show an increase in

intensity relative to peak #2. Peak #1 is the benzene e_{1g} (π) orbital and peak #3 contains contributions from 4 different levels, one of which is the a_{2u} (π) orbital while the other three are σ-type orbitals. Peak #2 represents the e_{2g} (σ) level. It is tempting to suggest that the π derived orbital peaks might be the only ones which are enhanced by potassium adsorption, while the σ levels remain constant. This would be surprising since the benzene bond is being weakened. (The data are inconclusive on this point, and require angularly resolved and polarized radiation studies.)

Another complementary effect would be the inability of benzene to donate charge into the metal if the population of the 6s Pt level was increased due to the potassium. We think, however, that this is a minor perturbation in comparison to donation into the e_{1g}^* anti-bonding level, because the analogous effect of bond weakening was not seen for CO. Recent calculations by Anderson (1983) show that changes in the occupation of the benzene e_{1g} antibonding level cause changes in the bending of the hydrogen atoms on benzene toward or away from the surface. Such calculations, however, yield information mainly on the hybridization of the carbon orbitals, not on the ease of C-H bond scission.

The apparent "screening" of the potassium by oxygen was also an interesting observation. K_2O is a promoter of both the ammonia synthesis and CO hydrogenation reactions on iron. Our result, however, implies that electronic promotion might not occur if the potassium is fully oxidized. We suggest that under the reducing conditions of both reactions, the potassium is not fully oxidized, since it is still capable of causing significant electronic promotion effects. It is also

interesting to note that this "screening" ability of oxygen was less noticeable on CO (our work) and N_2 (Paal, 1981).

4.3 Nitric Oxide (NO) adsorption on potassium-dosed Pt(111).

4.3.1 Thermal desorption studies.

The NO (mass 30) thermal desorption spectra (see Figure 4.30) are in agreement with previous work (Gland, 1980). Two sequentially filled states at 430 and 340 K are observed in the spectra. In addition, small amounts of N_2 (Figure 4.31) and traces of N_2O (Figure 4.32) were also desorbed. The relative distributions of nitrogen containing species which desorb are shown in Figure 4.33. After each experiment, AES and LEED analysis of the surface showed the presence of small amounts of platinum oxide, see Chapter 3. This decomposition of NO is attributable to the presence of defect sites (Gland, 1980) on the (111) surface plane estimated to be < 5% of monolayer coverage. Sharp (2x2) overlayer LEED patterns were observed for NO exposures of > 1 L.

Figures 4.34, 4.35, and 4.36 show the desorption spectra for NO, N_2 and N_2O obtained by varying the initial θ_K and dosing the surface with 1 L NO. The general feature observed with increasing potassium coverage is an increased yield of N_2 and N_2O in the desorption spectra indicating that NO was dissociated by potassium. As θ_K is increased, the intensities of the 340 and 430 K NO desorption peaks rapidly decrease and a broad desorption peak appears between 600 and 700 K, due to recombination of surface nitrogen and oxygen. No significant shifts in desorption temperatures of the peaks occur for the 340 and 430 K desorption states. Figure 4.37 presents the integrated distributions of N atoms among the NO, N_2, and N_2O species observed desorbing from the surface. The

intensity of the NO desorption peak decreases steadily with increasing θ_K.

Figures 4.38–4.41 show the desorption spectra and integrated distributions for $\theta_K = 0.5$ and NO doses of between 0.1 and 1 L. NO does not become the dominant desorbing species until the initial NO dose is greater than 0.5 L. This coincides with the appearance of the of the 340 K desorption state in the NO desorption spectra, (see Figure 4.38). In Figure 4.42 is shown the potassium desorption spectra following NO exposure to a potassium adlayer.

4.3.2 Discussion.

The general features of associative NO and CO adsorption on metals are similar. The major difference is that the gas phase NO molecule has one electron in the $2\pi^*$ antibonding orbital, while CO does not. NO was also found to react directly with potassium multilayers; hence potassium induced Pt-NO changes could not be verified.

Our data indicate, however, that NO was dissociated in an amount proportional to the potassium coverage on the surface. As seen in Figures 4.34 and 4.38 the dissociated NO adsorption state(s) filled first, followed by adsorption into the 340 and 430 K associatively adsorbed states. The undissociated states were not significantly altered in the presence of adsorbed potassium since their peak position remained essentially unchanged. On potassium, NO dissociates predominantly to N_2, with some N_2O.

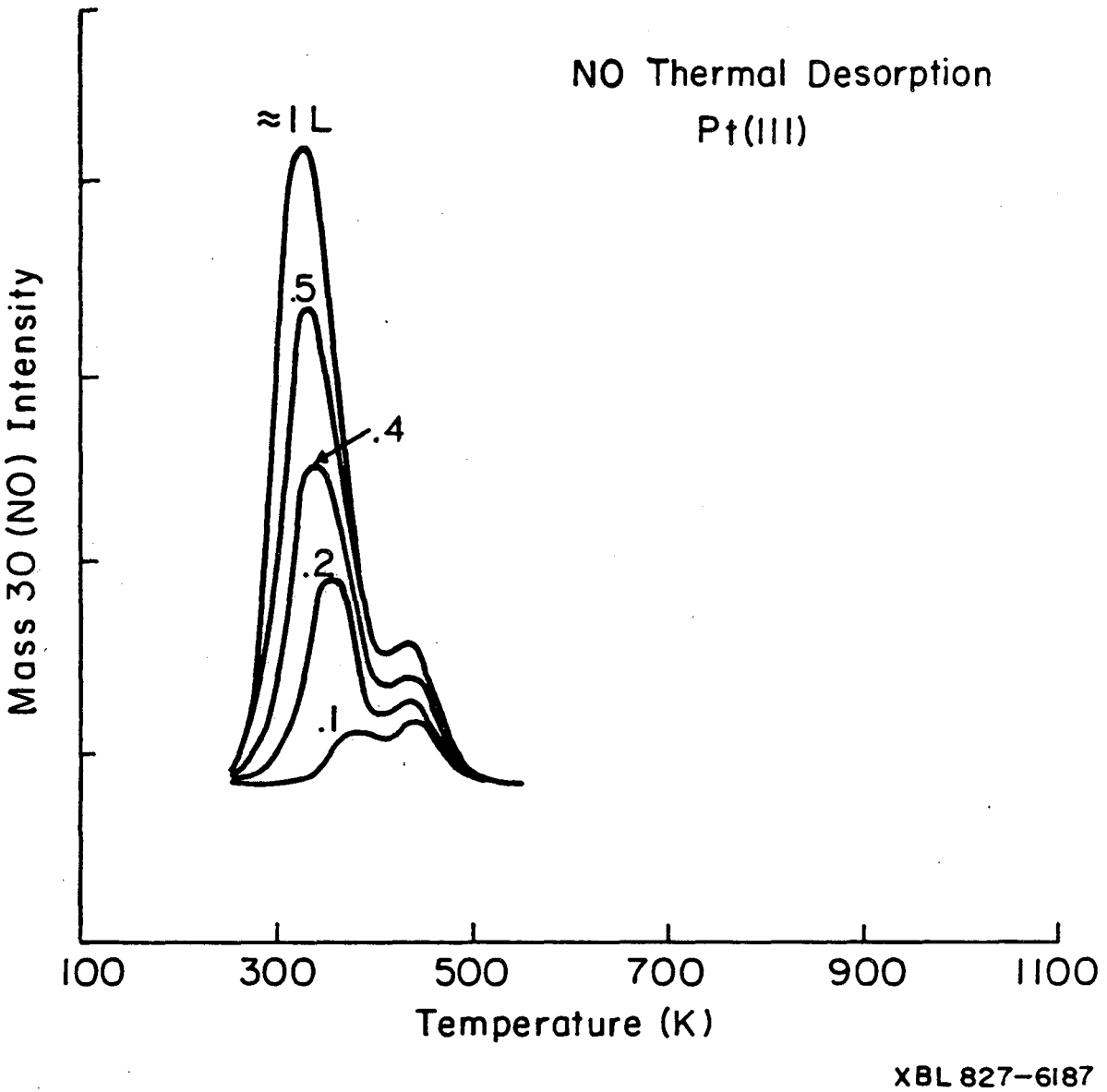
NO Thermal Desorption
Pt(111)
≈1 L
.5
.4
.2
.1
Mass 30 (NO) Intensity
100
300
500
700
900
1100
Temperature (K)
XBL 827-6187

Figure 4.30

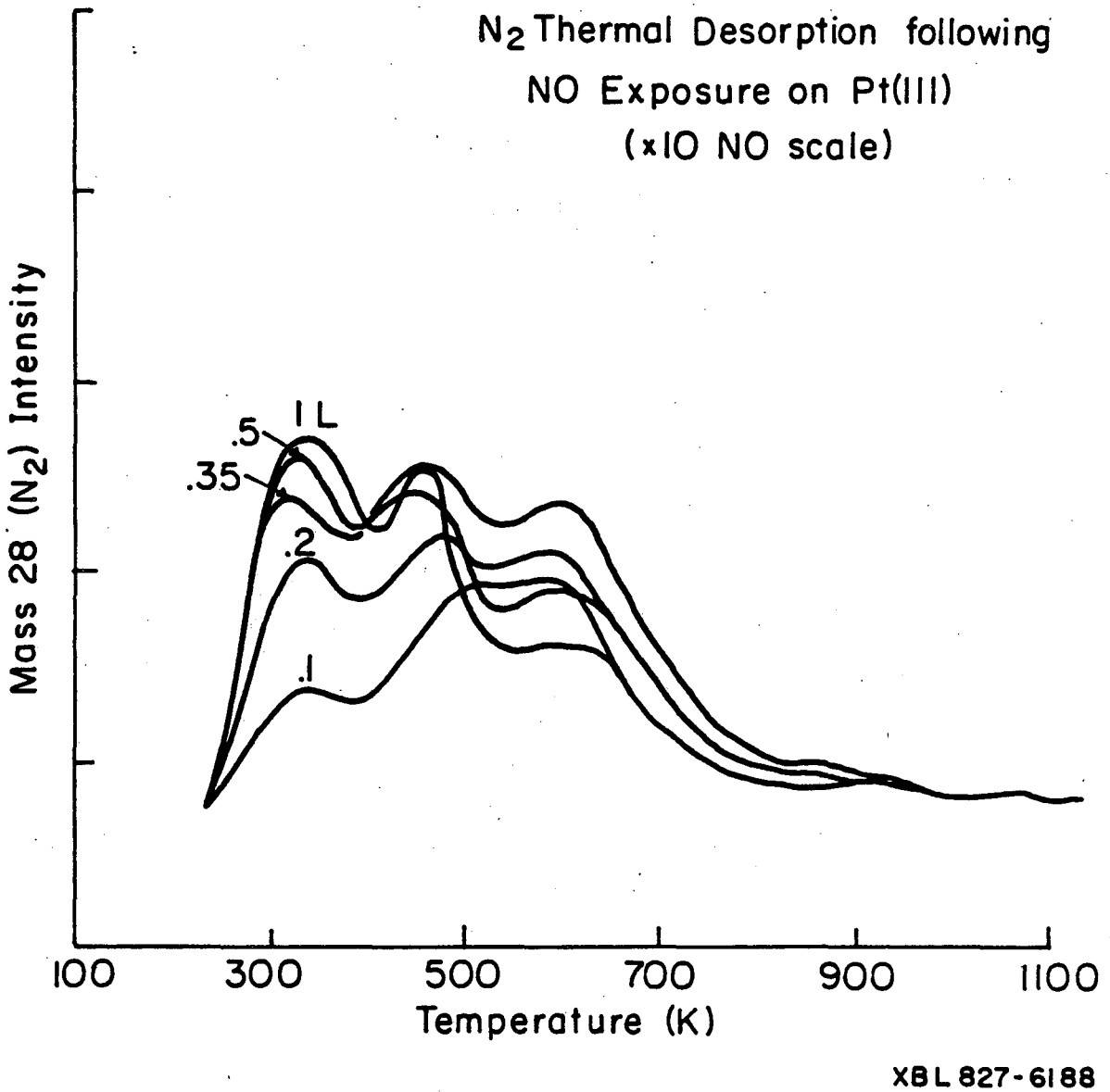
N2 Thermal Desorption following
NO Exposure on Pt(111)
(x10 NO scale)
Mass 28 (N2) Intensity
1 L
.5
.35
.2
.1
100
300
500
700
900
1100
Temperature (K)
XBL 827-6188

Figure 4.31

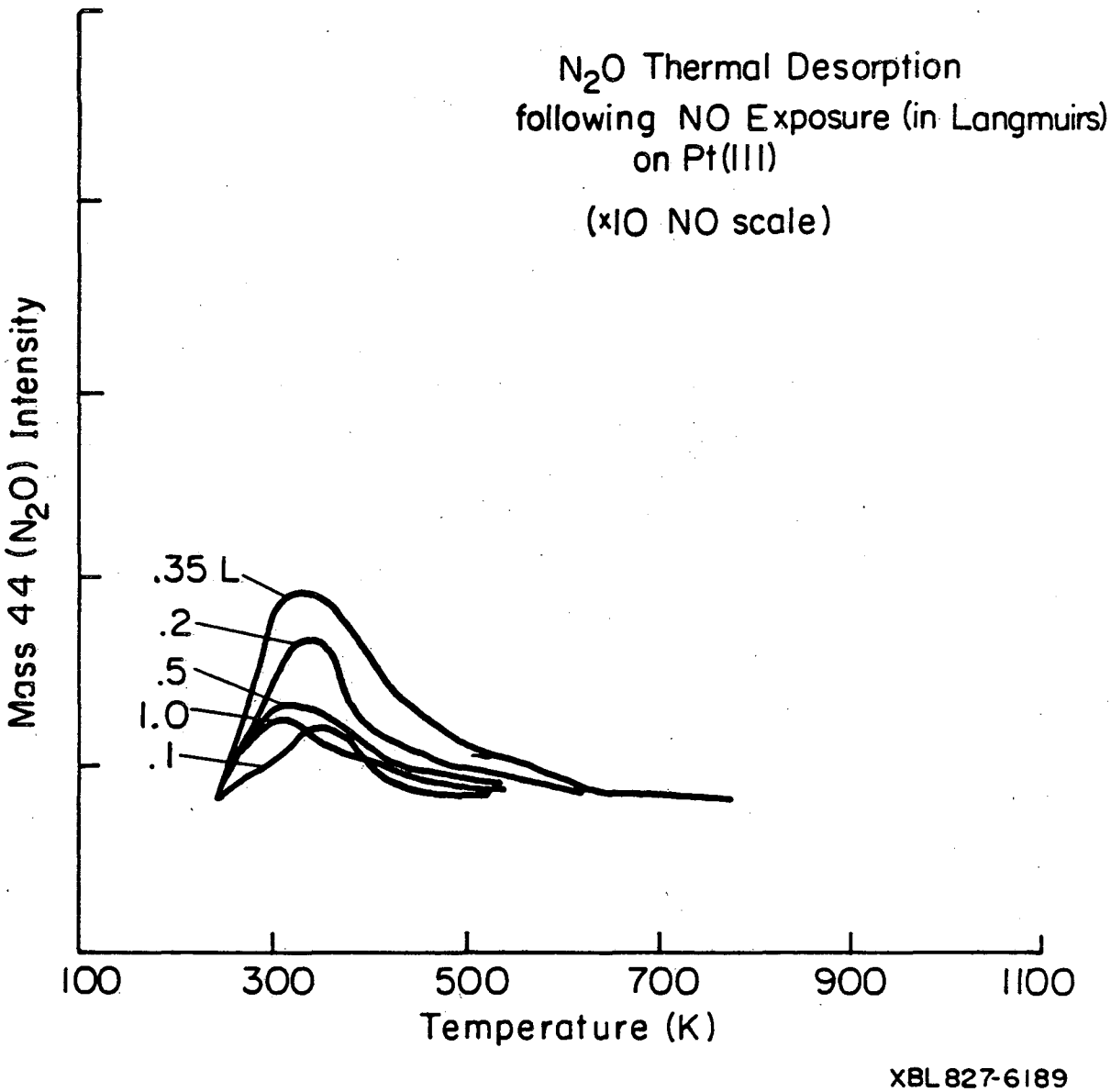
N_2O Thermal Desorption
following NO Exposure (in Langmuirs)
on Pt(111)
(x10 NO scale)
Mass 44 (N_2O) Intensity
.35 L
.2
.5
1.0
.1
100
300
500
700
900
1100
Temperature (K)
XBL 827-6189

Figure 4.32

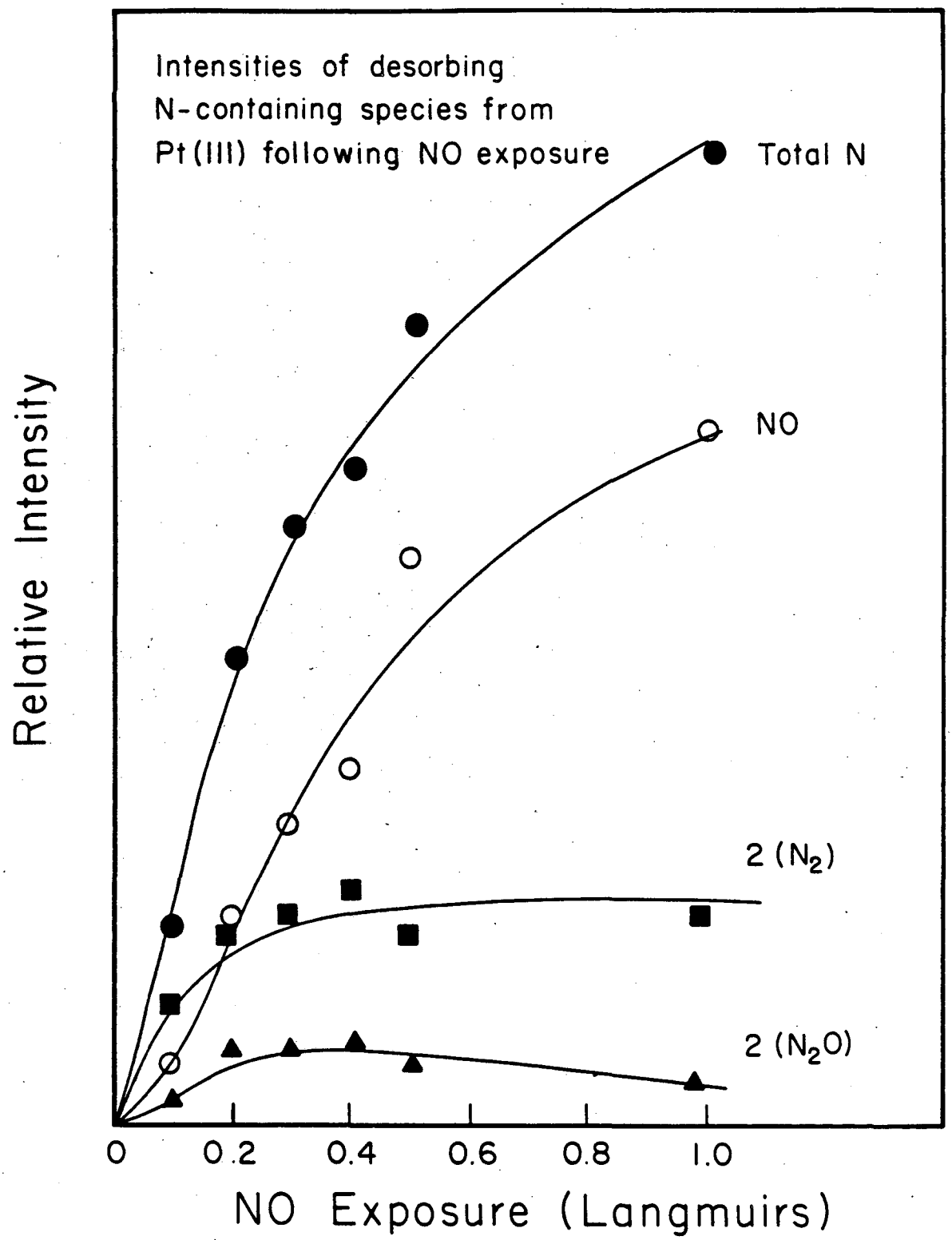

XBL 828-11090

Figure 4.33

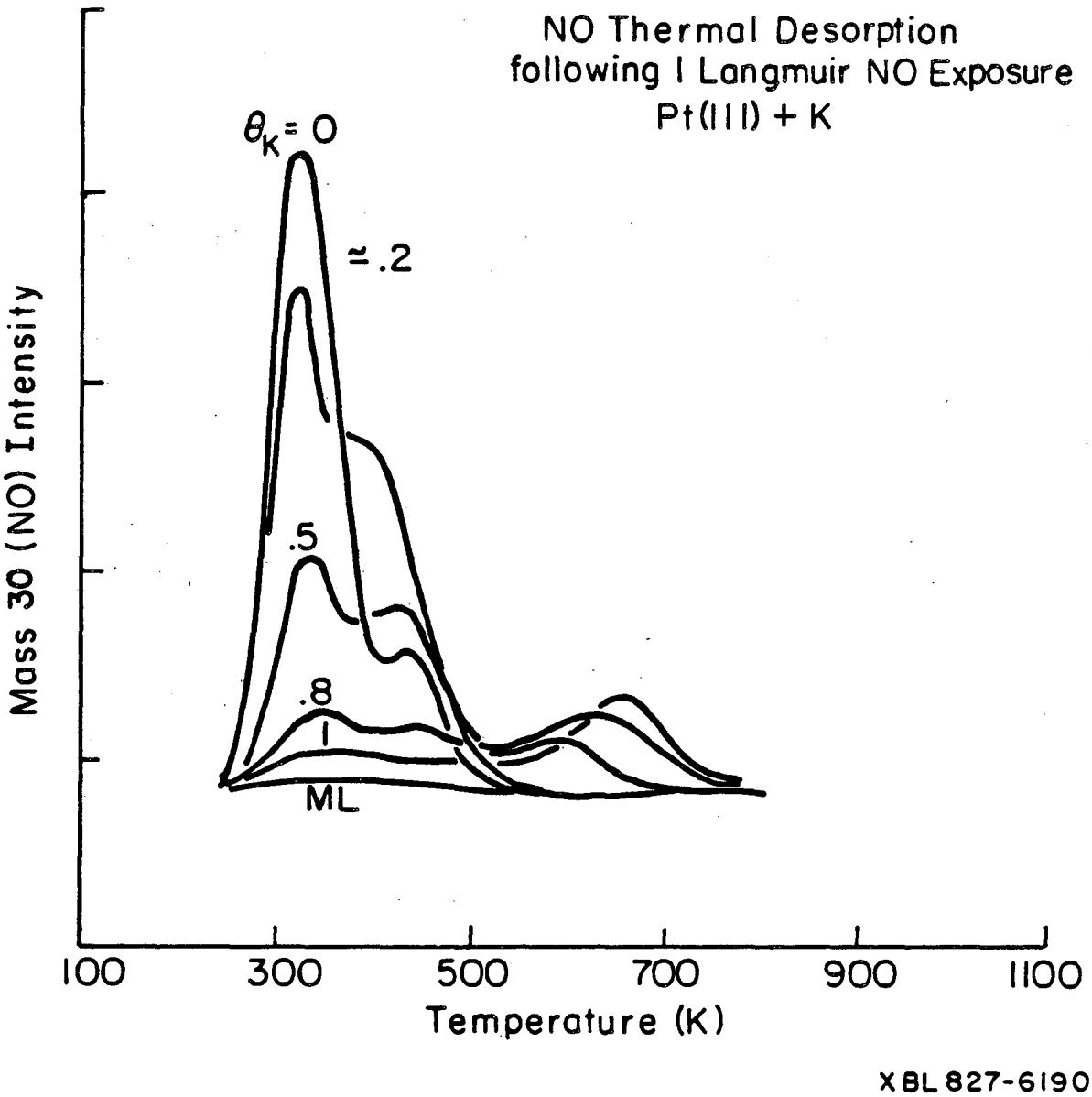
NO Thermal Desorption
following 1 Langmuir NO Exposure
Pt(111) + K
$\theta_K = 0$
≃ .2
.5
.8
1
ML
Mass 30 (NO) Intensity
100
300
500
700
900
1100
Temperature (K)
XBL 827-6190

Figure 4.34

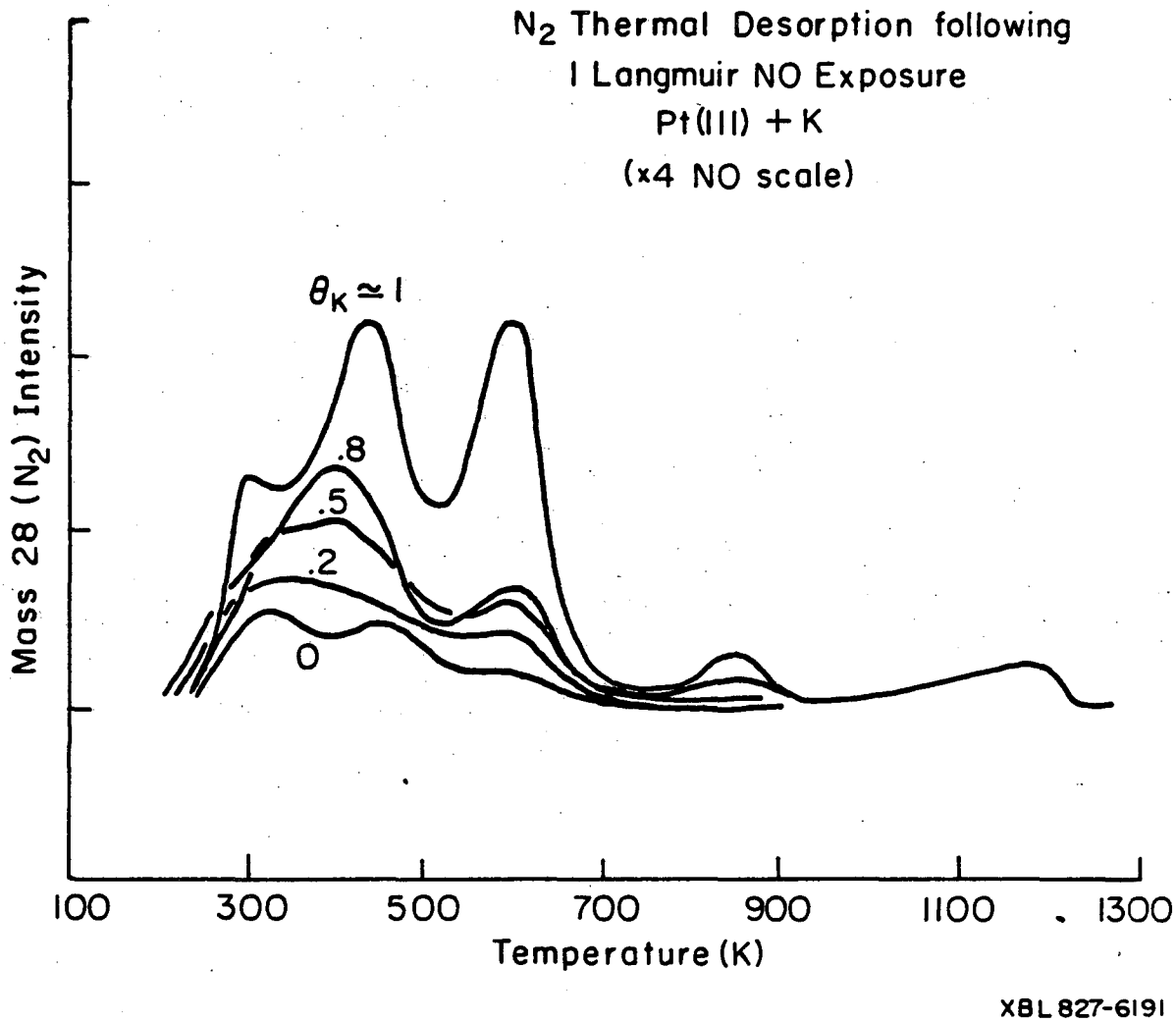
N2 Thermal Desorption following
1 Langmuir NO Exposure
Pt(111) + K
(x4 NO scale)
θK ≃ 1
.8
.5
.2
0
Mass 28 (N2) Intensity
100
300
500
700
900
1100
1300
Temperature (K)
XBL 827-6191

Figure 4.35

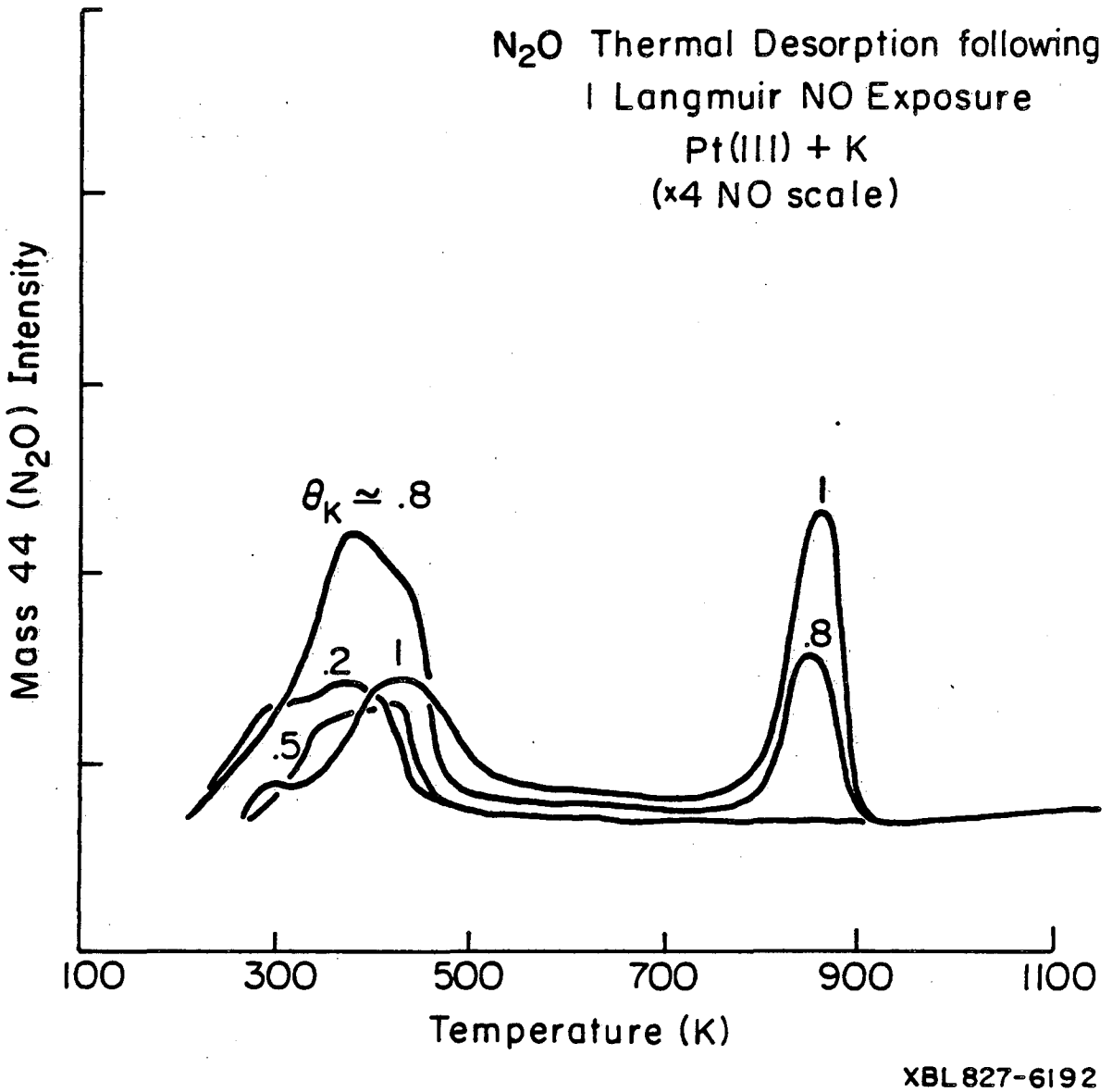
N2O Thermal Desorption following
1 Langmuir NO Exposure
Pt(111) + K
(x4 NO scale)
Mass 44 (N2O) Intensity
θK ≃ .8
.2
1
.5
1
.8
100
300
500
700
900
1100
Temperature (K)
XBL827-6192

Figure 4.36

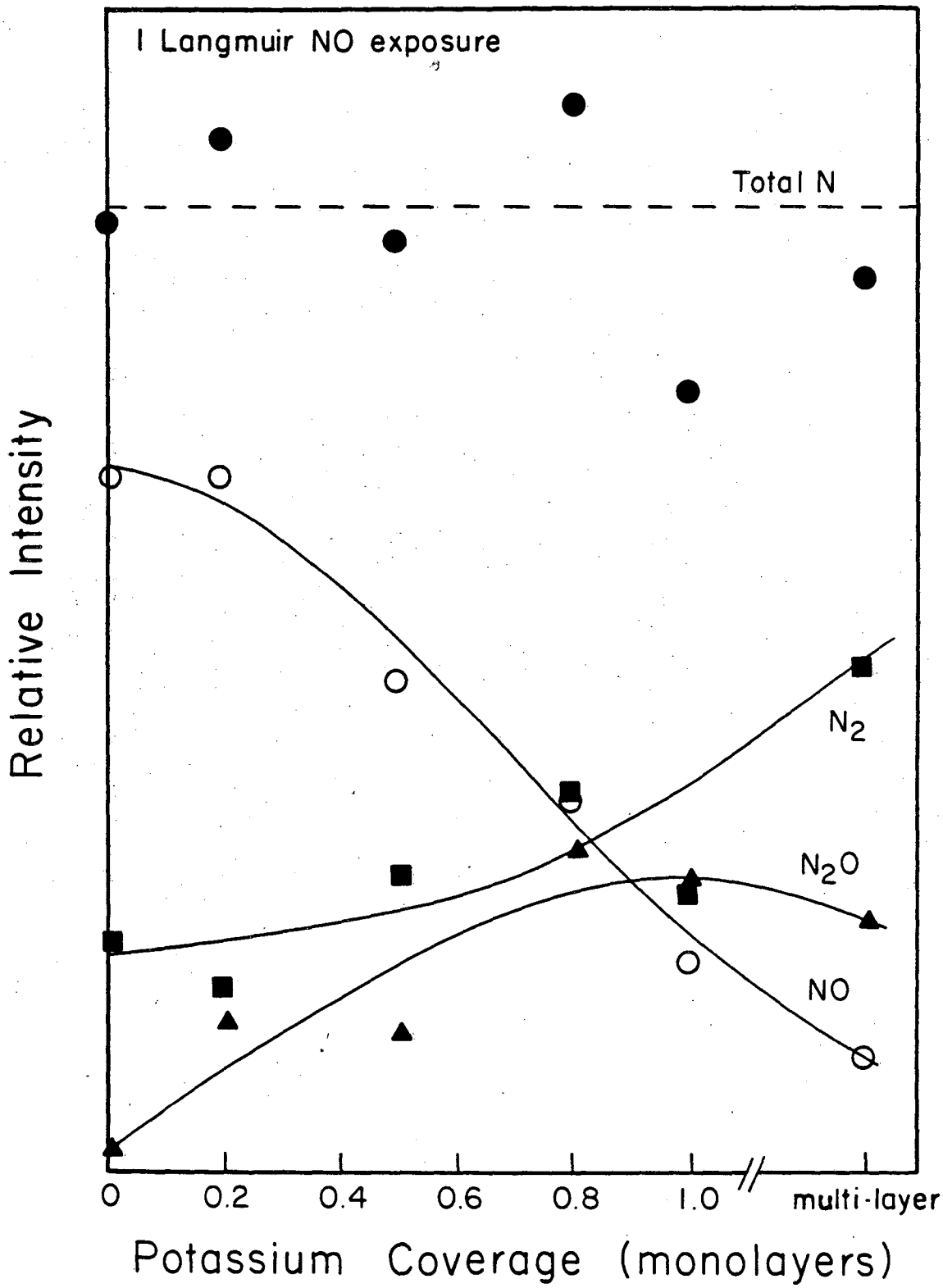

XBL 828-11088

Figure 4.37

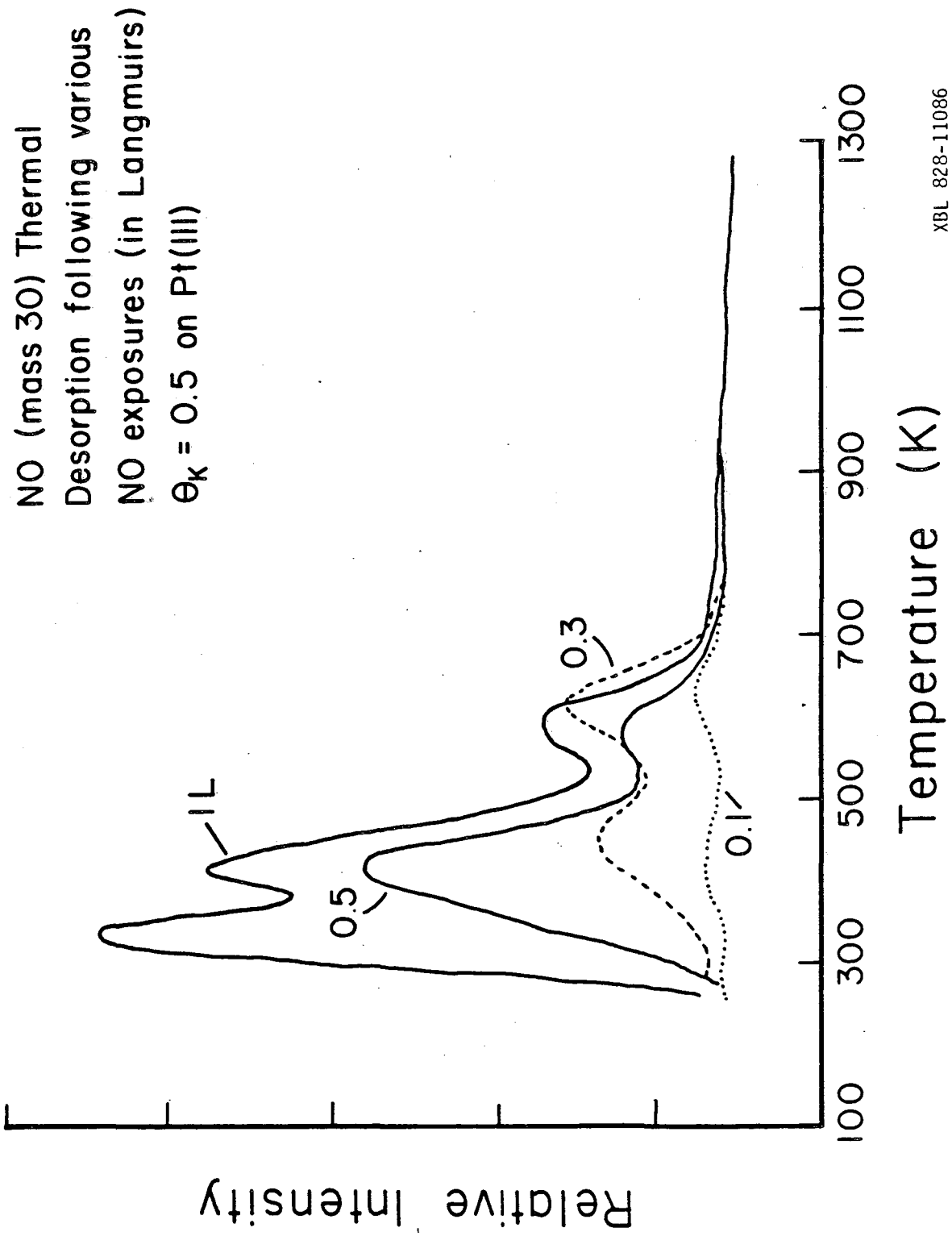
NO (mass 30) Thermal
Desorption following various
NO exposures (in Langmuirs)
θ_K = 0.5 on Pt(111)
1L
0.5
0.3
0.1
Relative Intensity
100
300
500
700
900
1100
1300
Temperature (K)
XBL 828-11086

Figure 4.38

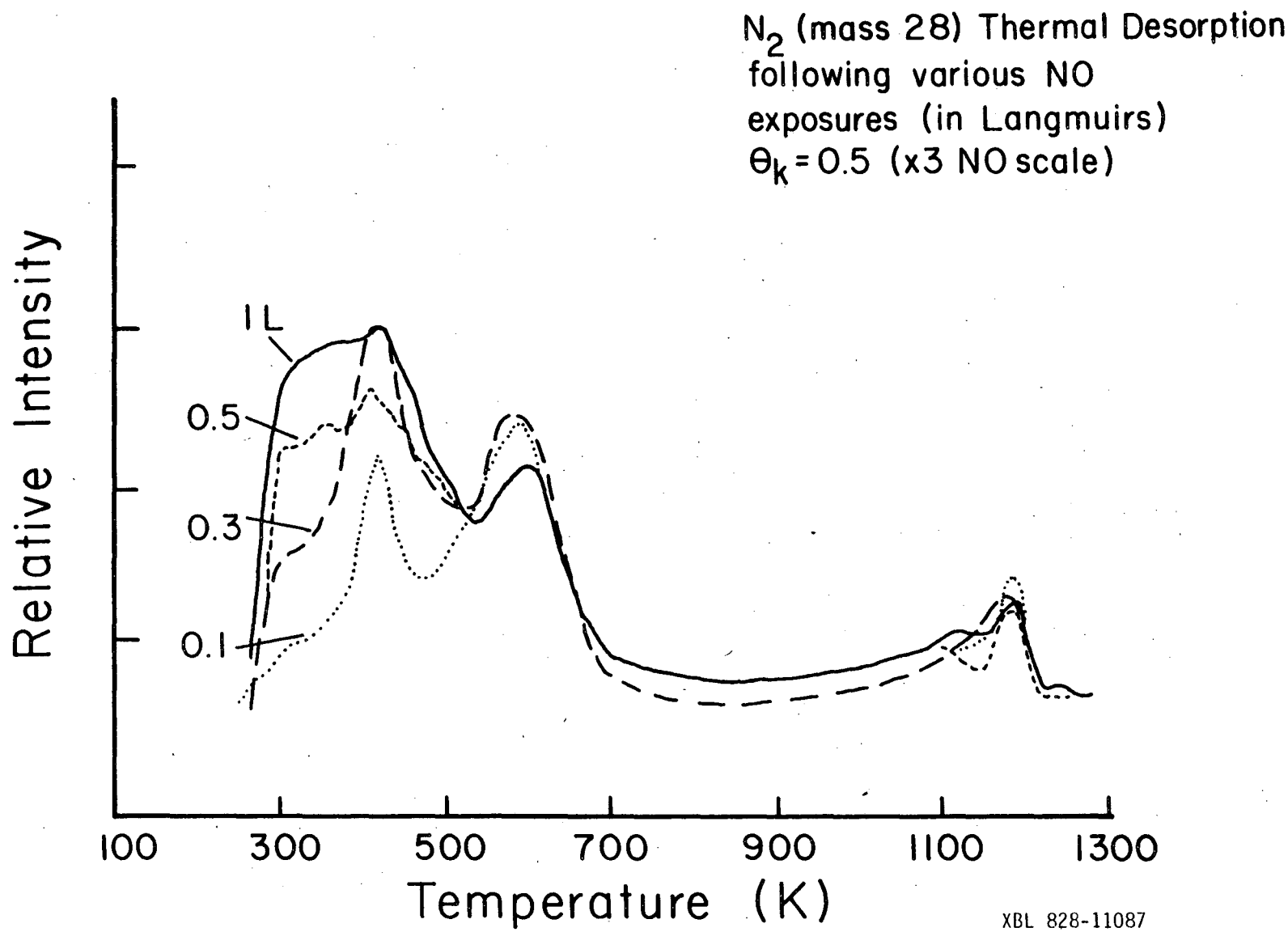
N_2 (mass 28) Thermal Desorption
following various NO
exposures (in Langmuirs)
$\theta_k = 0.5$ (x3 NO scale)
Relative Intensity
1L
0.5
0.3
0.1
100
300
500
700
900
1100
1300
Temperature (K)
XBL 828-11087

Figure 4.39

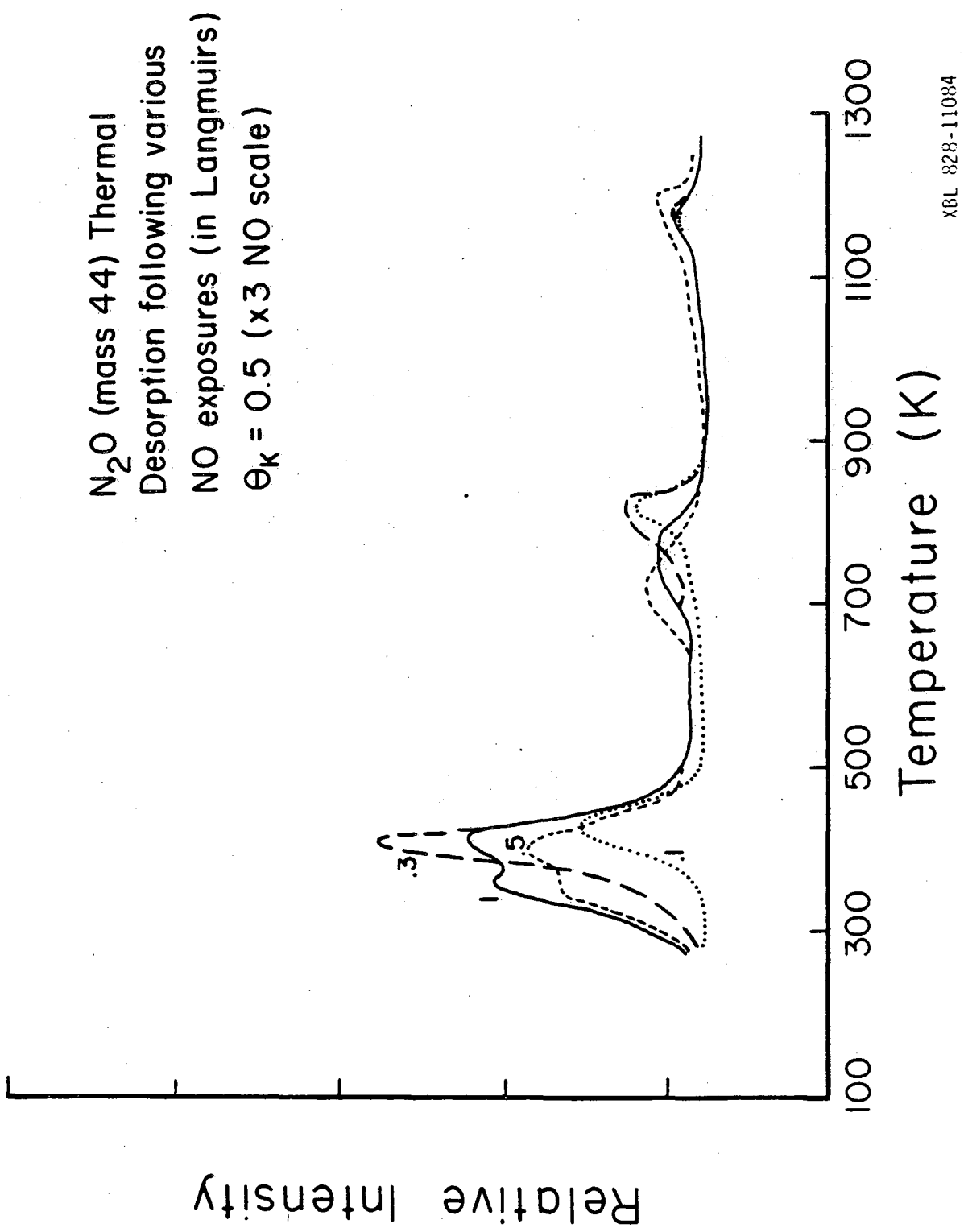
N_2O (mass 44) Thermal
Desorption following various
NO exposures (in Langmuirs)
θ_K = 0.5 (x3 NO scale)
.3
.5
1
1
100
300
500
700
900
1100
1300
Temperature (K)
Relative Intensity
XBL 828-11084

Figure 4.40

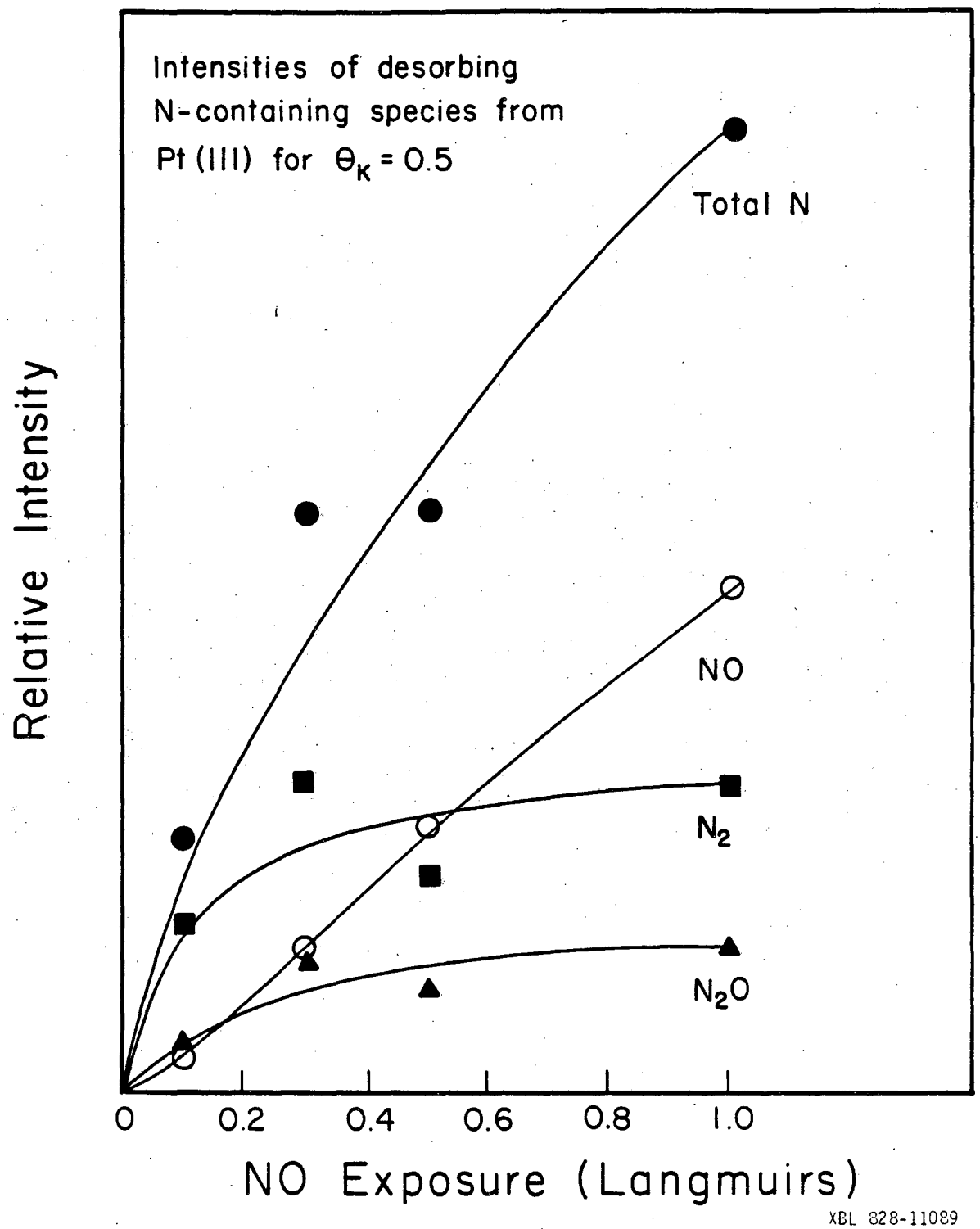
Intensities of desorbing
N-containing species from
Pt (III) for $\Theta_K = 0.5$
Total N
NO
N_2
N_2O
Relative Intensity
0
0.2
0.4
0.6
0.8
1.0
NO Exposure (Langmuirs)
XBL 828-11089

Figure 4.41

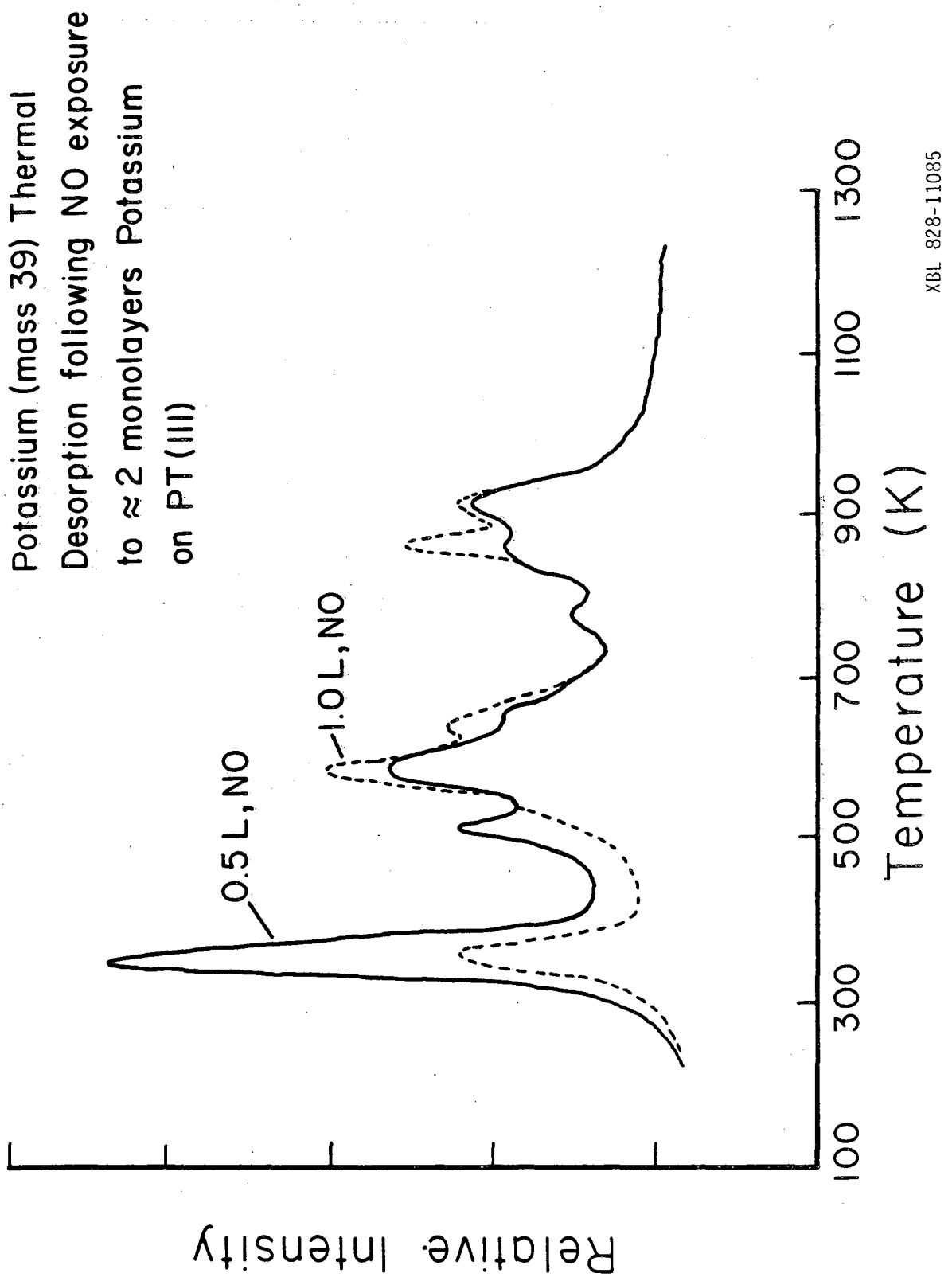
Potassium (mass 39) Thermal
Desorption following NO exposure
to ≈ 2 monolayers Potassium
on PT (III)
0.5 L, NO
1.0 L, NO
Relative Intensity
100
300
500
700
900
1100
1300
Temperature (K)
XBL 828-11085

Figure 4.42

4.4 Phosphorus triflouride (PF_3), acetonitrile (CH_3CN), and butene (C_4H_8) adsorption.

4.4.1 Thermal desorption studies.

The thermal desorption spectra of PF_3 on clean Pt(111) are shown in Figure 4.43. PF_3 exhibits first order desorption kinetics with a peak temperature of ~ 500 K and a FWHM of about 70 K, consistent with results published previously (Nitschke, 1981). Figure 4.44 shows the effect of various potassium coverages on the PF_3 desorption spectra. The amount of adsorbed PF_3 decreases with increasing potassium coverage. The blocking of sites by potassium was such that by Θ_K=0.5 (i.e. 50% of saturation coverage) no more PF_3 could be adsorbed. There also appears to be a slight decrease in the desorption peak temperature (≈ 25K), as well as an increase in the FWHM of the peaks from 70 to 130 K with increasing potassium coverage. PF_3 does not appear to adsorb on, or react with, a potassium multilayer. This is indicated both by the negligible amount of PF_3 adsorbed on K multilayers (as evidenced both in AES and TDS) and the K desorption spectra, found to be almost identical to that of clean K overlayers.

CH_3CN desorbed mostly intact from Pt(111) as has been observed in previous studies (Friend, 1981). Some dissociation occurred upon heating, as was monitored by AES following the thermal desorption cycle. Preadsorbed potassium was found to effectively block sites for acetonitrile adsorption, as was observed for PF_3 and butene, but no shifts in desorption peak temperature or width were detected.

The H_2 desorption spectrum following room temperature adsorption

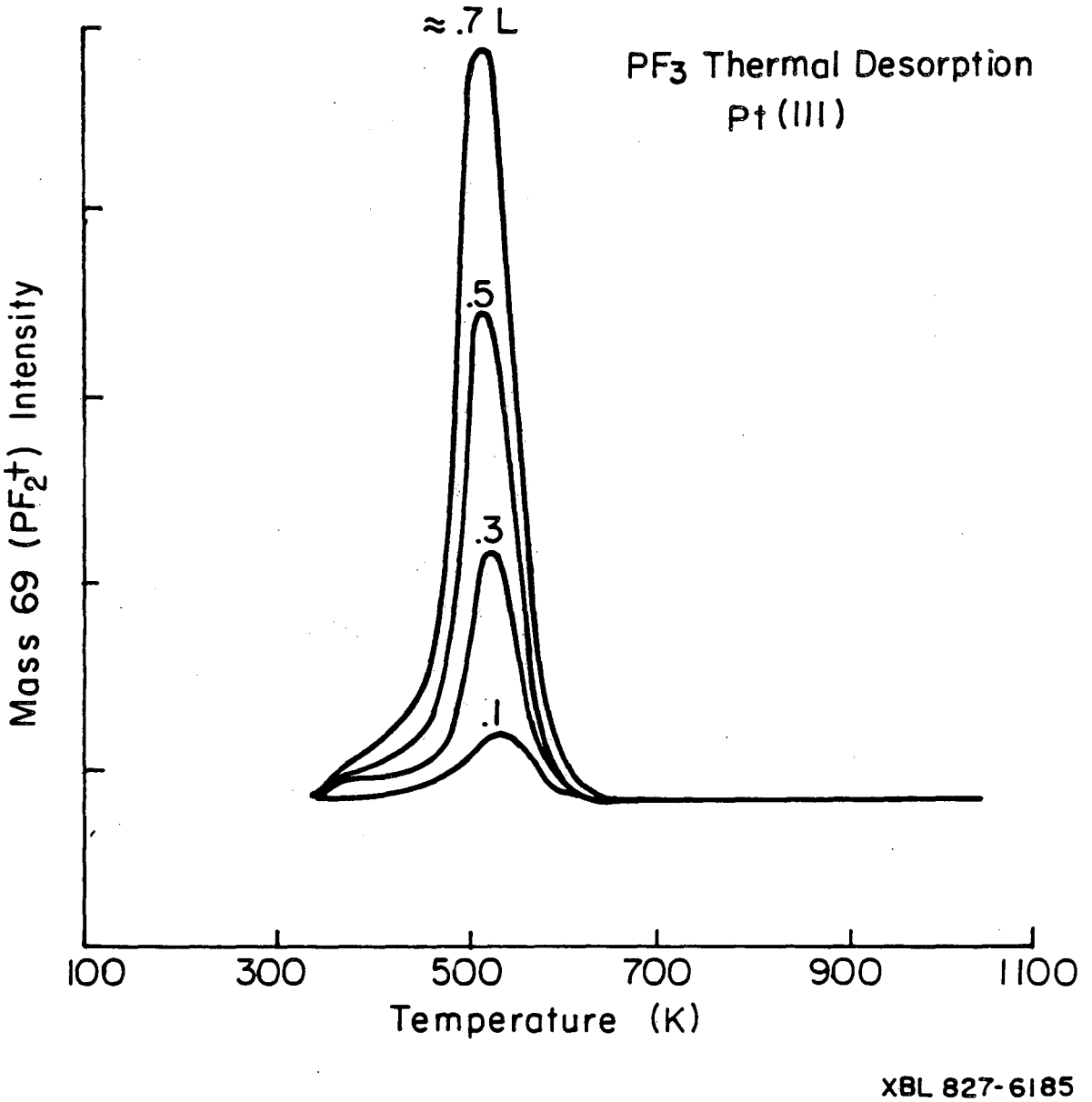
≈.7 L
PF3 Thermal Desorption
Pt (111)
.5
.3
.1
Mass 69 (PF2+) Intensity
100
300
500
700
900
1100
Temperature (K)
XBL 827-6185

Figure 4.43

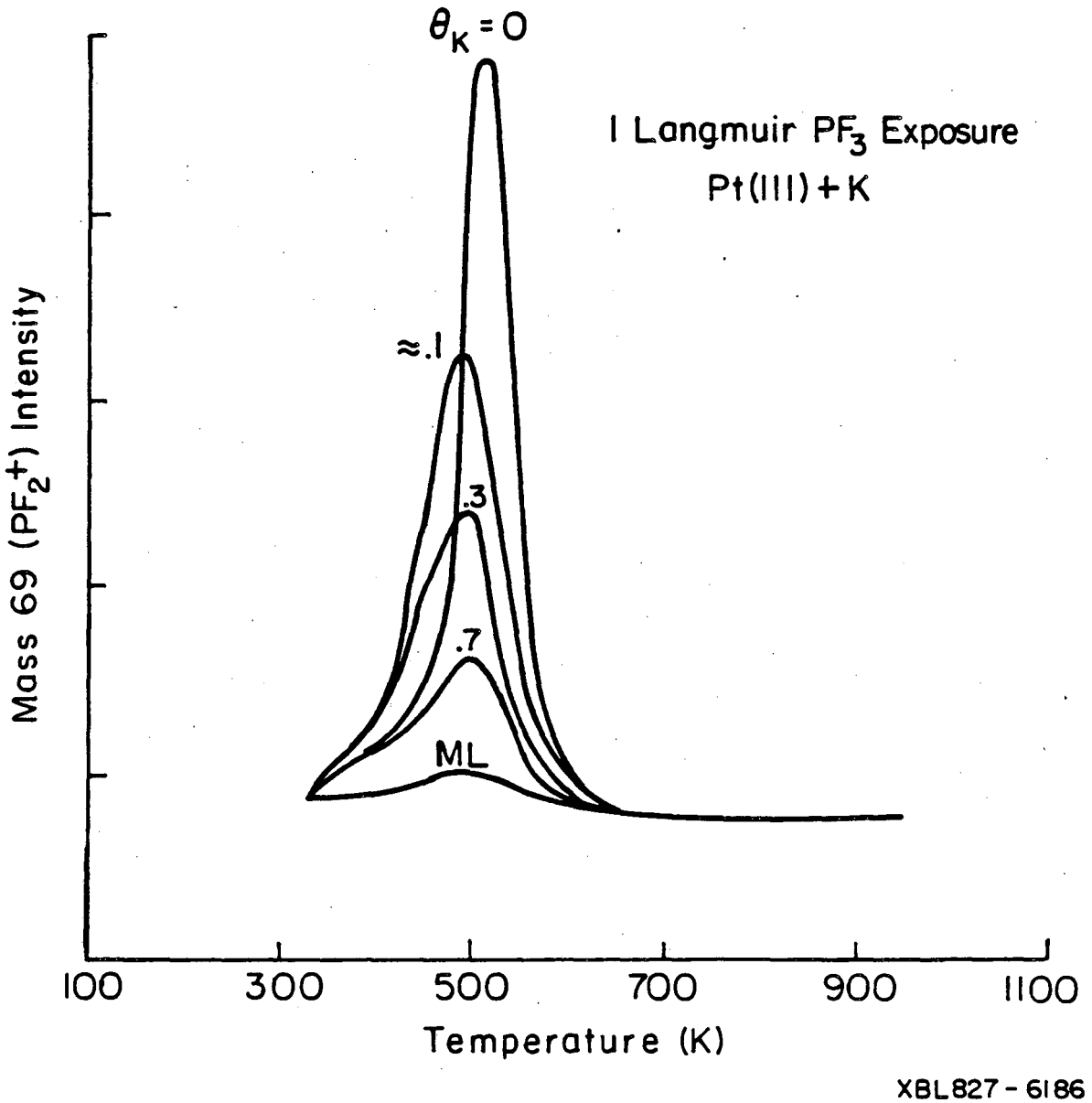
$\theta_K = 0$
1 Langmuir PF_3 Exposure
Pt(111) + K
≈.1
.3
.7
ML
Mass 69 (PF_2^+) Intensity
100
300
500
700
900
1100
Temperature (K)
XBL827-6186

Figure 4.44

of 1-butene on clean Pt(111), is identical to that of 2-butene (Salmeron, 1982). Both spectra are thought to result from the rapid formation of the stable butylidyne species upon adsorption (Koestner, 1983). No carbon containing species were observed in the desorption spectra. For a given exposure of 1-butene, much less is adsorbed onto the platinum surface if it is pre-dosed with potassium (see Figure 4.45). This decrease in coverage is not simply proportional to the potassium coverage; small potassium coverages have a large effect. For example, a potassium coverage of .5 monolayers (corresponding to an atomic ratio K/Pt of .16) reduces the butene adsorption by a factor of 5 following 10 L exposures. The drop in adsorption is due to physical blocking, not simply a change in the sticking coefficient. The second peak in the H_2 TDS curves for the potassium exposed surface appears slightly broadened and shifted to lower temperatures.

4.4.2 Discussion.

Adsorbed phosphorous trifluoride was found to desorb intact at about 500 K from both clean surfaces and surfaces partially covered with potassium. The thermal desorption spectra also showed some peak broadening, and a slight decrease in desorption maximum temperature with potassium. The lack of a large effect was at first surprising, since we had expected to observe effects similar to those seen for the K+CO+Pt(111) system, i.e. a 200K increase in desorption temperature. But by examing the relavant molecular orbitals, this behavior can be understood.

For PF_3 bound to a metal, the σ-donor energy level is located well below E_f at $\approx$ 8eV, while the 2π acceptor level is split into two levels (Nitschke, 1981) one located 4.5 eV below E_f and the other at 4 eV above

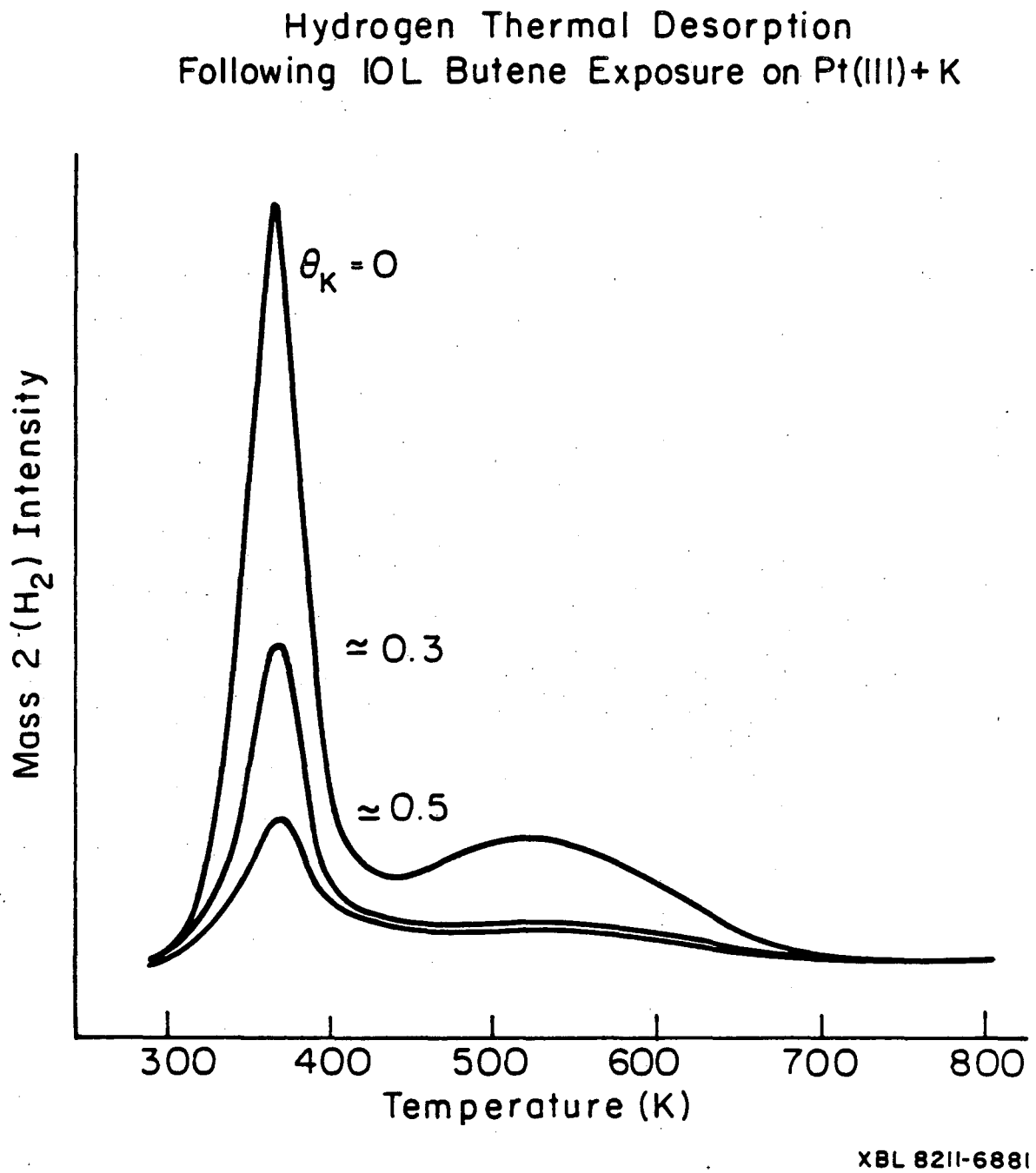
Hydrogen Thermal Desorption
Following 10L Butene Exposure on Pt(111)+K
$\theta_K = 0$
$\simeq 0.3$
$\simeq 0.5$
Mass 2 (H_2) Intensity
300
400
500
600
700
800
Temperature (K)
XBL 8211-6881

Figure 4.45

Approximate Energy Levels of PF_3
in the Gas Phase and on a Metal Surface

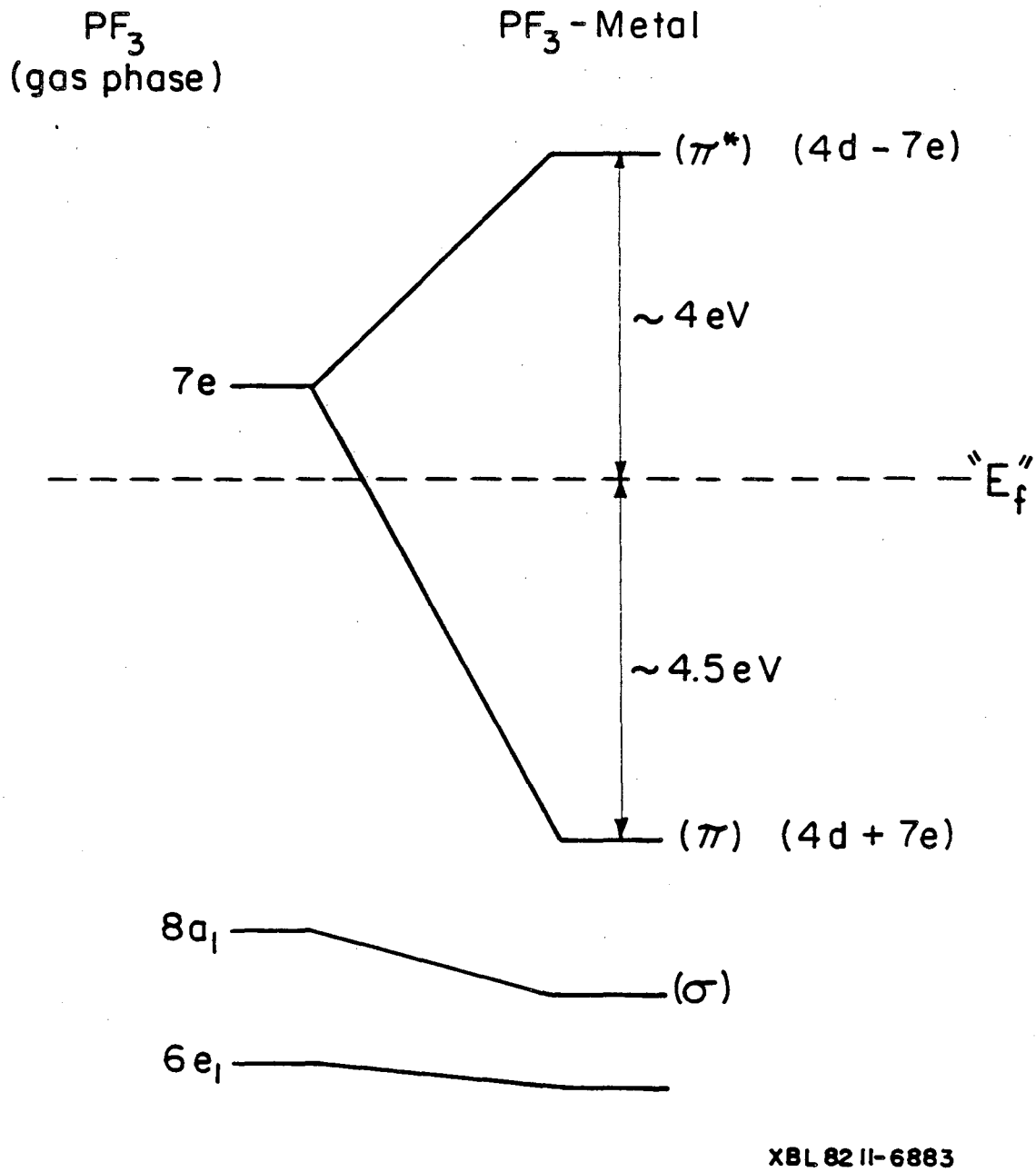

Figure 4.46

E_f (see Figure 4.46). The absence of significant potassium induced chemisorption changes in PF_3 can be explained by assuming that the σ donor levels and the bonding 2π-acceptor levels are fully occupied prior to potassium coadsorption, and that the nearest unoccupied PF_3 level is too far above E_f to accept electrons from the metal, even upon potassium coadsorption. One explanation for the slight drop in PF_3 desorption temperature is that there could be a decrease in 5σ (PF_3) to s-band (Pt) overlap, resulting from a filling of the 6s Pt band when potassium is adsorbed as mentioned above (Nitschke, 1981; Itoh, 1979).

For CO, which exhibits a large change in bonding when co-adsorbed with potassium, the 2π bonding orbital is located only $\approx$0.6-2.0 eV below E_f (Koel, 1983; Bosco, 1983). Here, the potassium is able to enhance the d-2π overlap, which strengthens the M-C bond and weakens the C-O bond (since the 2π level is antibonding between the C and O atoms), see Figures 4.1 and 4.2. CO is therefore more sensitive to changes in surface electron density.

Acetonitrile is known to be σ-bonded to metals via the lone pair orbital of its nitrogen (Friend, 1981). No accessible back-bonding levels are located near E_f, so there is no possibility of additional charge transfer between the metal and the unoccupied molecular orbitals. Therefore no significant changes in bonding were expected and none were found upon coadsorption of this molecule with potassium.

The stable structure of alkenes adsorbed on the Pt(111) surface at 300K is thought to be a R-C-M species (Koestner, 1983). Thus one does not expect any accessible adsorbate energy levels to exist near E_f since the highest σ-bonded levels are usually 5-15 eV below E_f.

The similar shape of the H_2 thermal desorption profiles following butene exposures with and without potassium pre-deposition is therefore expected, assuming that metal carbon bonding has an effect on the hydrogen desorption temperature. The changes induced in the second H_2 desorption peak are difficult to interpret and will require more information on the nature of the CH_n fragments believed to be present at these temperatures.

4.5 Literature Review of alkali coadsorption studies.

In this section I review the literature about alkali - molecular coadsorption systems. Most of the studies have involved CO, with the exception of the dinitrogen studies of Ertl and coworkers. The papers are discussed in chronological order.

4.5.1 CO + alkali promoter + Fe catalyst.

The effects of surface basicity on Fischer-Tropsch catalysts were discussed by Dry et al (1969). They reported that K_2O promoters on an iron catalyst, caused a 5 kcal/mole increase in the heat of adsorption of CO as measured by calorimetry. These authors suggested that the alkali atoms induced electronic changes at the surface which enabled stronger CO adsorption. They went on to postulate that a stronger M-C bond implied a weaker C-O bond which could then be hydrogenated more easily. At that time it was thought that the first step in CO hydrogenation was the formation of a surface enol intermediate $H-\underset{M}{C}-OH$. More recently, the enol-intermediate mechanism has been discredited, but their main observation of increased heat of desorption, and weakened carbon-oxygen bond, is still thought to be correct.

4.5.2 CO + K + Fe(110).

Broden et al (1979) published a paper discussing CO + K coadsorption on Fe(110). Using TDS, they also observed an increase in the heat of adsorption of CO when K was coadsorbed. By using UPS and XPS, they were also able to monitor the dissociation of CO. Upon heating, the dissociation probability was enhanced if potassium was coadsorbed. The authors showed, however, that the energy of dissociation was not

necessarily lowered by potassium. They argue instead that the increased CO dissociation was due to increased heat of adsorption, i.e. CO was adsorbed on the surface at a temperature more than 100 K higher than in the absence of potassium. At the higher temperature, dissociation becomes favored over desorption. From other evidence, they claimed that the potassium induced a localized effect on CO adsorption. By following the O(1s) level by XPS, they recorded the CO uptake as function of CO exposure. They found that CO coverage reached saturation rapidly on the clean Fe(110) surface, but that saturation was not reached until exposures of >400 L on the potassium covered surface. Thus, they claimed a large decrease in sticking coefficient with potassium. We believe that the sticking coefficient does go to zero, but that this is due instead to a real blocking of surface sites by potassium. Only by displacing potassium can CO be adsorbed on the "potassium covered" surface.

4.5.3 CO + K + Fe(100).

Benziger and Madix (1980) published a paper about several surface coadsorption systems on Fe(100). The aim of their research was to understand the effects of a variety of additives on CO hydrogenation. We review here only a small part of their effort, namely the interaction of CO and K on Fe(100). Their results were in quantitative agreement with those published by Broden (1979) on the Fe(110) surface: the dominant effect of K was to increase the binding energy of CO and to induce its dissociation. However, since the Benziger study involved TDS, XPS, and LCAO calculations, different types of information were obtained.

They also showed the effect of increasing potassium coverage on the CO thermal desorption spectra peak position. Increasing potassium coverage clearly caused an increase in the average temperature of desorption of the molecularly adsorbed CO, while at the same time increasing the fraction of dissociatively adsorbed CO. The dissociatively adsorbed peak showed a bond order between 1 and 2, implying limited mobility of the surface species. Contrary to Broden's study, Benziger concluded that the sticking coefficient remained constant up to 1 monolayer. Their XPS results showed two distinct states for CO adsorption, attributable to associatively and dissociatively adsorbed CO. They also concluded that the potassium effect is localized since the high temperature sites filled first.

In their LCAO calculations on small iron clusters, Benziger let the Fe 3d electrons interact with the 5σ and 2π CO levels, and the K 4s electron. They found that by donating the 4s electron into the d-band of Fe, potassium enhanced the backdonation into the CO 2π level. This accounted for the observed effects of increased heat of desorption and increased dissociation. They also showed that because of the large size of the atom, potassium could donate into the 2π CO level directly, thereby increasing these effects.

4.5.4 CO + alkali + Ni(100).

Kiskinova and coworkers have also performed a series of experiments involving alkali adsorption, coadsorption, and catalysis on nickel surfaces. They published a paper (Kiskinova, 1981) about CO adsorption on alkali covered Ni(100). On this surface, as with the iron surfaces, coadsorbed alkali (Na, K, and Cs) caused both an increase in the adsorption

energy of molecularly adsorbed CO, and an increase in the fraction of CO which dissociates. They concluded from their observations that the sticking coefficient dropped from .68 on the clean surface, to .3 at one monolayer alkali coverage. They noted the difference in C and O Auger lineshapes of molecularly and dissociatively adsorbed CO. The amount of CO which dissociated was proportional to the alkali coverage and to the electronegativity of the particular alkali used. The electronegativity decreases down the periodic table, thus Cs showed a greater effect than K or Na. We might add, however, that the larger effect could also be due to the increased size of Cs. They also noted that some disproportionation took place ($2CO \rightarrow CO_2 + C$).

4.5.5 $CO + KO_x + FeO$.

Keleman et al (1982) published a paper discussing CO adsorption on iron oxide in the presence of potassium. FeO is difficult to synthesize in a controlled way. According to the authors, however, once it is synthesized, it is relatively stable up to 650K. To oxidize the iron, they heated an iron single crystal to 700K in 2×10^{-7} torr O_2 for 14 hours. The surface prepared this way was FeO (wustite), as confirmed by XPS, UPS, and AES.

CO adsorbed on this surface with a relatively high sticking coefficient and desorbed intact with a peak maximum temperature at or below 400K. They did not observe CO disproportionation. Because of problems in interpretation of the UPS spectra, there is some ambiguity about whether or not the CO remained molecularly adsorbed with the carbon end down, as it does on most clean transition metals. Oxygen could be

adsorbed on the clean FeO surface, but was readily removed by heating to 600K. Oxygen preadsorption blocked the surface sites for CO adsorption.

CO adsorption was also studied with potassium coadsorbed on the surface. Potassium was vapor deposited from a KOH pellet and was shown (by UPS) to be adsorbed as KOH on the surface. Heating this KOH overlayer to 550K resulted in significant amounts of H_2O desorption, and the authors suggest that a monolayer of K + O remained adsorbed. This K + O overlayer appeared to have a stiochiometry of 2 to 1, but they claimed that it was not "K_2O".

When CO was adsorbed on this potassium covered surface, UPS showed it to be adsorbed molecularly as with the clean FeO surface. Curiously, the UPS peak positions appear within .1 eV of the same energy for both CO and KOH. Heating to 475 K caused CO to dissociate (as seen by the absence of the CO UPS peaks.) Further heating allowed the adsorbed carbon and oxygen to recombine and overcome the activation energy for desorption. The thermal desorption peak maximum increased to 625K with the potassium overlayer, from 400K on clean FeO.

4.5.6 Penning Ionization Studies of K/CO/Ni(111).

A series of surface Penning ionization electron spectroscopy (SPIES) experiments have recently been performed by Metiu and coworkers on the K/CO/Ni(111) system (Lee, 1983). In SPIES, a beam of metastable helium (or neon) atoms impinges upon the surface. If the surface is covered by a molecular adsorbate, the helium atom transfers its excitation energy to the molecule. This will then cause electron emission from the molecular orbital levels within the range of the excitation energy. SPIES is thus analogous to UPS, but has the added advantage that is

sees only the surface layer, while UPS probes 10-20 Å into the metal.

In Lee's experiment, the $2\pi^*$, $(1\pi + 5\sigma)$, and 4σ molecular orbital peaks of CO shifted to higher binding energy when potassium was coadsorbed. They also noted a significant increase in the intensity of the conjugate d - 2π level (relative to the other levels) with potassium. This is thus in good agreement with our result showing a decreased CO stretching vibrational frequency induced by potassium. Somewhat harder to understand is the shift to higher binding energy of the 4σ and $(1\pi + 5\sigma)$ levels. It is generally thought that the 1π level should be destabilized when the $2\pi^*$ CO level is filled, leading to a lower binding energy. An increase in final state screening should also cause the levels to move to lower binding energy (i.e. higher kinetic energy).

The initial state energy levels are normally considered pinned to the Fermi level, but as discussed above, this rule may break down if the local electrostatic potential is significantly changed. One final problem worth noting is that the position of the Fermi level is hard to determine in the SPIES experiment. Therefore the appearance of increased binding energy for all the levels may have arisen from a problem of referencing of E_f.

A temperature dependence study of the SPIES signal was also performed by Lee et al for the CO/K/Ni(111) system. They note that the CO signal decreased before the CO desorbed. This implied that dissociation was occurring upon heating to 600-640 K. This was confirmed by isotopic exchange thermal desorption studies which showed that exchange occurred at moderate to high potassium coverages, and at temperatures above 600K.

4.5.7 Electron Energy Loss Study of the CO/K/Ni(100) System.

Luftman and White (1983) are also currently studying the CO/K/Ni(100) system. Their thermal desorption studies show the same general behavior of most of the other alkali - CO systems: the heat of CO desorption increases with potassium coverage and a (presumably dissociated) CO state appears at about 700K. They also note that potassium is stabilized by CO analogous to what is observed for H_2O or O_2. They have also performed electron energy loss spectroscopy (EELS, not HREELS) and noted a decrease in the 2π (bonding) - 2π (antibonding) separation. They offer a more complete (qualitative) molecular orbital analysis than is reported elsewhere to account for the observed changes in TDS and EELS behavior. The essence of their argument is that potassium lowers the "site" electrostatic potential (what I have less rigorously called the "local work function"), causing the 2π gas phase reference level to be brought closer to the "$d\pi$" level (the bonding metal orbitals/band). By bringing them closer in energy, increased mixing will occur. Also the final state 2π (bonding) - 2π (anti-bonding) separation should decrease (assuming the overlap integral remains constant). They further argue that the $d\pi$ metal level should go to lower binding energy because of electron correlation effects, which will cause a further increase in the mixing.

At "press time" the author is aware of two additional studies: F. Hoffmann is studying the CO/K/Ru system by HREELS and has found similar vibrational behavior to what we have reported, but with additional features implying direct interactions. Kiskinova, Pirug, and Bonzel are studying the CO/K/Pt(111) system by XPS and UPS, and have offered a new interpretation of the potassium induced effects on that surface.

4.4.8 Fe + K + N_2.

The potassium and nitrogen on iron coadsorption system has been studied by Ertl et al (1979). This system is of direct relevance to the ammonia synthesis as the dissociative adsorption of nitrogen is thought to be the first and rate limiting step in the reaction. The industrial ammonia synthesis catalyst is in fact performed on a reduced iron catalyst which contains K_2O promoters, as well as some Al_2O_3 and SiO_2.

In their study, Ertl and coworkers showed that at 430K, the rate of dissociative nitrogen adsorption increased by at least two orders of magnitude when submonolayer amounts of potassium were present. They also showed that this was a result of both an increase in the heat of adsorption of molecularly adsorbed nitrogen from less than 9 kcal/mole to more than 11 kcal/mole, and a decrease in the activation barrier for dissociation.

From work function measurements, they showed that the enhanced dissociative adsorption was not simply correlated to the macroscopic work function, but was more likely related to the microscopic electronic structure in the immediate vicinity of the adsorbed potassium. Thus, the promoting action was localized as was observed for the Fe + K + CO systems discussed previously, where dissociative CO adsorption occurred. Somewhat surprisingly, they also observed a c(2x2) nitrogen overlayer LEED pattern even with potassium coadsorption.

They also studied the Fe + K + O + N_2 system (Paal, 1981) as it was previously shown that oxygen is required to thermally stabilize the potassium under reaction conditions. Coadsorbed oxygen blocked

nitrogen adsorption sites, lowering both the sticking coefficient and the total amount of nitrogen adsorbed on the Fe + K system. But the modified K + O overlayer was still able to dissociate N_2 as with the clean potassium overlayer.

Their interpretation of the potassium enhanced dissociation ability is similar to that given for CO. By lowering the energy spacing between the Fermi and vacuum levels, the normally unoccupied π^* N_2 orbital can be populated by backdonation from metal d-electrons, decreasing the activation barrier for dissociation.

4.6 Conclusion.

The general model which can be developed is that potassium (or any alkali) causes a change in the local electronic structure and fields at the surface of a transition metal, which then alters the chemisorption behavior of molecules such as CO or benzene. By lowering the surface dipole component of the work function, potassium enables the molecular orbitals lying near to E_f to interact more strongly with the metal. In the case of adsorbed CO, potassium causes the 2π orbital to increase its occupancy. This results in a strengthened carbon-metal bond, and a weakened carbon-oxygen bond. An added result is the change in site occupancy from top to bridged. This results from a competitive effect: for the high work function surface, the 5σ orbital dominates the bonding and preferentially chooses linear bonding to a single metal atom (top site). For the lower work function surface, back-bonding becomes more feasible, and CO moves to the higher coordination site to increase metal-2π overlap (i.e., the off diagonal overlap integral term in the Hamiltonian).

Adsorbed potassium caused a weakening of the benzene-metal bond. This is attributed to a decrease in the work function, which then allows the e_{1g}^{*} benzene level to be filled. This level is "anti-bonding" between the metal and carbon ring, and should cause a weakening of the bond.

The absence of significant potassium induced electronic effects on other systems studied can be attributed to the position of their molecular orbital levels. This type of analysis should be valid for most adsorption systems where a knowledge of "electronic promotion" is desired.

Chapter 5. The Use of Alkalis as Promoters: CO Hydrogenation Reactions

In this chapter, I report on our studies of CO hydrogenation performed on rhenium and iron foils. Rhenium has recently been shown to be a very active ammonia synthesis catalyst (Spencer, 1982b). Given the similar nature of the ammonia synthesis to CO hydrogenation, we had hoped to observe active and perhaps unique behavior for rhenium catalysts. Following a presentation of our results (sections 5.2-5.4), I review the recent literature on the subject of promoters for CO hydrogenation and offer some general conclusions (section 5.5).

The general changes we observe in product rates and selectivities when submonolayers of alkali are present on both rhenium and iron surfaces are qualitatively the same as are noted above for industrial catalysts. Decreased overall rates and product selectivity changes toward higher molecular weight species are observed on both surfaces. This is correlated with changes in CO dissociation. We offer a new interpretation of the catalytic role of alkalis on the carbonaceous layer that is formed as the reaction proceeds. We have also studied these surfaces following oxidation. As the degree of catalyst oxidation was increased, the active lifetime increased and the selectivity changed towards lower molecular weight species. Sulfur, on the other hand, poisoned the reaction.

5.1 Introduction

The hydrogenation of carbon monoxide is now being extensively studied as a substitute for conventional fuel sources (Vannice, 1976).

The reactions of CO and H_2 can be classified according to the products desired, as shown in Figure 5.1. The first is called the methanation reaction, and is normally carried out over a nickel catalyst. The second set of reactions is directed towards producing higher molecular weight hydrocarbon fuels such as gasoline, and is called the Fischer-Tropsch reaction. In the past it has often been carried out over promoted iron catalysts (Vannice, 1976). The final class of reactions which lead to desirable products (also sometimes called Fischer-Tropsch reactions) are those that produce oxygenated species such as ketones, alcohols, aldehydes, and carboxylic acids. For instance, both palladium (Hicks, 1983) and Zn-Cr-Cu (Natta, 1955) catalysts can produce methanol with high selectivity, while Rh_2O_3 and $LaRhO_4$ promoted with K_2O produce aldehydes and acids as well (Watson, 1982).

The conventional iron Fischer-Tropsch catalyst for producing higher molecular weight species is promoted with K_2O and Al_2O_3 (Anderson, 1956). Al_2O_3 is found mostly at the grain boundaries of the iron particles and is therefore considered a structural promoter. Potassium, on the other hand, is observed on the surface of both the Al_2O_3 and the active iron phases, and is generally thought to act as an electronic promoter.

CO bonds molecularly in many transition metals at room temperature, as noted in Chapter 4. On the other hand, H_2 is found to adsorb dissociatively on most metals with only a very small activation energy of dissociation. It was originally thought that molecular CO was first hydrogenated to form an enol, M-CH(OH), weakening the C-O bond, and eventually leading to C-O dissociation and/or chain growth (Storch,

Reaction Mechanisms for the Hydrogenation of Carbon Monoxide

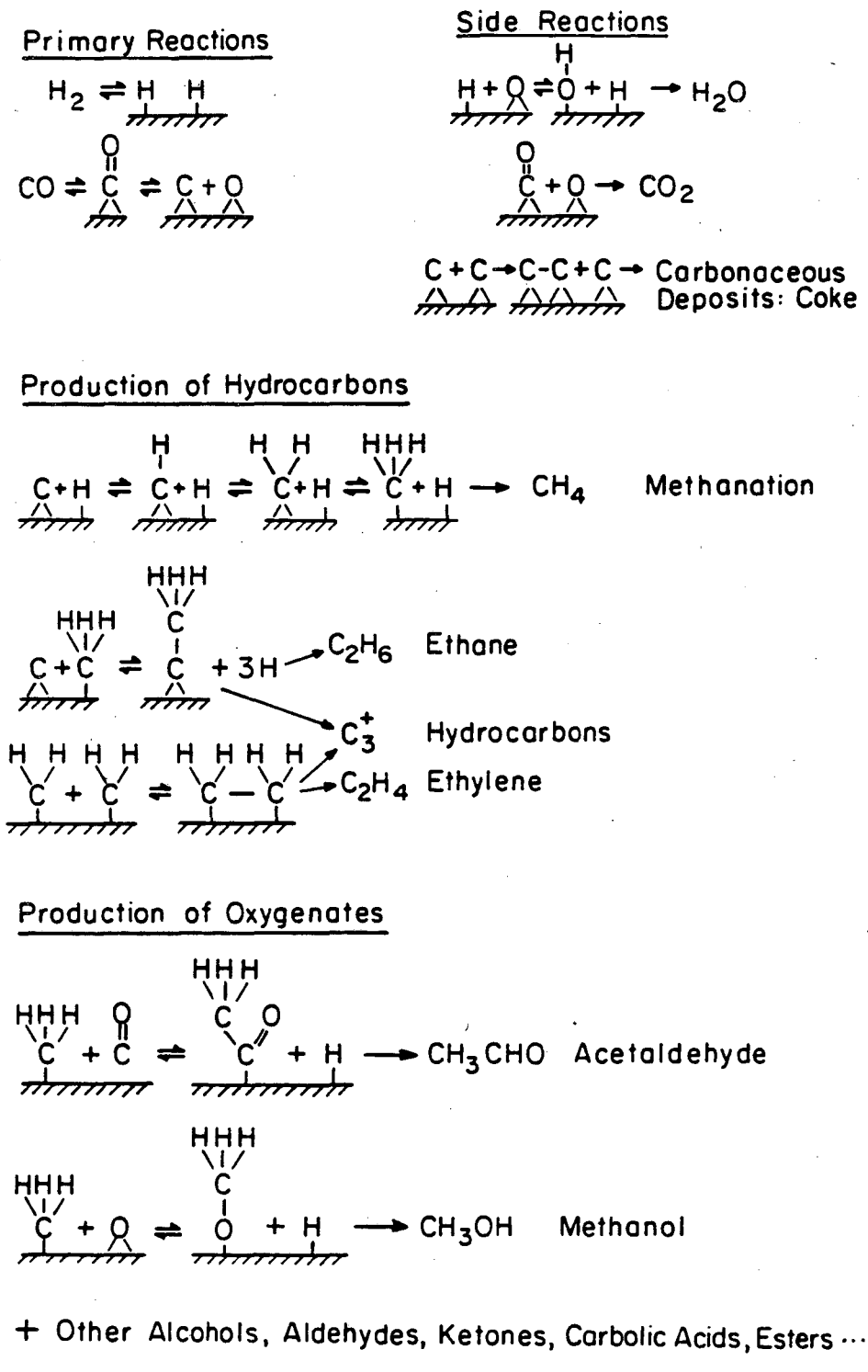

Figure 5.1

1951). More recently, it has been demonstrated that CO dissociates before hydrogenation takes place, and that the activation energy for dissociation is lowest at multiply coordinated sites (Ponec, 1978). There is considerable evidence for a favorable interaction between molecular CO and hydrogen on metal surfaces (Koel, 1983), but this interaction is probably not of major importance in CO hydrogenation reactions. Once dissociated, the various pathways that the surface carbon can follow are represented in Figure 5.1. For hydrogenation, atomic carbon and hydrogen combine stepwise to produce the various hydrocarbons. The production of oxygenated species follows a somewhat different pathway. The product distribution will depend on many parameters of both the catalyst composition and the reaction conditions. For instance, nickel catalysts do not dissociate as much CO as do iron catalysts. Under reaction conditions nickel is thought to have only about 10% of the surface covered with atomic carbon (Campbell, 1982), while on iron the active catalyst seems to be an iron carbide (Arakawa, 1983). Large differences in product distribution are observed between these two catalysts, perhaps resulting from their different reactivity towards CO.

Thermodynamics tells us two things about CO hydrogenation. First, since most of the desired reactions are exothermic, they are favored by lower temperatures - usually temperatures of 500-700K are used in order to optimize the rate of product formation. Secondly, from le Chatelier's principle, higher pressures are needed, since more moles of gas are consumed than are produced, especially when longer-chain hydrocarbon products are desired. Since our reactions were normally run at

about 32 psig, lower molecular weight products were expected to dominate.

Several characteristic changes are observed when alkali promoters are added to CO hydrogenation catalysts. These include selectivity changes to higher molecular weight species, higher alkene to alkane ratios, and more oxygenated species (Anderson, 1956). Most researchers also note an increased rate of carbon build-up, a lowering of the rate of methane formation, and changes in the active metal dispersion; see for instance, Arakawa (1983), Campbell (1982), and Gonzales (1982). In addition, several ultrahigh vacuum studies have recently been performed on the surface properties of alkalis when coadsorbed with CO and other small molecules. The main observations for the alkali + CO systems are: increased heat of adsorption, increased probability for dissociation, and a change in site occupancy from top to multiply coordinated. It is usually concluded that the changes in selectivity observed during CO hydrogenation are a result of the increased fraction of dissociated CO. This, in turn, is a result of greater backdonation into the CO 2π orbital.

5.2 Experimental

All work was performed in the combined ultrahigh vacuum - high pressure catalysis chamber described in Chapter 2. Following standard cleaning procedures (see section 2.3) a final heating was necessary to give an atomically smooth surface. Several reactions were run on surfaces which had not been annealed, and initial methanation rates were found to be as much as an order of magnitude greater than those from the flat surface. Sulfur and potassium were deposited as described in section 2.4. Oxygen was introduced at ca. 1×10^{-6} torr to oxidize both the

samples and the alkali adlayers. Oxidation could also be achieved by introducing water into the reaction cell before or during the reaction. The alkalis were readily oxidized at ambient temperature, while the clean iron and rhenium samples were heated at 400-500 and 800-900 C respectively to enhance the rate of low pressure oxidation. Water in the gas phase was much more effective in ensuring continued oxidation during the reactions. The "surface" iron oxides prepared by low pressure oxidation were reduced during the reactions.

Once the surface was prepared, the catalysis chamber was closed and a mixture of CO and H_2 gases was introduced. The $CO:H_2$ ratio was 1:4 with a total pressure of 32 psig except as noted. The sample was rapidly heated from room temperature to a given temperature (as monitored by a Pt/PtRh thermocouple wire) and samples were periodically introduced into the gas chromatograph by a gas sampling valve. Following a run, (usually from 1-5 hours) the catalysis chamber was evacuated. Then the sample was exposed to UHV, and AES and TDS were used to examine the surface.

5.3 Results

In Figure 5.2 we show an example of the results of methane accumulation versus time for a pre-oxidized iron foil. The runs were characterized by a brief induction time, followed by a long stable period, which would eventually decay after several hours. As discussed below, this decay is attributable to the slow build-up of a carbonaceous layer which poisoned the surface.

From the rate of methane production at various temperatures we were able to construct Arrhenius plots. In Figure 5.3 we show

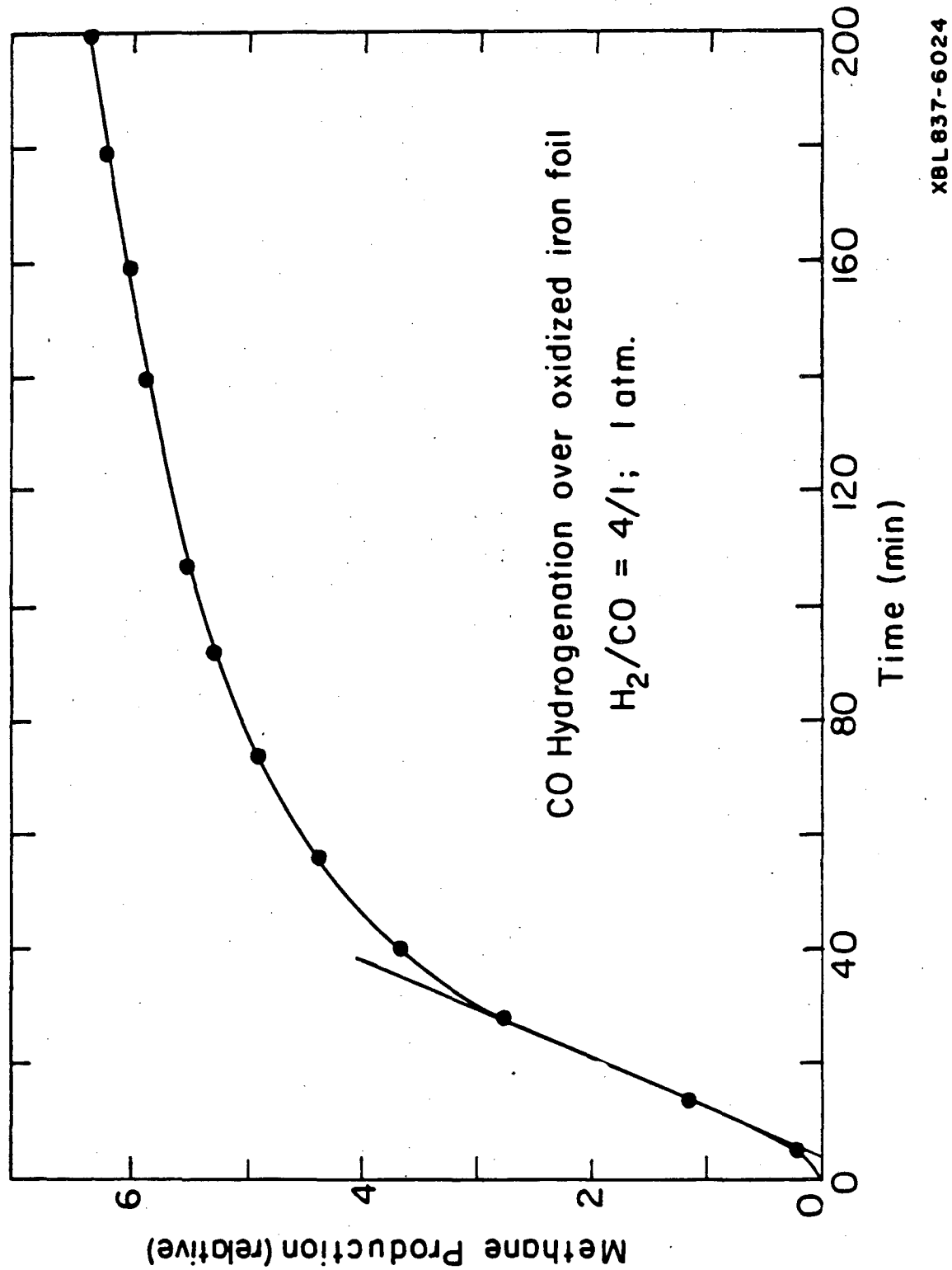
CO Hydrogenation over oxidized iron foil
$H_2/CO = 4/1$; 1 atm.
Methane Production (relative)
0
2
4
6
Time (min)
0
40
80
120
160
200
XBL837-6024

Figure 5.2

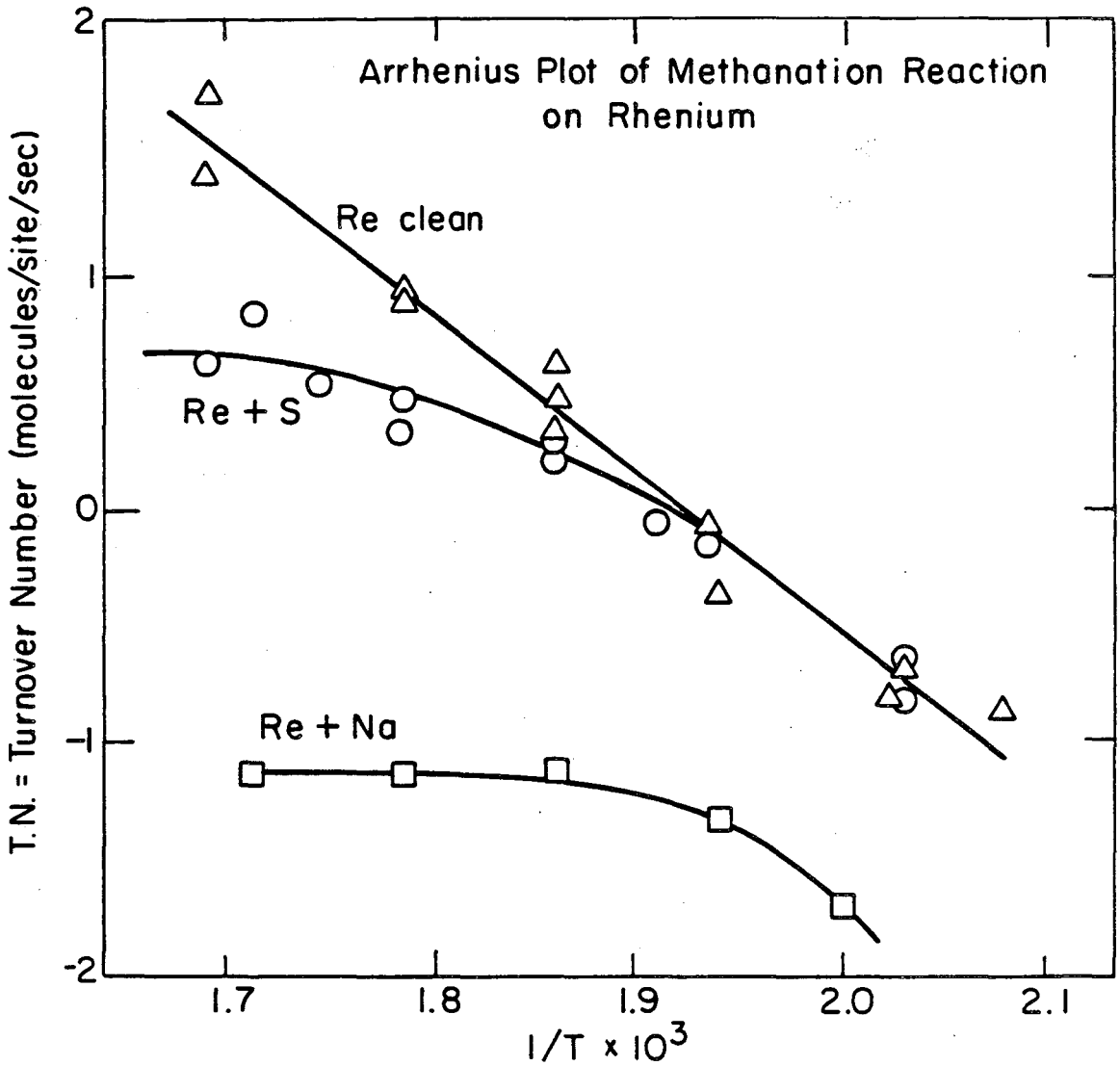

XBL 837-6025

Figure 5.3

Arrhenius plots for various runs on rhenium foil. This type of plot allowed us to determine the activation energy of the reaction, and the temperature at which surface poisoning began - where the linear Arrhenius curve started bending over (Goodman, 1980). Methane was the dominant product on most samples studied, but higher molecular weight alkanes and alkenes were also monitored.

The activation energies and the selectivities of Re and Fe foils are displayed in Figure 5.4. The turnover frequencies (molecules/site/sec) used are the maximum values reached by the catalyst following an induction period (usually <20 minutes after initiation). The turnover frequencies were calculated assuming an active number of surface sites of 10^{15} over which the catalyst was uniformly heated. (This number is hard to know accurately for several reasons. We believe, however, that it is correct to within 50%, because our results are in good agreement with the behavior of industrial iron Fischer-Tropsch catalysts at similar temperatures. In any case, it is the relative values, not so much the absolute ones, which are needed to discuss promoter effects.)

Figure 5.5 shows how the selectivities change as a function of temperature. As noted in Figure 5.4, the activation energy for ethylene is lower than that for methane. Thus methane production should be favored by higher temperatures, as is observed.

The main types of Fischer Tropsch catalyst poisoning are thought to be carbon or sulfur build-up. In Figure 5.6a we show an iron foil $dN(\varepsilon)$ AES spectrum before a catalyst run. Figure 5.6b shows a close-up of the carbon AES peak after two different reactions. The amount of carbon on the surface after a given run was a function of

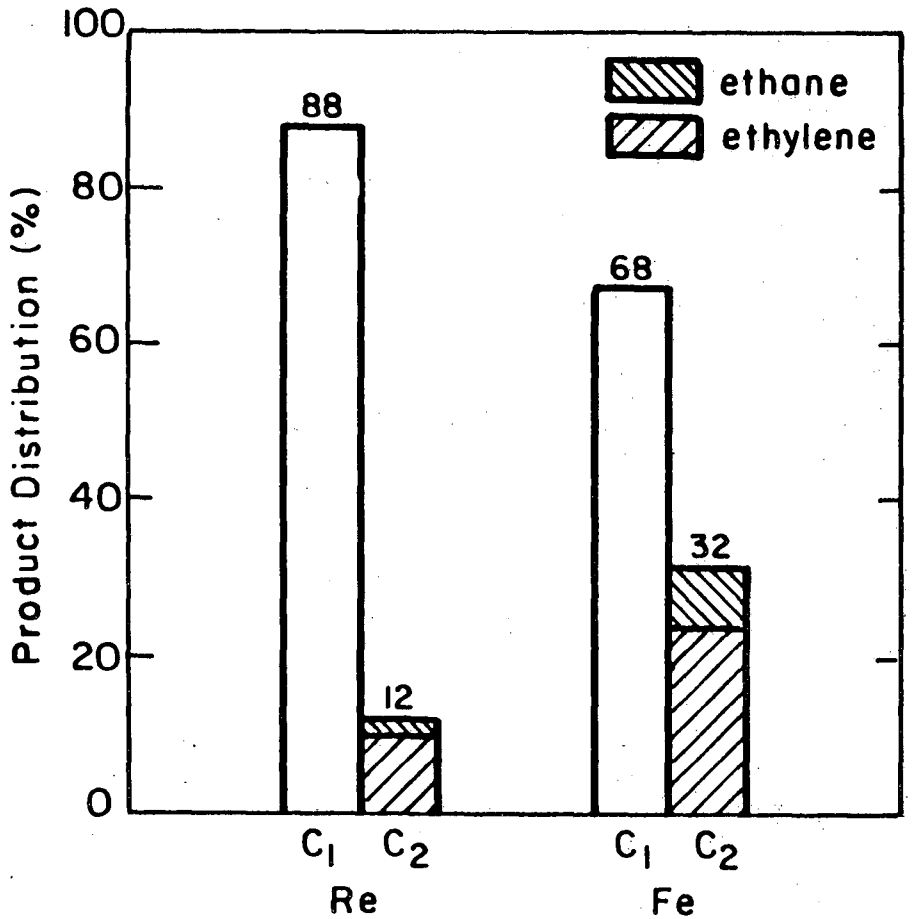

CO Hydrogenation
540 K $CO/H_2 = 1/4$
32 psi

	Re	Fe
Turnover Number (molecules/site/sec)	2	5
$E_a(CH_4)$	28	24
$E_a(C_2H_4)$	21	17

XBL 837-6026

Figure 5.4

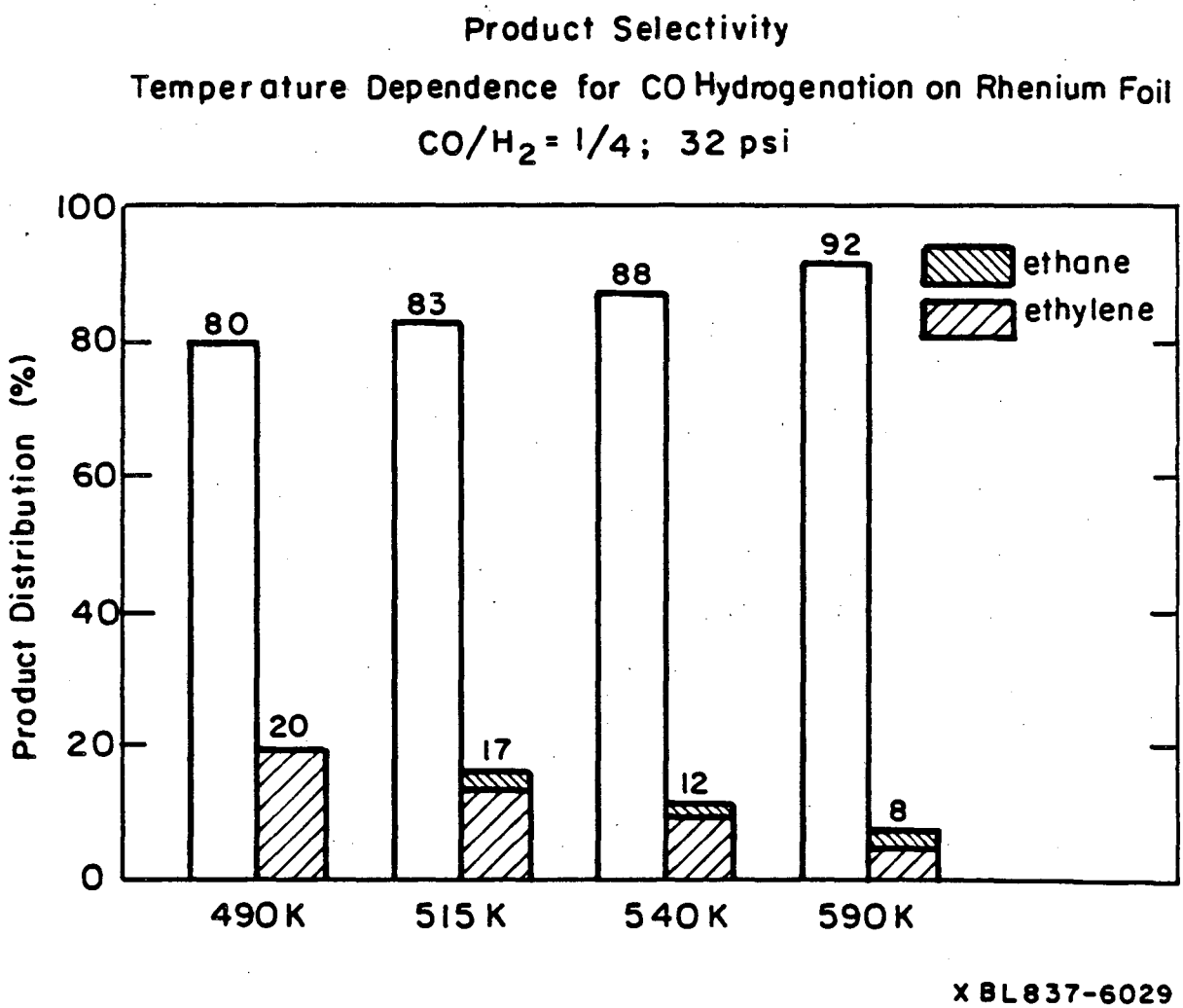
Product Selectivity
Temperature Dependence for CO Hydrogenation on Rhenium Foil
CO/H2 = 1/4; 32 psi
Product Distribution (%)
100
80
60
40
20
0
80
20
83
17
88
12
92
8
ethane
ethylene
490K
515K
540K
590K
XBL837-6029

Figure 5.5

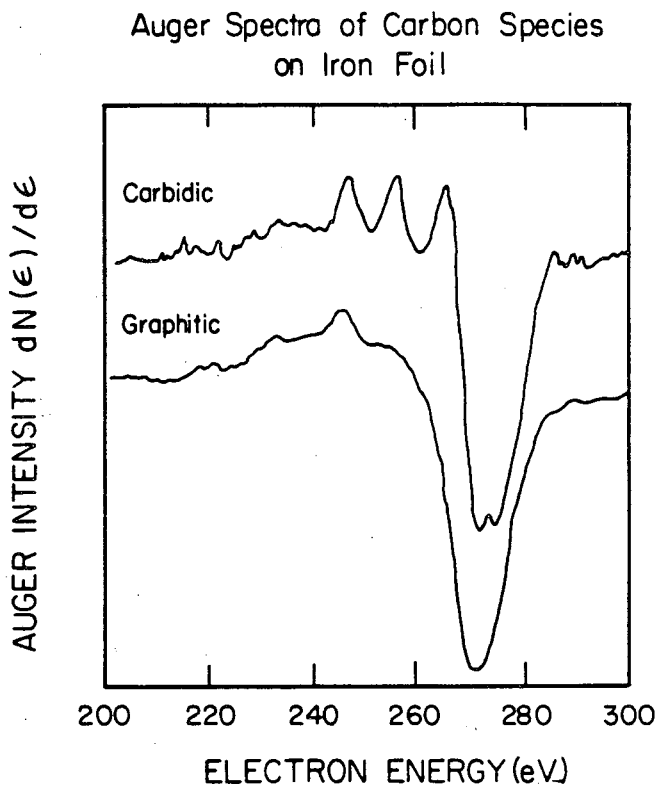

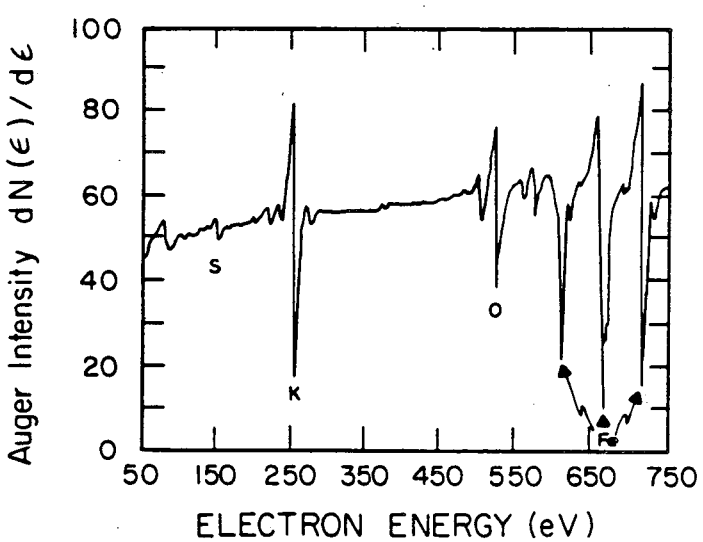

XBL 837-10729

Figure 5.6

Top panel - Close-up Auger spectra of carbon species.

Bottom panel - Promoted iron oxide sample

catalyst pretreatment, reaction temperature, and reaction time. Partial CO and H_2 pressures are also important in determining poisoning time.

Another type of poisoning was observed when sulfur was present on the surface. Sulfur changed the selectivity (towards methane), and it poisoned the surface, as observed in Figure 5.3, presumably by decreasing the number of active sites.

In Figure 5.7 and 5.8 we show the selectivities for the Re and Fe surfaces following oxygen and alkali promotion. The general pattern observed with alkali promoters was a change in selectivity towards higher molecular weight products as well as a decrease in the rate of methanation. The effect was more marked with rhenium than with iron, since clean iron already produces a large fraction of higher molecular weight species. In Figure 5.9 we show an Auger spectrum for a "clean" sample, and a sample following a reaction. In Figure 5.9b note the disappearance of the substrate metal peak with the continued appearance of the carbon, oxygen and alkali peaks. Thermal desorption of the overlayers following reactions showed significant amounts of H_2, H_2O, CO, CO_2, and various small hydrocarbons.

Preoxidation of the surface caused an opposite effect to what was observed with potassium addition: a higher selectivity towards methane. The rate changes with oxidation varied significantly with the extent of oxidation. A major problem occurred here concerning the number of active sites to be used in calculating turnover numbers. Oxidation tends to increase the surface area of the catalyst, even if the oxidation reaches only 10-20Å into the surface. A second, more complicating factor is that the degree of oxidation is not only a function of catalyst

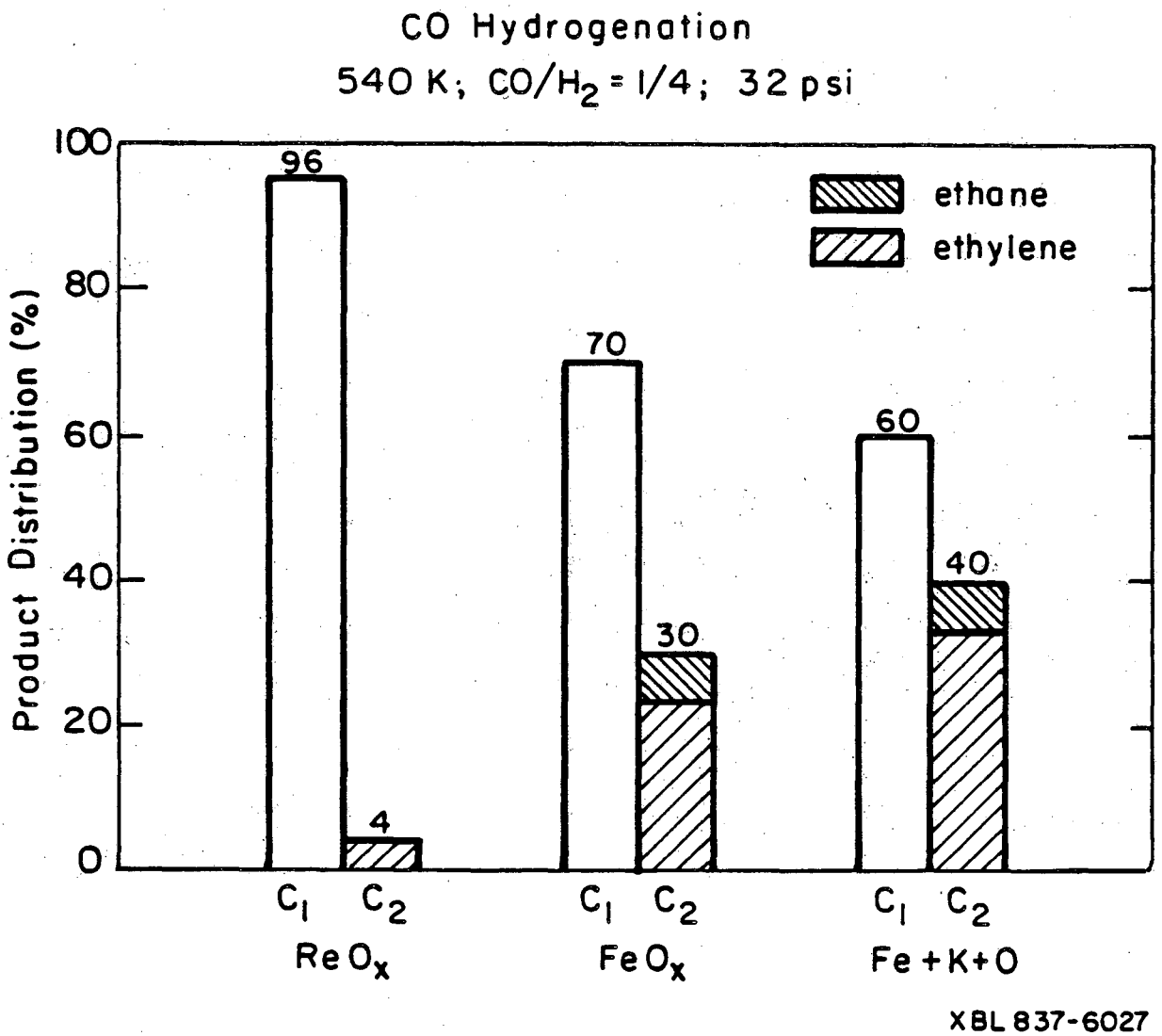
CO Hydrogenation
540 K; CO/H2 = 1/4; 32 psi
Product Distribution (%)
100
80
60
40
20
0
96
4
70
30
60
40
ethane
ethylene
C1 C2
ReOx
C1 C2
FeOx
C1 C2
Fe+K+O
XBL 837-6027

Figure 5.7

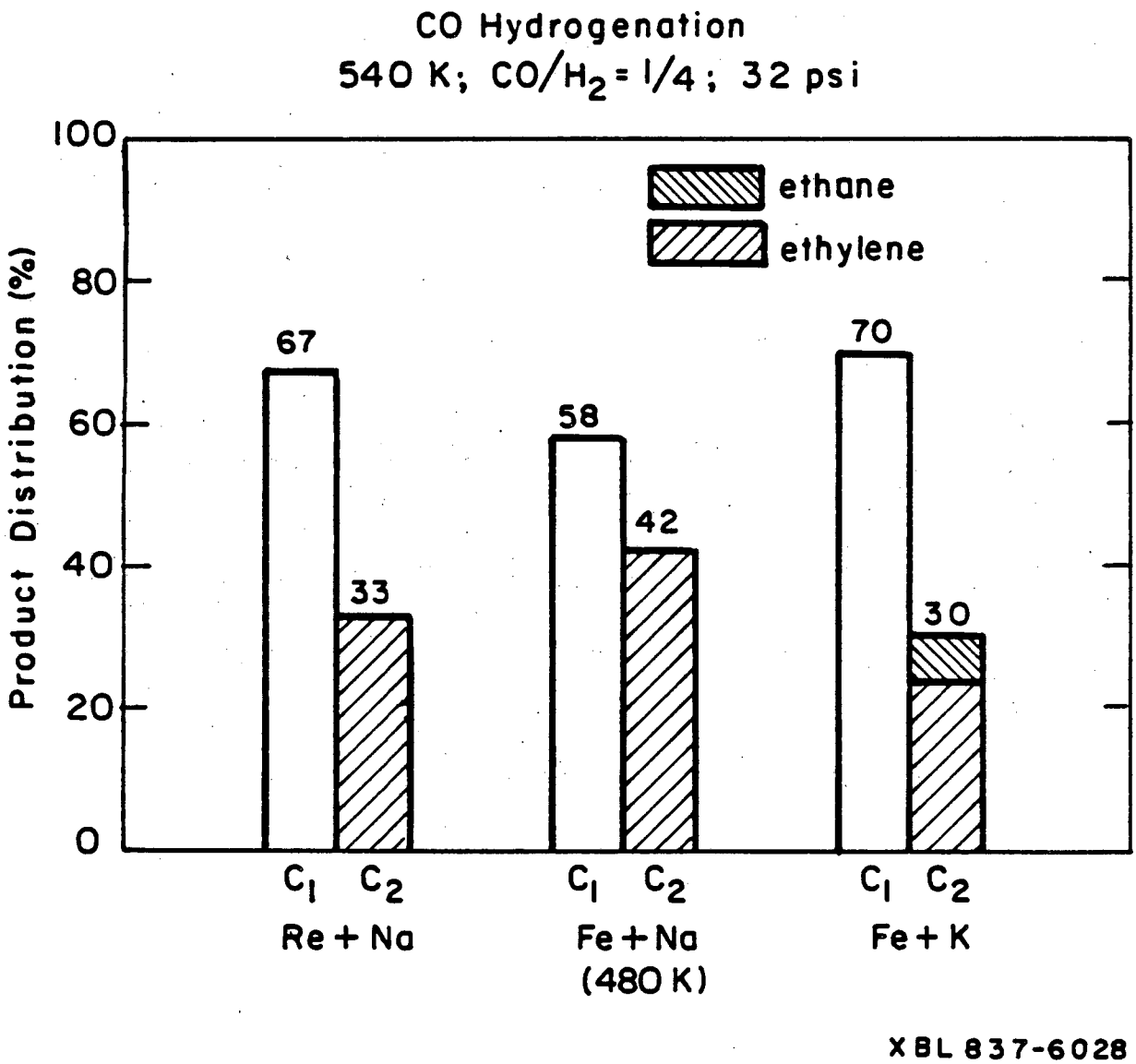
CO Hydrogenation
540 K; CO/H2 = 1/4 ; 32 psi
Product Distribution (%)
100
80
60
40
20
0
ethane
ethylene
67
33
58
42
70
30
C1 C2
Re + Na
C1 C2
Fe + Na
(480 K)
C1 C2
Fe + K
XBL 837-6028

Figure 5.8

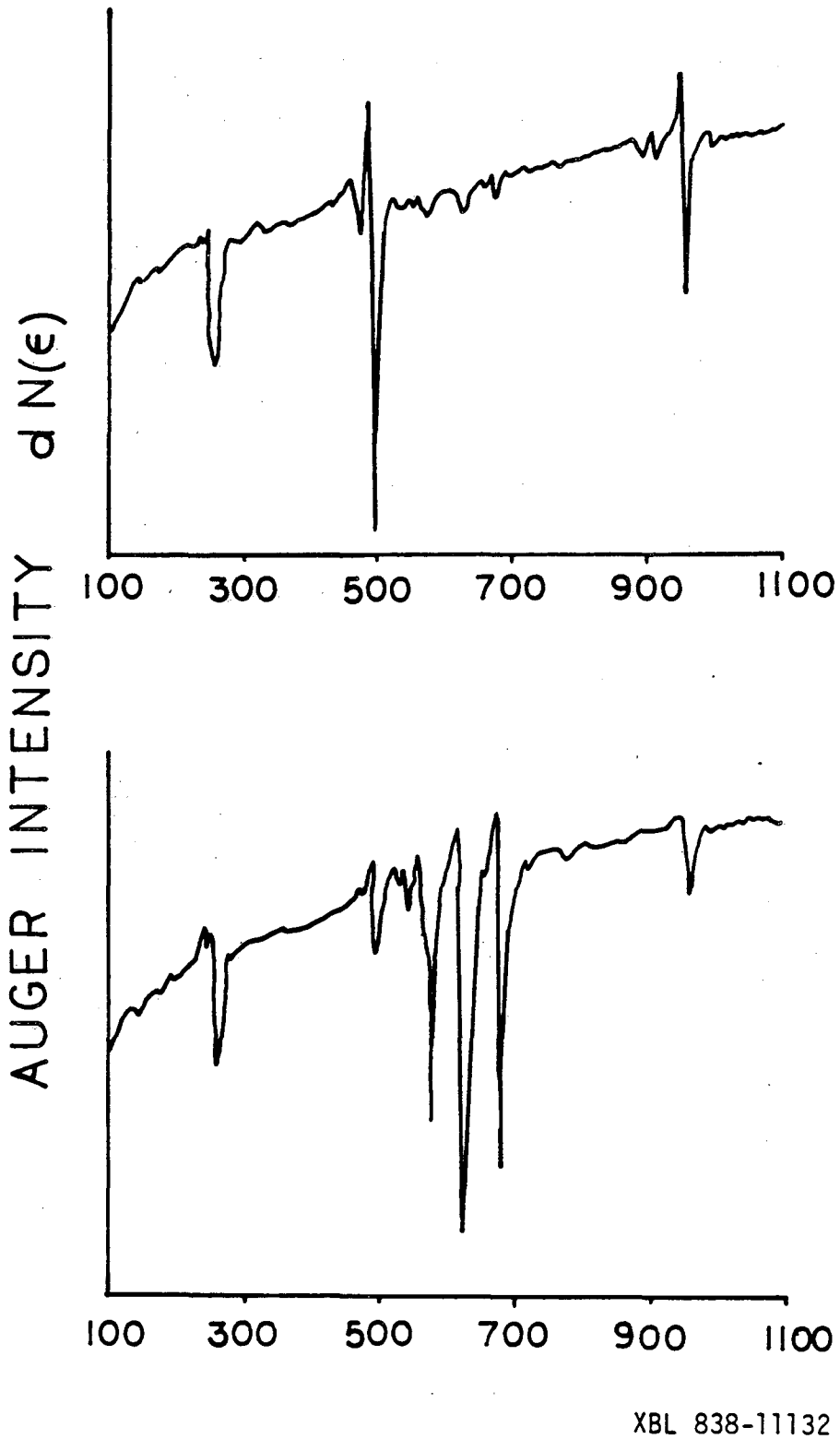

Figure 5.9 Auger spectra of an iron sample prior (bottom) to, and after (top) a reaction; sodium oxide promoted.

pre-treatment, but is constantly changing throughout the reaction as a function of catalyst temperature, reaction time, and partial pressures. Higher temperatures favor less oxygen incorporation in vacuum. Under high CO pressures (>1 atm), however, this is possibly compensated for by an increased rate of CO dissociation and subsequent oxygen incorporation. Thus the rates cited are the best values we could deduce from a knowledge of pre- and post-reaction surfaces. AES and TDS were used to help in this determination. In our runs with potassium the final rate and selectivity depended upon the exact extent of oxidation.

Gold, platinum and palladium, originally used as blanks as they are notoriously poor Fischer-Tropsch catalysts (Vannice, 1976), showed much lower activities than iron and rhenium. Palladium did prove interesting in that we were able to produce methanol (also note Poutsma, 1978; Fajula, 1982). We believe that palladium's ability to hold large amounts of hydrogen in the bulk is related to its unique ability of hydrogenating CO directly. Platinum and gold produce methane with >97% selectivity, but at rates two orders of magnitude slower than iron.

5.4 Discussion

The behavior of rhenium foil for CO hydrogenation was different from that of iron foil. Using initially clean surfaces, iron gave both faster rates and better selectivities towards higher molecular weight species. Because of the complexity of the mechanism, it is very hard to determine why some metals give faster rates than others, or what controls selectivity. Periodic trends show that the ability of a metal to dissociate CO decreases down or to the right in the periodic table. If CO hydrogenation activity were merely a function of the

ability of a metal to dissociate CO, perhaps Cr or Mo would be better catalysts than iron. In fact, poisoning by the buildup of carbonaceous deposits often determines the total yield of a particular catalyst sample; thus the metal which best dissociates CO may show the shortest active lifetime.

Carbon poisoning (coking), however, is not the same for all metals. Supported iron particles, for instance, seem to be quite reactive even after a bulk iron carbide is formed (Arakawa, 1983). On nickel methanation catalysts, on the other hand, no significant amount of carbon dissolves into the bulk, yet one monolayer of "graphitic" surface carbon is enough to poison the reaction (Goodman, 1980). This implies that the reaction can still run as long as some active metal is accessible at the surface.

On our samples, the degree of carbon build-up is measured by AES. This type of determination is of limited use because AES only sees the first few atomic layers. Since we could not vary the CMA detection angle in a systematic way, we cannot say with certainty whether the carbon we observed following a reaction is on the surface or in it. We can, however, distinguish between an active carbidic carbon, and an inactive graphitic one (see Figure 5.6). This classification has been discussed extensively by other authors and results from a comparison of the post reaction carbon AES peak shape with known peak shapes of metal-carbide and graphite surfaces. Our overlayers also contained large amounts of adsorbed (or trapped) oxygen and hydrogen, as was noticed in thermal desorption following the reaction. "Carbidic" carbon was the dominant surface species observed following low temper-

ature, short reaction time runs. "Graphitic" carbon was dominant following high temperature runs, or after flashing any post-reaction surface to >700K.

In general, alkalis on the surface accelerated the rate of carbon build-up, except if a reasonably high partial pressure of H_2O was in the gas phase. The increased carbon build-up is attributed to the ability of potassium to accelerate the dissociation of CO. By lowering the work function, potassium enables the metal to more easily backdonate into the CO 2π antibonding orbital (Nieuwenhuys, 1981), which then can readily dissociate at reaction temperatures.

On several runs, we also noted that only potassium (or sodium), oxygen, and carbon (i.e., not Fe or Re) were visible in the Auger spectra following a reaction. This was also observed by Bonzel and Krebs (1981), and they suggested that a potassium oxide layer was floating on top of a carbonaceous layer. We further suggest that the potassium oxide (or suboxide) layer can itself play an important role in the catalytic reaction. Alkalis have long been known to be used as catalysts in the steam gasification of carbon sources. Thus we must consider the possibility that the build-up of the carbonaceous layer is being hindered by the ability of alkali's to catalyze the reaction of water with carbon. In this model, potassium increases both the rate of CO dissociation (hence carbon build-up) and the rate of removal of the carbonaceous layer, once formed.

Another related reaction which has recently been discussed in the literature is CO hydrogenation over alkali-graphite intercalation compounds (Wen, 1980). Transforming this to our situation, if the

alkali metal atoms were inside the carbonaceous layer, then the alkali-carbon layer can itself become an active Fischer-Tropsch catalyst.

We also note that potassium caused a slight change in selectivity from alkanes to olefins, but the effect was less dramatic than was observed by Gonzales (1982). In Chapter 4, it was shown that the benzene-metal bond strength was decreased by coadsorbed potassium, and much less of the benzene dissociated upon heating. For CO hydrogenation, if the olefin (like benzene) were more weakly bound due to the presence of potassium, then its rate of desorption should be increased relative to that of the alkanes. The alkane to olefin selectivity change is therefore understandable since the olefin can desorb more easily once produced, instead of remaining adsorbed until fully hydrogenated.

The effect of oxidation on the iron and rhenium surfaces depended upon several parameters including: the degree to which the surface was oxidized, the temperature and time of the reaction, and the presence of sulfur or potassium on the surface. The extent of catalyst oxidation grew when water was introduced into the gas phase, enabling the surface to stay clean of the carbon build-up so apparent in most of the runs. Although the initial reaction rates did not increase, the rate of poisoning was slower for oxidized surfaces. As noted by Trimm (1980), the methanation activity of the metal can be roughly correlated with the heat of adsorption of oxygen. Surfaces that bond oxygen too strongly require higher temperatures to initiate methanation.

Another significant change induced by oxidation was the change in selectivity towards lower molecular weight species. By reducing both the amount of surface carbon and the number of adjacent metal atoms, the oxide surface does not permit extensive C-C bond formation. Thus the selectivity change can be rationalized by the decreased ability of C-C bonding. Finally we note that no significant amounts of oxygenates were detected over our low surface area rhenium and iron foils.

5.5 Literature Review.

Recently, Arakawa and Bell (1983), completed a study on the effects of potassium promoters on alumina supported iron catalysts for CO hydrogenation. Noting the decrease in both CO and H_2 uptake following reactions on potassium promoted catalysts, the authors concluded that potassium lowered the dispersion of iron on the surface. From isothermal desorption studies, they observed that potassium decreases the H_2 adsorption energy, while it increases the adsorption energy of CO. At very low potassium loadings, the overall rate of CO hydrogenation increases slightly, but decreases substantially with higher potassium concentrations. They also noted an increase in the ratio of C_2+ products compared to methane with an increasing K/Fe ratio, and a concomitant increase in the olefin to paraffin ratio. In their study, the ethanol yield was enhanced by increasing the K/Fe ratio, but the methanol yield remained unchanged. Increasing temperature on unpromoted surfaces, generally increased the methane selectivity and the paraffin to olefin ratios, but these temperature dependant changes were much less noticeable on potassium promoted surfaces.

Arakawa also noted that the rate of the water-gas shift reaction was increased proportionally with the potassium loading. Analysis of catalysts showed that potassium significantly increased the initial rate of carburization, while the final C/Fe ratio increased from .47 for unpromoted Fe, to .75 for K/Fe=0.2. This carbonaceous deposit could be removed by hydrogenation. This hydrogenation produced only paraffins on unpromoted samples, but equivalent amounts of olefins and paraffins on promoted iron (although at a slower rate). Curiously, carbon deposition from gaseous CO occured more rapidly when H_2 was present in the gas phase.

Gonzales and Miura (1982) studied the affects of alkali on CO hydrogenation over a silica supported ruthenium catalyst. They also claim that they observed a decrease in the rate of all hydrocarbon formation with potassium co-impregnation (the methane rates being slowed more than the rates of higher molecular weight products). However, contrary to Arakawa's iron study, they observed an increase in Ru dispersion from 13 to 19%. They claim that the activation energy from methanation was increased by potassium, while Campbell (1982) observed no changes in the activation energy on nickel. Gonzales also showed a two order of magnitude increase in olefin to paraffin ratio at 220C with potassium loaded to 10%. As noted in Arakawa's study, they showed that the change in space velocity (or contact time) only changed the olefin to paraffin ratio, not the C_1 to C_2 ratios. In a very interesting in situ infra-red experiment, Gonzales also showed that only top site CO was observed on potassium free Ru, under reaction conditions, but both top and bridged CO appeared on potassium

loaded Ru. This is in agreement with our UHV study on Pt, where potassium coadsorption caused a change in CO site occupancy from top to bridged. They went on to show that it was the bridged CO which was the most reactive.

Of course, one of the main problems encountered with studies on supported catalysts is that the support itself may play an important role in some part of the reaction. This can be remedied by using low surface area powders, foils, or single crystals. On foils and single crystals, one has the added advantage that a surface can be examined in UHV both prior to, and following, a reaction (see section 2 above). This type of study has been carried out for CO hydrogenation by several workers including Bonzel and Krebs on iron, Campbell and Goodman on nickel, and in our group on iron and rhenium.

Campbell and Goodman (1982) monitored the changes in CO hydrogenation over nickel which occured with potassium deposition. By observing H_2O desorption during a post-reaction flash to 600K, they claim that potassium is present during the reaction as a "solvated" species. This observation should be contrasted to the claim of Ertl and coworkers (1983) that potassium is coadsorbed with oxygen on iron catalysts under <u>ammonia</u> synthesis conditions.

As in the supported metal studies, Campbell shows that potassium decreases the methanation rate by a factor of 2 for 0.1 monolayer potassium. But they did not observe a change in activation energy. One of their interesting observations was an increase in the steady state carbon coverage from .1 to .3 monolayers when potassium was added to .1 monolayers.

This "carbidic" carbon was still active and did not show graphitization poisoning until over 700K. Contrary to some high pressure results seen on supported iron, they claim that potassium does in fact increase the rate of production of higher molecular weight species on nickel, i.e., it is not just a selective poison but an actual rate promoter. They conclude from their study, that since CO is more tightly bound with coadsorbed potassium, and since CO has a higher dissociation probability (and steady state carbon coverage), that C-C bond formation becomes favored over hydrogenation. They further conclude, in agreement with others, that hydrogenation must be the slow step as the CH_4 activation energy was not changed by potassium, only its rate of formation.

In the Bonzel and Krebs (1980) study of K_2CO_3 deposited on an iron foil, the authors claim that K_2CO_3 probably decomposed into a KOH like species under reaction conditions. They also observed an increased rate of carbon deposition (in agreement with Arakawa), decreased rates of methanation, and selectivity changes toward higher molecular weight species. Their most interesting observation was that the potassium and oxygen XPS signal remained relatively constant during the reaction, but the Fe substrate signal was replaced by a carbon signal on surfaces examined after a reaction. They thus postulate that a potassium salt is "floating" on top of a carbonaceous overlayer. We have also observed this behavior under certain conditions. This behavior lends support to a second interpretation for the role of alkali promoters for CO hydrogenation. On nickel, it is relatively clear from the Campbell study that carbon does not form an unreactive

graphitic overlayer at temperatures below 700K. Thus the major role of potassium here seems to be an an electronic promoter to facilitate the dissociation of CO. With iron (or rhenium) on the other hand CO dissociates much more easily, and infact, enables graphitization and the formation of carbides in the near surface region under reaction conditions. In this case, one must consider the possible role of alkalis as facilitating the removal of carbonaceous overlayers (although not the dissolved carbon). In this type of model, the metal substrate does the CO dissociation (or dissproportionation), while the alkali overlayer helps hydrogenate the carbonaceous overlayer. This alkali induced hydrogenation could proceed as in steam gasification (see Appendix D).

6. REFERENCES

Kenichi Aika, Humio Hori and Atsumo Ozaki, J. Cat., 27, 424 (1972).

T.A. Albright, Acct. Chem. Res., 15, 149 (1982).

K. Altenburg, H. Bosch, J.G. Van Ommen, and P.J. Gellings, J. Cat., 66, 1980, 326.

A. B. Anderson, Michael McDevitt, and F. L. Urbach, to be published.

R.B. Anderson, in: Catalysis, Volume 4, (Ed. P.H. Emmett) Reinhold, New York, 1956.

R.B. Anderson, J. Catal., 4, 56 (1965).

H. Arakawa and A. T. Bell, Ind. Eng. Chem. Proc. Des. Dev., 22, 97 (1983).

M. Araki and V. Ponec, J Catal., 44, 439 (1976).

U. Bardi and G. Rovida, in: Proc. ICSS-4 and ECOSS-3, Cannes, p. 325 (1980).

A. M. Baro and H. Ibach, J. Chem. Phys., 71, 4812 (1979).

J. Benziger and R. J. Madix, Surface Sci., 94, 119 (1980).

J.P. Biberian and M.A. Van Hove, Surf. Sci, in press, 1983.

G. Blyholder, J. Phys. Chem., 68, 2772 (1964).

H. P. Bonzel and H. J. Krebs, Surface Sci., 109, L527 (1981).

H. P. Bonzel and H. J. Krebs, Surface Sci., 91, 499 (1980).

F. Bozso, J. Arias, J.T. Yates, R.M. Martin, and H. Metiu, Chem. Phys. Lett., 94, 243 (1983).

G. Broden, G. Gafner and H. P. Bonzel, Surface Sci., 84, 119 (1979)

G. Broden, G. Pirug and H. P. Bonzel, Chem. Phys. Letters, 73(3), 506 (1980).

R. Burch, Acct. Chem. Res., 15, 24 (1982).

A.L. Cabrera, Heinz Heinemann and G.A. Somorjai, J. Cat., 75, 7 (1982).

A.L. Cabrera, N.D. Spencer, E. Kozak, P.W. Davies, and G.A. Somorjai, Rev. Sci. Instr., 53(12), 1888 (1982).

C. T. Campbell, G. Ertl, H. Kuipers, and J. Segner, Surf. Sci., 107, 207 (1981).

C. T. Campbell and D. W. Goodman, Surf. Sci., 123, 413 (1982).

C. T. Campbell and T. N. Taylor, Surf. Sci., (1983).

H.C. Chen and R.B. Anderson, J. Catal., 28, 161 (1973).

John K. A. Clarke and Anne C. M. Creaner, I&EC Product Research and Development, 20, 574 (1981).

Demuth and Eastman, Phys. Rev. B, 13(4), 1523 (1976).

J. E. Crowell, E. L. Garfunkel, and G. A. Somorjai, Surface Sci., 121, 301 (1982).

A. Crossley and D. A. King, Surface Sci., 95, 131 (1980).

F. Delanney, E. Tysoe, H. Heinemann, and G.A. Somorjai, to be published (1983).

L.C. De Menorval and J.P. Fraissard, Chem. Phys. Lett., 77(2), 309 (1981).

G. Doyen and G. Ertl, Surface Sci., 43, 197 (1974).

M. E. Dry, T. Shingles, L. J. Bishoff and G. J. Oosthuizen, J. Cat., 15, 190 (1969).

J. Drowart, in: Condensation and Evaporation of Solids, Eds. E. Rutner, P. Goldfinger and J. P. Hirth (Gordon and Breach, New York, 1964).

L. H. Dubois and G. A. Somorjai, Surface Sci., 91, 514 (1980).

P.H. Emmett and S. Brunauer, J. Am. Chem. Soc., 56, 35 (1934).

G. Ertl, Energetics of Chemisorption on Metals, in The Nature of the Surface Chemical Bond, North Holland (1979a).

G. Ertl, Cat. Rev. Sci. Eng., 21, 201 (1980).

G. Ertl, M. Grunze, and M. Weiss, J. Vac. Sci. Tech., 13, 314 (1976).

G. Ertl and J. Kuppers, Low Energy Electrons and Surface Chemistry, Verlag Chemie (1974) Weinheim.

G. Ertl, M. Neumann and K. M. Streit, Surface Sci., 64, 393 (1977).

G. Ertl, D. Prigge, R. Schloegl and M. Weiss, J. Cat. 79, 359 (1983).

G. Ertl and N. Thiele, Appl. Surf. Sci., 3, 99 (1979b).

G. Ertl, M. Weiss and S. B. Lee, Chem. Phys. Lett., 60, 391 (1979).

F. Fajula, R.G. Anthony, J.H. Lunsford, J. Catal., 73, 237, (1982).

A. G. Fedorus and A. G. Naumovets, Surface Sci., 21, 426 (1970).

D.L. Fehrs and R.E. Stickney, Surf. Sci., 24, 309 (1971).

T.E. Fischer and S.R. Keleman, J. Catal. 53, 24 (1978).

T.E. Fischer, S.R. Keleman, and R.S. Polizzotti, J. Catal., 69, 345 (1981).

C. M. Friend, E. L. Muetterties, and John L. Gland, J. Phys. Chem., 85, 3356 (1981).

H. Froitzheim, H. Hopster, H. Ibach and S. Lehwald, Appl. Phys., 13, 147 (1977).

E. L. Garfunkel, J. E. Crowell and G. A. Somorjai, J. Phys. Chem., 86, 310 (1982).

E. L. Garfunkel, J. J. Maj, M. H. Farias, J. E. Frost, and G. A. Somorjai, Journal of Physical Chemistry, (1983).

E. L. Garfunkel and G. A. Somorjai, Surface Sci., 115, 441 (1982).

R. L. Gerlach and T. N. Rhodin, Surface Sci., 19, 403 (1970); 17, 32 (1969).

E. Gillet and B. Gruzza, Surf. Sci., 97, 553 (1980).

J. L. Gland and B. A. Sexton, Surface Sci., 94, 355 (1980); and R. J. Gorte, L. D. Schmidt and J. L. Gland, Surface Sci., 109, 367 (1981).

S. Glasstone, K.J. Laidler and H. Eyring, The Theory of Rate Processes, McGraw-Hill, New York (1941).

R. Gorte and L. Schmidt, Surf. Sci., 76, 559 (1978).

R.D. Gonzalez and Hiroshi Miura, J. Catal., 77, 338 (1982).

D.W. Goodman, R.D. Kelley, T.E. Madey, and J.T. Yates, J. Catal., 63, 226 (1980).

F. Haber, Z. Electrochem., 16, 244 (1910).

T. Halachev and E. Ruckenstein, J. Catal, 73, 171 (1982).

Katsumi Hanji, Hasime Shimuzu, Hitoshi Shindo, Takaharu Onishi, and Kenzi Tamaru, J. Res. Inst. Catalysis, Hokkaido Univ., 28(3), 175 (1980).

W. Heegemann, K.H. Meister, E. Bechtold and K. Hayek, Surf. Sci., 49, 161 (1975).

C.R. Helms, H.P. Bonzel and S. Keleman, J. Chem. Phys., 65, 1773 (1976).

J. Holzl and F.K. Schulte, Work Function of Metals, in Solid Surface Physics, Springer, 1979.

F. Hoffmann, private communication, 1983.

P. Hofmann, K. Horn, and A.M. Bradshaw, Surf. Sci., 105, L260 (1981).

B.A. Hutchins, T.N. Rhodin, and J.E. Demuth, Surf. Sci., 54, 419 (1976).

H. Ibach and D.L. Mills, Electron Energy Loss Spectroscopy and Surface Vibrations, Academic Press, London, 1982.

H. Itoh and A. B. Kunz, Chem. Phys. Lett., 64(3), 576 (1979).

Alan Jones and Brian D. McNicol, J. Catal., 47, 384 (1977).

J. E. Katz, P. W. Davies, J. E. Crowell and G. A. Somorjai, Rev. Sci. Instr., 53(6), 785 (1982).

S.R. Keleman, T.E. Fischer, and J.A. Schwartz, Surf. Sci., 81, 440 (1979).

S.R. Keleman, A. Kaldor and D. J. Dwyer, Surface Sci., 121, 45 (1982).

D.A. King, Chem. and Phys. of Solid Surf. II, CRC Press (1979).

M. Kiskinova, Surface Sci., 111, 584 (1981).

M. Kiskinova and D. W. Goodman, Surf. Sci., 108, 64 (1982).

M. Kiskinova, G. Pirug, and H.P. Bonzel, Surf. Sci., in press (1983).

M. Kiskinova, L. Surnev and G. Bliznakov, Surface Sci. 104, 240 (1981).

B. E. Koel, D. E. Peebles, and J. M. White, Surf. Sci., 125, 709 (1983).

R. J. Koestner, M. A. Van Hove, and G. A. Somorjai, ChemTech, 13(6), 376 (1983).

Kotz and Purcell, Inorganic Chemistry, p890, Saunders, 1977.

H. J. Krebs and H. P. Bonzel, Surf. Sci., 99, 570 (1980).

H. J. Krebs, H. P. Bonzel and G. Gafner, Surf. Sci., 88, 269 (1979).

E.L. Kugler and F.W. Steffgen, Eds., Hydrocarbon Synthesis from Carbon Monoxide and Hydrogen, Am. Chem. Soc. (1979).

I. Langmuir and K.H. Kingdon, Science, 57, 58 (1923); Proc. Roy. Soc. A107, 61 (1925).

I. Langmuir and J.B. Taylor, Phys. Rev., 44, 6 (1933).

J. Lee, C.P. Hanrahan, J. Arias, R.M. Martin, and H. Metiu, to be published, 1983.

S.B. Lee, M. Weiss and G. Ertl, Surface Sci., 108, 357 (1981).

S. Lehwald, H. Ibach, and J.E. Demuth, Surface Sci., 78, 577 (1978).

R.F. Lin, D.F. Ogletree, M.A. Van Hove, and G.A. Somorjai, to be published.

A. Lindgren and L. Walden, Surface Sci., 89, 319 (1979).

H. Luftman, Y.M. Sun, and J.M. White, to be published, 1983.

H. Mayer, Z. Physik, 115, 729 (1940).

J. J. McCarroll, Surface Sci., 53, 297 (1975).

D.W. McKee and D. Chatterji, Carbon, 13, 381 (1975).

G. B. McVicker and M. A. Vannice, J. Cat., 63, 25 (1980).

A. Mittasch, Geschichte der Ammoniak Synthese (Verlag Chemie, Berlin, 1951).

C.A. Mims and J.K. Pabst, Fuel, 62, 176 (1983).

D. R. Monroe and R. P. Merrill, J. Catalysis, 65, 461 (1980).

T. du Motay, Br. Pat. 2548 (1867).

E. L. Muetterties, J. R. Bleeke, E. J. Wucherer, and T. Albright, Chem. Rev. 82, 499 (1982).

G. Natta, in: Catalysis, Vols. 3 & 5 (P.H. Emmett, ed.) Reinhold, New York, 1955.

F.P. Netzer, E. Bertel, and J.A.D. Matthew Surf. Sci., 92, 43 (1980).

F.P. Netzer and J.U. Mack, J. Chem. Phys., 79(2), 1017 (1983).

B. E. Nieuwenhuys, Surface Sci., 105, 505 (1981).

F. Nitschke, G. Ertl, and J. Kuppers, J. Chem. Phys., 74(10), 5911, (1981).

P. R. Norton, J. W. Goodale and E. B. Selkirk, Surface Sci., 83, 189 (1979).

A. D. Novaco and J. P. McTague, Phys. Rev. Letters, 38, 1286 (1977).

A. D. Novaco and J. P. McTague, J. Physique, Colloq., 38.

G.L. Nyberg and N.V. Richardson, Surf. Sci., 85, 335 (1979).

Motomu Oh-Kita, Hideo Midorikawa, Ken-ichi Aika, and Atsumu Ozaki, J. Cat., 70, 384 (1981).

A. Osborne and C.S. Donahue, PET/CBM Personal Computer Guide, Osborne/McGraw-Hill, Berkeley (1980).

Z. Paal, G. Ertl, and S.B. Lee, Appl. Surf. Sci., 8, 231 (1981).

C.A. Papageorgopoulus and J.M. Chen, Surf. Sci., 52, 40 (1975).

L. Pauling, The Nature of the Chemical Bond, Cornell University Press (1960) Ithaca, New York.

L.A. Petermann, Prog. Surf. Sci., 3, 1 (1972).

G. Pirug, H. P. Bonzel, and G. Broden, Surf. Sci., 122, 1 (1982).

V. Ponec, Cat. Rev. Sci. Eng., 18, 151 (1978).

V. Ponec, Surf. Sci., 80, 352 (1979).

D. Post and E. J. Baerends, Surf, Sci., 109, 167 (1981).

M.L. Poutsma, L.F. Elek, P.A. Ibarbia, A.P. Risch, and J.A. Rabo, J. Catal., 52, 157 (1978).

N.K. Ray and A.B. Anderson, Surf. Sci., 125, 803 (1983).

P.A. Redhead, Vacuum 12, 203 (1962).

A. Redondo, Y. Zeiri and W.A. Goddard, Phys. Rev. Lett., 49(25), 1847 (1982).

M.W. Roberts and C.S. McKee, Chemistry of the Metal-Gas Interface, Oxford Univ. Press (1978).

A. Rosen, E. J. Baerends and D. E. Ellis, Surface Sci., 82, 139 (1979).

SAES Getters/USA Inc., Colorado Springs, CO.

W.M.H. Sachtler, Catal. Rev., 14, 193 (1976).

M. Salmeron and G. A. Somorjai, J. Phys. Chem., 86, 341 (1982).

L. D. Schmidt and R. Gomer, J. Chem. Phys., 45, 1605 (1966).

E. Shustorovich and R. Baetzold, Appl. of Surf. Sci., 11/12, 693 (1982).

G. A. Somorjai, Chemistry in Two Dimensions: Surfaces, Cornell University Press (1981).

G. A. Somorjai and M. A. Van Hove, Adsorbed Monolayers on Solid Surfaces (Springer, 1979).

N. D. Spencer and G. A. Somorjai, Reports on Progress in Physics, The Institute of Physics, 46,1, 1 (1983).

N.D. Spencer and G.A. Somorjai, J. Catal., 78, 142 (1982).

P.C. Stair, J. Am. Chem. Soc., 104(15), 4044 (1982).

Steininger, Lehwald, and Ibach, Surf. Sci., 123, 264 (1982).

F. Stoop, F.J.C.M. Toolenaar, and V. Ponec, J. Catal., 73, 50 (1982).

H.H. Storch, N. Golumbic, and R.B. Anderson, The Fischer-Tropsch and Related Syntheses, Wiley, New York, 1951.

S. J. Tauster, S. C. Fung, R. T. K. Baker, and J. A. Horsley, Science, 211, 1121 (1981).

J.M. Thomas and R.M. Lambert, eds., Characterization of Catalysts, Wiley (1980).

F.C. Tompkins, Chemisorption of Gases on Metals, Academic Press, London (1978).

J. Topping, Proc. Roy. Soc. (London) A, 114, 67 (1927).

D.L. Trimm, Design of Industrial Catalysts, Elsevier, Amsterdam (1980).

Min-Chi Tsai and E. L. Muetterties, J. Am. Chem. Soc., 104, 2534 (1982).

M.A. Van Hove, S.Y. Tong, and N. Stoner, Surf. Sci., 54, 259 (1976).

M.A. Vannice, Cat. Rev. Sci. Eng., 14(2), 153 (1976).

M.A. Vannice, J. Cat., 74, 199 (1982).

R.A. Van Santen, private communication, 1983.

M.J. Veraa and A.T. Bell, Fuel, 57, 194 (1978).

J.C. Vickerman, K. Christmann, and G. Ertl, J. Catal., 71, 175 (1981).

K. Wandelt, H. Hulse, and J. Kuppers, Surf. Sci., 104, 212 (1981); and J. Kuppers, K. Wandelt, and G. Ertl, Phys. Rev. Lett., 43, 928 (1979).

C. Wagner, J. Chem. Phys., 21, 1819 (1953).

P.R. Watson and G.A. Somorjai, J. Catal., 74, 282 (1982).

W.H. Weinberg, R.M. Lambert, C.M. Comrie, and J.W. Linnett, Surf. Sci 30, 299 (1972).

Wen-Yang Wen, Cat. Rev.-Sci. & Eng., 22, 1 (1980).

D. H. Winicur, J. Hurst, C.A. Becker and L. Wharton, Surface Sci., 109, 263 (1981).

J.T. Yates, Vacuum, 31, 715 (1981).

J.T. Yates, in press, 1983.

R.F. Hicks, Q.J. Yen, and A.T. Bell, to be published.

M. Primet, J.M. Bassett, M.V. Mathieu, and M. Prettre, J. Cat. 29, 213 (1973).

Appendices 190

A. Classification of additives 191

A.1 Introduction 191

A.2 Operational (Macroscopic) Categories of Catalyst Additives 192

A.3 Fundamental (Microscopic) Categories of Catalyst Additives 193

B. Thermal Desorption Spectroscopy: Practice and Theory... 197

B.1 Theory of Rate Processes 198

B.2 The Thermal Desorption Equations 204

B.3 Aspects of the Thermal Desorption Experiment 212

B.4 Problems in Thermal Desorption Analysis 216

C. Sulfur as an additive 220

C.1 Introduction 220

C.2 Experimental 221

C.3 Results 223

C.4 Discussion 228

C.4.1 The Effect of Potassium 228

C.4.2 The Effect of Sulfur 229

D. Review of related uses of alkali promoters in catalysis.... 232

D.1 Carbon Gasification 232

D.2 Ammonia Synthesis 238

E. PET computer programming for surface science 240

E.1 Introduction 240

E.2 Computer Controlled Thermal Desorption Spectroscopy E-2 241

E.3 Computer Control for Photoelectron and Auger Spectroscopy 242

E.4 Auger/ESCA Display Program 243

Appendix A. Categories of Additives for Metal and Oxide Catalysts.

A.1 Introduction.

Catalyst components may be roughly divided into three groups: the active component (often a transition metal), the support (such as silicon oxide or aluminum oxide), and the additives (such as promoters or selective inhibitors). Certain components may serve more than one structural or functional purpose, but these general distinctions should be useful.

In choosing a catalyst, excluding economic considerations, one is usually interested in finding a combination of components which will optimize: 1) overall rate, 2) selectivity, and 3) lifetime of the catalyst for any given reaction. These three factors of rate, selectivity, and lifetime are operational parameters which can be readily measured from product yields and distibutions.

In developing a classification scheme for catalyst additives, it is important to first operationally classify them in terms of their macroscopic effects. Once this is achieved, a more fundamental classification scheme is required to define the way in which the additive interacts on the microscopic level with the reactants and intermediates, as well as the active metal component of the catalyst.

We propose the following four fundamental catagories of additives to distinguish between their microscopic properties: electronic (chemical), surface structural, support/textural, and bifunctional. Although many of these properties have been discussed in the literature recently, it is important to bring them together to begin developing a complete model of promoter action in catalysis. Some useful papers are:

Burch (1982), Ponec (1979), Sachtler (1982), Vickerman (1981), Yates (1981), Ponec (1979), Stair (1982), Stoop (1982), Fischer (1981), Halachev (1982), and Benziger (1980). The rest of this section will be devoted to defining both the operational and fundamental categories, Methods of catalyst preparation or regeneration will not be discussed.

A.2 Operational (Macroscopic) Categories of Catalyst Additives.

1) The overall rate is generally considered to be the rate of conversion of reactants to products. Any additive which increases the rate of reaction can therefore be considered a rate promoter. The overall rate of a catalytic reaction can be increased in a number of ways. Standard techniques include increasing the surface area of the active component and optimizing temperature, pressure, mass transport, and other reaction conditions.

2) Given the difficulty and expense of separation techniques, a major interest of the chemical industry is not the total rate of conversion of reactants to products, but the selective conversion to (a) specific product(s). The selectivity of the catalyst is a measure of the relative rates of competing reaction pathways. Additives are now routinely used both to promote the conversion to desired products, as well as to suppress undesirable reaction pathways. In general, any additive which induces a desirable change in selectivity can be considered a selectivity promoter.

3) Most catalysts have a definite lifetime for a given reaction after which they become inactive. This may range from several hours

for certain supported platinum catalysts to several months for some iron catalysts. The loss of activity may be the result of surface poisoning, such as an inactive carbon or sulfur adlayer, or a loss of particle dispersion by sintering. Any additive which increases the useful lifetime of a catalyst, whether it be by maintaining dispersion (textural promoter) or reducing coking and poisoning, can be called a lifetime promoter.

A.3 Fundamental (Microscopic) Categories of Catalyst Additives.

Many hypotheses have been developed over the past fifty years concerning reaction dynamics on catalytic surfaces, but it was not until very recently that conclusive evidence could be given to verify one or another microscopic model of a catalytic reaction. The atomic level techniques involve the study of adsorbed species on solid surfaces under ultrahigh vacuum conditions, and actual in situ studies of catalytic surfaces by infrared spectroscopy and and electron microscopy (see section 2.5.3).

In addition to the relatively simple systems which have recently been studied (using single crystal metal surfaces as model catalysts with adsorbates such as H_2, N_2, CO, NO, O_2, and C_2H_4), researchers in various laboratories are also probing the microscopic state and function of catalyst additives and alloys. We now define the four fundamental categories of the known (and possible) functions that additives have at the atomic level.

1. An electronic promoter is an additive that interacts directly with the active component of the catalyst and modifies its surface

electronic properties. The electronic promoter itself is not the catalyst but only modifies an existing active catalyst. This may, but not necessarily, involve a change in oxidation state of the active component. Electronic promoters are usually of two general types:

a) The first type changes the oxidation state of the substrate metal, but still permits adsorption. Examples of this are the oxidizing and some sulfiding pretreatment additives.

b) The second type does not change the oxidation state, but modifies the electronic properties of the active component. This category of additive function is commonly called the ligand effect, and can be further subdivided into those additives which affect the surface over a relatively long range (perhaps by donating or withdrawing electrons from the delocalized s-bands of the metal), and those which exhibit only nearest neighbor effects (presumably by modifying the localized d-orbitals).

2. A structural additive of the active metal surface is one whose dominant effect is to change some properties of the metal surface by altering the structure (or composition) of the region surrounding the active metal atoms. Electronic effects on the metal centers are considered secondary here. Two important types of structural additives are the ensemble size and face-selective additives.

a) An ensemble size additive is one in which the active metal component of the catalyst is diluted in a matrix of inactive atoms. Several alloy systems are believed to belong to this class of additives. For example, the group IB elements Cu, Ag, and Au, when alloyed with the platinum group metals sometimes exhibit this behavior. In practice, however, it

is difficult to distinguish between the ensemble effect and a weakly perturbing ligand effect.

By diluting the active metal in an "inert" matrix, bridged and multiple bonding sites may disappear, as well as those sites important for bond-breaking. This aspect of adsorbates is variously referred to as geometric, structural, template, or coordination effects in the surface science literature. The exact role that the ensemble effect has in catalysis, of course, differs from one reaction or surface to another.

b) A face-selective additive stabilizes a certain crystallographic orientation of small supported metal clusters. For example, the Ni(111) crystallographic surface is known to reorient to a (100) orientation in the presence of sulfur; also the Pt(100) to (111) (ie. 5x20) transition is known to be stabilized by the presence of potassium. Different faces of the same metal have been shown to exhibit remarkably varied catalytic behavior. The most striking example of this has been in the ammonia synthesis, where Fe(111) was shown to produce ammonia at 418 times the rate of Fe(100), Spencer (1982).

3. Support (or textural) additives have long been used in the construction of catalysts. Here, the additive interacts most directly with the support, not the active metal component. Perhaps the most common function for such additives is to stabilize a high surface area of the active component, preventing sintering. MgO and CaO, when added to iron catalysts, are thought to function in this way. Another class of additive is believed to block certain support sites which are undesirable for the synthesis. A third type of additive provides a "sink" to which impurities segregate, keeping the active component clean.

One of the more interesting, although controversial, support effects is the recent observation of "strong metal support interactions" (SMSI) (Tauster, 1981). One reaction where SMSI is observed is in the hydrogenation of CO on rhodium catalysts. Rh on TiO_2 catalysts, after high temperature reduction, shows little sign of hydrogen or CO adsorption, and its catalytic activity changes dramatically relative to that observed for reduction of rhodium on SiO_2. One of the dominant interpretations (as put forth in Tauster, et al) is that for high dispersion, TiO_2 donates electrons into the Rh, filling up its d-shell, making it more like Ag, Au, or Pt in its catalytic activity. [We believe that this interpretation is wrong and that what is observed is due to encapsulation or a new $Rh_xTi_yO_z$ phase.]

Nevertheless, the idea of support induced electronic interactions should, in principle, be considered. A related observation is that particle size appears crucial in determining electronic properties. In a very interesting set of NMR experiments, DeMonorval (1981) showed that the adsorbed hydrogen signal (for H_2 on a platinum catalyst) shifted significantly when catalyst particles of less than a 30 Å diameter were prepared. For large metal clusters, however, significant charge transfers from or to the support are unlikely from electrostatic considerations.

4. A <u>bifunctional</u> (or trifunctional) additive does not promote the active component, but adds a second catalytic surface. For example, the Pt-Pd-Rh auto emissions catalyst where NO_x is reduced on the Rh surface, while CO and unburned hyrocarbons are oxidized on the Pt surface. The bifunctional additive thus enables the dual catalyst to perform two (or more) separate reactions on the different surfaces.

Appendix B. Thermal Desorption Spectroscopy: Theoretical and Practical Aspects

The desorption of atoms and molecules from a solid surface can be achieved by any of several means, including thermal desorption, photodesorption, electron (and ion) stimulated desorption, and field desorption. In this section, I will discuss the theory and practice of thermal desorption spectroscopy (TDS, also known as temperature programmed desorption (TPD), with special reference to experiments performed in ultrahigh vacuum. Although TDS can in principle offer quantitative information on a great variety of thermodynamic and kinetic aspects of adsorption and desorption phenomena, it has been my experience that it is very difficult to get accurate "numbers" out. The new molecular beam surface scattering techniques offer a more quantitative analysis of these surface phenomena, but at a great cost in time and money. The great advantage of TDS is that it is a relatively simple way of getting semi-quantitative thermodynamic data, and is especially appropriate for understanding trends in chemisorption, of the type discussed in this thesis.

This appendix is outlined as follows: 1) brief review of statistical mechanical theory of rate processes, 2) the derivation of the thermal desorption equations, 3) the thermal desorption experiment, and 4) experimental and theoretical problems in analysis. Several excellent introductions to thermal desorption can be found in the literature, including: King (1979), Peterman (1972), Redhead (1962), Ertl (1979a), Tompkins (1978), Somorjai (1981), Roberts (1978), Gorte (1978), and Yates (1983).

B.1 Theory of Rate Processes

From quantum mechanics the potential energy of any reacting species can be determined as a function of bond distance (see Figure B.1a). By taking the classical path of lowest energy through the saddle, can plot the "reaction coordinate" an energy profile of the reaction, Figure B.1b.

For any given case, one can define the equilibrium constant, K_c as:

$$K_c = \frac{\text{concentration in final state}}{\text{concentration in initial state}} \qquad \text{Eqn. B.1}$$

$$= \frac{N_f}{N_i} \text{ (constant V; N = number of molecules)}$$

$$= \frac{F_f}{F_i} \text{ (F = molar partition function)}$$

$$= \frac{f_f}{f_i} \text{ (f = the atomic partition function)}$$

The atomic partition function, f, is give by

$$f = \sum_i g e^{-\varepsilon_i/kT} \text{ (where g is the degeneracy of the } i^{th} \text{ level)}$$

Since the system is quantized, the reaction coordinate for any two states can be depicted by Figure B.2a,

where $\varepsilon_f' = \varepsilon_o + \varepsilon_f$ (where ε_o is the zero point energy difference). The total equilibrium constant is then:

$$K_c = \frac{F_f}{F_i}$$

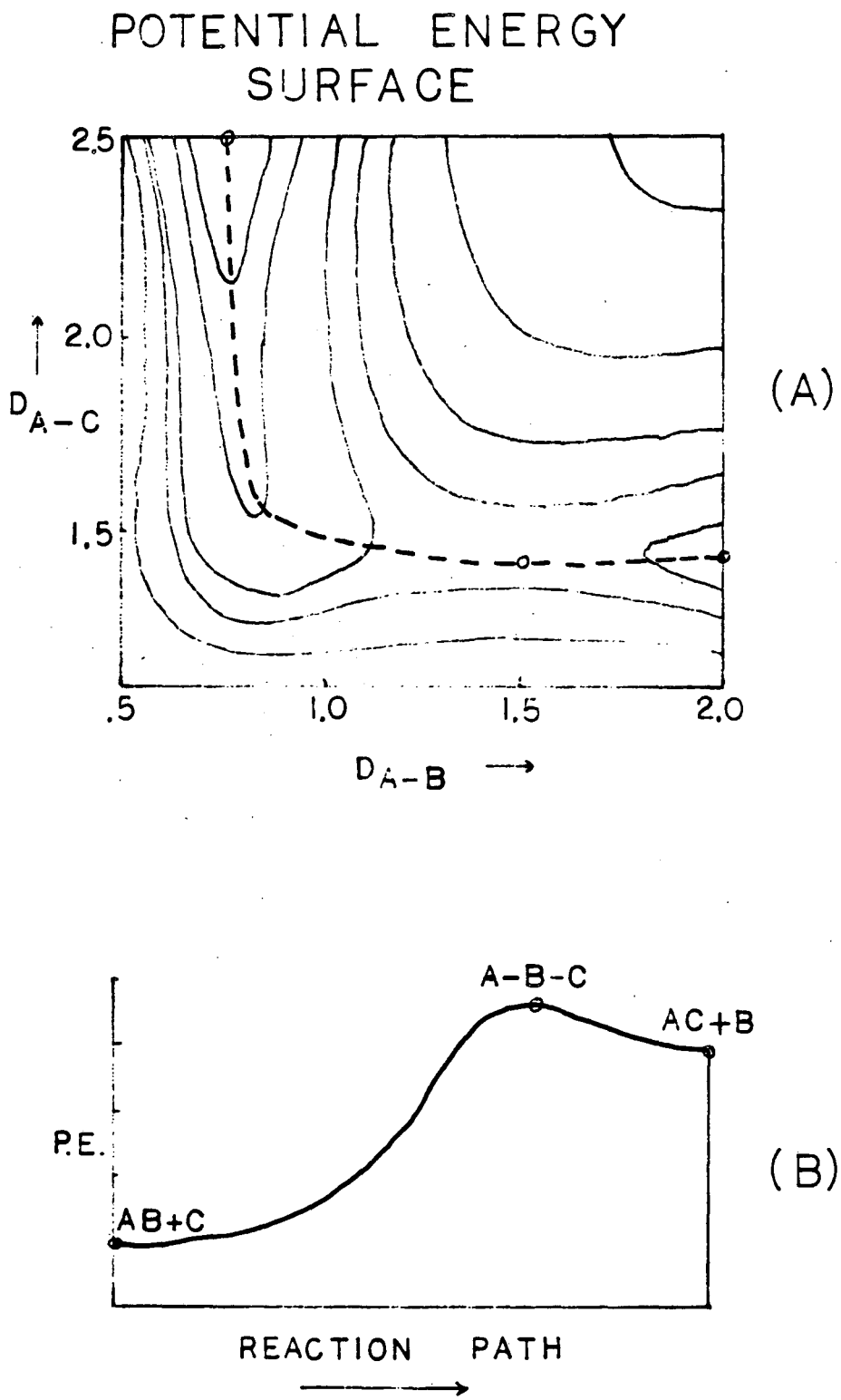

XBL 838-11080

Figure B.1

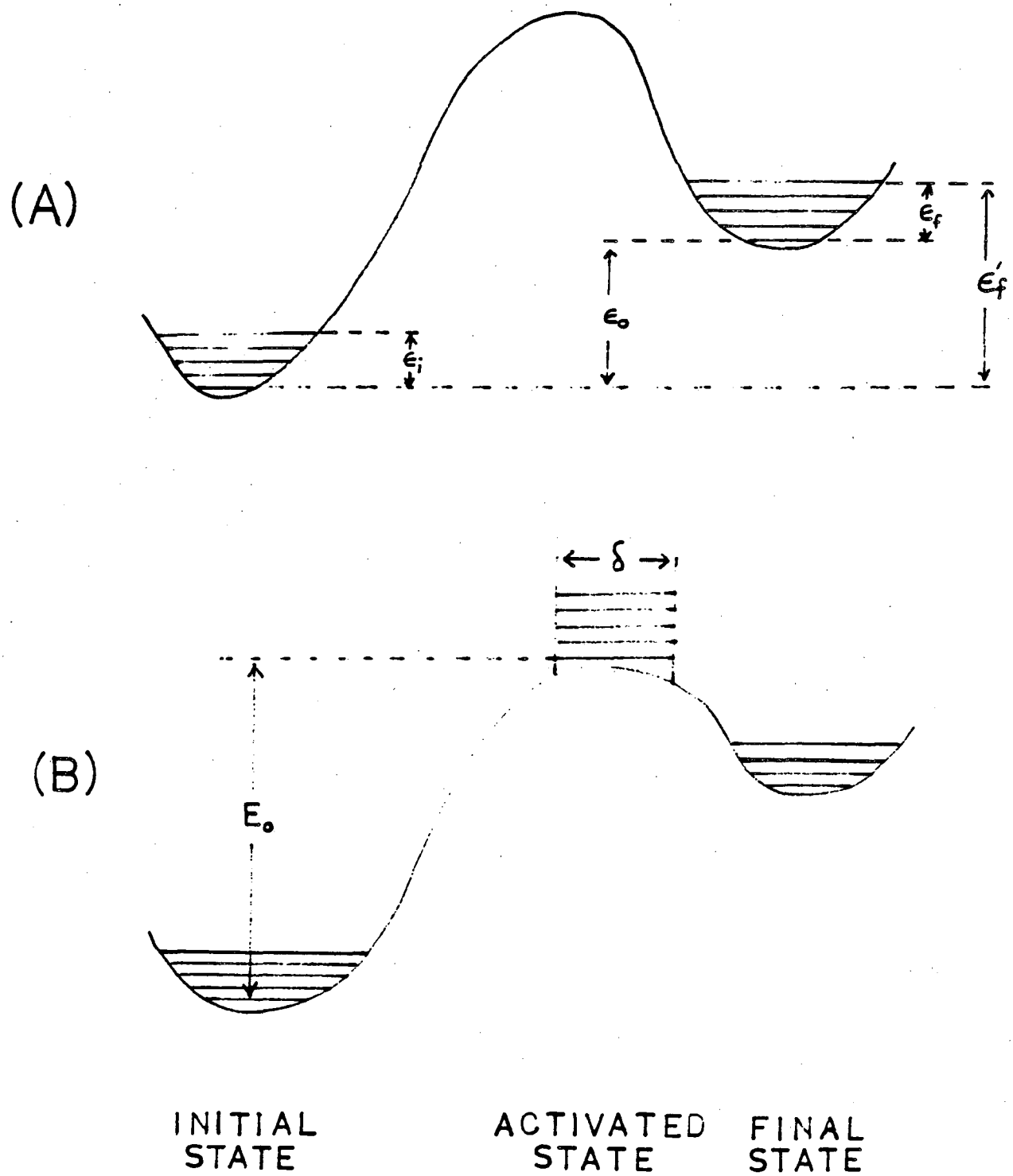

XBL 838-11079

Figure B.2 (from Glasstone)

where

$$F_f = \sum_i g e^{-\varepsilon_f' f/kT} = e^{-\varepsilon_o/kT} \sum_i g\, e^{-\varepsilon_f/kT}$$

(and $F_i = \ldots$).

The "absolute rate theory" (or "transition state theory") assumes that an "activated complex" exists and is in quasi-equilibrium with the initial state. The transition state model is shown in Figure B.2b.

One can define an equilibrium constant between the initial and activated states as:

$$K^{\ddagger} = \frac{C^{\ddagger}}{\prod_i C_i} \qquad \text{Eqn. B.2}$$

From the kinetic theory of gases, the mean velocity of an atom or molecule passing through the barrier is

$$\langle \frac{dx}{dt} \rangle = \frac{k_b T}{2\pi m^*} \text{ (where } m^* \text{ is the effective mass of the complex).}$$

The average time, τ, for crossing through the barrier is

$$\tau = \frac{\delta}{\langle \frac{dx}{dt} \rangle} = \delta \sqrt{\frac{2\, m^*}{k_b T}} \text{ where } \delta \text{ is the width of the barrier.}$$

If we then assume that every atom or molecule which has enough energy to reach the barrier passes through it, then the rate of reaction can be expressed as

$$\frac{-dN}{dt} = \frac{C^{\ddagger}}{\tau} = C^{\ddagger}\sqrt{\frac{k_bT}{2\Pi m^*}} \cdot \frac{1}{\delta} = k \prod_i C_i \ . \qquad \text{Eqn. B.3}$$

So the rate constant is

$$k = \frac{C^{\ddagger}}{\prod_i C_i} \sqrt{\frac{k_bT}{2\Pi m^*}} \cdot \frac{1}{\delta}$$

And $\frac{C^{\ddagger}}{\prod_i C_i} = K_c^{\ddagger} = \frac{F^{\ddagger''}}{\prod_i F_i} = \frac{F^{\ddagger'}}{\prod_i F_i} e^{-E_o/RT}$

where $F^{\ddagger''}$ and $F^{\ddagger'}$ are the partition function for the activated complex with and without the (molar) zero point energy included.

We now make the further assumption that one of the vibrational degrees of freedom (along the reaction coordinate) should be "frozen out" and converted into a translational degree of freedom:

$$F^{\ddagger'} = F^{\ddagger} f_{tr} = F^{\ddagger} \sqrt{\frac{2\Pi m^* k_bT}{h}} \cdot \delta$$

Thus, we have:

$$k = \frac{k_bT}{h} \frac{F^{\ddagger}}{\prod_i F_i} e^{-E_o/RT} \qquad \left(\text{where } \frac{k_bT}{h} \approx 10^{13} \text{ at RT}\right) . \qquad \text{Eqn. B.4}$$

Since (quantum mechanically) we must consider that the complex will not necessarily go through the final state but may fall back into the initial state from the activated state, we add the transmission coefficient (α).

$$k = \frac{k_bT}{h} \alpha K^{\ddagger} \quad \text{where } K^{\ddagger} = \frac{F^{\ddagger}}{\prod_i F_i} e^{-E_o/RT}$$

This can be reexpressed in somewhat more useful thermodynamic terms as:

$$-\Delta G^{\ddagger} = RT\ln K^{\ddagger} \quad \text{(free energy of activation)} \qquad \text{Eqn. B.5}$$

$$\text{so } k = \alpha \frac{k_b T}{h} e^{-\Delta G^{\ddagger}/RT} = \alpha \frac{k_b T}{h} e^{-\Delta H^{\ddagger}/RT} e^{\Delta S^{\ddagger}/R}$$

but, we usually measure the energy, E, at constant volume or pressure;

$$E_p = RT + \Delta H^{\ddagger} = E_a$$

$$\text{so } k = \alpha e \frac{K_b T}{h} e^{-E_a/RT} e^{\Delta S^{\ddagger}/R}$$

$$\text{or more simply } k = \nu e^{-E_a/RT} \qquad \text{Eqn. B.6}$$

where $\nu = \alpha e \frac{K_b T}{h} e^{\Delta S^{\ddagger}/R}$ is called the pre-exponential factor.

B.2 The Thermal Desorption Equations

For adsorption (as distinct from a gas phase process), the potential energy diagram is somewhat different than the biomolecular reaction case expressed in Figure B.1b. Instead, the reaction coordinate will resemble Figure B.3a or B.3b.

The distance along the reaction coordinate needed to reach the barrier is infinite (unless there exists an activation energy for adsorption). In practice we assume that it is finite (~2-5Å) and perform the calculation accordingly. It is useful at this point to distinguish between the two types of adsorption described in Figures B.3a and B.3b. In Figure B.3a, level B is considered a physisorbed state (also sometimes called a precursor state), while F Fig. B.3a and b is the chemisorbed state shown with and without an activation energy of adsorption. The physisorbed or precursor state can be roughly defined as a state with a heat of adsorption of less than 10 Kcal/mole. In Figure B.3b, dissociatve chemisorption is shown, in this case with a large activation energy for dissociation. Note the difference between the heat of chemisorption (A-B), and the heat of desorption (C-B), the difference being the activation energy for dissocation (A-C).

Returning now to our rate expresion we have

$$k = \alpha e \frac{k_b T}{h} e^{\Delta S^{\ddagger}/RT} \quad e^{-E_a/RT} = \nu e^{-E_a/RT}$$

To find the rate of desorption, $-dN_a/dt$, from a surface we merely multiply by the concentration (for first order desorption):

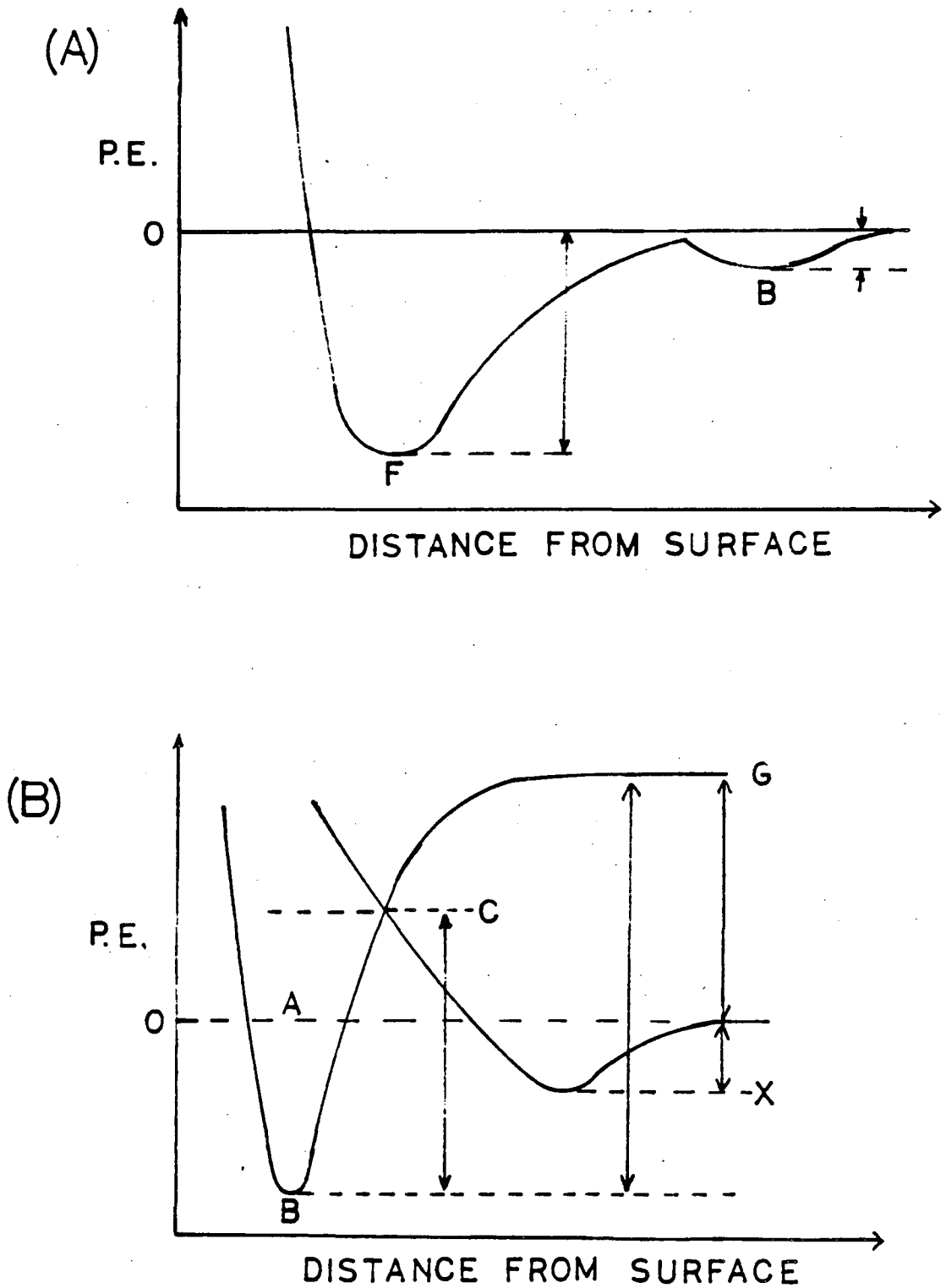

XBL 838-11078

Figure B.3 (from Tompkins)

$$\frac{-dN_a}{dt} = k \cdot N_a = \nu \cdot N_a \cdot e^{-E_d/RT} \qquad \text{Eqn. B.7}$$

where E_d = activation energy of desorption

ν_1 = preexponential factor, $\approx 10^{13}$ sec^{-1}

N_a = concentration of adsorbate

In general, for n^{th} order desorption we have

$$\frac{dN_a}{dt} = N_a^n \nu e^{-E_d/RT}$$

In the thermal desorption experiment one usually measures the pressure as a function of time (or temperature). In general, the change in pressure is proportional to the rate of desorption, minus the pumping speed (above steady state). In most UHV chambers it is now reasonable to assume that the pumping speed is fast compared to the "characteristic time" for desorption, and we have:

$$\frac{-dN_a}{dt} = \frac{S}{Ak_bT} \Delta P$$

where S = pumping speed

A = surface area of sample

ΔP = change in pressure

For a linear heating rate of the sample, $T = T_o + \beta t$, where $\beta = dT/dt$, i.e. the heating rate. If we assume that ν and E_d are coverage independent, then we can solve our equation to find the temperature at which the desorption rate is a maximum:

$$\frac{d^2N}{dT^2} = 0, \text{ (for desorption rate maximum)}$$

$$\frac{dN}{dt} = \frac{dN}{dT} \cdot \frac{dT}{dt} \quad \text{or} \quad \frac{dN}{dT} = \frac{dN}{dt} / \beta$$

Solving further:

$$- \frac{dN}{dT} = \frac{N_a^n}{\beta} \nu e^{-E_d/RT} \qquad \text{Eqn. B.9}$$

For n = 1 (first order desorption) we get:

$$\frac{d^2N}{dT^2} = 0 = \frac{d}{dT} \left(\frac{N_a}{\beta} \nu e^{-E_d/RT} \right) \qquad \text{at } T = T_p$$

or

$$\left(\frac{\nu}{\beta}\right) N_a \, e^{-E_d/RT_p} \quad \left(\frac{\nu}{\beta}\right) e^{-E_d/RT_p} = \left(\frac{N_a \nu}{\beta}\right) e^{-E_d/RT_p} \left(\frac{E_d}{RT_p^2}\right)$$

rearranging we get:

$$\left(\frac{\nu}{\beta}\right) e^{-E_d/RT_p} = \frac{E_d}{RT_p^2} \qquad \text{Eqn. B.10}$$

For first order desorption with $\nu = 10^{13}$ s^{-1} and

$= 10^2$-10^3 K/s) we get

$$E_d \simeq .06 \, (T_p) \text{ in kcal/mole.} \qquad \text{Eqn. B.11}$$

For n = 2 we get

$$\left(\frac{2n_p\nu}{\beta}\right)e^{-E_d/RT} = \left(\frac{E_d}{RT_p^2}\right) \qquad \text{Eqn. B.12}$$

where $\frac{1}{2}n_o = n_p$ which is the coverage at $T = T_p$.

For first order desorption, the peak position should be independent of coverage. First order desorption kinetics are typical for physisorption and associative chemisorption. Here the T_p and FWHM are coverage independent. For second order desorption, the peak position should decrease with increasing coverage. Adsorbed hydrogen exhibits second order desorption behavior as it is dissociatively adsorbed. For zeroth order desorption kinetics the peak position should increase with increasing coverage (or temperature). Examples of zeroth order kinetics are metal and metal oxide (i.e. multilayer) desorption.

In some instances, several states will exist on the surface, giving rise to several peaks. The most simple solution is:

$$\frac{dN_t}{dt} = \sum_i \frac{dN_i}{dt} \quad \left(\text{where } \frac{dN_t}{dt} \text{ is the total desorption distribution from } i \text{ states}\right)$$

Usually, however, one does not find ideal desorption behavior. Often E_{ad} and/or ν are coverage dependent. Also, precursor states modify desorption kinetics as discussed in Section B.4.

Before discussing the thermal desorption experiment, it is worth commenting briefly on an added complication of desorption phenomena.

If an atom or molecule is relatively free to move along the surface then the partition F_{ads} (F_i in Eqn. B.4) should be relatively large as in a 2-D gas. $F_{trans} \approx 10^{10}$ per degree of translational freedom. On the other hand, if the molecule is confined to a certain site on the surface F_{ads} will be smaller: F_{ads} (immobile) $< F_{ads}$ (mobile). Since F_{ads} is larger for the 2-D gas, the rate constant, k(mobile), will become smaller than k(immobile). This can be visualized graphically as follows: consider a metal surface onto which is placed an adatom such as sulfur which does not bond strongly with a molecule such as CO or H_2. The potential energy of an adsorbate on the clean and modified surfaces can be represented as in Figure B.4a. A change in the potential energy contour for an adsorbate along the surface will cause a change in mobility of the adsorbate. This will become manifest in a change in the preexponential factor (i.e., the surface entropy component) of an Arrhenius type desorption equation (Eqn. 4). In terms of the thermal desorption experiment this means that (all other things being equal) the temperature of the maximum rate of desorption will be lower for an immobile layer than a mobile one. A change in the preexponential factor by three orders of magnitude would cause a change in peak temperature by about 50 K for adsorbed CO or benzene. (N.B. This argument assumes that $F^{\ddagger}$, the partition function in the activated complex, does not change much.)

If, on the other hand, the surface additive affects the depth of the chemisorption potential well and not the diffusion energy along

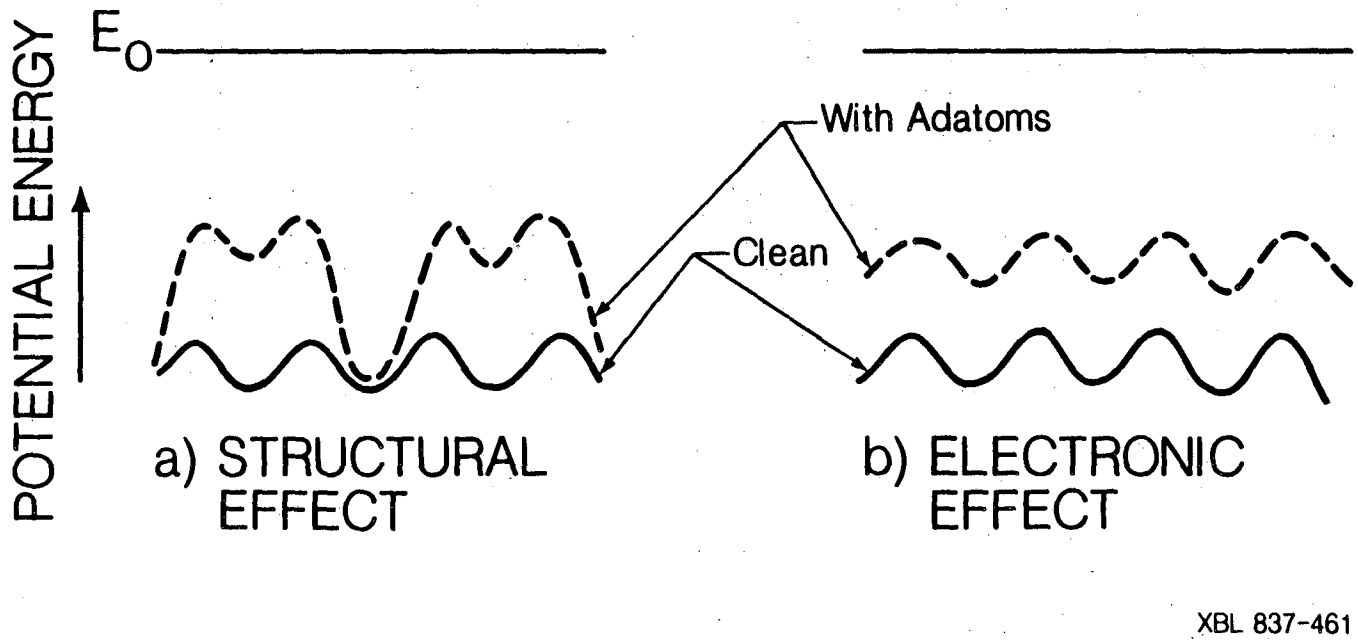
POTENTIAL ENERGY
E_0
With Adatoms
Clean
a) STRUCTURAL EFFECT
b) ELECTRONIC EFFECT
XBL 837-461

Figure B.4

the surface, then the dominant change will occur with the E_a (or ΔH_{ads}) term, and not with the preexponential factor. This is depicted in Figure B.4b. In this extreme, the structural effects as well as changes in transition state geometry are excluded, and the variations in desorption are due to a change in the ability of the metal substrate to bond with an adsorbate, i.e. the depth of the potential well. I believe that this type of discussion is necessary to enable an understanding our coadsorption systems as well as others.

B.3 Aspects of the Thermal Desorption Experiment

Desorption from single crystals is the most common method now used to determine heats of adsorption; the interpretation of desorption from polycrystalline wires and foil becomes much more complicated because of multiple adsorption states. Once cut and polished, the crystal can be mounted in one of serveral manners. The thermal desorption experiment requires a sample mount and heating design such that the desorption signal detected comes from the sample, and not the support. Wire supports, such as Ta, W, or Pt are often used because of their small surface area. Passing a current through the wires causes them to heat up, which in turn heats the sample by conduction. Electron bombardment heating is also possible, but often causes thermal and electron stimulated desorption from surfaces other than the desired one. The problems of desorption from undesirable surfaces should be minimized by mounting the sample such that only line of sight desorption reaches the detector (usually a quadrupole mass spectrometer).

The choice of power supply can also be important: DC currents are preferred since AC heating can cause unwanted 60 cycle noise in the desorption spectra. Computer controlled ramping with feedback circuitry is the most desirable method of heating, enabling variations in heating rates and curves (linear, logarithmic, etc.). More primitive methods without feedback suffice, if the heating curve can be accurately reproduced between runs. This yields less quantitative results, but all of the trends should be apparent.

Finally, it should be noted that if quantitative measures of coverage are desired, other methods of calibration must be used in conjunction with TDS peak measurements. These can include LEED, structure/coverage determination, Auger uptake curves, radio tracer techniques, or molecular beam methods.

Before explaining all of the problems associated with thermal desorption, it is worth digressing for a moment to discuss adsorption. Although several different definitions are used, the concept of a sticking coefficient is a useful one. The sticking coefficient S_o (at zero coverage) can be defined as the probability that an incident gas molecule will become trapped in a chemisorbed state. The condensation coefficient (α) refers to the probability that the incident molecule will be trapped in) a physisorbed (precursor or chemisorbed) state. By definition $0 \leqslant S_o \leqslant \alpha \leqslant 1$.

To a first approximation, for sticking with precursor states we have:

$$S_o = \alpha \left[1 + \frac{\nu_d e^{-\varepsilon_d/RT}}{\nu_a e^{-\varepsilon_a/RT}} \right]^{-1}$$

where E_a refers to the activation energy for going from the physisorbed to the chemisorbed state. For low T, $S_o \longrightarrow \alpha$, and for high T, $S_o \longrightarrow \alpha\ (1+\nu_d/\nu_a)^{-1}$.

The sticking probability also sometimes defined as:

$$S(\theta,T) = S_o(1-\theta)e^{-E_a/RT}$$

If we neglect the exponential term we can display the most common types of sticking probability behavior as follows:

1) 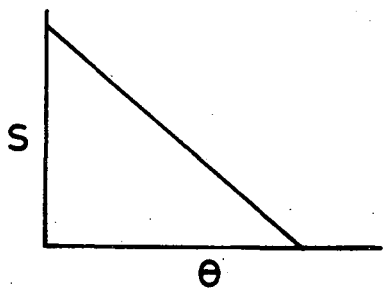

$S = S_o(1-\theta)$ Langmuir behavior

2) 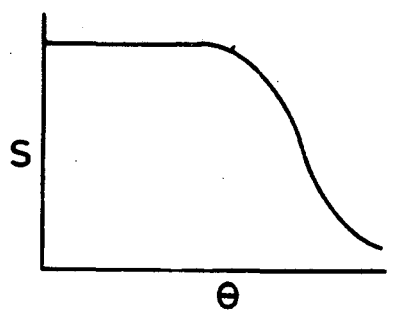

$S = S_o(1-\theta)^n$ $n<1$ (or others see below) Sticking with precursor states

3) 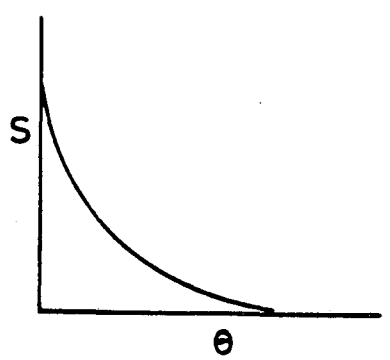

$S = S_o(1-\theta)^2$ Dissociative adsorption with no precursor states. Two sites needed.

4) 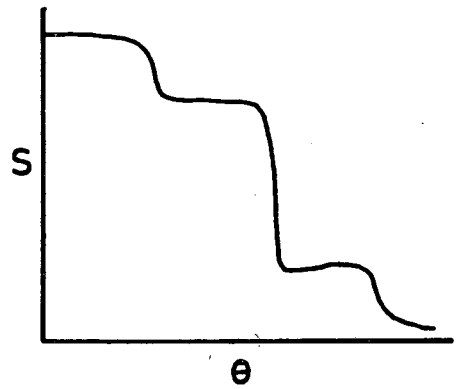

reconstructions or ordered phases.

5) 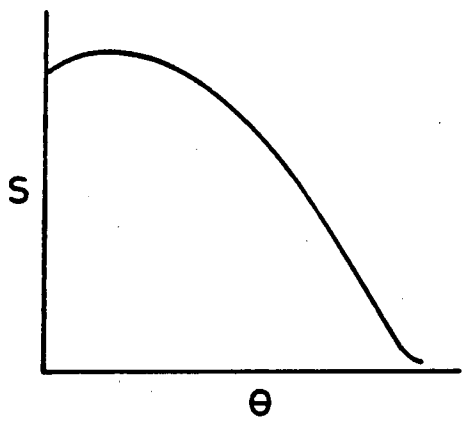

Island growth with strong attractive lateral interactions.

B.4 Problems in Thermal Desorption Analysis

There are many problems with both the experimental and theoretical aspects of thermal desorption. At the experimental level, we know that we can rarely exclude edge, support, pumping speed, and wall effects from contributing to the desorption spectra from a single crystal surface. These all have a tendency to broaden the peak. However, in experiments such as those reported in Chapter 4 of this thesis, these effects are minor compared to the major changes in chemisorptive strength induced by the coadsorption of alkali atoms. Although a quantitative analysis is somewhat difficult, qualitative trends are preserved. It is desirable, nevertheless, to minimize the various experimental sources of error by using a molecular doser and a line of site desorption shield around the detector. "Wall effects" can lead to a misinterpretation of the order of a reaction (first order desorption will resemble zeroth order desorption) and to spurious peaks (from displacement). We have minimized these by using an off axis manipulator where the crystal is placed ≈2 cm from the QMS ionizer. One should also be careful to ensure that the detector responds linearly over the region studied if peak areas are to be used. Finally, it is imperative that the surface be heated in a uniform way and be clean and flat--impurities and or roughness can cause drastically different thermal desorption behavior.

In addition to experimental difficulties, several theoretical problems arise in describing simple desorption processes. As noted before, a molecule or atom may adsorb by first entering into a physisorbed or precursor state, and then falling into a chemisorbed

state. The reverse can happen for desorption, and this leads to a change in the desorption equation.

The importance of the precursor state in TDS is that only a fraction, W, of the molecules which go from the chemisorbed to the precursor state will desorb. The energy imparted to the desorbing species may cause lateral motion in the precursor state, not motion normal to the surface needed for desorption. The rate to go from the chemisorbed to the precursor state is:

$$-\frac{dN}{dt} = \nu N e^{-E/RT} \text{ (1st order)}$$

And if only a fraction, W, go on to desorb:

$$-\frac{dN}{dt} = W\nu N_s \theta e^{-E/Rt} \qquad \text{Eqn. B.13}$$

where θ is the fractional coverage, and where W, to a first approximation, can be represented as

$$F = f_d + f_m \left[1 - (1 + \frac{fd}{fa})^{-1} \; [1 - \frac{K\theta}{1-\theta}]^{-1}\right]$$

where:

f_a = probability of becoming chemisorbed from a precurser state.

f_d = scattered into gas phase from unoccupied site.

f_d = scattered into gas phase from occupied site.

f_m = probability of hopping to nearest neighbor from unoccupied site.

$K = f_d'/(f_a+f_d)$

The f values an be approximated from sticking profiles. As W is decreased the spectrum broadens and T_p goes up in temperature. One must be careful here: for first order desorption, T_p decreases with increasing coverage if a precursor state exists, giving the appearance of second order kinetics.

For molecularly adsorbed CO on Pt(111) the peak temperature decreases by at least 50K with increasing coverage, as well as broadening the FWHM. This can be explained by 1) precursor states, 2) two overlapping states (i.e. top and bridge), 3) lateral interactions causing E_{ad} (or ν) to vary with coverage, 4) second order desorption, etc. The TDS experiment is inclusive here; one must go to other methods, such as UPS, HREELS, or molecular beam techniques to help resolve the discrepancy.

Another problem is that of "lateral interactions": The thermal desorption spectrum is not only a result of substrate-adsorbate interactions, but of adsorbate-adsorbate ones as well. These may be attractive and/or repulsive, and will vary with coverage, temperature, and composition. In general this can be solved by modifying the exponential term to include coverage dependence.

$$-\frac{dN_a}{dt} = \nu N_a e^{-[E_d(o) + zwf(\theta)]/RT} \qquad \text{Eqn. B.14}$$

where: z desribes the lattice type

w is an interaction potential

and $f(\theta)$ is a function of coverage

With lateral interactions, curious spectra often result. For example, two peaks may appear in the desorption spectrum, where the first is due to chemisorption with strong repulsive nearest neighbor interactions, and the second is due to "normal" first or second order behavior. Less confusing, but still troublesome, is the downward shift in desorption concentration with increasing coverage which may lead one to assume second order desorption, instead of first order desorption with repulsive lateral interactions (see Chapter 3).

A more basic problem is that the theory assumes that the transition state model is applicable to the surface. Thus, all the questionable assumptions of gas phase transition state theory (and more) deserve attention. For instance, should all the degrees of freedom of the desorption complex be weighted the same as in the gas phase, and are they in equilibrium?

Another problem of transition state theory is how to determine the transmission coefficient, α, noted earlier. By definition, α, is a function of temperature and may be very small yielding small preexponentials 10^2-10^5 sec^{-1}. Some add an additional tunneling term.

Finally, we note that Goddard and coworkers (Redondo, 1983) have shown that a simple rate expression can be derived from a classical stochastic diffusion theory. They claim that their theory gives much better correspondence with experimental data than that obtained by transition state theory.

Despite all these objections, thermal desorption should, and will, continue to be useful for obtaining information about the thermodynamic and kinetic phenomena occurring at surfaces.

Appendix C. A Comparison of Sulfur and Potassium Additive Effects.

C.1 Introduction.

Submonolayer coverages of various atomic additives (modifiers) have recently been studied on many transition metal surfaces to help understand promoting and poisoning effects in catalysis (see Appendix A). Some investigators have argued that the dominant effect of certain additives is to physically block or dilute the catalytically active metal component for adsorption or reaction (see for example Sachtler, 1976). This is also called an ensemble or structural effect. Others have pointed to the changes in heat of adsorption of CO or H_2 and conclude that these results are due to electronic interactions between the additive and the metal atoms. This is called a chemical, ligand, or electronic effect. Other conventions have also been employed such as surface acidity or basicity to describe electronic effects (Stair, 1982). In fact, a constant source of confusion in the recent literature on surface additives can be traced back to the lack of agreement in terminology. We will use the idea of structural and electronic effects as developed in Appendix A.

In this section we report about the chemical properties of carbon monoxide and benzene when coadsorbed with sulfur on the Pt(111) surface, and compare the sulfur behavior with that of potassium which was presented in Chapter 4. For the purpose of discussion, some of the results reported earlier are recounted here. For potassium, it was shown that an electronic effect is the dominant cause of the observed changes in desorption of CO and benzene. With sulfur coadsorption, on the other hand, "structural" effects might be more important than electronic ones

in altering the desorption behavior of these molecules.

C.2 Experimental.

A Pt(111) sample was mounted in the TDS chamber described in section 2.1. To achieve the desired coverages, sulfur was either deposited at a constant rate for a certain time and then monitored by AES, or the surface was saturated with sulfur and then heated, desorbing sulfur, until a desired coverage was reached. For the CO and sulfur coadsorption system we were interested in four coverage regimes: clean Pt(111), $\theta_S = 0.25$, $\theta_S = 0.33$, and $\theta_S > 0.5$, (where θ_S is the sulfur coverage relative to the platinum monolayer atomic density). After sufficient sulfur deposition on a clean Pt(111) surface, an ordered $(\sqrt{3}x\sqrt{3})R30°$ sulfur overlayer structure could be obtained by heating to 700-900K. A second lower coverage, (2x2) sulfur overlayer structure was obtained by heating to 1000-1150K. No other LEED patterns were visible at higher or lower coverages, consistent with previously reported results (Heegemann, 1975). Since sulfur is generally believed to occupy the highest coordination site available on metal surfaces, the two overlayer LEED patterns are most likely due to the sulfur overlayers depicted in Figures C.1a and C.1b.

The potassium deposition techniques and overlayer behavior on Pt(111) has been described in detail in Chapters 2 and 3 above. CO and benzene exposures were accomplished using a needle doser in front of the sample. Heating rates for the thermal desorption spectra were $\approx 30\ K\ s^{-1}$.

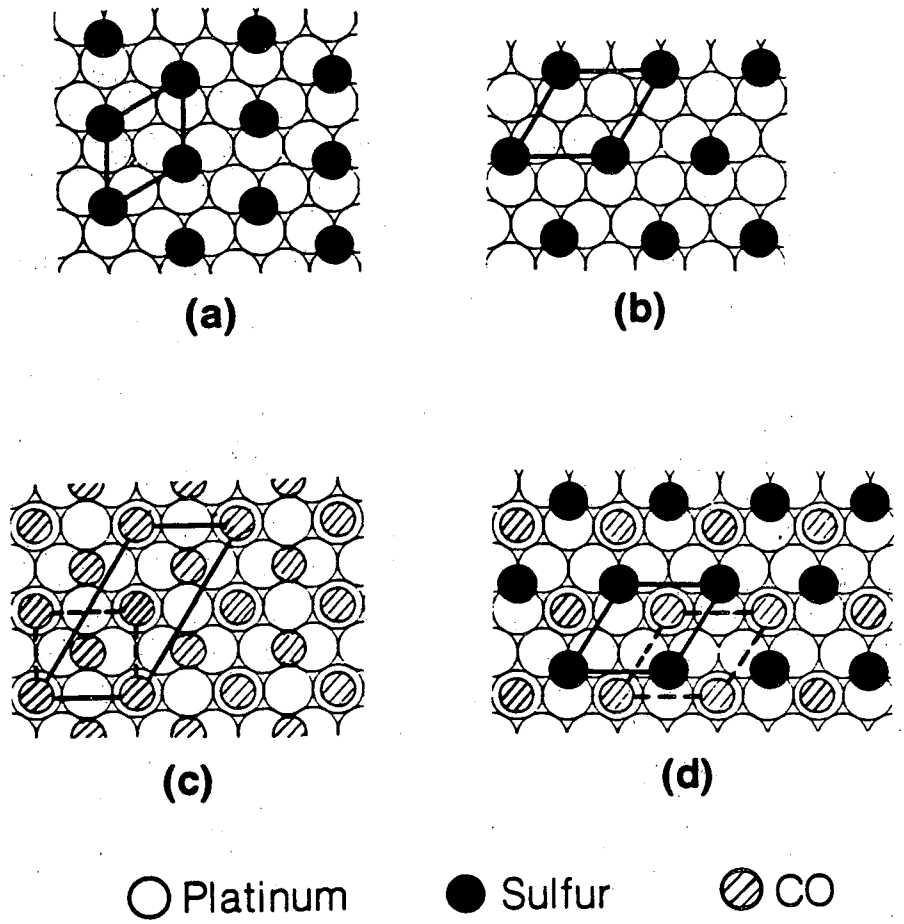

XBL 837-460

Figure C.1

C.3 Results

C.3.1 Chemisorbed carbon monoxide.

Carbon monoxide adsorbed on Pt(111) has been extensively studied by many researchers (see Steininger, 1982, and references therein). At low coverages, CO adsorbs on top sites on platinum, while at higher coverages bridged sites become occupied. Although there has been some disagreement in the literature, it is now thought that the top and bridge sites are the only ones occupied, although some tilting may occur (Biberian, 1983).

With the Pt(111) sample held at 170K, a CO exposure of greater than 1 langmuir (1 L = 1 x 10^{-6} torr s) was sufficient to yield a c(4x2) overlayer LEED pattern. LEED and HREELS analyses (Biberian, 1983) have shown this pattern to correspond to a real space representation described in Figure C.1c, and a coverage of $\Theta_{CO} \approx 0.5$. In Figures C.2a and C.2b we show the CO thermal desorption spectra following 1L and 0.4L exposures. Note the increase in peak area and concomitant decrease in temperature of the peak maximum for the higher exposure. This effect is thought to be due to repulsive lateral interactions between the CO molecules.

Figure 4.8 shows the saturation coverage CO thermal desorption spectra as a function of potassium coverage on the Pt(111) surface. Of importance here is to note the large increase in heat of adsorption with increasing potassium coverage. Also, the change in heat of adsorption was a continuous function of both CO and K coverage, as shown in Figures 4.5, 4.6 and 4.7.

The p(2x2) sulfur overlayer structure on Pt(111) allowed significant CO adsorption following a 0.4 L exposure as can be observed in figure

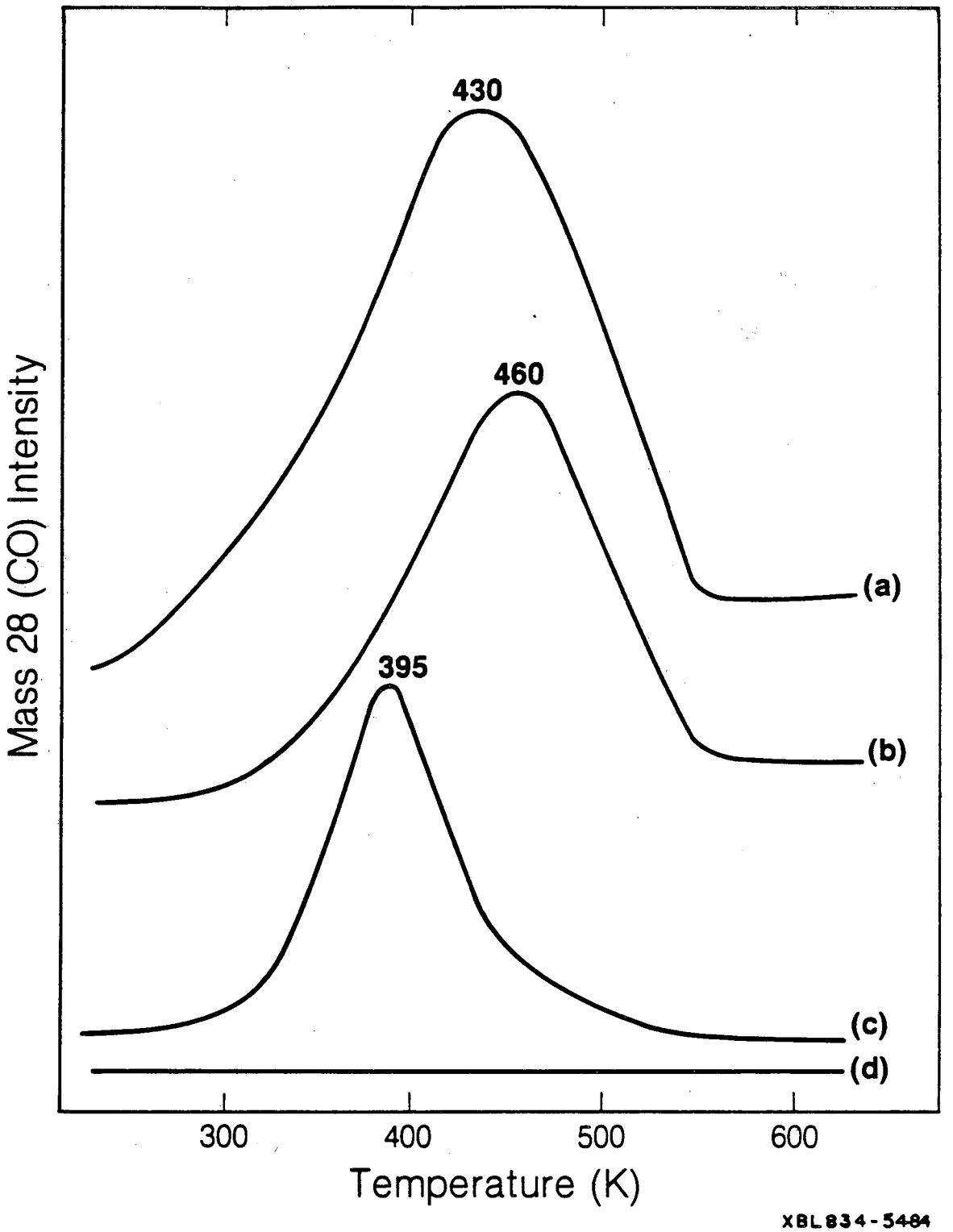

Figure C.2

Carbon monoxide thermal desorption from Pt(111) (a) + (b) and Pt(111) + sulfur (c) + (d).

C.2c. In addition, the desorption peak temperature was shifted by about 65K from a 0.4 L exposure on clean Pt(111), Figure C.2b. Higher CO exposures on the p(2x2) sulfur overlayer resulted in no additional adsorption. In Figure C.2d we show the CO thermal desorption following a 0.4 L CO exposure on the Pt(111) + ($\sqrt{3}$x $\sqrt{3}$)R30° sulfur surface. Similar spectra, showing little or no CO desorption, were observed for higher CO exposures as well as for higher sulfur coverages. No new, or altered, LEED patterns were observed following CO exposure. The CO thermal desorption peak area for the Pt(111) + p(2x2) sulfur + 0.4 L CO overlayer (Figure C.2c) was ≈ 1/2 that of the Pt(111) + c(4x2) CO overlayer (Figure C.2a).

In Figure C.1d, we show what we believe is the real space representation of a the p(2x2) overlayer structure with coadsorbed CO and S. With a p(2x2) overlayer array of sulfur atoms sitting in hollow sites, there exists another (2x2) mesh of single platinum atom sites with no coordinated sulfur atoms, where CO could be adsorbed. This model of coadsorption is consistent with the observations that the (2x2) sulfur overlayer LEED pattern was not changed when CO was adsorbed and the the CO thermal desorption peak area for the c(4x2) CO structure on clean Pt(111) (with a known coverage of $\Theta_{CO} \approx 0.5$) was twice that of the p(2x2) S + CO overlayer structure, with Θ_S=0.25 and Θ_{CO}=0.25. Assuming that this model is correct, each sulfur atom blocks three platinum substrate atoms from adsorption. This is also seen from the virtually complete blocking of CO adsorption on the($\sqrt{3}$x$\sqrt{3}$)R30° sulfur overlayer surface where Θ_S=0.33, Figure C.2d.

This p(2x2) overlayer structure with one platinum atom and one CO

molecule per unit cell is ideally suited for a dynamical LEED intensity analysis due to the small size of the unit cell. Such an analysis might yield valuable information concerning bond length distortions in coadsorption systems.

C.3.2 Chemisorbed benzene.

The thermal desorption spectrum of benzene on Pt(111) was shown in Figure 4.21. For low exposures, most of the benzene decomposes upon heating, with hydrogen being the main species monitored in the desorption spectrum, while for higher exposures, some of the benzene desorbs intact.

In Figure 4.23 was shown the thermal desorption spectra for benzene desorbing from Pt(111) with various coverages of potassium. Here we can see that a 200K decrease in benzene desorption edge maximum with potassium coadsorption, the opposite of what was observed for CO.

In Figure 4.24 we contrasted the effect that adsorbed potassium has on benzene desorption with the effect that is seen with potassium oxide. In the potassium oxide case, potassium was first deposited to $\Theta_K \approx 0.3$, then the surface was exposed to 5 L oxygen. Oxidation of the potassium made the effect on benzene practically disappear.

The effect of sulfur on the desorption of benzene is shown in Figure C.3. The dominant features are a slight drop in temperature of the desorption rate maximum, and an effective blocking of adsorption sites. A more thorough understanding of the adsorption states would be required to claim that one state is blocked, while another is filling in.

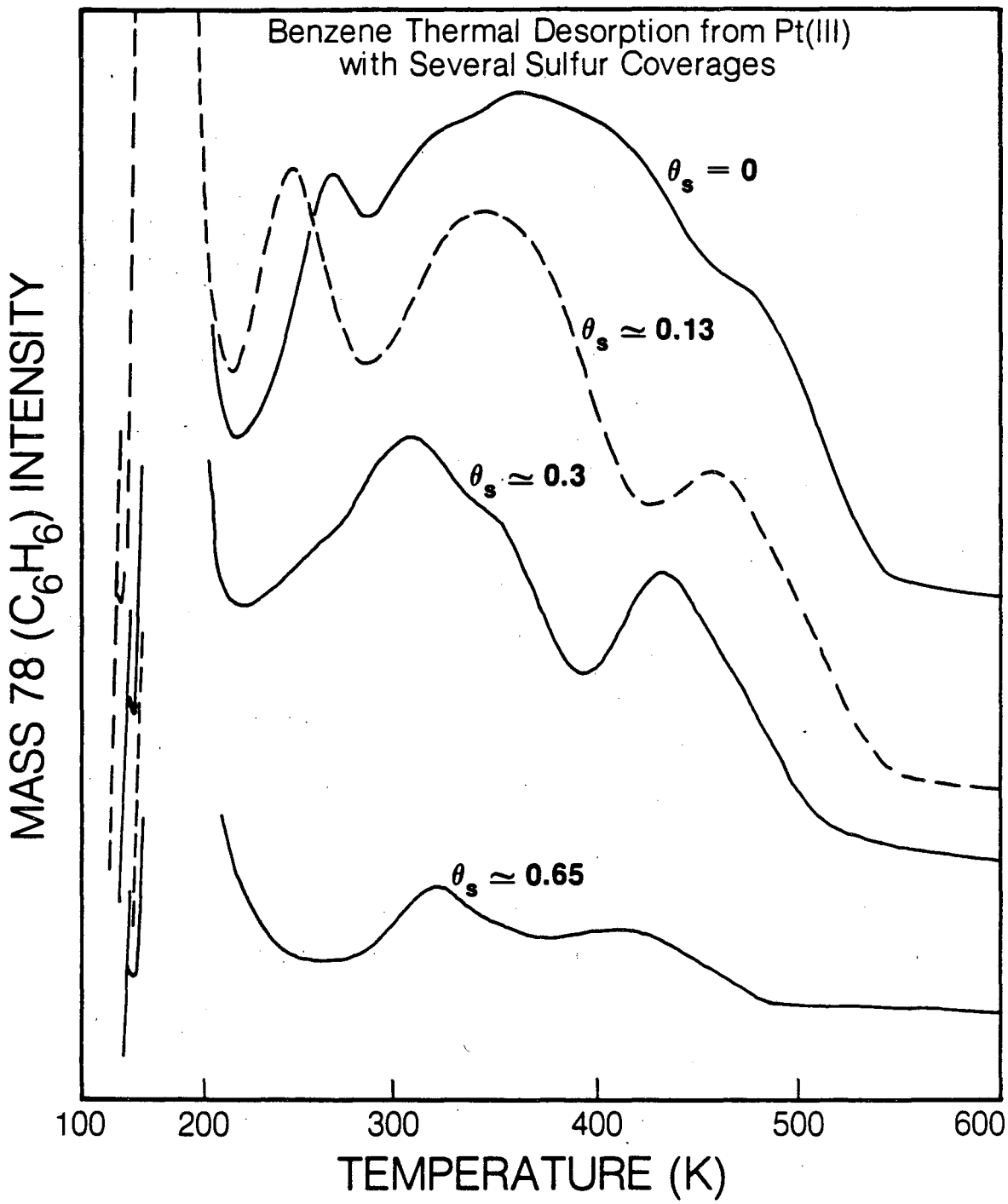

XBL 837-459

Figure C.3

C.4 Discussion

We chose to study CO and benzene and their interaction with sulfur (following low temperature exposure) on Pt(111) because both molecules had shown large changes when coadsorbed with potassium in earlier studies. Because of the different electronegativities of potassium and sulfur, we expected different effects on the chemisorption of these molecules. Our results show that on Pt(111) coadsorbed potassium caused a 200K increase in the temperature of desorption of CO, and a 200K decrease in the maximum temperature of desorption of benzene. Adsorbed sulfur, on the other hand, caused a decrease in the desorption temperature of both CO and benzene.

C.4.1 The effect of potassium.

The large potassium induced change in desorption temperature of both CO and benzene seems to be due to a strong substrate mediated electronic interaction. For CO, if site blocking (structural) effects were important, the thermal desorption peak should have moved down in temperature, not up, as explained in Appendix B. More evidence supporting an electronic interpretation comes from the TDS, photoemission, and high resolution electron energy loss (HREELS) results (see chapter 4). The results also indicate that the electronic interaction is mediated by the substrate (i.e. it is not a direct interaction) and is effective over at least several interatomic spacings.

By coadsorbing oxygen, the effect of potassium on the chemisorption of benzene almost disappeared, as we show in Figure 4.24. This further supports the model of an electronic effect for the potassium induced

changes. If structural effects occurred, we would have expected the oxidation to cause an even greater change in thermal desorption peak temperature.

C.5.2 The Effect of Sulfur.

The interpretation of the effect of coadsorbed sulfur on CO and benzene is less clear. We observed a decrease in the temperature of CO desorption from Pt(111) when sulfur (an electronegative species) was added (figure C.3c). This might be expected since coadsorbed potassium (electropositive) caused a large increase in the CO desorption temperature. Surprisingly, analogous effects were not seen for benzene adsorption: both potassium and sulfur caused a decrease in the benzene desorption temperature.

In Figure 4.29 we show a molecular orbital diagram for a metal-benzene system analogous to our surface. What is of interest here is the e_{1g}^{*} level lying just above E_f. If potassium on the surface can lower this level enough to be populated, it should weaken the benzene-metal interaction (as we observe). Our UPS results show a slight increase in binding energy of the lower lying benzene levels suggest that the e_{1g}^{*} level may also be lowered. Thus the interpretation of potassium as inducing substrate mediated electronic interactions for the chemisorption of both benzene and CO is consistent.

But why then did sulfur cause a decrease in desorption temperature of benzene as well as CO? Recent work on "electron acceptors" shows that the work function of a metal does not behave in a simple manner (Shustorovich, 1982). From the point of view of adding an electron acceptor (such as sulfur) to the surface, the dipole created between

the atoms and their image charge should increase the work function. But with adsorbed chlorine, for instance, sometimes a decrease in work function is observed. This can be rationalized by noting that the adsorbate-image dipole is not the only dipole component of the work function (see Figure 3.1). A second, and perhaps more important, dipole component comes from the bulk electron spillover into the vacuum. The changes in wavefunction spillover character due to adsorbates can thus overcompensate the adsorbate-image dipole component.

To follow this argument to its logical conclusion, we would say that with sulfur, as with potassium, a decrease in work function causes the benzene e_{1g}^{*} level to be populated, decreasing the benzene-substrate bond energy. However similar reasoning should lead us to predict that potassium and sulfur should have the same effect on coadsorbed CO. This was not observed: potassium and sulfur showed opposite effects on the CO desorption temperature. We are therefore led to discount the work function model as determining the sulfur-benzene coadsorption system.

We can, however, explain the decrease in CO and benzene desorption temperature (when sulfur is coadsorbed) as being due to a structural effect. This would result from a change in the preexponential factor (ν) as described in Appendix B. By blocking the mobility of CO or benzene along the surface, the preexponential factor in the desorption equation should increase, which (for constant ΔH_{ads}) will cause a decrease in peak temperature in the thermal desorption spectrum. Since this is consistent with the data, we tend to favor structural effects as dominating desorption behavior for the sulfur coadsorption

systems. Certainly electronic effects will exist, as evidenced by the slight increase in vibrational frequency of CO when other electron acceptors, such as chlorine or oxygen, are coadsorbed with CO on supported platinum (Primet, 1973), but we believe these are not the dominant effect.

Appendix D. Review of Related Uses of Alkali Additives in Catalysis.

This section contains a brief literature review of the use of alkali promoters for carbon gasification and ammonia synthesis. A review of alkali promoters for CO hydrogenation was given in section 5.5 above. For carbon gasification, alkalis are actually the catalyst, not simply a promoter of another metal. Nevertheless, the similarities between the various reactions warrents consideration here of the use of alkalis for gasification.

D.1 Carbon Gasification.

The gasification of coal or any other carbon source to produce H_2 and CO (syngas) is a necessary first step in the synthetic fuels industry (Kugler, 1978). The resultant CO and H_2 can be further reacted over a methanation or Fischer-Tropsch catalyst to give useful products such as methane, alcohols, or long chain hydrocarbons (e.g. gasoline).

The steam gasification of carbon usually requires high temperatures (>1000K), since it is a highly endothermic reaction.

(1) $C + H_2O \rightarrow H_2 + CO$ $\Delta H = +31$ kcal/mole

Several other simple reactions which can take place under gasification conditions are represented below:

(2) $2C + O_2 \rightarrow 2CO$ $\Delta H = -53$ kcal/mole

(3) $C + CO_2 \rightarrow 2CO$ $\Delta H = +41$ kcal/mole

(4) $CO + H_2O \rightarrow CO_2 + H_2$ $\Delta H = -10$ kcal/mole

(5) $C + 2H_2 \rightarrow CH_4$ $\Delta H = -18$ kcal/mole

(6) $CO + 3H_2 \rightarrow CH_4 + H_2O$ $\Delta H = -49$ kcal/mole

In addition to these reactions, similar reactions can occur in the gasification of crude hydrocarbon sources:

(7) $-CH_2- + H_2O \rightarrow CO + 2H_2$ $\Delta H = +36$ kcal/mole

(8) $-CH_2- + 1/2O_2 \rightarrow CO + H_2$ $\Delta H = -22$ kcal/mole

In several of the industrial gasification processes, no catalyst is used. However others, such as the Exxon and Kellog processes do employ alkali carbonates or hydroxides to catalyze the reaction. In fact, alkali and alkaline earth metals have been known for over 100 years to be active gasification catalysts (Motay, 1867). The recent awareness in energy conservation has renewed interest in trying to understand the basic science of alkali catalyzed coal gasification. The most readily observed catalytic consequence of adding alkali salts is that the gasification rates increase (at constant temperature) and the agglomeration (caking) of the carbon source is decreased.

Several mechanistic pathways have been postulated for the various alkali catalyzed gasification reactions, of which we will briefly discuss three. Veraa and Bell (1978) have proposed a sequence of reaction steps to explain the catalytic gasification cycle:

(9) $M_2CO_3 + 2C \rightarrow 2M + 3CO$

(10) $2M + 2H_2O \rightarrow 2MOH + H_2$

(11) $CO + H_2O \rightarrow CO_2 + H_2$

(where M = an alkali metal)

(12) $2MOH + CO_2 \rightarrow M_2CO_3 + H_2O$

(13) $C + H_2O \rightarrow H_2 + CO$

McKee and Chatterji (1975) offer a slightly different reaction sequence where equations 11 and 12 are replaced by:

(14) $2MOH + CO \rightarrow M_2CO_3 + H_2$

However, the overall reaction is still represented by equation 13.

One problem with these two postulated pathways, as pointed out by Wen (1980) is that from a thermodynamic point of view the lithium salt should be the least active, but in actual experiments it displayed the highest reactivity. Wen argues that the active catalyst is not an alkali salt, but rather an intercalated alkali-graphite or alkali-amorphous carbon compound. He shows how the Fermi level of graphite (a semi-metal) is effectively shifted to higher energy when an alkali metal enters the space between the graphite layers, making it more metallic, and a better electron donor. One important consequence of the metallic character of alkali intercalation is that the modified graphite (or aromatic carbon chain) can easily adsorb hydrogen. For instance the following class of organic salts are readily hydrogenated, while the neutral organic molecules are relatively stable.

(15)

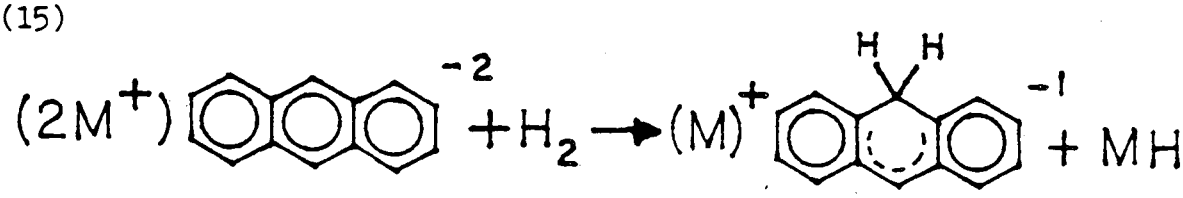

These complexes also adsorb CO and can therefore be used as CO hydrogenation catalysts.

Wen postulates the following mechanism for steam gasification of carbon sources.

(16) $M_2CO_3 + 2C \rightarrow 2M + 3CO$

(17) $2M + 2nC \rightarrow 2C_nM$

(18) $2C_nM + 2H_2O \rightarrow 2nC + 2MOH + H_2$

(19) $2MOH + CO \rightarrow M_2CO_3 + H_2$

---

(20) $C + H_2O \rightarrow CO + H_2$

A similar mechanism would hold for MOH as the starting material instead of M_2CO_3. He also notes that the diffusion of alkali metals through the carbonaceous material should be relatively facile either as M(g) or as MOH. The main difference between this mechanism, and the ones proposed by Veraa (1978) and McKee (1975), is that the Wen mechanism presumes that the alkali metal is intercalated when it reacts with H_2O, while the other two state merely that atomic alkali atoms react with H_2O without specifying the location of the alkali. The Veraa and McKee mechanisms are therefore, more general.

Other reactions are known to take place on alkali - graphite intercalation compounds. In addition to CO hydrogenation, these include the hydrogenation of the carbon substrate to form light hydrocarbons, as well as the hydrogenation of benzene to cyclohexane.

The third mechanism which has been postulated is called the phenolate mechanism and is supported by the work of Mims (1983) as

well as the work done in our laboratory (Delanney, 1983). The key intermediate shown in these studies is the phenolate species as represented in equation 21.

(21) 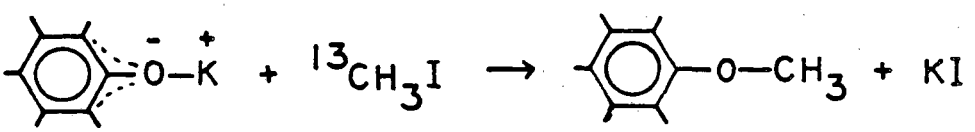

The existence of this species has been demonstrated indirectly by an ion exchange surface methylation technique (Mims), and from stoichiometric arguments (Delanney). In the methylation experiment, ^{13}C enriched CH_3I is added to a carbon source impregnated with potassium carbonate (spherocarb) and the resultant methylated solid is characterized by ^{13}C nmr.

In the Mims study, it was shown that a carbon sample with KOH impregnation, followed by methylation form a stable intermediate. The intermediates formed at 970K by heating the sample in He or by initiating gasification are the same. This methylated intermediate demonstrates the prior existence of the phenolate.

Delanney et al have recently shown that KOH on a graphite powder reacts with steam in two successive stages. In the first stage, hydrogen and hydrocarbons are evolved at a high rate, but no CO or CO_2 is detected. This stage ceases after the equivalent of 0.5 molecules H_2 per potassium atom are produced. This is attributed to the dissociative adsorption of water to form -C-H and -C-OH (phenol) groups. The phenol group then reacts readily with KOH to form C-O-K (phenolate) species. The existence of the phenolate is strongly supported by the observation that 0.5 molecules H_2 are produced per potassium atom. This species

is found to form at an appreciable rate between 800-950K. By 950K, most of the initial potassium salt will be converted to C-O-K.

During the second stage of the reaction (at temperatures between 950-1000K) the gasification proceeds more slowly. It will, however, preceed indefinitely, and the rate can be increased by further increasing the temperature. Here, we also note the production of one H_2 molecule per equivalent CO molecule. We believe that this stage results from the decomposition of the phenolate species to give CO, K_2O, and metallic potassium. Then, K_2O and metallic potassium combine with H_2O to produce H_2 and KOH again. For a real catalyst, poisoning occurs by alkali complexation with impurities such as silicon or various metals.

Once CO and H_2 are made by steam gasification, their further reaction to form methane and water is exothermic, and is normally carried out on a nickel catalyst at 600K. Because of the high cost of the heating required for steam gasification, it would be desirable to convert the carbon source directly to methane or other hydrocarbons. For instance the following reaction is virtually thermoneutral:

$$(22) \quad 2C + 2H_2O \rightarrow CH_4 + CO_2 \qquad \Delta H = 3.6 \text{ kcal/mole}$$

Alkalis are able to induce this reaction. In addition, higher molecular weight species were produced (which are known to be produced over alkali intercalated graphite). The formation of the stable phenolate intermediate seems however to result in these reactions being stoichiometric at temperatures below 800-900K.

What is needed (from the point of view of a phenolate mechanistic scheme) is a metal which can aid in the dissociative adsorption of a

significant amount of strongly bound water on the carbon. At the same time the metal must not be so strongly bound that the formation of a stable phenolate-like intermediate freezes out the reaction, requiring excessively high temperatures to complete the catalytic cycle.

D.2 The Ammonia Synthesis.

The commercial development of the direct synthesis of ammonia occured in the first two decades of the twentieth century (Haber, 1910). The catalyst was (and still is) formed from Fe_3O_4 (magnetite), with Al_2O_3 and K_2O additives. The catalyst powder is first reduced under hydrogen to form metallic iron particles, which contain a small amount of K and O on the surface. Studies have shown that the Al_2O_3 is located between the iron particles, presumably as a structural promoter. Thermodynamic and kinetic constraints require that the reaction be run at moderate temperatures (500C) and high pressures (>100 atm.)

It was shown as early as 1934 that nitrogen adsorption was the rate limiting step in the overall synthesis (Emmett, 1934). More recently it has been shown that the dissociative adsorption of nitrogen is the slow step, while molecular adsorption is the weakly bound precursor state (Ertl, 1976). The dissociative adsorption of hydrogen is facile on iron at reaction temperatures. It is also found that the (111) crystallographic face is much more active for dissociating nitrogen, while the (110) face is the least active (Ertl, 1980). Very similar face selectivities were observed for the ammonia synthesis, where the (111) face was found to be 418 times more active than the (110) face. Although the energetics are different, the molecular mechanism of ammonia synthesis is analogous to the methanation reaction:

(23) N_2 (g) $\rightleftharpoons$ N_2 (ads) $\rightleftharpoons$ 2N (ads)

(24) H_2 (g) $\rightleftharpoons$ 2H (ads)

(25) N (ads) + H (ads) $\rightleftharpoons$ NH (ads)

(26) NH (ads) + H (ads) $\rightleftharpoons$ NH_2 (ads)

(27) NH_2 (ads) + H (ads) $\rightleftharpoons$ NH_3 (ads) $\rightleftharpoons$ NH_3 (g)

However, in the methanation reaction, it is the final hydrogenation of the surface CH_3 species which is thought to be rate limiting, while in the ammonia synthesis the dissociation of N_2 is rate limiting.

The function and state of potassium in the ammonia synthesis is still under investigation, but the picture which has emerged can be described as follows. Potassium and oxygen are coadsorbed both on the active iron and on the Al_2O_3 phase. The iron, reduced from its Fe_3O_4 starting form, appears to contain a significant amount of nitrogen dissolved in it, perhaps forming a nitride in the near surface region. As noted above in section 5.9, the surface potassium helps both to increase the N_2 adsorption energy and to decrease the activation energy for its dissociation. This effect is more pronounced on the Fe(110) and (100) planes, which are normally very poor at dissociating nitrogen compared to the (111) face (Ertl, 1980).

APPENDIX E

The Use of the PET-Commodore Computer for Surface Science Studies

E.1 Introduction

Most modern microcomputers, when combined with an appropriate interface, can be used to control and/or monitor scientific instruments. We are currently using the PET-Commodore 2001, 32K Personal Computer to facilitate several different types of surface science studies, including: 1) multichannel thermal desorption spectroscopy (TDS monitors the gaseous species desorbed from asurface as it is heated), 2) Auger electron spectroscopy (AES monitors surface atomic composition), and 3) photoelectron spectroscopy (which measure electrons emitted from both the valence-UPS- and core-XPS, regions). Other researchers in the UC Berkeley Chemistry Department, with the help of the Electronics Shop, have used the PET to monitor gas chromatography, and gas phase laser spectroscopy.

With the development of a series of software programs, the main advantages to be gained by using the computer over conventional techniques are: permanent storage of data on diskettes, and post processing of the data to integrate, differtiate, signal average, or "zoom-in" on data. The computer can also accurately control the electronic power supplies and analyzers used to collect data, and even saves money in the case of Auger and photoelectron spectroscopy since no "System Control" or multichannel analyzer is needed (with the PHI system).

The programs are self explanatory in that once a program is loaded and running the screen prompts the user with a series of simple questions. An overview of each of the programs is given in the following pages and some directions/commands are explained where needed. Should changes be desired, the reader is referred to Osborne (1980) for an introduction about the computer and BASIC programming. Steve Smiriga and Henry Chan of the U.C. B. Chemistry Electronics shop can be consulted for more substantial changes in hardware or machine language programming.

A schematic diagram of our computer, instrumentation, and interface is given in Figure E.1. The interface includes a 12 bit A/D converter, a 16 bit D/A converter, an 8 channel multiplexer, a 32 bit upcounter, and a voltage to frequency converter with a hardware timer. The computer has a 6502 (8 bit) microprocessor with 32K RAM. This is sufficient for most of our needs. Programming is done in BASIC for the interactive parts, while machine language is used for data collecting (because speed is important). [On a few occasions it would have been better to have had 64K or 128K RAM. Since 16 bit microprocessors are becoming more popular, we would recommend the larger size for someone who does not already have a 32K computer.]

E.2 Computer Controlled Thermal Desorption Spectroscopy

Using the current software, the computer is capable of scanning and monitoring the intensities of up to 8 different mass channels on a UTI 100C mass spectrometer, and one temperature, at a maximum rate of about 20 per second. The computer, program, and interface should work

equally well on any quadrupole mass spectrometer which can take a 0-10V mass programing input signal and give a 0-10V output for intensity. The program and interface have been designed to enable the user to change the electrometer gain; however, some undesirable noise appears using this option with the UTI 100C. The software consists of two programs, both of which are loaded from the disk into the PET RAM (active memory) by pressing the SHIFT/RUN key with the diskette in disk drive 0. The first program combines an interactive "parameter set-up" section with a post-processing graphics routine, while the second contains a series of machine language subroutines enabling fast data collection, storage, and retrieval. A listing of the two programs is giving in Table E.1.

In Figure E.2 is shown an interactive flow chart describing the prompting questions and their function. In the post-processing part, the temperature scale must be normalized before meaningful plots are made. This is usually accomplished by creating peaks of any gas (with leak value) at two different temperatures, and then using the scaling factors and offsets to center the display. Nonlinear thermocouple behavior can be corrected for either in the computer or by changing the temperature scale of the plot.

E.3 Computer Control for Photoelectron and Auger Spectroscopy

The "ESCA" Programs for Auger, ESCA (XPS) and UPS include a set of 4 programs; an interactive BASIC program and a machine language program for taking data, and two more for post-processing. The programs are listed in Table E.2. The main interactive program

enables data to be taken, stored, and for spectra to be subtracted from each other. In Figure E.3 is shown the flow diagram for this program.

E.4 Auger ESCA Display Program

When using the Auger/ESCA Display program, all files to be displayed must have been stored previously while within the main Auger/ESCA data collection program. The Auger/ESCA Display program operates in two input modes, the Command Mode and the Display Mode. In the Command Mode, the program will ask for a "COMMAND *" and await input from the keyboard followed by a carriage return. In general this mode used to recall data from the disk and display it. The Display mode interacts with the user by merely hitting keys to affect the display: neither the "COMMAND" prompt, nor the keys hit will appear on the screen. Both modes work on data which has been placed into a buffer in the PET memory; the original data on the disk remains intact. Note that in the descriptions below, parentheses denote shifted keys, i.e. (S) means shift S.

First a few remarks about the end points of the display. When a data file is first read in from disk 1, the x-axis endpoints are set to those of the "raw" data as entered in the main ESCA program, VI and VF. The Y axis is set to run from 0 to 100K counts, but only a portion is displayed by the "Autoscaler". VI and VF can be changed in the command mode, i.e. if the spectra were miscalibrated, via the "X" command. This will not change the data, but on the voltages displayed on the x-axis. More often, however, one would wish to simply change

the displayed initial and final voltages DVI and DVF, to zoom in on a peak. For intance, in changing DVI and DVF all the data remains the same in the PET memory, the only real change is that fraction of memory which is displayed. In general most Display mode commands use and modify DVI and DVF. The one exception is "S" (smoothing) within the Display mode which changes the intensities of only that fraction of the spectra displayed.

COMMAND MODE:

G - Get data from disk in drive 1, wipes existing data in buffer.

D - Displays the data with dots between VI and BF and cause the program to enter display mode.

L - Displays the data with lines connecting the dots.

H - Plots latest displayed data on EPSON plotter

X - Sets VI and VF to desired values. Does not alter data.

R - Resets VI and VF to their original value as stored on diskette.

A - Autoscales the data between DVI and DVF.

Y - Set Counts for top and bottom limits, as opposed to being autoscaled.

S - Smoothes data with 3 point smoothing routine, and redisplays it.

I - Integrates displayed data and re-enters display mode.

(I) - Differentiates data.

Q - Quit ESCA Display program and return to main data collection program.

B - Subtracts a given baseline from all data.

(Q) - Clears the screen.

DISPLAY MODE:

A, H, S, L and D are the same as in Command Mode.

(D) - Re-displays data using present cursor points.

(U) - Turns on the cursor (to zoom in).

(V) - Turns off the cursor.

(- Moves the cursor left.

) - Moves the cursor right.

Z - Turns on the repeat mode, so you don't have to press the cursor keys over and over.

(Z) - Turns off the repeat mode.

(() - Sets the left cursor point.

()) - Sets the right cursor point.

E - Puts cursor position in eV on screen.

R - Returns to the command mode.

B - Replaces the data between cursor points with a straight line.

(2) - Contracts along Y axis.

(8) - Expands along Y axis.

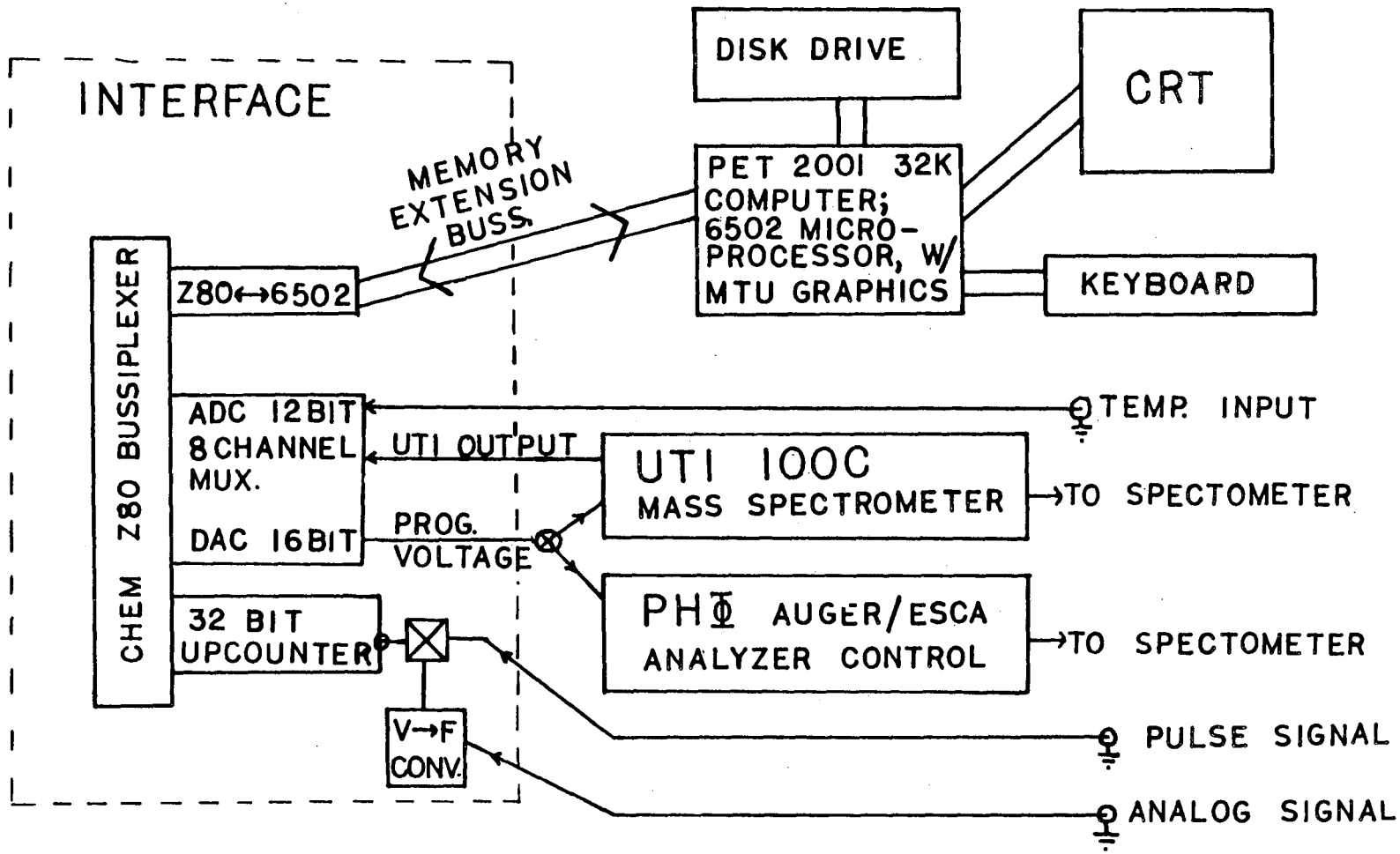

XBL 838-11147

Figure E.1

Thermal Desorption Program

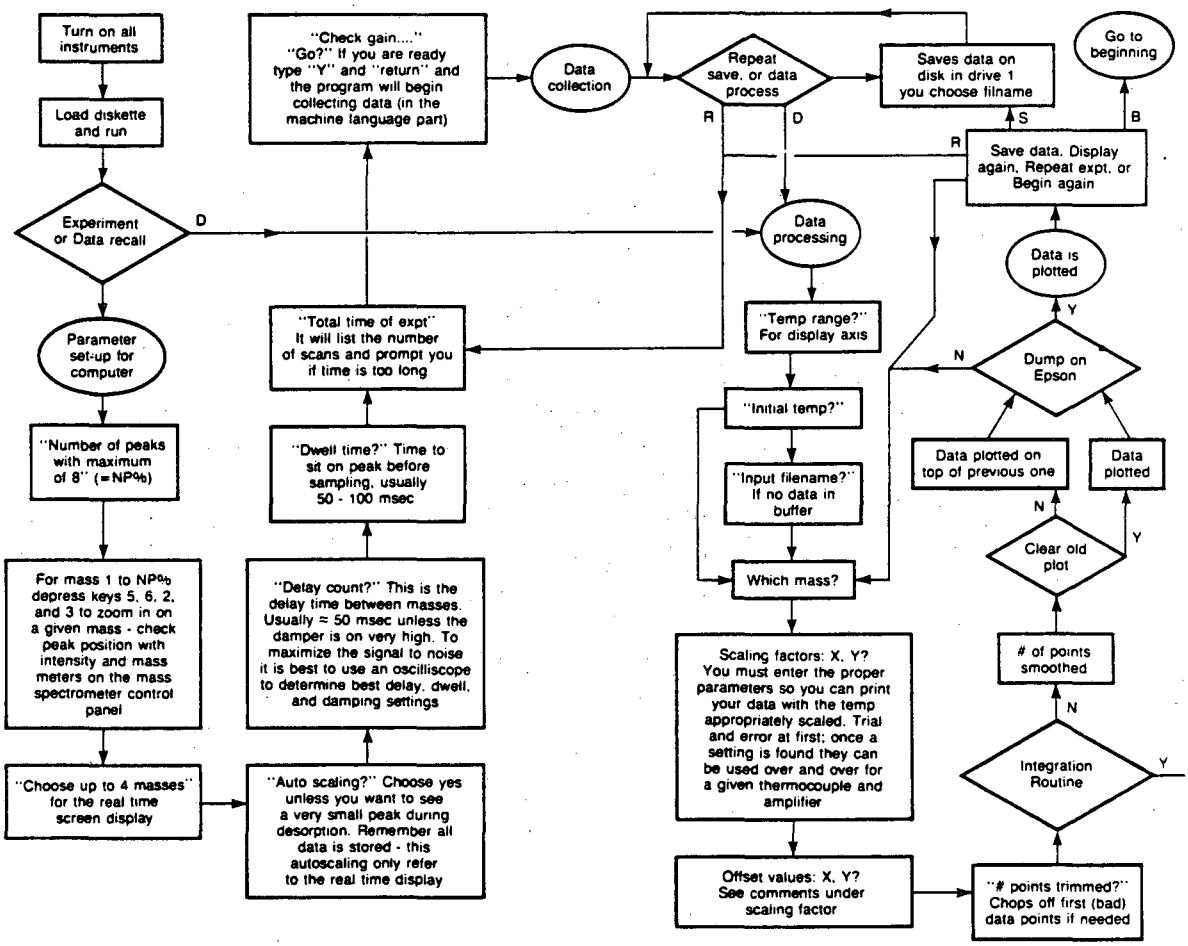

XBL 838-3055

Figure E.2

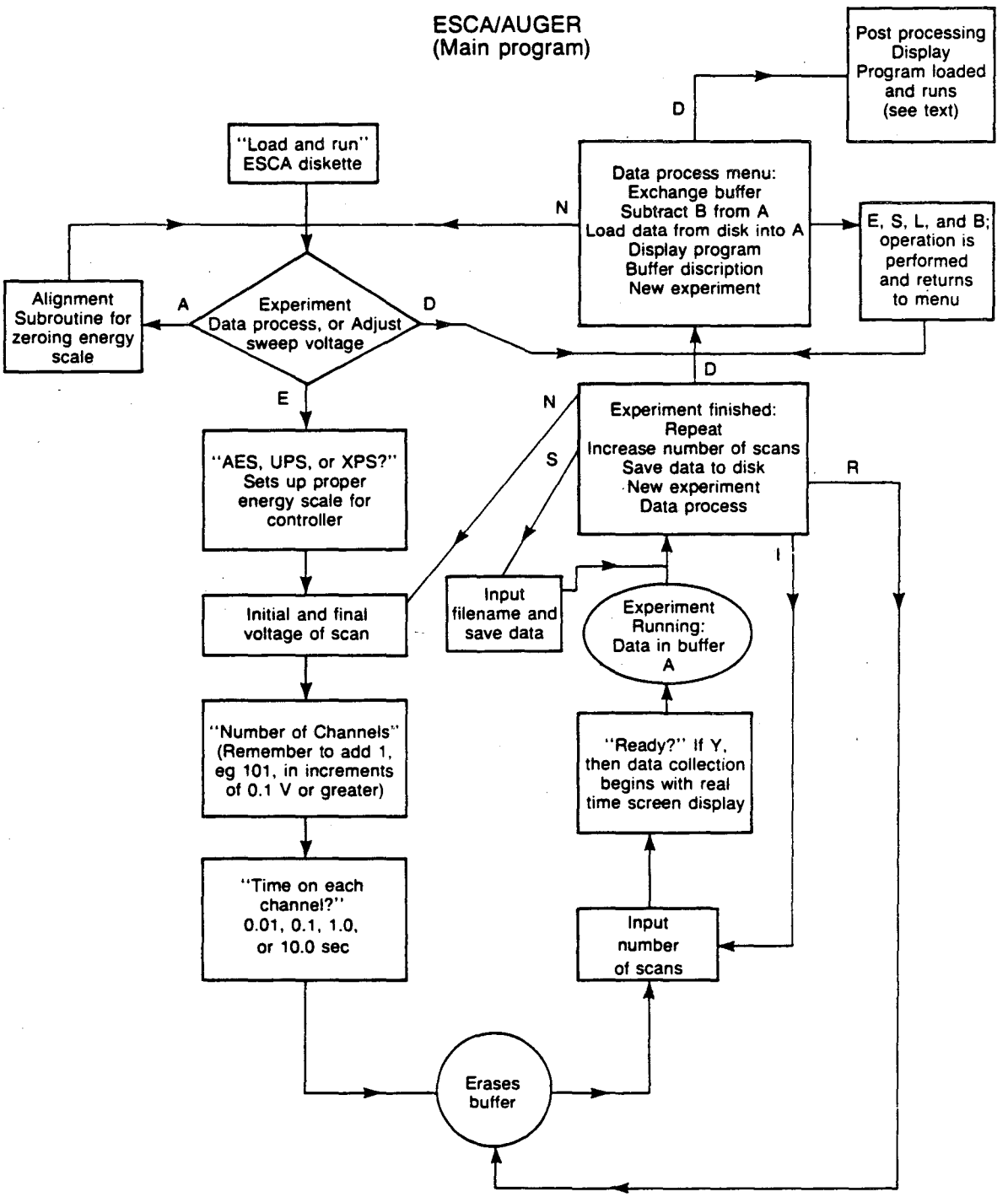

XBL 838-11081

Figure E.3

TABLE E.1

```
100 REM *UTI TDS3"
110 POKE 48895,38
120 POKE 49150,1:POKE 53,40
130 DIM MS%(8),GN%(8),DA(8),DS%(4)
140 POKE 35939,128:POKE 35943,145
150 POKE 35937,255:POKE 35936,255
160 POKE 35923,146:POKE 35922,6
170 POKE 35911,128:POKE 35907,128
180 PRINT"EXPERIMENT, OR DATA RECALL"
190 INPUTK$
200 IFK$="D"THEN1450
210 IFK$="E"THEN230
220 GOTO180
230 GOSUB 810
240 DA=DA(1):GOSUB 1420:POKE 35922,GN%(1)
250 POKE 53,40:POKE 1,0:POKE 2,40
260 PRINT"CHECK GAIN SWITCH, DAMPER CONTROL, TEMP AMP, AND CRYSTAL POSITION"
270 INPUT "GO ";K$:IF K$<>"Y"THEN 270
280 POKE 48895,38:SYS(24352):POKE 49151,3
290 POKE 24321,0:POKE 24322,0:POKE24325,1:POKE 24326,0
300 POKE 20504,0:POKE 20507,0
310 PRINT"0000 *"DT%"MS INTO EXPERIMENT"
320 PRINT"0 SCREEN PASS"
330 PRINT"MASS"DS%(1)
340 PRINT"**********************************"
350 PRINT"MASS"DS%(2)
360 PRINT"**********************************"
370 PRINT"MASS"DS%(3)
380 PRINT"**********************************"
390 PRINT"MASS"DS%(4)
400 PRINT"";
410 PRINT ""
420 SYS (20704)
430 PRINT"":POKE 49150,1
440 PRINT"REPEAT,SAVE,OR DATA PROCESS"
450 INPUT K$
470 IF K$="R"THEN GOSUB 1240:GOTO250
480 IF K$="S"THEN GOSUB 520:GOTO440
490 IFK$="D"THENGI=2:GOTO1490
500 PRINT"":GOTO 440
510 END
520 REM* SAVE DATA ON DISK*
530 PRINT"SAVE DATA ON DISK"
540 PRINT"PLACE DISK IN DRIVE #1"
550 INPUT "O.K. ";K$
560 IF K$<>"Y" THEN 550
570 OPEN 1,8,15:PRINT#1,"I1"
580 INPUT#1,A$
590 IF VAL(A$)<>0 THEN PRINT"DISK INITIALIZE ERROR; TRY AGAIN":CLOSE1:GOTO55
600 INPUT "FILE NAME";FM$
610 FL$="1:"+FM$+",SEQ,WRITE"
620 OPEN 2,8,4,FL$
630 INPUT#1,A$,B$,C$,D$
640 IF VAL(A$)=0 THEN 670
650 PRINT"ERROR "A$,B$,C$,D$
660 PRINT"TRY AGAIN":CLOSE2:CLOSE1:GOTO550
670 PRINT"COMMENT":INPUT CM$
680 PRINT#2,CM$
690 PRINT"SAVING DATA; PLEASE WAIT"
700 PRINT#2,NP%
710 FOR I=1 TO NP%
720 PRINT#2,MS%(I):NEXT
730 FOR I=1 TO NP%
740 PRINT#2,GN%(I):NEXT
750 PRINT#2,DT%:PRINT#2,TT%
760 PRINT#2,FS%
770 MF%=INT(FS%/256):LF%=FS%-256*MF%
780 POKE39,LF%:POKE38,MF%:SYS(22368)
790 PRINT "DONE":CLOSE 2:CLOSE 1
800 RETURN
810 REM  **  PARAMETER SETUP  **
820 INPUT "NUMBER OF PEAKS WITH MAX OF 8";NP%
830 IF NP%>8 THEN GOTO 820
840 FOR I=1 TO NP%
850 PRINT "MASS"I;:INPUTMS%(I):NEXT
860 PRINT"MASSES OPEN FOR D TO A ADJUSTMENT
870 PRINT"USE THE KEY '5' FOR COARSE UP"
880 PRINT"              '6' FOR COARSE DOWN"
890 PRINT"              '2' FOR FINE UP"
900 PRINT"              '3' FOR FINE DOWN"
910 PRINT"USE 'RETURN' TO REGISTER THE MASS"
920 DA=65535:FOR I=1 TO NP%
930 IF PEEK(151)=27 THEN 930
940 PRINT "FOR MASS #"MS%(I);
950 A=PEEK(151)
960 IF A=34 THEN GOSUB 1360
970 IF A=41 THEN GOSUB 1340
980 IF A=18 THEN GOSUB 1400
990 IF A=25 THEN GOSUB 1380
1000 IF A<>27 THEN 950
1010 POKE 158,0
1020 PRINT DA:DA(I)=DA:POKE158,0:GN%(I)=1:NEXT
1030 FOR I=20528 TO 20535:POKE I,0:NEXT
1040 PRINT"CHOOSE UP TO 4 MASSES FOR SCREEN DISPLAY"
1050 PRINT"AVAILIABLE MASSES ARE"
1060 FOR I=1 TO NP%:PRINTMS%(I)",";:NEXT:PRINT:PRINT
1070 RJ=1
1080 PRINT "AUTO-SCALING?";:INPUT G$
1090 IF G$="Y" THEN TS%=2000:RJ=2
1100 FOR I=1 TO NP%
1110 PRINT"DISPLAY"I"IS MASS":INPUT DS%(I):K=1
1120 IF MS%(K)=DS%(I)THEN 1150
1130 K=K+1:IF K>NP% THEN PRINT"MASS" DS%(I)"NOT FOUND":GOTO 1110
1140 GOTO 1120
1150 IF RJ=2 THEN L=0: GOTO1170
1160 PRINT "TOP SCALE (1 TO 5376 IN BINARY STEPS)":INPUT TS%:L=0
1170 IF(2^L)*42=> TS% THEN 1190
1180 L=L+1:GOTO 1170
1190 POKE(20528+K-1),L*8+I
1200 IF I=4 GOTO1206
1205 NEXT
1206 INPUT "DELAY COUNT (8-255)";DC%
1207 IF(DC%<8)OR(DC%>255)THEN1206
1208 POKE 21089,DC%:POKE 21093,DC%
1210 PRINT"DWELL TIME, MINIMUM OF 50 MSEC"
1220 INPUT MT%:DT%=MT%/.256:IF DT%<180 THEN 1210
1230 K=INT(DT%/256):POKE 20482,K+1:POKE 20481,DT%-K*256
1240 PRINT "TOTAL TIME OF EXPERIMENT IN SEC."
1250 INPUT TT%:TR%=TT%/(DT%*.000256)
1260 PRINT"TOTAL # OF SCAN IS" TR%
1270 IF (TR%*(NP%+1))>5056 THEN PRINT "NOT ENOUGH STORAGE SPACE":GOTO 1240
1280 FS%=TR%*(NP%+1)*2+10240
1290 K=INT(FS%/256):POKE20486,K:POKE20485,FS%-K*256
1300 POKE 20501,NP%:FOR I=1 TO NP%
1310 K=INT(DA(I)/256):POKE(20544+(I-1)*3),K:POKE(20544+(I-1)*3+1),DA(I)-K*256
1320 POKE(20544+(I-1)*3+2),GN%(I)
```

```
1330 NEXT:RETURN
1340 IF DA>65436 THEN RETURN
1350 DA=DA+100:GOTO 1420
1360 IF DA<100 THEN RETURN
1370 DA=DA-100:GOTO 1420
1380 IF DA>65535 THEN RETURN
1390 DA=DA+1:GOTO 1420
1400 IF DA<1 THEN RETURN
1410 DA=DA-1:GOTO 1420
1420 K=INT(DA/256)
1430 POKE 35937,K:POKE 35936,DA-K*256
1440 RETURN
1450 PETMEM:GI=1
1460 L=0:G1=0:XP=0:H=0:H1=0:H2=0
1470 REM ** VISIBLE MEMORY PLOTTING ROUTINE FOR THERMAL DESORPTION **
1480 REM ** PLOT AND LABEL AXES **
1490 INPUT "TEMP. RANGE";TR
1500 INPUT "INIT. TEMP";T1
1510 ON GI GOTO1750,1970
1520 CLEAR:VISMEM
1530 GMODE 1:DT=9:FORY=0TO100STEP10
1540 MOVE 12,Y*1.8+15:CHAR STR$(Y)
1550 NEXTY
1560 MOVE 10,50:CHROT1:CHAR"RELATIVE INTENSITY":CHROTO
1570 MOVE 80,0:CHAR "   TEMPERATURE (K)"
1580 LINE 40,20,305,20
1590 LINE 40,20,40,200
1600 FOR Y=0TO20STEP2
1610 Y1=Y*DT+20
1620 LINE 38,Y1,40,Y1
1630 NEXT Y
1640 TS=TR/200
1650 DX=265/TS
1660 FOR X=0 TO TS
1670 X1=X*DX+40
1680 LINE X1,18,X1,20
1690 S=T1+X*200
1700 MOVE X1-15,10:CHAR STR$(S)
1710 NEXT X
1720 RETURN
1730 INPUT#2,K$:SQ=VAL(K$):RETURN
1740 REM ** INPUT FILE DATA **
1750 OPEN 1,8,15:XP=0
1760 INPUT"DIRECTORY";K$
1770 IFK$="Y"THEN DIRECTORY
1780 PRINT"PUT DATA DISKETTE IN DISK DRIVE #1"
1790 INPUT "FILENAME";FM$
1800 FL$="1:"+FM$+",SEQ,READ"
1810 OPEN2,8,4,FL$
1820 INPUT#1,A$,B$,C$,D$
1830 IF VAL(A$)=0 THEN 1860
1840 PRINT"ERROR "A$,B$,C$,D$
1850 PRINT "TRY AGAIN":CLOSE2:CLOSE1 :GOTO1750
1860 INPUT#2,CM$:PRINT"COMMENT: "CM$
1870 PRINT"LOADING DATA, PLEASE WAIT"
1880 GOSUB1730:NP%=SQ
1890 REM ** INPUT MASS NUMBERS **
1900 FOR I=1TONP%:GOSUB1730:MS%(I)=SQ:NEXT
1910 REM ** INPUT GAIN(S) **
1920 FOR I=1TO NP%:GOSUB1730:GN%(I)=SQ:NEXT
1930 REM ** INPUT DWELL TIME, TOTAL TIME, AND TOTAL # OF DATA POINTS **
1940 GOSUB1730:DT%=SQ:GOSUB1730:TT%=SQ:GOSUB1730:FS%=SQ
1950 SYS(22432):CLOSE 2:CLOSE1
1960 FS%=PEEK(2)*256+PEEK(1)-1
1970 PRINT"THERE ARE"NP%" MASSES"
1980 FOR I=1TO NP%
1990 PRINT"MASS"I" IS"MS%(I)" WITH GAIN"GN%(I): NEXT
2000 PRINT "DWELL TIME IS"DT%
2010 PRINT "TOTAL TIME OF EXPERIMENT IS"TT%"SECONDS"
2020 PRINT "TOTAL NUMBER OF DATA POINTS IS"INT((FS%-10240)/NP%/2)
2030 INPUT"WHICH MASS";MS%:K=1
2040 IF MS%(K) =MS% THEN 2070
2050 K=K+1:IF K>NP%THENPRINT"MASS"MS%" NOT FOUND":GOTO 2030
2060 GOTO 2040
2070 INPUT"SCALING FACTORS";FX,FY
2080 INPUT"X,Y OFFSET VALUES";OX,OY
2090 B=40+OX
2100 INPUT"NO.OF POINTS TRIMMED";PT
2110 INPUT"INTEGRATION";I$
2120 TU=300:TV=150
2130 IF I$="N" THEN 2230
2140 INPUT"TEMP. BOUNDARIES FOR INTEGRATION";QA,QB,QC,QD
2150 TA=40+265*(QA-T1)/TR
2160 TB=40+265*(QB-T1)/TR
2170 TC=40+265*(QC-T1)/TR
2180 TD=40+265*(QD-T1)/TR
2190 INPUT"UPPER TEMP. OF PLOT";QU
2200 TU=40+265*(QU-T1)/TR
2210 INPUT"CENTER TEMP. OF PLOT";QV
2220 TV=40+265*(QV-T1)/TR
2230 INPUT "NUMBER OF POINTS TO BE SMOOTHED";NS%
2240 IF(NS%<1)OR((NS%*FX)>127)OR((NS%*FY)>127)OR(NS%>15)THEN 2230
2250 POKE 1,0:POKE 2,40
2260 POKE 0,K*2:POKE20640,NS%
2270 POKE 20643,(NP%+1)*2
2280 POKE 20642,INT(NS%*FX)
2290 POKE 20644,INT(NS%*FY)
2300 POKE20649,PT+1:POKE20650,8:POKE24328,0:POKE24324,0
2310 MF%=INT(FS%/256):LF%=FS%-MF%*256
2320 POKE20647,LF%:POKE20648,MF%
2330 TJ=10240+(NP%+1)*2*PT
2340 TJ=(PEEK(TJ)*256+PEEK(TJ+1))/FX
2350 POKE20651,1:POKE20652,0
2360 A%=INT(TU/256):B%=TU-A%*256
2370 POKE20664,B%:POKE20665,A%
2380 A%=INT(TV/256):B%=TV-A%*256
2390 POKE20672,B%:POKE20673,A%
2400 A%=INT(TA/256):B%=TA-A%*256
2410 POKE20674,B%:POKE20675,A%
2420 A%=INT(TB/256):B%=TB-A%*256
2430 POKE20676,B%:POKE20677,A%
2440 A%=INT(TC/256):B%=TC-A%*256
2450 POKE20678,B%:POKE20679,A%
2460 A%=INT(TD/256):B%=TD-A%*256
2470 POKE20680,B%:POKE20681,A%
2480 INPUT"CLEAR OLD PLOT ";K$:IFK$="Y"THEN GOSUB 1520
2490 VISMEM
2500 SYS(22048)
2510 IO=PEEK(20645)
2520 H=PEEK(20651)+PEEK(20652)*256
2530 IM=PEEK(20646)
2540 HM=PEEK(20682)+PEEK(20683)*256
2550 HA=PEEK(20684)+PEEK(20685)*256
2560 HB=PEEK(20686)+PEEK(20687)*256
2570 HC=PEEK(20688)+PEEK(20689)*256
2580 HD=PEEK(20690)+PEEK(20691)*256
2590 H2=PEEK(20692)+PEEK(20693)*256
2600 H1=PEEK(20694)+PEEK(20695)*256
2610 A2=PEEK(20696)+PEEK(20697)*256
2620 A1=PEEK(20698)+PEEK(20699)*256
2630 AT=PEEK(20701)+PEEK(20702)*256
2640 ID=PEEK(20653)
```

```
2650 IFHD<>0THEN2670
2660 HD=PEEK(20661)*256+PEEK(20660)+B:ID=PEEK(20663)*256+PEEK(20662):TD=HD
2670 IF I$="N" THEN 2720
2680 SL=(ID-IM)/(HD-HM)
2690 A1=A1-H1*(ID+SL*(HA/2+HB/2-HD))
2700 A2=A2-H2*(ID+SL*(HC/2+HD/2-HD))
2710 AT=AT-HD*(ID-SL*HD/2)
2720 MOVE 230,190:CHARFM$
2730 MOVE 190,180:CHARCM$
2740 MOVE 255,170:CHAR"MASS:";STR$(MS%)
2750 MOVE 240,0:CHAR"X,Y:";STR$(FX);STR$(FY)
2760 MOVE 230,160:CHAR"SMOOTHING:";STR$(NS%)
2770 MOVE 190,150
2780 CHAR"OFFSET VALUES:";STR$(OX);STR$(INT(IO))
2790 IF I$="N" THEN 2930
2800 LINE TA,25,TA,28
2810 MOVE TA+10,25
2820 CHAR STR$(INT(A1))
2830 LINE TB,25,TB,28
2840 LINE TC,25,TC,28
2850 MOVE TC+10,25
2860 CHAR STR$(INT(A2))
2870 LINE TD,25,TD,28
2880 MOVE 210,140
2890 CHAR"TOTAL AREA:";STR$(INT(AT))
2900 DOTL 2,2
2910 LINE TJ+8,ID-SL*HD-IO+50,TD,ID-IO+50
2920 DOTL 2,0
2930 GET K$:IF K$=""THEN2930
2940 PETMEM:INPUT "DUMP ON EPSON?";K$
2950 IFK$<>"Y"THEN1970
2960 PRINT "TURN ON EPSON; WHEN READY TYPE ANY KEY"
2970 GETK$:IFK$=""THEN 2970
2980 OPEN 4,4
2990 BG$=CHR$(27)+CHR$(75)+CHR$(144)+CHR$(1)
3000 PRINT#4,CHR$(27);"A";CHR$(8)
3010 FOR I=44824 TO 44863
3020 PRINT#4,BG$;
3030 MB%=INT(I/256):LB%=I-256*MB%
3040 POKE1,LB%:POKE2,MB%
3050 POKE652,74:POKE653,74:POKE654,74:POKE655,74
3060 SYS(640):PRINT#4,CHR$(10)
3070 PRINT#4,BG$;
3080 POKE1,LB%:POKE2,MB%
3090 POKE652,234:POKE653,234:POKE654,234:POKE655,234
3100 SYS(640):PRINT#4,CHR$(10):NEXT:CLOSE4:GOTO1970
```

TABLE E.2

```
100 REM****ESCA PROGRAM - UPDATED BY KG 4/83****
110 POKE53,62:HP=8*4096+12*256
120 POKE 35929,128:POKE35943,145
130 POKE35937,255:POKE35936,255
140 POKE35923,146:POKE35922,6
150 POKE35911,128:POKE35907,128
160 POKEBP+235,146:REM *INITIALIZE 8255RUN
170 DIM PS$(1),NM$(1),VI(1),VF(1),NC%(1),VC(1),TC(1),AD(1),NS%(1),MX(1),MN(1
180 AD(0)=62*256
190 AD(1)=70*256
200 REM
210 REM
220 PRINT"MAIN MENU"
230 PRINT"EXPERIMENT"
240 PRINT"DATA PROCESS"
250 PRINT"ADJUST SWEEP VOLTAGE"
260 INPUT "ENTER CHOICE";K$
270 K$=LEFT$(K$,1)
280 IF K$="E"THENGOSUB330:GOTO310
290 IF K$="D"THENGOSUB1100:GOTO310
300 IF K$="A"THENGOSUB1280:GOTO310
310 GOTO 220
320 REM
330 REM*EXPERIMENT DRIVER*
340 PRINT"RUN EXPERIMENT"
350 PRINT"ENTER"
360 INPUT"UPS, XPS, OR AUGER";PS$
370 IFPS$="U"THENPS$(0)="UPS":SF=1.55:GOTO400
380 IFPS$="X"THENPS$(0)="XPS":SF=1.827:GOTO400
390 IFPS$="A"THENPS$(0)="AUGER":SF=1.55:GOTO400
400 INPUT"INITIAL , FINAL VOLTAGE";VI,VF:VI(0)=VI/SF-3:VF(0)=VF/SF-3
410 IF(VI<0)OR(VF>2000)OR(VF<VI)THENGOSUB1410:PRINT"";:GOTO400
420 INPUT"# OF CHANNELS";NC%:NC%(0)=NC%
430 IFNC%>1000THENGOSUB330:PRINT"";:GOTO420
440 VC=(VF-VI)/(NC%(0)-1):VC(0)=VC/SF
450 IF(VC<.1)OR(INT(VC*10)<>VC*10)THENGOSUB1410:PRINT"";:GOTO420
460 PC%=NC%/300+1
470 INPUT"TIME (SEC.) ON EACH CHANNEL";TC:TC(0)=TC
480 IF(TC=.01)OR(TC=.1)OR(TC=1)OR(TC=10)THEN500
490 GOSUB1410:PRINT"";:GOTO470
500 IFTC=.01THENCT%=60
510 IFTC=.1THENCT%=61
520 IFTC=1THENCT%=62
530 IFTC=10THENCT%=63
540 GOSUB 1830
550 PRINT"# OF SCANS";
560 INPUT NS%
570 REM
580 REM****SETUP FOR EXPERIMENT UNTIL 800****
590 MB%=AD(0)/256:LB%=AD(0)-MB%*256
600 POKE20483,LB%:POKE20484,MB%
610 POKE20496,EM
620 MB%=NS%/256:LB%=NS%-MB%*256
630 POKE20497,LB%:POKE20498,MB%
640 MB%=NC%/256:LB%=NC%-MB%*256
650 POKE20501,LB%:POKE20502,MB%
660 POKE20506,CT%
670 POKE20505,PC%
680 MB%=NC%(0)/256:LB%=NC%(0)-MB%*256
690 POKE20506,(LB%+1)AND255:POKE20507,(MB%+1)AND255
700 VS=65535-VI(0)*30:MB%=VS/256:LB%=VS-MB%*256
710 POKE20508,LB%:POKE20509,MB%
720 VS=VC(0)*30:MB%=VS/256:LB%=VS-MB%*256
730 POKE20510,LB%:POKE20511,MB%
740 POKE20514,10:POKE20515,0
750 INPUT "READY ";K$
760 IF K$<>"Y"THEN 750
770 GOSUB2620:REM*AXIS*
780 PRINT"USE '<' TO ABORT; 'C' TO STOP SCAN"
790 POKE49150,3
800 MB%=ON%/256:LB%=ON%-MB%*256
810 POKE36074,CT%-48:POKE36074,CT%
820 POKE20490,0:POKE20491,0:POKE20492,0:POKE20493,0
830 POKE75,LB%:POKE76,MB%:SYS(20608)
840 NS%(0)=PEEK(20482)*256+PEEK(20481)
850 MX(0)=PEEK(20534)*256+PEEK(20535)
860 MN(0)=PEEK(20538)*256+PEEK(20539)
870 IFPEEK(20480)AND8THENGOSUB1830
880 IFPEEK(20480)AND4THENPRINT"DATA OVERFLOW"
890 IFPEEK(20480)AND32THENPRINT"SCAN # OVERFLOW"
900 PRINT"FINISH SCAN FINISHED: TYPE ANY KEY TO CONTINUE":GET:
910 GETK$:IFK$=""THEN910
920 POKE 49150,1
930 REM* AFTER EXPERIMENT*
940 PRINT"EXPERIMENT IS DONE"
950 PRINT" "
960 PRINT"REPEAT EXPERIMENT"
970 PRINT"INCREASE # OF SCAN"
980 PRINT"SAVE DATA ON DISK"
990 PRINT"NEW EXPERIMENT"
1000 PRINT"DATA PROCESS"
1010 INPUT"ENTER CHOICE";K$
1020 IFK$="R"THEN GOSUB 1440:GOTO540
1030 IFK$<>"I"THEN1060
1040 GOSUB1440:EM=0:INPUT"# OF ADDITIONAL SCANS";AS%
1050 NS%=NS%(0)+AS%:GOTO580
1060 IFK$="S"THEN GOSUB 1520:GOTO1090
1070 IFK$="N"THEN GOSUB1830:GOTO400
1080 IFK$="D"THEN GOTO 1100
1090 GOTO 930
1100 REM*DATA PROCESS DRIVER*
1110 PRINT"DATA PROCESS"
1120 PRINT" "
1130 PRINT"EXCHANGE BUFFERS (A<->B)"
1140 PRINT"SUBTRACT B FROM A"
1150 PRINT"LOAD DATA FROM DISK TO BUFFER A"
1160 PRINT"BUFFER DISCRIPTION"
1170 PRINT"DISPLAY AND POSTPROCESSING"
1180 PRINT"NEW EXPERIMENT"
1190 INPUT"ENTER CHOICE";K$
1200 IFK$="E"THENGOSUB1920:GOTO1260
1210 IF K$="S"THENGOSUB2720:GOTO1260
1220 IFK$="L"THENGOSUB2080:GOTO1260
1230 IFK$="B"THENGOSUB2350:GOTO1260
1240 IFK$="D"THENGOSUB2510:GOTO1260
1250 IFK$="N"THENRETURN
1260 GOTO1100
1270 REM
1280 REM*ALIGNMENT DRIVER*
1290 PRINT"ADJUSTMENT OF SWEEP VOLTAGE"
1300 PRINT"ENTER 'E' TO EXIT THIS MODE"
1310 INPUT "ENTER VOLTAGE (0-2000 V.)";K$:VT=VAL(K$)/1.55-1.5
1320 IFK$="E"THEN 1390
1330 DA=65535-30*VT:IF DA<0 THEN 1380
1340 K=INT(DA/256):POKE35937,K:POKE35936,DA-K*256
```

```
1350 PRINT"ADJUST FOR THE RIGHT VOLTAGE"
1360 PRINT"TYPE ANY KEY TO CONTINUE"
1370 GETK$:IFK$=""THEN1370
1380 GOTO 1290
1390 RETURN
1400 REM
1410 REM*ERASE LAST LINE*
1420 PRINT"                                        "
1430 RETURN
1440 REM*PRINT EXP. PARAMETER*
1450 PRINT"EXPERIMENT"
1460 PRINTPS$(0)" "NM$(0)
1470 PRINT"FROM"VI" TO "VF" EV"
1480 PRINT"WITH "NC%(0)" CHANNELS"
1490 PRINT"VOLTAGE INCREMENT OF"VC" EV"
1500 PRINT"TIME ON EACH CH. IS"TC(0)"SEC."
1510 RETURN
1520 REM*SAVE TO DISK*
1530 PRINT"SAVE BUFFER A TO DISK"
1540 PRINT"PUT DISK IN DRIVE # 1"
1550 INPUT"WANT DIRECTORY";K$
1560 IFK$<>"Y"THEN1590
1570 DIRECTORY D1
1580 IFVAL(DS$)<>0THENPRINT""DS$:GOTO1540
1590 INPUT"FILE NAME ";FM$
1600 INPUT"COMMENT";NM$(0)
1610 DOPEN#2,(FM$),D1,W
1620 IFVAL(DS$)<>0THENPRINT""DS$:GOTO1540
1630 PRINT"SAVING DATA; PLEASE WAIT"
1640 PRINT#2,PS$(0)
1650 PRINT#2,NM$(0)
1660 PRINT#2,VI(0)
1670 PRINT#2,VF(0)
1680 PRINT#2,NC%(0)
1690 PRINT#2,VC(0)
1700 PRINT#2,TC(0)
1710 PRINT#2,NS%(0)
1720 PRINT#2,MX(0)
1730 PRINT#2,MN(0)
1740 MB%=AD(0)/256:LB%=AD(0)-MB%*256
1750 POKE1,LB%:POKE2,MB%
1760 EN=AD(0)+NC%(0)*2-1
1770 MB%=EN/256:LB%=EN-MB%*256
1780 POKE39,LB%:POKE38,MB%
1790 SYS(22368)
1800 DCLOSE#2
1810 RETURN
1820 REM
1830 REM*ERASE BUFFER A*
1840 MB%=AD(0)/256:LB%=AD(0)-MB%*256
1850 POKE1,LB%:POKE2,MB%
1860 SYS(21440):REM*ZERO BUFFER*
1870 POKE20481,0:POKE20482,0
1880 POKE20485,0:POKE20486,0
1890 POKE20516,48:POKE20517,48:POKE20518,48:POKE20519,48
1900 SYS(24352):REM*CLEAR VISMEM*
1910 RETURN
1920 REM*EXCHANGE BUFFER  A<->B*
1930 PRINT"EXCHANGE BUFFERS A<->B":TR=TI+60
1940 PS$=PS$(0):PS$(0)=PS$(1):PS$(1)=PS$
1950 NM$=NM$(0):NM$(0)=NM$(1):NM$(1)=NM$
1960 VI=VI(0):VI(0)=VI(1):VI(1)=VI
1970 VF=VF(0):VF(0)=VF(1):VF(1)=VF
1980 NC%=NC%(0):NC%(0)=NC%(1):NC%(1)=NC%
1990 VC=VC(0):VC(0)=VC(1):VC(1)=VC
2000 TC=TC(0):TC(0)=TC(1):TC(1)=TC
2010 AD=AD(0):AD(0)=AD(1):AD(1)=AD
2020 MX=MX(0):MX(0)=MX(1):MX(1)=MX
2030 MN=MN(0):MN(0)=MN(1):MN(1)=MN
2040 NS%=NS%(0):NS%(0)=NS%(1):NS%(1)=NS%
2050 IFTI<TRTHEN2050
2060 RETURN
2070 REM
2080 REM*LOAD FROM DISK TO BUFFER A*
2090 PRINT"LOAD DATA FROM DISK TO BUFFER A"
2100 PRINT"PUT DISK IN DRIVE # 1"
2110 INPUT"WANT DIRECTORY ";K$
2120 IFK$<>"Y"THEN2150
2130 DIRECTORY D1
2140 IFVAL(DS$)<>0THENPRINT""DS$:GOTO2100
2150 INPUT"FILE NAME ";FM$
2160 DOPEN#2,(FM$),D1
2170 IFVAL(DS$)<>0THENPRINT""DS$:GOTO2100
2180 INPUT#2,PS$(0)
2190 INPUT#2,NM$(0)
2200 INPUT#2,VI(0)
2210 INPUT#2,VF(0)
2220 INPUT#2,NC%(0)
2230 INPUT#2,VC(0)
2240 INPUT#2,TC(0)
2250 INPUT#2,NS%(0)
2260 INPUT#2,MX(0)
2270 INPUT#2,MN(0)
2280 MB%=AD(0)/256:LB%=AD(0)-MB%*256
2290 PRINT"LOADING DATA; PLEASE WAIT"
2300 POKE1,LB%:POKE2,MB%
2310 SYS(22432)
2320 DCLOSE#2
2330 RETURN
2340 REM
2350 REM*BUFFER DISCRIPTION*
2360 PRINT"BUFFER DISCRIPTION"
2370 FOR I=0 TO 1
2380 PRINT"BUFFER "CHR$(65+I)" STARTS AT PAGE"AD(I)/256
2390 PRINT"EXPERIMENT "PS$(I)" "NM$(I)
2400 PRINT"FROM"VI(I)" TO "VF(I)" EV"
2410 PRINT"WITH "NC%(I)" CHANNELS"
2420 PRINT"VOLTAGE INCREMENT OF"VC(I)" EV"
2430 PRINT"TIME ON EACH CH. IS"TC(I)"SEC."
2440 PRINT"# OF SCAN IS"NS%(I)
2450 PRINT"MAX. IS"MX(I)"; MIN. IS"MN(I)
2460 PRINT"":NEXT
2470 PRINT"TYPE ANY KEY TO CONTINUE"
2480 GETK$:IFK$=""THEN2480
2490 RETURN
2500 REM
2510 REM*DISPLAY DATA ON VISMEM*
2520 PRINT"THE DISPLAY ROUTINE ONLY WORKS ON DISK  DATA"
2530 INPUT "WANT TO SAVE DATA TO DISK BEFORE IT IS   OBLITERATED";K$
2540 IFK$="Y"THENGOSUB1520
2550 C$=CHR$(34):PRINT"POKE53,95:DLOAD"C$"RDISP $5F-60"C$
2560 PRINT"NEW"
2570 PRINT"DLOAD "C$"RICKDISPLAY"C$
2580 PRINT"RUN"
2590 POKE158,4
2600 FORI=623TO629:POKEI,13:NEXTI
2610 END
2620 REM*DISPLAY AXIS*
2630 PRINT""
2640 PRINT"▌":PRINT"▌"
2650 FORYC=1TO4:PRINT"▌":PRINT"▌":PRINT"▌":PRINT"▌":NEXT
2660 PRINT"▌"MID$(STR$(VI),2)"V.";
```

```
2670 XB=40*NC%/PC%/300-LEN(STR$(VF))-1
2680 IFXB<(LEN(STR$(VI))+2)THENXB=LEN(STR$(VI))+3
2690 IFXB>36-LEN(STR$(VF))THENXB=36-LEN(STR$(VF))
2700 PRINTTAB(XB)MID$(STR$(VF),2)"V.";
2710 RETURN
2720 PRINT"CHECK FOR MIN AND MAX ":TR=TI+90
2740 MS=INT(AD(0)/256):LS=AD(0)AND255
2750 POKE1,LS:POKE2,MS
2760 MS=INT((NC%-1)/256):LS=(NC%-1)AND255
2770 POKE21664,LS:POKE21665,MS
2780 MS=INT(AD(1)/256):LS=AD(1)AND255
2790 POKE35,LS:POKE36,MS
2800 SYS(21696)
2802 MN=PEEK(21669)+PEEK(21670)*256-(PEEK(21671)AND1)*(2^16)
2804 MX=PEEK(21672)+PEEK(21673)*256-(PEEK(21674)AND1)*(2^16)
2810 PRINT"MIN AND MAX IN DIFFERENCE SPECTRUM ARE":PRINTMN,MX
2830 MN(0)=0:MX(0)=MX-MN
2840 MS=INT(AD(0)/256):LS=AD(0)AND255
2850 POKE1,LS:POKE2,MS
2860 MS=INT((NC%-1)/256):LS=(NC%-1)AND255
2870 POKE21664,LS:POKE21665,MS
2880 MS=INT(AD(1)/256):LS=AD(1)AND255
2882 POKE35,LS:POKE36,MS
2890 SYS (21888)
2900 IFTI<1RTHEN2900
2910 RETURN
```

```
100 REM ** DISPLAY PROGRAM ** UPDATED JULY 1982 BY RG
110 PRINT"MORGAN ESCA DISPLAY PROGRAM"
120 A$="123456789012345678901234 5":A$=A$+A$+A$+A$+A$+A$+A$+A$
130 B$="    ";LL$=CHR$(13)+""+"":CT=100:SYS(256*97)
140 OPEN 144,4:PRINT#144,CHR$(27);"A";CHR$(8):GMODE1
150 H$="                                        "+CHR$(13)+""
160 DIM D%(1100),P(2,0)
170 Y2=100000:YT=Y2:YS=180/Y2
180 BG$=CHR$(27)+CHR$(75)+CHR$(205)+CHR$(255)+CHR$(0)+CHR$(0)
190 FOR I=768TO796:READ A:POKE I,A:NEXT
200 SV=PEEK(42)+256*PEEK(43)
210 DATA 162,200,173,0,0,157,0,0,202,208,1,96
220 DATA 169,40,24,109,3,3,144,3,238,4,3,141,3,3,76,2,3
230 PRINT""
240 PRINT"COMMAND     *    (SEE LIST OF COMMANDS)";LL$;:PETMEM:INPUTC$
250 PRINT"                    ":C$=LEFT$(C$,1)
260 IFC$="A"THEN GOSUB 690:GOTO240
270 IFC$="G" GOTO 1410
280 IFC$="Q" GOTO 1800
290 IF C$="L" GOTO540
300 IFC$="H" THENGOSUB 410:GOTO 240
310 IFC$="I" GOTO 63999
320 IFC$="*" GOTO 1540
330 IFC$="B" GOTO 630
340 IFC$="R" GOTO 610
350 IFC$="*" THEN PRINT"";:PETMEM:GOTO 240
360 IFC$="X"THENGOTO520
370 IFC$="Y" GOTO 840
380 IF C$="D" GOTO 1600
390 IF C$="S" GOTO1880
400 PRINT"INVALID COMMAND":GOTO 240
410 GOSUB 650
420 HS=(WR-WL)/40:NT=CT*INT(.9999+(WL/CT)):HH=HS/7.99
430 FOR I=1 TO 40:VM=I+36863:W=WL+HS*I
440 MB%=INT(VM/256):LB%=VM-256*MB%:POKE771,LB%:POKE772,MB%
450 POKE 774,PEEK(SV+3)-1:POKE 775,PEEK(SV+4)
460 PRINT#144:SYS(768)
470 IF W<NT GOTO 480
480 PRINT#144,"        ";BG$;CHR$(0);CHR$(0);
490 PRINT#144,CHR$(255);A$;
500 NEXT I
510 RETURN
520 PRINT"EV INIT.";W1;LL$;:INPUTW1
530 PRINT"EV FINAL",W2;LL$;:INPUTW2:GOTO240
540 WL=W1:WR=W2:PVMEM:DF=1:XFFLG0
550 IF DF THEN GOSUB 650
560 XS=265/(X2-X1):XO=-X1*XS+40
570 I=X1:JM I*XS+XO,D%(I)*YS+YO
580 FORI=X1+1 TO X2
590 JD I*XS+XO,D%(I)*YS+YO
600 NEXTI:GOTO900
610 W1=F1:W2=F2:WL=W1:WR=W2:S7=F7:GOTO240
620 REM ** ADD VARIABLE BASELINE ROUTINE HERE
630 INPUT"BASELINE COUNT TO SUBTRACT";T
640 FOR I=X1 TO X2:D%(I)=D%(I)-T:NEXTI
650 X1=INT((WL-F1)/WS):IF X1<0 THEN X1=0
660 X2=INT(.99+(WR-F1)/WS):IF X2>F7 THEN X2=F7
670 WL=F1+X1*WS:WR=F1+X2*WS:RETURN
680 PRINT "";B$;B$;INT(YB);"-";INT(YT);"COUNTS":RETURN
690 GOSUB 650
```

```
700 PRINT"AUTOSCALING, PLEASE WAIT"
710 Y1=D%(X1):Y2=Y1
720 FORI=X1+1TOX2:T=D%(I)
730 IFT>Y2THENY2=T
740 IFT<Y1THENY1=T
750 NEXT
760 YS=155/(Y2-Y1):YO=-Y1*YS+25
770 YT=Y2:YB=Y1
780 RETURN
790 GOSUB 650
800 XS=265/(X2-X1):XO=-X1*XS+40
810 FOR I=X1 TO X2
820 JM INT(I*XS+XO),INT(D%(I)*YS+YO):WRPIX
830 NEXT I:RETURN
840 PRINT"MAX COUNT",Y2,LL$;:INPUTY2
850 PRINT"MIN COUNT",Y1,LL$;:INPUTY1
860 GOSUB 760:GOTO240
870 WL=W1:WR=W2:XFFLG0
880 DF=1
890 IF DF THEN GOSUB 790
900 GOSUB 680:PVMEM
910 GET C$:IF ZM AND(C$="") THEN C$=LC$:GOTO 940
920 IF C$="" GOTO 910
930 PRINT"                    "
940 LC$=C$:IFC$="5"GOTO910
950 IFC$="R"GOTO240
960 IFC$=","GOTO1190
970 IFC$="."GOTO1200
980 IFC$="("GOTO1360
990 IFC$=")"GOTO1340
1000 LC$="5":IFC$="A"GOTO 1250
1010 IFC$="D"GOTO680
1020 IFC$="*"THEN CLEAR:DF=0:GOTO 910
1030 IFC$="2"GOTO240
1040 IFC$="["GOTO1300
1050 IFC$="]"GOTO1330
1060 IFC$="<"GOTO1280
1070 IFC$=">"GOTO1270
1080 IFC$="["GOTO1380
1090 IFC$="5"GOTO1880
1100 IFC$="B"GOTO1220
1110 IFC$="="GOTO1290
1120 IFC$="Z"THEN ZM=1:POKE33767,154:GOTO 910
1130 IFC$="J"THEN ZM=0:POKE33767,32:GOTO 910
1140 IFC$="L"GOTO550
1150 IFC$="E"GOTO1260
1160 IFC$="/"THENGOSUB520:GOTO910
1170 IFC$="H"THENGOSUB410:GOTO910
1180 PRINT"INVALID COMMAND":GOTO 910
1190 T=1/YS:YT=YT-T:YB=YB+T:YS=YS*1.1:GOTO 890
1200 T=1/YS:YT=YT+T:YB=YB-T:YS=YS*.9:GOTO 890
1210 IFCL=CRTHENPRINT"CURSOR ERROR":GOTO910
1220 T=(D%(CR)-D%(CL))/(CR-CL):NT=D%(CL)-CL*T
1230 FORI=CL TO CR:D%(I)=NT+I*T:NEXT
1240 JL CL*XS+XO,D%(CL)*YS+YO,CR*XS+XO,D%(CR)*YS+YO:GOTO 910
1250 GOSUB 690:GOTO 890
1260 GRACSR:JM CX*XS+XO,168:JA",";STR$(INT(CC));"]":GOTO1320
1270 JA"L":CL=CX:GOTO 910
1280 JA"R":CR=CX:GOTO 910
1290 X1=CL:X2=CR:GOSUB 670:RG=1:GOSUB 1610:GOSUB800:GOTO910
1300 CX=INT((X1+X2)/2)
1310 CC=F1+WS*CX:PRINTH$;"     X=";CC;" Y=";D%(CX)
1320 JM CX*XS+XO,D%(CX)*YS+YO:GRACSR:GOTO910
1330 GRACSR:GOSUB 680:GOTO 910
1340 IF CX=X2 GOTO 910
1350 CX=CX+1:GRACSR:GOTO 1310
1360 IF CX=X1 GOTO 910
1370 CX=CX-1:GRACSR:GOTO 1310
1380 PRINT#144,"X=";F1+WS*CX;" Y=";D%(CX):PRINT#144," ":GOTO 910
1390 S7=INT((W2-W1)/WS-.99):IFS7<=0THENPRINT"ERROR: BAD ENDPOINTS":GOTO240
1400 REM ** INPUT DATA
1410 INPUT"DISK( FILENAME";F$:IFF$=""GOTO240
1420 DOPEN#8,(F$),D1
1430 IF DS<>0 THEN PRINT DS$:CLOSE8:GOTO 240
1432 PRINT"LOADING DATA; PLEASE WAIT"
1440 INPUT#8,D1$:INPUT#8,TT$:INPUT#8,W1
1450 INPUT#8,W2:INPUT#8,S7:INPUT#8,WS
1460 INPUT#8,TP:INPUT#8,SW:INPUT#8,Y2:INPUT#8,Y1:SP=1:LP$=DT$:DOSE8:GO
1470 F1=W1:F2=W2:F7=S7:FS=WS:WL=W1:WR=W2
1480 MS=INT(S7/256):LS=S7AND255
1490 POKE 24576,LS:POKE 24577,MS
1500 POKE24591,0:SYS(6*4096+2*16)
1510 IFPEEK(24578)=0 THEN 1520
1512 PRINT"ARRAY NOT FOUND"
1520 IF DS<>0 THEN PRINT"GET ERROR"
1530 CLOSE8:GOTO 240
1540 T=1/WS
1550 FOR I=X1+1TO X2
1560 D%(I-1)=(D%(I)-D%(I-1))*T
1570 NEXT I
1580 TT$="D%("+TT$+")"
1590 GOTO 1250
1600 REM ** PLOT AND LABEL AXES
1610 CLEAR:VISMEM
1620 GMODE 1:DT=9:FOR Y=0TO100 STEP 10
1630 MOVE12,Y*1.8+15:CHAR STR$(Y):NEXTY
1640 MOVE 10,50:CHROT1:CHAR"RELATIVE COUNTS": CHROTO
1650 MOVE80,0:CHAR"ELECTRON ENERGY (EV)"
1660 LINE40,20,305,20:LINE40,20,40,200
1670 FOR Y=0TO20 STEP2:Y1=Y*DT+20
1680 LINE 30,Y1,40,Y1:NEXTY
1690 IF (WR-WL)<11 THENDV%=1:GOTO1750
1700 IF (WR-WL)<51 THENDV%=5:GOTO1750
1710 IF (WR-WL)<101 THENDV%=10:GOTO1750
1720 IF (WR-WL)<301 THENDV%=25:GOTO1750
1730 IF (WR-WL)<1001 THENDV%=100:GOTO1750
1740 IF (WR-WL)<2001 THENDV%=300:GOTO1750
1750 TS=(WR-WL)/DV%:DX=265/TS
1760 FOR B=0 TO TS:XA=B*DX+40
1770 LINEXA,18,XA,20: S=WL+B*DV%
1780 MOVE XA-15,10:CHAR STR$(S):NEXTB:IFRG=1 THEN RG=0:RETURN
1790 RG=0:GOTO870
1800 PRINT#144:CLOSE144
1810 C$=CHR$(34):PRINT"POKE53,62:DLOAD"C$"ESCA18 $50-$60"C$
1820 PRINT"NEW"
1830 PRINT"DLOAD"C$"ESCA1"C$
1840 PRINT"RUN"
1850 POKE158,4
1860 FORI=623TO629:POKEI,13:NEXTI
1870 END
1880 D%(S7+1)=D%(S7): D%(S7+2)=D%(S7)
1910 MS=INT(S7/256):LS=S7AND255
1920 POKE24576,LS:POKE24577,MS
1930 POKE24591,1:SYS(6*4096+2*16)
     GOTO1600
```

This report was done with support from the Department of Energy. Any conclusions or opinions expressed in this report represent solely those of the author(s) and not necessarily those of The Regents of the University of California, the Lawrence Berkeley Laboratory or the Department of Energy.

Reference to a company or product name does not imply approval or recommendation of the product by the University of California or the U.S. Department of Energy to the exclusion of others that may be suitable.

TECHNICAL INFORMATION DEPARTMENT
LAWRENCE BERKELEY LABORATORY
UNIVERSITY OF CALIFORNIA
BERKELEY, CALIFORNIA 94720